

Diss. ETH No. 15086

**A Combined Approach using
Calorimetry and IR-ATR Spectroscopy
for the Determination of
Kinetic and Thermodynamic Reaction Parameters**

A dissertation submitted to the
SWISS FEDERAL INSTITUTE OF TECHNOLOGY ZURICH

for the degree of
Doctor of Technical Sciences

presented by
Andreas Zogg
Dipl. Chem. ETH
born November 26, 1974
citizen of Grabs SG

accepted on the recommendation of
Prof. Dr. K. Hungerbühler, examiner
Prof. Dr. M. Morari, co-examiner
Prof. Dr. F. Stoessel, co-examiner
Dr. U. Fischer, co-examiner

Zurich 2003

ISBN Nr. 3-906734-33-1

To my parents

Preface

This thesis is based on research performed at the Safety and Environmental Technology Group of the Swiss Federal Institute of Technology (ETH) in Zurich between 1999 and 2003. The ETH research fund is gratefully acknowledged for providing a significant part of the necessary funding (Project TH-13./99-3).

First of all I would like to thank my supervisor, Professor Dr. K. Hungerbühler for having accepted and supported my research project in the field of reaction calorimetry and kinetic evaluation, as well as Prof. Dr. M. Morari and Prof. Dr. F. Stoessel for their assistance as co-examiners. Especially I would like to thank Dr. U. Fischer for managing the project during its initial stage and for his advice during the whole research phase.

Sincere thanks are extended to Hans-Peter Schläpfer from the mechanical and Max Wohlwend from the electronic workshop for their great and inspiring support during the construction of the presented reaction calorimeter.

Special thanks are also addressed to Dr. J. Pastré, who started this project in 1997 and kindly introduced me into the subject, to I. Zürcher who carried out her Diploma thesis within this project in 2001 and finally to S. Gianoli and F. Visentin who will carry on the project in future.

I am also grateful to Dr. J. Schildknecht of Roche Pharma, Dr. F. Mascarello, Dr. A. Keller, J. Jeisy and B. Leuthe of Roche Vitamin and Dr. C. Heuberger of Novartis for their inspiring suggestions and support during the construction of the reaction calorimeter, to Dr. M. Linder, Dr. B. Schenker, and all other people of Mettler Toledo for their support during the redesign of the presented reaction calorimeter and for their efforts to turn the developed calorimeter into a commercial product.

I would also like to thank Dr. E. Zass for supporting me in gathering reference data for the epoxidation reaction, Dr. W. Stahel for inspiring discussions on the mathematical part of this work and all members of the institute and especially all members of the Safety and Environmental Technology Group who supported me during the doctoral studies.

My greatest appreciation is reserved for my family and my parents Blanca and Dr. Martin Zogg. Without their unique support this work would not have been possible. Especially I would also like to thank my brother Dr. David Zogg for his great assistance in the field of control engineering.

CONTENT

Abstract	VII
Zusammenfassung	IX
Symbols, Operators, and Abbreviations	XI
Overview	XIX
1 Introduction	1
1.1 Context and Motivation	1
1.1.1 The Chemical reaction at the core of Integrated Process Development	1
1.1.2 Bottleneck: Parameters for empirical reaction models.....	2
1.2 Goal of the Thesis	4
1.3 Suitable analytical setups for kinetic and thermodynamic screening	5
2 Theoretical Background	8
2.1 Reaction calorimetry	8
2.1.1 Overview on the basic reaction calorimeter types	9
2.1.2 Isothermal, isoperibolic, adiabatic and temperature programmed operation mode	11
2.1.3 Steady-state heat-flow balance of the different calorimeter types	12
2.1.4 Dynamics of an isothermal reaction calorimeter.....	24
2.1.5 Assessment of the three basic reaction calorimetric principles	27
2.2 IR-ATR Spectroscopy	30
2.3 Evaluation of calorimetric and spectroscopic data	32
2.3.1 Overview and goal.....	32
2.3.2 Evaluation methods for isothermal calorimetric reaction data	33
2.3.3 Evaluation methods for isothermal spectroscopic reaction data	42
2.3.4 Combined evaluation of spectroscopic and calorimetric data.....	47
2.3.5 Model selection.....	48

3	The new Calorimeter.....	49
3.1	Historical development.....	49
3.2	Requirements for the new reaction calorimeter	50
3.2.1	Accuracy of the calorimeter	53
3.2.2	Time constants of the calorimetric signals.....	56
3.3	Concept for the realization	57
3.3.1	Selection of appropriate construction materials	57
3.3.2	Split fast and slow heat-flow changes by introducing an intermediate thermostat	57
3.3.3	Steady-state temperature profiles of the new calorimeter at different operating conditions	64
3.3.4	Hot spots on the surface of the compensation heater	67
3.3.5	Calculation concept for the inner (reactor) thermostat.....	69
3.3.6	Calculation concept for the intermediate (jacket) thermostat.....	69
3.4	Design of the new calorimeter.....	70
3.4.1	Complete reactor and overview	70
3.4.2	Copper Jacket	72
3.4.3	Cover, connections and magnetic coupling.....	75
3.4.4	Cooler, Peltier elements and T_{Pelt} sensors.....	78
3.4.5	Compensation heater	80
3.5	Setup and peripheral devices of the whole apparatus.....	81
3.6	Software and controller	82
3.7	From measured signals to calorimetric data	89
3.7.1	Calculation of q_{tot} by combination of the inner and outer heat-flow balance.....	89
3.7.2	Calculation of the total heat pumped by the Peltier elements q_{Cooling} ...	91
3.7.3	Calculation of q_{Stirr} and q_{Loss}	96
3.7.4	Final calculation formula for q_{tot} and filtering of the required measurement signals	99

4	Evaluation of the Calorimetric and Spectroscopic Data, a new Combined Approach.....	100
4.1	<i>Historical background.....</i>	100
4.2	<i>Requirements.....</i>	100
4.3	<i>Concept of the evaluation method.....</i>	103
4.3.1	Combined evaluation algorithm	103
4.3.2	Model selection.....	106
4.3.3	Step by step evaluation procedure	107
4.4	<i>Mathematical formulation of the combined evaluation algorithm.....</i>	109
4.4.1	Pre-treatment of the infrared data.....	109
4.4.2	Pre-treatment of the calorimetric Data.....	110
4.4.3	Step by step explanation	110
4.5	<i>Automatic calculation of the combined objective function ΔComb....</i>	114
5	Applications and Results	122
5.1	<i>Overview</i>	122
5.2	<i>Neutralization of NaOH with H₂SO₄.....</i>	123
5.2.1	Evaluation of the calorimetric data.....	123
5.3	<i>Hydrolysis of acetic anhydride.....</i>	126
5.3.1	Combined evaluation of the infrared and calorimetric data.....	126
5.3.2	Simultaneous evaluation of all measurements at all temperatures....	133
5.3.3	Summary of all results	134
5.4	<i>Epoxidation of 2,5-di-tert-butyl-1,4-benzoquinone</i>	135
5.4.1	Combined evaluation of the infrared and calorimetric data.....	136
5.4.2	Testing different reaction models.....	146
5.4.3	Simultaneous evaluation of all experiments at all temperatures.....	153
5.4.4	Analysis of the automatic scaling method.....	157

6	Final Discussion and Conclusions	160
6.1	New reaction calorimeter	160
6.1.1	Accuracy and time constants of the new calorimeter	162
6.1.2	Comparison mathematical – measured baseline	165
6.1.3	Calibration of the Peltier elements	166
6.1.4	Time correction of the baseline signal (q_{Cooling})	167
6.1.5	Influence of the ambient temperature	168
6.2	Evaluation of the calorimetric data	169
6.3	Combined evaluation of calorimetric and infrared data	170
6.3.1	Feasibility study with a simple reaction example	172
6.3.2	Increased information content by measuring two different analytical signals	172
6.3.3	A more complex reaction with different feasible reaction models	173
6.3.4	Comparison of the three evaluation types: Separate Calorimetric, separate infrared and combined evaluation	174
6.3.5	Determination of pure component spectra	175
6.3.6	Limits of the IR-ATR (infrared) signal	176
6.3.7	Limits of the model-based evaluation	177
7	Outlook	178
7.1	Reaction calorimeter	178
7.1.1	Reactor redesign	178
7.1.2	Ideas for future developments	181
7.1.3	Ideas for the improvement of the heat-flow balance calculations	182
7.2	Evaluation algorithm	183
8	References	185

Appendix	A 1
A Reaction Calorimetry	A 1
<i>A.1 Combinations and further developments of the three basic reaction calorimetric principles (isothermal)</i>	<i>A 1</i>
B Infrared Spectroscopy	A 3
<i>B.1 Applicability of Lambert Beer's Law in ATR spectroscopy</i>	<i>A 3</i>
<i>B.2 Evaluation methods that do not require a reaction model</i>	<i>A 7</i>
<i>B.3 Comparison and combination of model-based and model-free evaluation methods</i>	<i>A 13</i>
C Construction details of the new reaction calorimeter	A 15
<i>C.1 IR-ATR Probe and Teflon inliner</i>	<i>A 15</i>
<i>C.2 Stirrer</i>	<i>A 16</i>
<i>C.3 Thermal insulation</i>	<i>A 16</i>
<i>C.4 Stirrer Engine</i>	<i>A 16</i>
<i>C.5 Baffles</i>	<i>A 16</i>
<i>C.6 Position of the temperature sensors inside the copper jacket</i>	<i>A 17</i>
<i>C.7 Cooler, peltier elements and cooling liquid</i>	<i>A 18</i>
<i>C.8 Periphery devices according to Figure 3-14</i>	<i>A 22</i>
D Calculation details required for the heat-flow balance of the new reaction calorimeter	A 25
<i>D.1 Determination of S, R and κ</i>	<i>A 25</i>
<i>D.2 Determination of k_{Loss}</i>	<i>A 31</i>
<i>D.3 Mathematical baseline for the calculation of q_{tot}</i>	<i>A 33</i>
E Applications: Experimental procedures and additional Calculations	A 34
<i>E.1 Neutralization of NaOH with H_2SO_4</i>	<i>A 34</i>
<i>E.2 Hydrolysis of Acetic Anhydride</i>	<i>A 35</i>
<i>E.3 Epoxidation of 2,5-di-tert-butyl-1,4-benzoquinone</i>	<i>A 50</i>
<i>E.4 Industrial reaction examples</i>	<i>A 68</i>
<i>E.5 Heterogeneous Reaction Example</i>	<i>A 73</i>

ABSTRACT

To meet the need for a systematic and quick gathering of **kinetic and thermodynamic reaction parameters** in early phases of process design a **small reaction calorimeter (25 to 45 ml) with an integrated IR-ATR probe** was developed during this work. Such a device is of particular importance for new fine-chemical and pharmaceutical products, where typically only small amounts of test substance are available and time-to-market is crucial. The new prototype reaction calorimeter uses a copper block as an intermediate thermostat instead of a double wall vessel (typically glass) with a circulation fluid. The reaction temperature is controlled at **isothermal conditions using the Power-Compensation principle**. To allow an **online measured baseline** (compensate changes of the heat transfer through the reactor wall during the reaction) **an additional heat-flow balance using Peltier elements is implemented and was patented**. This combination shortens the time required for a reaction experiment because **calibration steps are not required**, and enables the connection of several devices to the same cryostat (parallelisation). The new calorimeter has a very **small time constant of about 4 s** and is therefore ideally suited to measure **fast and highly exothermal** reactions at isothermal conditions. The performance and the accuracy of the new device will be demonstrated based on several reaction examples:

- ❖ The **neutralization of NaOH with H₂SO₄** (measured reaction enthalpy at 25 °C: -134 ± 1 kJ/mol, literature reference: -139.1 kJ/mol).
- ❖ The **hydrolysis of acetic anhydride** (measured reaction enthalpy at 25 °C: -60 ± 5 kJ/mol, measured first order rate constant: $2.9 \cdot 10^{-3} \text{ s}^{-1}$, $E_A = 56$ kJ/mol, literature references: -63 ± 2 kJ/mol, and $2.76 \pm 0.06 \cdot 10^{-3} \text{ s}^{-1}$, $E_A = 57$ kJ/mol).
- ❖ Two **highly exothermal industrial reactions** (maximal reaction power of ≈ 2.5 kW/l). In both examples the advantage of an online measured calorimetric baseline is clearly demonstrated.

Furthermore a **new evaluation principle** for the measured reaction data will be presented that allows the identification of the unknown reaction parameters such as rate constants, activation energies, reaction orders and reaction enthalpies. The evaluation is based on an empirical reaction model. **In contrast to conventional evaluation procedures the infrared and calorimetric data are simultaneously evaluated**. Therefore a new evaluation algorithm was developed, using nonlinear optimization, in order to estimate all unknown reaction parameters in a single step. **Neither pure infrared spectra of the involved chemical components nor any calibrations are required**. The performance of the new evaluation algorithm will be demonstrated by analyzing the following reaction examples:

- ❖ The **two step consecutive epoxidation** of 2,5-di-tert-butyl-1,4-benzoquinone
- ❖ The **hydrolysis of acetic anhydride**.

ZUSAMMENFASSUNG

Im Rahmen dieser Arbeit wurde ein **kleinvolumiges Reaktionskalorimeter (25 bis 45 ml)** mit einer **integrierten IR-ATR Sonde** entwickelt. In frühen Phasen der Prozessentwicklung soll damit dem Bedarf einer schnellen Erfassung von **kinetischen und thermodynamischen Reaktionsparametern** entsprochen werden. Speziell in der Feinchemikalien und pharmazeutischen Industrie ist ein solches Gerät von besonderer Bedeutung weil gewöhnlich nur geringe Testsubstanzmengen vorhanden sind und die Produkteinführungszeit möglichst kurz gehalten werden muss. An Stelle des üblichen doppelwandigen Reaktormantels (z.B. Glas) mit zirkulierender Kühlflüssigkeit, wird im neu entwickelten Reaktionskalorimeter ein Kupferblock als Zwischenthermostat eingesetzt. Die Reaktionstemperatur wird **mittels Power-Compensation Prinzips isotherm geregelt**. Um eine **online Messung der Basislinie** (kompensiert Veränderungen des Wärmedurchgangs an der Reaktorwand während einer Reaktion) zu ermöglichen, wurde eine **zusätzliche Wärmeflussbilanz mittels Peltierelementen implementiert und patentiert**. Diese Kombination verkürzt die benötigte Zeit für ein Reaktionsexperiment weil **keine Kalibrationsschritte mehr notwendig** sind, und ermöglicht den Anschluss mehrerer solcher Geräte an den selben Kryostaten (Parallelisierung). Das neue Reaktionskalorimeter weist eine sehr **kleine Zeitkonstante von ca. 4 s** auf und ist folglich bestens geeignet um schnelle und **stark exotherme Reaktionen** unter isothermen Bedingungen zu messen. Das Leistungsvermögen und die Genauigkeit des neuen Kalorimeters werden anhand von mehreren Beispielreaktionen gezeigt:

- ❖ Die **Neutralisation von NaOH mit H₂SO₄** (gemessene Reaktionsenthalpie bei 25 °C: -134 ± 1 kJ/mol, Literaturreferenz: -139.1 kJ/mol).
- ❖ Die **Hydrolyse von Acetanhydrid** (gemessene Reaktionsenthalpie bei 25 °C: -60 ± 5 kJ/mol, gemessene Geschwindigkeitskonstante erster Ordnung: $2.9 \cdot 10^{-3} \text{ s}^{-1}$, $E_A = 56$ kJ/mol, Literaturreferenz: -63 ± 2 kJ/mol, und $2.76 \pm 0.06 \cdot 10^{-3} \text{ s}^{-1}$, $E_A = 57$ kJ/mol).
- ❖ Zwei **stark exotherme Reaktionsbeispiele aus der Industrie** (maximale Reaktionsleistung ≈ 2.5 kW/l). Bei beiden Reaktionsbeispielen konnte der Vorteil einer online gemessenen Basislinie klar gezeigt werden.

Des Weiteren wird ein **neues Auswertungsprinzip** für die gemessenen Reaktionsdaten vorgestellt, welches die Identifikation unbekannter Reaktionsparameter (Geschwindigkeitskonstanten, Aktivierungsenergien, Reaktionsordnungen und Reaktionsenthalpien) erlaubt. Die Auswertung basiert auf einem empirischen Reaktionsmodell. **Im Gegensatz zu konventionellen Auswertungsverfahren werden die Infrarot- und Kalorimetriedaten simultan ausgewertet.** Dazu wurde ein neuer Auswertungsalgorithmus entwickelt, basierend auf nichtlinearer Optimierung, um alle unbekannt Reaktionsparameter in einem einzigen Schritt zu bestimmen. **Weder Reininfrarotspektren der involvierten chemischen Komponenten noch Kalibrationen irgend einer Art sind erforderlich.** Die Leistungsfähigkeit des neuen Auswertungsalgorithmus wird anhand der Analyse folgender Reaktionsbeispiele demonstriert:

- ❖ Die **Zweischritt Epoxidierung** von 2,5-di-tert-butyl-1,4-benzochinon.
- ❖ Die **Hydrolyse von Acetanhydrid.**

SYMBOLS, OPERATORS, AND ABBREVIATIONS

<i>Symbol</i>	<i>Unit</i>	<i>Description</i>
# Hits	-	Number of same optimal solutions found for the non-linear identification of the reaction model parameters $\theta_{1..Np}$.
α	-	Weighting factor used for a Pareto diagram.
κ	W/K	Heat conduction coefficient of the Peltier elements.
$\Delta\Delta T_{Pelt}$	K	Device specific parameter to compensate the sensor offset of T_{Pelt}^{up} and T_{Pelt}^{down} .
ΔA or $\Delta A(\theta_{1..Np})$	-	Remaining sum of squares of the linear least squares fit of A_{Data} in order to estimate the pure component spectra. Equals the infrared objective function in the combined evaluation of calorimetric and infrared data. It is a function of the reaction model parameters $\theta_{1..Np}$.
$\Delta A'$	-	$\Delta A - \Delta A_{min}$
ΔA_k	-	Remaining sum of squares of the linear least squares fit of A_{Data} in order to estimate the pure component spectra at the k'th wave number.
ΔA_{min}	-	Minimum of the function $\Delta A(\theta_{1..Np})$. It is equal to the minimal possible model fit error of the infrared data.
$\Delta Comb$	-	Combined objective function used for the simultaneous evaluation of calorimetric and infrared data. Requires the knowledge of ΔQ_{min} , ΔA_{min} , S_Q , and S_{IR} .
$\Delta Comb^*$		$\Delta Q - \Delta Q_{min} + \Delta A - \Delta A_{min}$
ΔH	J/mol	Total measured enthalpy, including the reaction enthalpy $\Delta_r H$ and the heat of mixing Q_{mix} and an eventual heat of phase transfer Q_{phase} .
$\Delta_r H$ ($\Delta_r H_1$, $\Delta_r H_2$)	J/mol	Reaction enthalpy (first and second reaction enthalpy for a consecutive reaction).
ΔQ or $\Delta Q(\theta_{1..Np})$	W ²	Remaining sum of squares of the linear least squares fit of q_{Data} in order to estimate the reaction enthalpies. Equals the calorimetric objective function in the combined evaluation of calorimetric and infrared data. It is a function of the reaction model parameters $\theta_{1..Np}$.
$\Delta Q'$	W ²	$\Delta Q - \Delta Q_{min}$
Δq_0	W	Difference of $q_{Comp,0}$ and $q_{Cooling,0}$
$\Delta q_{accu,rel}$	[%]	Instantaneous relative heat accumulation error
$\Delta Q_{accu,rel}$	[%]	Integrated relative heat accumulation error
ΔQ_{min}	W ²	Minimum of the function $\Delta Q(\theta_{1..Np})$. It is equal to the minimal possible model fit error of the calorimetric data.
λ_W	W/(m·K)	Heat conduction coefficient of the reactor wall.
$\tilde{\nu}$	cm ⁻¹	Wave number

Symbols, Operators, and Abbreviations

$\theta_{1..Np}$		Reaction model parameters such as rate constants, activation energies or reaction orders.
θ_i		i 'th reaction model parameter.
$\theta_{1..Np}^{Comb,1}$		Reaction model parameters determined by a first combined evaluation of calorimetric and infrared data (using $S_{Q,1}$ and $S_{IR,1}$).
$\theta_{1..Np}^{Comb,2}$		Reaction model parameters determined by a second and final combined evaluation of calorimetric and infrared data (using $S_{Q,2}$ and $S_{IR,2}$).
$\theta_{1..Np}^{IR}$		Reaction model parameters determined by a separate infrared evaluation.
$\theta_{1..Np}^Q$		Reaction model parameters determined by a separate calorimetric evaluation.
ρ_r	kg/m ³	Density of the reaction mixture
τ	s	Time constant
A	m ²	Total heat-transfer area of the reactor wall.
A	-	Reaction spectrum. Matrix of absorbance values ($N_t \times N_\lambda$)
A^*	-	Reaction spectrum reduced by PCA ($N_t \times N_\lambda$).
A_{calc}	-	Calculated reaction spectrum (based on a reaction model, $N_t \times N_\lambda$).
$A_{calc,k}$	-	Calculated reaction spectrum at the k 'th wave number (based on a reaction model, $N_t \times 1$).
A_{Data} or $A_{Data,measured}$	-	Matrix containing all infrared measurements (pre-treated reaction spectra A) of all experiments that are evaluated.
$A_{Data,calculated}$	-	Matrix containing all calculated infrared reaction spectra of all experiments that are evaluated.
$bl()$	W	Baseline function.
C	mol/l	Matrix of concentrations profiles ($N_t \times N_C$)
c	mol/l	Concentration time profile
$c_{A(B,C...)}$	mol/l	Concentration of component A, B, C ...
c_{A0}	mol/l	Initial concentration of component A.
C_{abs}	mol/l	Matrix of abstract concentration profiles obtained by a principal component analysis ($N_t \times N_{PC}$)
C_{calc}	mol/l	Calculated matrix of concentration profiles (based on a reaction model, $N_t \times N_C$)
$c_{calc,s}$	mol/l	Calculated concentration profile of component s (based on a reaction model).
c_{dos}	mol/l	Dosing concentration.
$c_{measured,s}$	mol/l	Measured concentration profile of component s .
$c_{p,dos}$	J/(mol·K)	Heat capacity of the dosed liquid.
$c_{p,r}$	J/(mol·K)	Heat capacity of the reaction mixture
$c_{p,tot}$	J/(kg·K)	Heat capacity of the reactor content (including reaction mixture and reactor inserts).

C_{real}	mol/l	Matrix of physical meaningful concentration time curves ($N_c \times N_c$)
d_R	m	Diameter of the stirrer
dt_{after}	s	Minimum time delay before the next switching of the control parameters.
dt_{before}	s	Time delay. Control parameters are switched dt_{before} seconds before the start and the stop of the dosing.
E	l/mol	Matrix of pure component spectra ($N_c \times N_\lambda$)
e		White noise error
$E_A (E_{A,1}, E_{A,2})$	J/mol	Arrhenius activation energy (first and second activation energy for a consecutive reaction).
$e_{A, B, C \dots}$	-	Pure spectra vector of component A, B, C ...
E_{abs}	l/mol	Matrix of abstract pure spectra obtained by principal component analysis ($N_{PC} \times N_\lambda$)
E_{calc}	l/mol	Calculated matrix of pure component spectra (based on a reaction model, $N_c \times N_\lambda$)
E_{real}	-	Matrix of physical meaningful pure component spectra ($N_c \times N_\lambda$)
f	mol/s	Feed rate
f_A	-	Scaling function for the infrared data.
f_Q	-	Scaling function for the calorimetric data.
h_j	W/(m ² ·K)	Jacket-side heat-transfer coefficient
h_r	W/(m ² ·K)	Reactor-side heat-transfer coefficient
I_{Comp}	A	Current of the compensation heater
I_{Pelt}	A	Current of the Peltier elements
$k (k_1, k_2)$	(l/mol) ⁿ⁻¹ /s	Reaction rate constant of a n'th order reaction (first and second step in a consecutive reaction).
k_0	(l/mol) ⁿ⁻¹ /s	Initial n'th order rate constant.
k_{Lid}	W/K	Empiric proportional coefficient for the calculation of q_{Lid} . It depends on the reaction conditions.
k_{Loss}	W/K	Empiric proportional coefficient for the calculation of q_{Loss} . It does not depend on the reaction conditions.
$k_{Loss,a}$	W/K ²	Device specific parameter used to calculate k_{Loss} as a function of the temperature. It was pre calibrated.
$k_{Loss,b}$	W/K	Device specific parameter used to calculate k_{Loss} as a function of the temperature. It was pre calibrated.
$k_{Loss,opt}$	W/K	Optimal k_{Loss} value determined by linear least squares optimization.
L	m	Thickness of the reactor wall
$Max_{\Delta T}$	K	Maximum allowed deviation from the set point.
Max_{dT}	K/s	Maximum allowed change of T_r
m_{tot}	kg	Mass of the reactor content (including reaction mixture and reactor inserts).

Symbols, Operators, and Abbreviations

n (A, B, C ...)	mol	Number of moles (of components A, B, C ...)
	-	Reaction order
N_C	-	Number of chemical components in the reaction system.
$N_{C,abs}$	-	Number of absorbing chemical components in the reaction system.
Ne	-	Newton number
N_{exp}	-	Number of experiments that are evaluated at the same time.
N_{ν}	-	Number of wave numbers
$N_{Mean,D}$	-	Number of points used for the moving average filter of T_r (D part).
$N_{Mean,PI}$	-	Number of points used for the moving average filter of T_r (P and I part).
N_{Mean}^{dt}	-	Number of points used for the moving average filter to calculate Max_{dT} .
N_{ν}	-	Number of wave numbers
N_{obs}	-	Number of concentration observations.
N_P	-	Number of reaction model parameters
N_{PC}	-	Number of principal components
N_R	-	Number of reactions
n_S	s^{-1}	Reversions per second of the stirrer
N_t	-	Number of time samples
$N_{t,IR}$	-	Number of time samples in A_{Data} .
$N_{t,Q}$	-	Number of time samples in q_{Data} .
ord_C	-	Reaction order of the catalyst concentration in the epoxidation experiment (used for both consecutive reaction steps).
$ord_{C,1}, ord_{C,2}$	-	Reaction order of the catalyst concentration in the epoxidation experiment (used for the first and second consecutive reaction step respectively).
ord_P	-	Reaction order of the tert-butyl hydroperoxide.
$P_{Peltier}$	W	Power consumption of the Peltier elements.
$P_{Stirrer}$	W	Power consumption of the stirrer engine.
q	W	heat flow
q_{accu}	W	Heat flow caused by heat accumulation.
$q_{Baseline}^{measured}$	W	Measured baseline (based on $q_{Cooling}$ and q_{Comp})
$q_{Baseline}^{mathematical}$	W	Mathematical baseline (based on assumptions).
q_{Comp}	W	Power consumption of the compensation heater.
$q_{Comp,0}$	W	Power consumption of the compensation heater before the start of a reaction.
$q_{Cooling}$	W	Total cooling power of the Peltier elements. In chapter 5 and 6 the term $q_{Cooling}$ is used instead of $q_{Cooling,corr}$.
$q_{Cooling,0}$	W	Total cooling power of the Peltier elements before the start of a reaction.
$q_{Cooling,corr}$	W	Time corrected $q_{Cooling}$

$q_{Cooling,exp}$	W	Expected ideal $q_{Cooling}$
$q_{Cooling,SS}$	W	Steady-state approximation of $q_{Cooling}$
q_{Data} OR $q_{Data,measured}$	W	Vector containing all calorimetric measurement data (pre-treated q_{tot}) of all experiments that are evaluated.
$q_{Data,calculated}$	W	Vector containing all calculated calorimetric data of all experiments that are evaluated.
q_{Dos}	W	Heat flow caused by the dosing of a liquid into the reaction mixture.
q_{Flow} $q_{Flow,1}$	W	Heat flow from the reactor content through the reactor wall into the reactor jacket.
$q_{Flow,2}$	W	Heat flow from the intermediate thermostat to the cooling liquid.
$q_{Fluid,IN}$	W	Heat flow introduced by the cooling liquid.
$q_{Fluid,OUT}$	W	Heat flow removed by the cooling liquid.
q_{Lid}	W	Heat flow from the reactor content through the reactor lid.
q_{Loss}	W	Heat loss to the environment.
$q_{Loss,0}$	W	Heat losses to the environment before the start of a reaction.
q_{Loss}^{Pelt}	W	Heat flow caused by the passive thermal conduction of the Peltier elements.
$q_{Loss,SS}^{Pelt}$	W	Steady-state approximation of q_{Loss}^{Pelt}
q_{mix}	W	Heat flow caused by heat of mixing.
Q_{mix}	J	Total heat revealed by mixing two different liquids.
q_{Ohm}	W	Heat flow caused by the electrical resistance of the Peltier elements.
$q_{Ohm,SS}$	W	Steady-state approximation of q_{Ohm}
q_{Pelt}	W	Heat flow caused by the Peltier effect.
$q_{Pelt,SS}$	W	Steady-state approximation of q_{Pelt}
q_{phase}	W	Heat flow caused by phase changes.
Q_{phase}	J	Total heat revealed or consumed by phase change processes.
q_{React}	W	Reaction power
q_{Stirr}	W	Heat flow caused by the stirring of the reaction mixture.
$q_{Stirr,0}$	W	Heat flow caused by the stirrer before the start of a reaction.
q_{tot} q_{React}^{tot}	W	Total power consumption or production during a reaction measurement. It contains the reaction power q_{React} and any other thermally active processes such as heat of mixing (q_{mix}) or heat of phase change (q_{phase}).
Q_{tot}	J	Total produced or consumed heat during a reaction measurement.
r	mol/(l·s)	Reaction rate
R	Ω	Electrical resistance of the two Peltier elements in series.
R	J/(mol·K)	Ideal gas constant
r or $r(t)$	mol/(l·s)	Reaction rate
r_A (B, C ...)	mol/(l·s)	Reaction rate of component A, B, C ...

Symbols, Operators, and Abbreviations

S	V/K	Seebeck coefficient of the two Peltier elements in series.
S_{IR} or $S_{IR,1 \dots 2}$	-	Automatically calculated scaling factor for the infrared objective function (ΔA). Used for the combined evaluation of calorimetric and infrared data. $S_{IR,1}$ is used for the first, $S_{IR,2}$ for the second and final combined evaluation
S_Q or $S_{Q,1 \dots 2}$	W^2	Automatically calculated scaling factor for the calorimetric objective function (ΔQ). Used for the combined evaluation of calorimetric and infrared data. $S_{Q,1}$ is used for the first, $S_{Q,2}$ for the second and final combined evaluation
T	-	Transformation matrix
T_{Amb}	K	Ambient temperature. If used in the context of the new reaction calorimeter it is equal to $T_{Amb,3}$.
$T_{Amb,0}$	K	Ambient temperature before the start of a reaction.
$T_{Amb,1}$	K	Ambient temperature sensor number 1.
$T_{Amb,2}$	K	Ambient temperature sensor number 2.
$T_{Amb,3}$	K	Ambient temperature sensor number 3.
T_C	K	Temperature of the compensation heater wall.
T_{Cry}	K	Temperature of the cooling liquid provided by the cryostat (new reaction calorimeter).
T_{Dos}	K	Temperature of the dosed liquid.
t_f	s	Elapsed time until the end of the reaction.
t_i	s	i'th point in time
T_j	K	Jacket temperature. a) Equals the temperature of the cooling liquid in a conventional reaction calorimeter. b) Equals the mean value of $T_{j,2}$ to $T_{j,5}$ to describe the temperature of the copper block in the new reaction calorimeter.
$T_{j,0}$	K	Jacket temperature before the start of a reaction.
$T_{j,1} \dots T_{j,6}$	K	Different temperature sensors in the copper jacket.
$T_{T,1}, T_{T,2}$		
$T_{j,OUT}$	K	Temperature of the cooling liquid leaving the jacket of a conventional reaction calorimeter.
$T_{j,IN}$	K	Temperature of the cooling liquid entering the jacket of a conventional reaction calorimeter.
T_{PC}	K	Cold-side temperature of the Peltier elements.
T_{Pelt}^{down}	K	Temperature of the thermocouple used to measure T_{PH} .
T_{Pelt}^{up}	K	Temperature of the thermocouple used to measure T_{PC} .
T_{PH}	K	Hot-side temperature of the Peltier elements.
T_r	K	Reaction temperature
$T_{r,set}$	K	Set point of the reaction temperature controller (inner thermostat).
T_{ref}	K	Reference temperature.

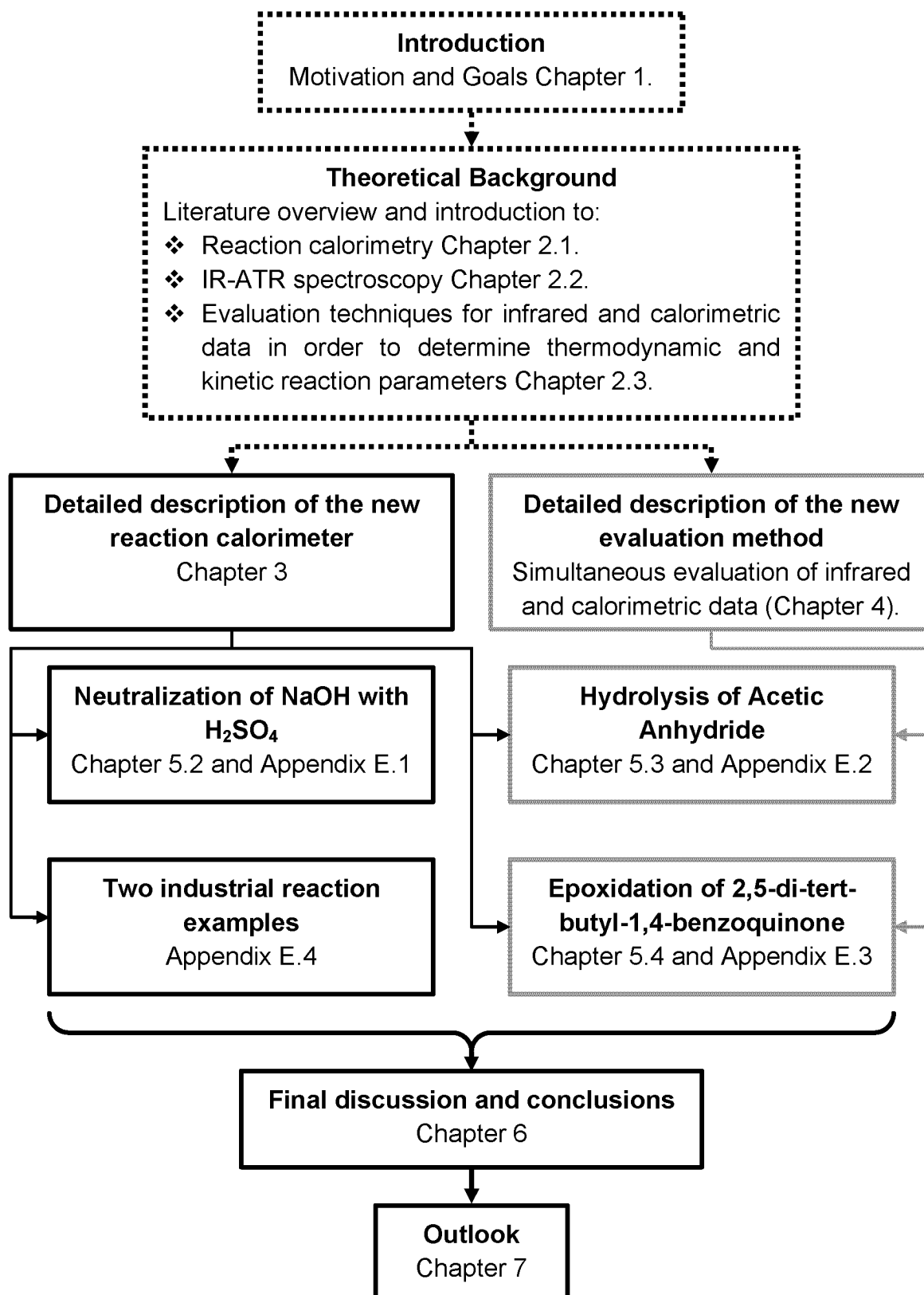
T_W	K	Temperature of the reactor wall
T_{WC}	K	Temperature of the cooler wall.
U	W/(m ² ·K)	Overall heat-transfer coefficient
u, u'		Output of a system
U_{Comp}	V	Voltage of the compensation heater
U_{Pelt}	V	Voltage of the Peltier elements
v_{dos}	l/s	Dosing rate
V_r	l	Volume of the reaction mixture.
W_{IR}	-	Weighting factor for infrared data.
W_Q	W ²	Weighting factor for calorimetric data.
$X_{thermal}$	-	Thermal conversion
y, y'		Input into a system

Operator	Example	Description
$\hat{}$	\hat{a}	Estimation of value a
$+$	A^+	Pseudo inverse of the Matrix A $A^+ = (A^T \times A)^{-1} \times A^T$
T	A^T	Transposed Matrix A
\times		Matrix multiplication
\cdot		Scalar multiplication
<i>correction</i>	<i>correction</i> ($q_{Cooling}$)	Time correction as described in chapter 3.7.2
$\ \cdot \ _2^2$	$\ A\ _2^2$	Sum of all squares of all matrix elements of A . Equal to the square of the second norm of matrix A .

Abbreviation	Description
Eval.	Evaluation
Cal. Eval.	Separate evaluation of the calorimetric data.
IR Eval.	Separate evaluation of the infrared data.
Comb. Eval.	Combined evaluation of the calorimetric and infrared data.
Classic Cal. Eval.	Classic separate evaluation of the calorimetric data by integration.
Classic IR Eval	Classic separate evaluation of the infrared data by single wave number (univariate) analysis.
ATR	Attenuated Total Reflection
DSC	Differential Scanning Calorimeter
IR	Infrared (4000 ... 600 cm ⁻¹)
SMCR	Self-Modeling Curve Resolution
PCA	Principal Component Analysis
ITTFA	Iterative Target Testing Factor Analysis
ALS	Alternating Least Squares
EFA	Evolving Factor Analysis
RFA	Resolving Factor Analysis

OVERVIEW

The following figure shows an overview on this work including references to the corresponding Chapters.



1 INTRODUCTION

1.1 Context and Motivation

1.1.1 *The Chemical reaction at the core of Integrated Process Development*

The context of this work is the integrated process development in the **fine chemical or pharmaceutical industry**. An integrated process development considers environmental, economic and safety aspects as objectives of process development.

From the entire chemical production process, this work will **focus on the optimization of the reaction step** only, which represents the core of the process. For this process step the chances of a “win-win” situation with respect to economic, environmental and safety objectives are high. Many measures focused on the improvement of either economic, ecological or safety aspects only, will automatically contribute to an improvement in the other two objectives. Thus improving the reaction step is an important task of an integrated process development and has a crucial effect on the overall performance of the production process. The following example shall illustrate the “win-win” situation in the context of reaction optimization:

One main task of process optimization aims at choosing operating conditions favoring the synthesis of the main product and minimizing unwanted by-products. A high yield or a high space-time yield does not only signify a higher economic profit from product sales but also means an efficient use of raw materials and energy (e.g. less energy required for subsequent separations) and less waste that has to be treated or deposited [Heinzle et. al. 98], [Koller et. al. 98], and [Jödicke et. al. 99]. The latter advantages signify an environmentally more friendly process and **improved eco-efficiency** [Heinzle et. al. 97], [Hungerbühler et. al. 98], and [Mak et. al. 97].

Process development and optimization in pharmaceutical and fine chemical industry starts when the target chemical structure and a possible synthesis path were found by chemical research. It will end when the production was successfully implemented in the pilot plant and the final production plant. **However the optimization of a process should start as early as possible during the development phase** in order to have a maximum of reaction and process parameters that can still be changed. Therefore this work will focus on the early phases of process development.

1.1.2 Bottleneck: Parameters for empirical reaction models

Many tasks of process development can only be carried out or are at least supported if a reaction model and the corresponding parameters are known. Such examples are reported by [Göhring et. al. 96], [Guntern et. al. 98], [Lundstrom et. al. 98], [Lehtonen et. al. 97], and [Dyer et. al. 02]. **However the reliability and usefulness of the calculated data strongly depends on the quality of the applied reaction parameters and the chosen reaction model.**

Of course most of the chemical reactions applied in fine chemical and pharmaceutical production are rather complex from a mechanistic point of view. However based on a common chemical knowledge it should be possible to guess an appropriate **empirical reaction model** for most of the reactions. Such an empirical reaction model has to fulfill the needs of the early process development and does not have to represent deeper insight of the reaction step. Thus an empirical reaction model will only describe the **most important main and side reactions with as little reaction parameters as possible**. This will minimize the effort needed to identify the unknown reaction parameters and increase the robustness of the model in the later application. Of course there will be cases where several empirical reaction models are equally likely, and thus further investigations are required in order to allow a reasonable **model selection**.

As mentioned all reaction models will contain unknown reaction parameters such as rate constants, activation energies, reaction orders, phase change rates, diffusion coefficients or reaction enthalpies. Unfortunately it is a fact that in fine chemical and pharmaceutical production for a large majority of reactions there is **hardly any knowledge about these kinetic and thermodynamic reaction parameters**. Although many different analytical techniques have been developed during the past decades and various mathematical evaluation algorithms exist to extract the desired information. Therefore the use of reaction model-based optimization tools is impeded and e.g. the identification of optimal and safe reaction conditions will be difficult [Guntern et. al. 98] and [Keller 98].

As there is a big lack of information, crucial for a successful and fast reaction optimization in early phases of process development, **this thesis contributes tools that will help to fill this gap of knowledge**. The actual situation is characterized by the following problems:

- ❖ As time-to-market is crucial for competitiveness most of the existing appropriate analytical techniques are impeded because they still **require too much time** (e.g. if calibration or sampling is required).
- ❖ Many analytical techniques that would be easy and fast to use **do not reveal the required information** or the reaction proceeds too fast.
- ❖ Not all of the desired reaction parameters can be measured directly but are the result of a complex evaluation of the basic measurement data. Such **evaluations are often time consuming** or require a sophisticated mathematical knowledge.
- ❖ Especially in early phases of process development there might be **insufficient amounts of the essential test compounds** available to carry out the required analytics.

Besides these technical lacks, addressed by this thesis, there are also some rather strategic obstacles:

- ❖ Process optimization remains a **second-class activity**, because short term tasks of high priority absorb most of the available management attention during the whole manufacturing process [*Regenass 97*].
- ❖ Looking at **economic benefits only** it is likely that the costs for optimizing and investigating the reaction might be considered to be larger than the benefits by an increased efficiency of the reaction.

These strategic obstacles might be the reason why the “win-win” situation for economic and environmental objectives in process optimization is not yet reached. New penalties on environmental pollution, the Kyoto protocol or an increase of the energy prices will favor an integrated process development. Consequently more time and money will be provided for an in-depth reaction characterization and optimization. However the technical lacks mentioned above will be addressed in this work as described in the following Chapter.

1.2 Goal of the Thesis

This thesis tackles the technical lacks mentioned before by improving and creating tools that **provide kinetic** (rate constants, activation coefficients, reaction orders ...) **and thermodynamic parameters** (reaction enthalpies ...) of a chemical reaction in early stages of process development. Therefore the goal of the thesis is to:

- ❖ Develop a **new small-scale reaction calorimeter (25 to 45 ml)** that allows an accurate measuring of the reaction power. In order to reduce the experiment time **neither calibrations of the heat-transfer coefficients nor the heat capacity** (see also Chapter 7.1.3) of the reactor content should be required. The new reactor must be combined with an IR-ATR probe that allows **simultaneous measurement of mid-infrared spectra**.
- ❖ Enlarge the application area of standard reaction calorimeters for **fast and strongly exothermal reactions**.
- ❖ Develop a new evaluation method that allows a **simultaneous evaluation of the two measured data sets (calorimetric and infrared data)** in order to identify the desired reaction parameters (kinetics and thermodynamics) in one single step. The evaluation method should be completely automatic. It should not require any further information, such as calibration data or pure component spectra, in order to allow a fast and easy application.
- ❖ Test the new calorimeter and the combined evaluation method with **industrial as well as standard reaction examples**.
- ❖ Show the benefits and limitations of the combination of calorimetric and infrared measurements.
- ❖ Verify whether a simultaneous evaluation of the two data sets (calorimetric and infrared data) can improve the identification of the desired reaction parameters compared to a separate evaluation.
- ❖ Develop a method that allows a systematic selection of the most likely reaction model if several possibilities are reasonable.

The focus of this thesis lies on reactions of the **fine chemical and pharmaceutical** production. The kinetic and thermodynamic parameters can then be used to investigate and optimize the chemical reaction step on the basis of an empirical reaction model.

1.3 Suitable analytical setups for kinetic and thermodynamic screening

The chemical system should be investigated in a test reactor that is as similar as possible to the final production reactor [Evans et al. 80]. For the fine chemical and pharmaceutical production, batch or semi-batch reactors are common. Thus a similar reactor should be used for the test experiments. For the task of early process optimization a reactor volume in the range of 50 ml is appropriate ([Harre et al. 01], [Harre et al. 99] and [Van Loo et al. 02]) as scale-up to industrial size is not completely unreasonable. In contrast to smaller scale automated screening reactors ([Harre et al. 99] and [Laird 01]), mixing, feed- and temperature programming, as well as the heat transfer from reactor to jacket can all be carried out in a manner which resembles the industrial conditions. However data gathered from such a reactor should always be verified in a bench- or pilot plant system.

The temperature controlling of the reactor content is another crucial point of the setup. As most chemical and physical changes taking place during a reaction step depend on the temperature, the evaluation of the measured data will be much easier if isothermal conditions are fulfilled [Karlsen et al. 87, a] and [Schlegel et al. 97]. As soon as the signals of the applied analytical sensors also depend on the temperature (e.g. spectroscopy), isothermal conditions are requisite.

A unique technique for the simultaneous determination of kinetic and thermodynamic parameters is calorimetry [LeBlond et al. 96]. Kinetic information emerges as rates of heat evolution or absorption, and thermodynamics as the integrated heats (enthalpies) of the chemical and physical processes taking place [Landau 96]. Numerous different calorimetric techniques are available, such as DSC (Differential Scanning Calorimetry), Micro Calorimetry, Bomb Calorimetry, Solution Calorimetry, ARC (Accelerating Rate Calorimetry) and Reaction Calorimetry. As in reaction calorimetry the system is investigated under conditions that are similar to the normal production reactor, it is the appropriate technique for the purpose of reaction optimization.

Reaction calorimetry was widely applied to investigate thermodynamic and kinetic parameters of chemical reactions [Regenass 83], [Becker 68], [Pastré 00], [Pastré et al. 01], [Sempere et al. 98], [Balland et al. 00], [Ubrich et al. 99], [LeBlond et al. 96], [Dyer et al. 02], and [Stappers et al. 02]. A theoretical and historical background of reaction calorimetry will be given in Chapter 2.1.

However [Hugo 93] discussed rules for the applicability of thermo-kinetic measurements and concluded that only for simple and homogeneous reactions meaningful results can be obtained from thermo-kinetic measurements alone. For more complex reactions additional information by the way of chemical analysis is

needed for the determination of reaction kinetics. Similar, [LeBlond *et. al.* 96] and [Stoessel 97] stated that the correspondence between chemical and thermal conversion must be verified by other analytical techniques. Particularly in the case of consecutive or parallel reaction mechanisms difficulties arise when the total reaction power has to be allocated to each reaction step [Regenass 83] and [Sbirrazzuoli *et. al.* 00].

It is therefore common to combine reaction calorimetry with other analytical techniques in order to make the results more reliable or to get additional information. However as the aim of this work is to provide a fast and easy to use tool, additional analytical techniques have to fulfill the following requirements:

- ❖ The technique should be online. Thus no samples have to be taken. Traditional methods for the determination of kinetics are based on concentration data given by various sampling techniques and chemical analysis. However these techniques show two main drawbacks: 1) Some species (e.g. mean products) may be very unstable and thus the sampling will be impeded. 2) The development of a reliable analytical method for some of the reactive species may take too much time.
- ❖ It should not be necessary to calibrate the system for each new reaction.
- ❖ The analytic sensor should not influence the calorimetric measurement and vice versa.

Analytical sensors that fulfill these requirements are listed below. They are separated into two groups: A) Sensors that can reveal information that is specific for the different chemical compounds in the reaction mixture and B) sensors that reveal overall information about the reaction mixture, similar to reaction calorimetry.

- A. IR – ATR (Infrared, Attenuated Total Reflectance), NIR (Near Infrared), UV-VIS (Ultraviolet – Visible) and Raman probes; Gas consumption / production measurement.
- B. Pressure-, pH sensor, turbidity and stirrer torque measurement.

For this work the IR-ATR technique was chosen because of its wide application range. For a detailed discussion of the IR-ATR technology see Chapter 2.2. Pressure and stirrer torque are also measured but were not included in the present evaluation.

The combination of calorimetry and infrared spectroscopy is a standard combination [am Ende et. al. 99], [Landau et. al. 95, a], [LeBlond et. al. 98], [Ubrich et. al. 99] and [Nomen et. al. 01]. The combination of these two techniques is interesting because not only the measured signals differ but also its source. These differences are explained in **Table 1-1**.

Table 1-1: Comparison of infrared spectroscopy and reaction calorimetry

	<i>IR Spectroscopy</i>	<i>Reaction Calorimetry</i>
Source of the measured signal	All absorbing components of the reaction mixture. Integral kinetic signal proportional to the component concentrations.	Physical or chemical processes that deliver or consume heat. Examples are chemical reactions , mixing of different fluids or phase changes. Differential kinetic signal proportional to the reaction rates.
Primary measured signal	Absorption of infrared light by excitation of molecular vibrations	Temperature of the reaction mixture.
Secondary measured signals	none	Electrical power consumption, Mass flows .
Physical value used for the identification of reaction parameters	Equal to the measured signal	Energy required by the calorimetric system to control the reaction temperature at a certain level.
Physical property that relates the evaluated signal to a chemical reaction model	Pure spectra of the components in mixture.	Reaction enthalpies , heat of mixing or heat of phase change.

Table 1-1 shows that the information delivered by the two techniques might be complementary in many cases. For example it becomes clear that reaction calorimetry detects many more effects than just the chemical reaction [Becker 68]. As these effects (e.g. heat of mixing) are not detected by the infrared signal, they can be identified.

A further advantage of a combination of these two analytical techniques is that eventual non idealities of both measurement techniques like baseline drifts or deviations from Lambert Beer's law (see Chapter 2.2) can be detected.

2 THEORETICAL BACKGROUND

2.1 Reaction calorimetry

As discussed in the previous Chapter, reaction calorimetry is a suitable tool for the purpose of kinetic and thermodynamic screening in early stages of process development. A review on the principles and the development of different types of reaction calorimeters is presented by [Becker 68], [Karlsen et. al. 87, a], [Landau 96] and [Regenass 97]. A comprehensive overview on different calorimetric principles and their application in research and commercial devices is given by [Pastré 00]. A rather general overview about calorimetry is given by [Hemmingner et. al. 84].

In the following section the most important aspects and problems of reaction calorimetry will be discussed. As mentioned before, reaction calorimetry only focuses on calorimetric devices that resemble the later production-scale reactors of the corresponding industrial processes. In addition to substance specific data (e.g. heat capacity and enthalpy of reaction) they should also indicate equipment specific data (e.g. effects of stirring or heat transfer) that might be useful hints in the context of scale-up. Therefore this Chapter will not discuss thermal analysis devices such as DSC (Differential Scanning Calorimeter) or other micro calorimetric devices that differ significantly from the production-scale reactor.

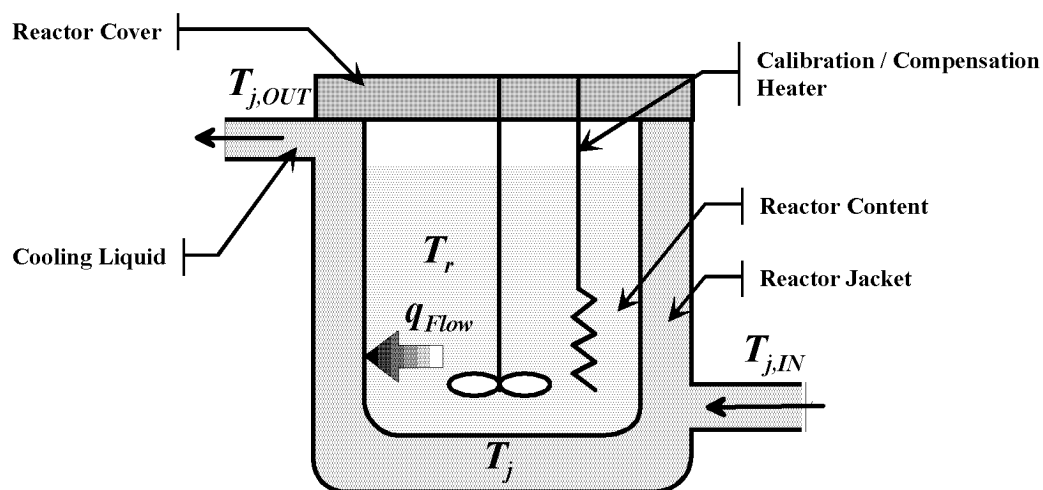


Figure 2-1: Standard setup of a reaction calorimeter.

Most of the existing reaction calorimeters consist of a reaction vessel and a surrounding jacket with a circulating fluid that transports the heat away from the reactor (see **Figure 2-1**). Such devices can be classified according to their measurement and control principles into three categories (of course many other classifications would be possible): 1) Heat-Flow, 2) Power-Compensation, and 3) Heat-Balance reaction calorimeters. They will be shortly described in the following subchapter.

2.1.1 Overview on the basic reaction calorimeter types

Heat-Flow reaction calorimeter

The temperature of the reactor content (T_r) is controlled by varying the temperature of the cooling liquid (T_j). The heat flow from the reactor content through the wall into the cooling liquid (q_{Flow}) is determined by measuring the difference between reactor-content and cooling-liquid temperature. In order to convert this temperature signal into a heat-flow signal (units watt), a heat-transfer coefficient has to be determined using a calibration heater. To allow a fast control of the T_r , the flow rate of the cooling liquid through the jacket should be high. The Heat-Flow principle was developed by Regenass and co-workers ([Regenass 76] and [Martin 75]). Most of the commercially used reaction calorimeters are based on the Heat-Flow principle, such as the RC1 from [Mettler Toledo] (based on the work of Regenass, [Riesen et. al. 85]), the SysCalo's from [Systag] and the Simular from [HEL] ([Singh 97]). A detailed calculation of the complete heat-flow balance is given in Chapter 2.1.3.2.

Power-Compensation reaction calorimeter

The temperature of the reactor content (T_r) is controlled by varying the power of a compensation heater inserted directly into the reactor content. As with an electrical heater cooling is not possible, the compensation heater always maintains a constant temperature difference between the reactor jacket and the reactor content. Thus "cooling" is achieved by reducing the power of the compensation heater. The heat flow from the reactor content through the wall into the cooling liquid is typically not determined because the reaction power is directly visible in the power consumption of the compensation heater. The temperature of the cooling liquid (T_j) is controlled at a constant temperature by an external cryostat. The Power-Compensation principle was first implemented by Andersen ([Andersen 66] and [Andersen 69]) and was further developed by [Köhler et. al. 72], [Hentschel 79] and [Schildknecht 81]. [Pollard 01] and [Pastré et. al. 01] reported a small scale Power-Compensation calorimeter. A commercial Power-Compensation calorimeter is the AutoMate [Simms et. al. 00] and the Simular (combined with Heat Flow [Singh 97]) from [HEL]. A detailed calculation of the complete heat-flow balance is given in Chapter 2.1.3.3.

Heat-Balance reaction calorimeter

The temperature of the reactor content (T_r) is controlled by varying the temperature of the cooling liquid (T_j). The heat flow from the reactor content through the wall into the cooling liquid (q_{Flow}) is determined by measuring the difference between jacket inlet ($T_{j,IN}$) and outlet temperature ($T_{j,OUT}$) and the mass flow of the cooling liquid. Together with the heat capacity of the cooling liquid the heat-flow signal is directly determined without calibration. The Heat-Balance principle was first implemented by [Meeks 68]. Commercial versions are the RM200 from [Chemisens], SysCalo 2000 Series from [Systag] and the ZM-1 from [Zeton Altamira] (developed in collaboration with Moritz and co-workers [Pauer et. al. 99]). A detailed calculation of the complete heat-flow balance is given in Chapter 2.1.3.4.

Combinations and further developments

Many more reaction calorimeters were developed during the past years (Peltier, isoperibol, differential ... calorimeters). Some of them are based on the three basic principles mentioned above or combine several of them into one device. They are described in the Appendix A.1.

A complete redesign of the Power-Compensation technique using Peltier elements and a copper jacket as an intermediate thermostat will be presented in this work (see Chapter 3).

2.1.2 Isothermal, isoperibolic, adiabatic and temperature programmed operation mode

Calorimetric applications can also be distinguished by their way of controlling the reaction temperature. As shown in **Table 2-1** not all of three measurement principles described above are suitable for the different control modes. As mentioned in Table 2-1 the isothermal operation mode is supposed to be the easiest in application because no heat accumulation by the reactor contents has to be considered. Thus no heat capacities as a function of T_r of the reaction mixture as well as of the reactor inserts (e.g. stirrer, sensors, baffles ...) are required. However in reality due to the non idealities of the control circuits of the calorimeters and the principles of heat flow, the reaction temperature cannot be controlled strictly isothermal (see Chapter 2.1.4). If the deviations are significant, heat accumulation terms have to be considered despite the "isothermal" operation mode (see Chapters 3.2.1, 6.1.1, and 7.1.3). As mentioned in Chapters 1.3 and 2.2 isothermal conditions are preferred for the application within this work and therefore the future discussions will focus on this operation mode.

Table 2-1: Different ways of controlling the reaction temperature T_r in a reaction calorimeter.

¹⁾ No applications found in literature.

	T_r	T_j	<i>Special requirements</i>
Isothermal	Controlled at a constant level	<i>Heat Balance and Heat Flow:</i> T_j is varied to control T_r <i>Power Compensation:</i> T_j is controlled at a constant level, lower than T_r	-
Isoperibolic	Uncontrolled	<i>Heat Balance and Heat Flow</i> Controlled at a constant level	The heat capacity of the reaction mixture, inserts and part of the reaction wall must be known as a function of T_r .
Temperature Programmed	Controlled to follow a certain temperature program	<i>Heat Balance and Heat Flow:</i> T_j is varied to control T_r <i>Power Compensation ¹⁾:</i> T_j is controlled to follow the same temperature program as T_r but at a constant lower level.	The heat capacity of the reaction mixture, inserts and part of the reaction wall must be known as a function of T_r .
Adiabatic	Only measured	<i>Heat Balance ¹⁾ and Heat Flow:</i> T_j is controlled to avoid heat losses (close to T_r).	The heat capacity of the reaction mixture, inserts and part of the reaction wall must be known as a function of T_r .

2.1.3 Steady-state heat-flow balance of the different calorimeter types

The only heat flow considered so far is the heat flow through the reactor jacket (Figure 2-1, q_{Flow}). For the case of an isothermal reaction run the main heat flows that have to be considered in a reaction calorimeter are shown in **Figure 2-2**.

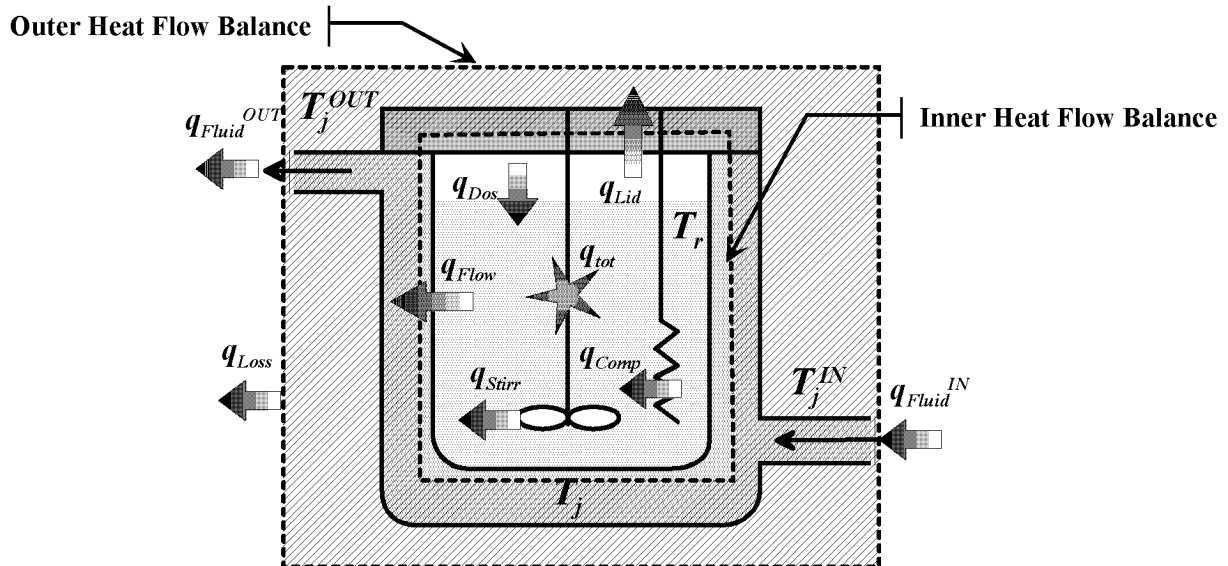


Figure 2-2: Main heat flows that have to be considered in a reaction calorimeter running at isothermal conditions.

For the following discussions ideal isothermal controlling of the reaction temperature T_r will be assumed. Therefore in Figure 2-2 no heat accumulation terms of the reaction mixture and the reactor inserts are shown. However this assumption does not hold for all applications and apparatuses. In Chapter 2.1.4 a short discussion on non ideal behavior is given.

The task of the calorimeter is to determine the total heat production / consumption during a chemical reaction q_{tot} [W]. Generally any kind of physical process in which heat is released or absorbed is measured. Therefore the heat flow q_{tot} can be expressed as follows:

$$q_{tot} = q_{React} + q_{Mix} + q_{Phase} \quad (2-1)$$

Where q_{React} is the reaction power [W], q_{mix} the heat flow occurring due to non ideal mixing of different fluids and q_{Phase} the heat flow due to phase change processes [W]. For a simple one-step reaction at constant pressure the reaction power can be further expressed as follows:

$$q_{React} = -\Delta_r H \cdot V_r \cdot r \quad (2-2)$$

Where $\Delta_r H$ is the reaction enthalpy [J/mol], V_r the volume of the reaction mixture [l] and r the reaction rate [mol/(l·s)].

The heat evolved by the stirrer q_{Stirr} [W] can be described by [Zogg 93]

$$q_{Stirr} = Ne \cdot \rho_r \cdot n_s^3 \cdot d_R^5 \quad (2-3)$$

Where Ne is the Newton number [-], ρ_r the density of the reaction mixture [kg/m³], n_s the revolutions per second of the stirrer [s⁻¹] and d_R the diameter of the stirrer [m].

The heat flow caused by the dosing of reactants q_{Dos} [W] can be expressed as:

$$q_{Dos} = f \cdot c_{p,Dos} \cdot (T_{Dos} - T_r) \quad (2-4)$$

where f is the feed rate [mol/s], $c_{p,Dos}$ is the specific heat capacity of the dosed liquid [J/(mol·K)] and T_{Dos} [K] is the temperature of the dosed liquid.

The crucial heat flow q_{Flow} shown in Figure 2-2 will be explained in details in the following Chapter. All other heat flows shown in Figure 2-2 are discussed in Chapters 2.1.3.2, 2.1.3.3, 2.1.3.4 as their calculation and inclusion in the heat-flow balances depend on the reaction calorimetric principle applied.

2.1.3.1 Heat flow through a plane reactor wall

Before looking at the individual heat-flow balances of the different reaction calorimeters, the heat flow through the reaction wall into the reactor jacket q_{Flow} (see Figure 2-2) shall be discussed [Zogg 83] and [VDI Wärmeatlas]. **Figure 2-3** shows the steady-state temperature profile when heat flows from the reactor content through the reactor wall into the cooling liquid. Generally the temperature of the reactor content T_r and the cooling liquid T_j are assumed to be homogeneous except to a small film layer close to the reactor wall (without convection). Thus the heat transfer can be separated into three different steps: 1) The reactor-side heat transfer, described by the heat-transfer coefficient h_r [W/(m²·K)]. 2) The heat conduction through the reactor wall, described by the thickness of the wall L and the heat conduction coefficient λ_w [W/(m·K)]. And 3) the jacket-side heat transfer, described by the heat-transfer coefficient h_j [W/(m²·K)]. The heat flow $q_{Flow,r}$ on the reactor side (Figure 2-3) can be expressed as follows:

$$q_{Flow,r}(t) = A \cdot \lambda_w \cdot \left. \frac{\partial T_w}{\partial l} \right|_L = A \cdot h_r \cdot (T_r(t) - T_w(L,t)) \quad (2-5)$$

Where A is the total heat-transfer area [m²], l the position inside the wall, and T_w the temperature of the reactor wall. The heat flow $q_{Flow,j}$ on the jacket side (Figure 2-3) can be expressed as follows:

$$q_{Flow,j}(t) = A \cdot \lambda_w \cdot \left. \frac{\partial T_w}{\partial l} \right|_0 = -A \cdot h_j \cdot (T_j(t) - T_w(0,t)) \quad (2-6)$$

Steady-state heat-flow approximation

At steady state, when the temperature profile and all the heat flows do not change in time the heat flow entering the reactor wall must be equal to the heat flow leaving the wall and no heat accumulation takes place inside the wall. The steady-state heat flow q_{Flow} can therefore be expressed as follows:

$$q_{Flow} = q_{Flow,r} = q_{Flow,j} \quad (2-7)$$

At steady-state conditions the temperature profile inside the reactor wall is linear because only heat conduction is taking place (shown in Figure 2-3). Therefore the following two conditions are further fulfilled:

$$\left. \frac{\partial T_W}{\partial l} \right|_0 = \left. \frac{\partial T_W}{\partial l} \right|_L = const \quad and \quad \left. \frac{\partial T_W}{\partial l} \right|_0 \cdot L = T_W(L) - T_W(0) \quad (2-8)$$

By combining Equations (2-5) to (2-8) the following expression for the steady-state heat flow through the reactor wall is obtained:

$$q_{Flow} = U \cdot A \cdot (T_r - T_j) \quad (2-9)$$

where U is the overall heat-transfer coefficient [$W/(m^2 \cdot K)$]. It consists of the three main heat-transfer resistances defined before:

$$\frac{1}{U} = \frac{1}{h_r} + \frac{L}{\lambda_w} + \frac{1}{h_j} \quad (2-10)$$

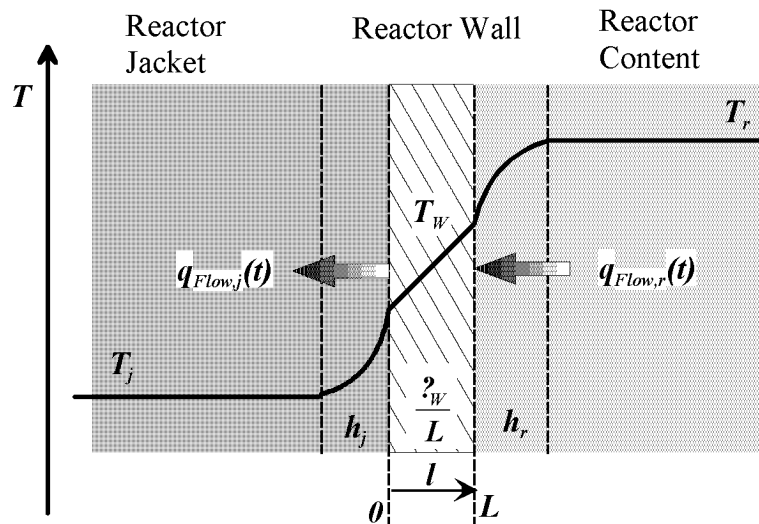


Figure 2-3: Steady-state temperature profile ($q_{Flow,j} = q_{Flow,r}$) when heat flows from the reactor content ($T = T_r$) through the reactor wall ($T = T_w(l)$) into the cooling liquid of the jacket ($T = T_j$).

The two steady-state heat-transfer coefficients h_r and h_j [$W/(m^2 \cdot K)$] could be further described by physical properties of the system. For the reactor-side heat-transfer coefficient h_r the following Equation could be used, that was established for stirred tank reactors (valid as long as the Reynolds number is in the range of $10^2 \dots 4 \cdot 10^5$ and the Prandtl number in the range of $2 \dots 2 \cdot 10^3$) [VDI Wärmeatlas, Equation Ma 4]:

$$h_r = \frac{\lambda_r}{d_R} \cdot C \cdot \left(\frac{n_S \cdot d_R^2 \cdot \rho_r}{\eta_r} \right)^{2/3} \cdot \left(\frac{\eta_r \cdot c_{p,r}}{\lambda_r} \right)^{1/3} \cdot \left(\frac{\eta_r}{\eta_r(L)} \right)^{0.14} \quad (2-11)$$

Where C is a geometric factor (see [VDI *Wärmeatlas*] section Ma for further details) [-], λ_r the thermal conductivity coefficient of the reaction mixture [W/(m·K)], d_R the diameter of the stirrer [m], n_S the revolutions per second of the stirrer [s⁻¹], ρ_r the density of the reaction mixture, η_r the dynamic viscosity of the reaction mixture ($\eta_r(L)$ denotes the dynamic viscosity of the mixture on the reactor wall) and $c_{p,r}$ the heat capacity of the reaction mixture [J/(kg·K)]. According to Equation (2-11) the overall heat-transfer coefficient U in Equation (2-9) is strongly dependent on the physical properties of the investigated chemical reaction mixture.

An analogous equation for the reactor jacket can only be given when the geometric design is known. However most of the reaction calorimeters consist of a double wall jacket similar to the one shown in Figure 2-1. For such a jacket design no adequate heat transport models could be found in literature. Similar to h_r , h_j depends on the main physical properties of the cooling liquid. It should be considered that they can change as a function of T_j .

Thus U generally varies during the measurement of a chemical reaction because of mainly two reasons:

1. h_r varies because the physical properties of the reaction mixture change during a reaction (e.g. viscosity increase during a polymerization reaction).
2. Depending on the calorimetric system chosen, h_j may vary because the jacket temperature T_j varies during the measurement of a reaction and consequently the physical properties of the cooling liquid that determine h_j .

Not only U but the total heat-transfer area A in Equation (2-9) can also change during a reaction measurement because of dosing, density or vortex changes.

When Equation (2-9) is applied to calculate calorimetric signals, the temperature of the cooling liquid T_j should be further analyzed. Depending on the geometry of the jacket and the heat-flow rate of the cooling liquid, its temperature may vary over the reaction jacket due to heat absorbed or released from the reactor. Therefore a corrected jacket temperature should be used in Equation (2-9).

Dynamic heat flow

As mentioned Equation (2-9) is only valid at steady-state conditions, when the heat flow through the reactor wall is constant. However if a reaction is taking place, the heat flow through the reactor wall might vary depending on the calorimetric principle applied (see also Chapter 2.1.5). It is therefore important to look at the dynamic heat transfer through the reactor wall.

In a dynamic heat transport situation, the temperature profile shown in Figure 2-3 will change with time. Therefore heat accumulation occurs inside the reactor wall as well as the reactor and jacket-side film layer and thus the first law of thermodynamics has to be solved as a partial differential equation of time and position (see e.g. [VDI Wärmeatlas], [Hemminger et. al. 84]).

This task is relatively easy for the reactor wall because only heat conduction is taking place (Fourier equation for heat conduction). Therefore Equations (2-5) and (2-6) are correctly describing the heat flow on the surfaces of the reactor wall as long as the thermal conductivity λ_w does not depend on temperature. The solution of the resulting partial differential equation is not the scope of this work, a possible approach (neglecting the curvature of the reactor wall) is given by Karlsen [Karlsen et. al. 87, b]. [Zaldivar et. al. 96] describes a more accurate wall model including the shape of the reactor.

The heat transfer inside the cooling liquid and the reaction mixture is more complex because heat conduction as well as heat transport by convection are taking place. As Figure 2-3 indicates, the temperature profile in the jacket- and reactor-side films are therefore no more linear even at steady state and computational fluid dynamics would have to be used in order to describe the dynamic temperature profile inside the two fluids. The situation gets even more complex as the heat-transfer coefficients h_r and h_j in Equations (2-5) and (2-6) are also depending on physical properties of the fluids that might significantly change as a function of temperature (see Equation (2-11)).

No literature reference could be found that exactly describes the dynamic heat transfer from the reactor content through the reactor wall into the cooling liquid. [Karlsen et. al. 87, b] calculated the dynamic heat transfer but neglected changes of h_r and h_j as well as heat accumulation inside the films on the reactor wall.

Generally the dynamic heat flow is completely neglected and the steady-state Equation (2-9) is also used to calculate a time-varying calorimetric signal. The subject of the dynamic heat transfer will be further discussed in the context of the overall dynamic behavior of the calorimeters in Chapter 2.1.4.

2.1.3.2 Steady-state isothermal heat-flow balance of a Heat-Flow reaction calorimeter

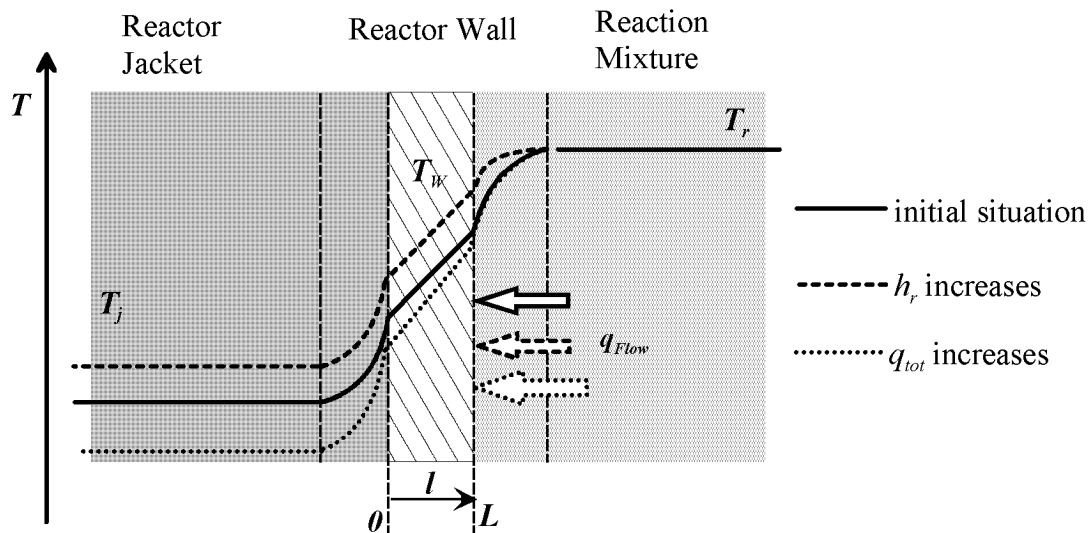


Figure 2-4: Steady-state temperature profile in a Heat-Flow reaction calorimeter when heat flows from the reactor content ($T = T_r$) through the reactor wall ($T = T_W(l)$) into the jacket ($T = T_j$). The reactor temperature is controlled at isothermal conditions by varying T_j .

Figure 2-4 shows the steady-state temperature profile through the reactor wall at different operating conditions. The straight black line represents the initial situation assuming e.g. $h_r = h_j = \lambda_W / L$, constant q_{tot} (Equation (2-1)) and therefore constant heat flow (q_{Flow} see also Chapter 2.1.3.1) through the reactor wall. There are basically two different events that will cause a change of this situation:

- 1) A change of the reactor-side heat transfer, e.g. **an increasing h_r** . Therefore the overall heat-transfer coefficient U (Equation (2-10)) will increase. The resulting temperature profile is shown by the dashed line. As q_{tot} does not change, q_{Flow} is not allowed to change as well because T_r is controlled at isothermal conditions. Therefore the temperature profiles inside the cooling liquid and the reactor wall will only be shifted to another level but do not change their shape (Assuming that h_j and λ_W are independent of temperature). However as h_r is increased the temperature difference $T_r - T_W(L)$ has to decrease in order to keep q_{Flow} constant. Thus the jacket temperature T_j will have to be increased by the controller in order to keep T_r constant.
- 2) A change of the total heat production / consumption q_{tot} , e.g. **an increasing q_{tot}** . The resulting temperature profile is shown by the dotted line. As q_{tot} increases, also q_{Flow} has to increase because T_r is controlled at isothermal conditions. Assuming that h_r , h_j and λ_W are independent of the temperature, they remain constant and thus the jacket temperature T_j has to be lowered by the controller in order to keep T_r constant.

2 Theoretical Background

According to Figure 2-4 the reactor wall as well as the cooling liquid are the main dynamic elements in a Heat Flow reaction calorimeter as their temperatures change during a reaction measurement. The temperature of the cooling liquid T_j was assumed to be homogeneous over the whole reactor jacket except the jacket side film layer. This assumption is reasonable as long as the flow of the cooling liquid is fully turbulent. If T_j is not homogeneous, the measured jacket temperature has to be replaced by a mathematically modified jacket temperature ([RC1 Handbook], [Landau 96]).

Only the inner heat-flow balance shown in Figure 2-2 ($q_{Comp} = 0$ W) has to be considered for reaction calorimeters based on the Heat-Flow principle. The bound of the steady-state heat-flow balance is the outer reactor wall ($l=0$) including the jacketed side film layer described by h_j . The steady-state isothermal heat-flow balance can thus be expressed as follows:

$$q_{Stirr} + q_{Dos} + q_{tot} = q_{Flow} + q_{Lid} \quad (2-12)$$

Where q_{tot} [W] is the total heat release or uptake of the reaction mixture (Equation (2-1)). The heat flows q_{Dos} and q_{Stirr} were already explained in Equations (2-4) and (2-3).

The heat flow through the reactor wall q_{Flow} [W] is generally calculated according to the steady-state Equation (2-9) though the heat flow through the reactor wall is clearly dynamic. This could lead to errors if q_{tot} , calculated by Equation (2-12), is used to get kinetic informations (see discussion in Chapter 2.1.5).

However the overall heat-transfer coefficient U and the heat-transfer area A in Equation (2-9) are usually unknown and can change during the course of a reaction (see Chapter 2.1.3.1). Conventionally these two parameters have to be calibrated by means of a calibration heater (see Figure 2-1) before and after a reaction experiment. Such a calibration is not possible during the reaction as q_{tot} has to be zero. Therefore a change of U or A caused by the chemical reaction will cause an error in the measured q_{tot} .

The remaining heat flow in Equation (2-12) is q_{Lid} the heat losses through the reactor lid. It is strongly dependent on the convection conditions inside the reactor and on the temperature of the reactor lid. E.g. q_{Lid} could be expressed as follows:

$$q_{Lid} = k_{Lid} \cdot (T_r - T_{Amb}) \quad (2-13)$$

Where k_{Lid} is an empiric proportional coefficient [W/K] depending on the reaction conditions and T_{Amb} is the ambient temperature [K].

2.1.3.3 Steady-state isothermal heat-flow balance of a Power-Compensation reaction calorimeter

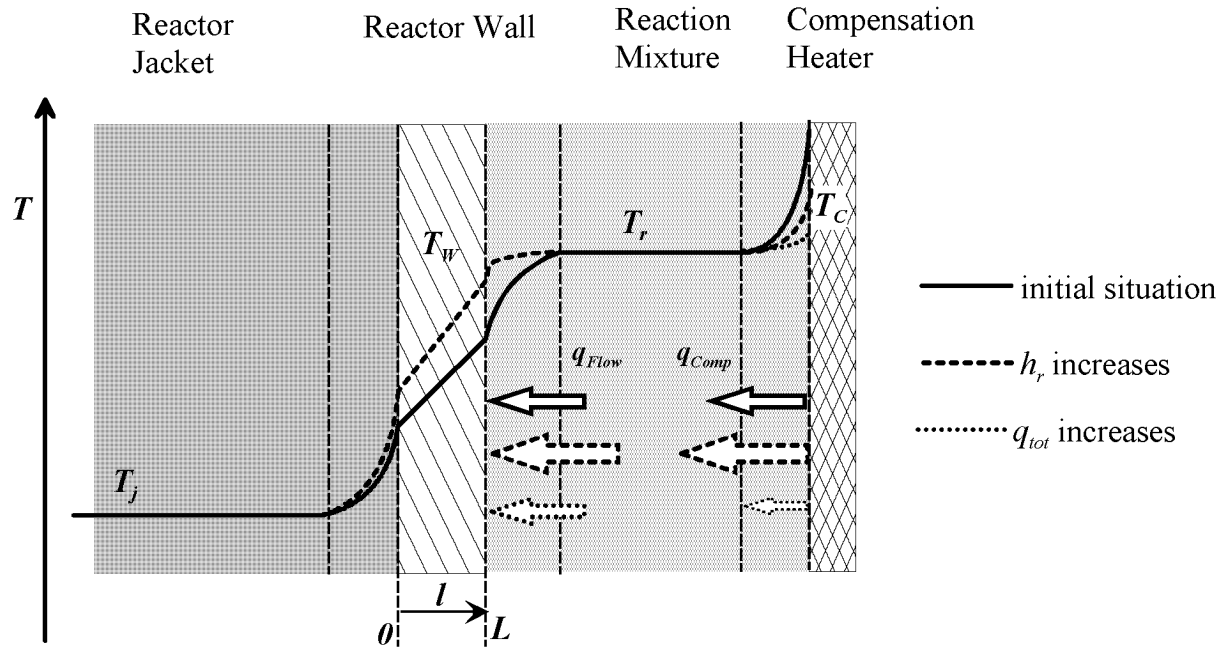


Figure 2-5: Steady-state temperature profile in a Power-Compensation calorimeter when heat flows from the compensation heater ($T = T_c$) into the reactor ($T = T_r$) and from the reactor through the reactor wall ($T = T_w(l)$) into the jacket ($T = T_j$, controlled isothermally by an external cryostat). The reactor temperature is controlled at isothermal conditions by varying the power of the compensation heater (q_{Comp}).

Figure 2-5 shows the steady-state temperature profile from the compensation heater through the reactor content and wall into the cooling liquid at different operating conditions. The straight black line represents the initial situation assuming e.g. $h_r = h_j = \lambda_w / L$, no heat release or uptake ($q_{tot} = 0$, Equation (2-1)) and therefore constant heat flow through the reactor wall (q_{Flow} see also Chapter 2.1.3.1) and constant power of the compensation heater q_{Comp} . There are basically two different events that will cause a change of this situation:

2 Theoretical Background

- 1) A change of the reactor-side heat transfer, e.g. an **increasing** h_r . The resulting temperature profile is shown by the dashed line. The heat flow q_{tot} does not change and h_j as well as λ_W are assumed to be independent of the temperature. Therefore the overall heat-transfer coefficient U (Equation (2-10)) will increase and as T_r and T_j are controlled at isothermal conditions q_{Flow} will increase (Equation (2-9)). The temperature difference $T_r - T_W(L)$ has to decrease. An increased q_{Flow} is compensated by an increased q_{Comp} released by the compensation heater. Assuming identical heat-transfer conditions on the heater wall as on the reactor wall, the heat-transfer coefficient on the heater wall will increase as well. Thus the temperature of the compensation heater (T_C) might decrease, as indicated in Figure 2-5 however this depends on the situation. It is also very likely that the heat-transfer coefficient on the heater wall is larger than h_r on the reactor wall if the compensation heater is placed close to the stirrer.
- 2) A change of the heat release or uptake, e.g. an **increasing** q_{tot} . The resulting temperature profile is shown by the dotted line. In order to keep T_r constant the power released by the compensation heater (q_{Comp}) is decreased. h_r , h_j and λ_W do not change and T_j as well as T_r . Therefore q_{Flow} and the temperature profile through the reactor wall will remain constant. As q_{Comp} is decreased and the heat transfer on the heater wall does not change, T_C will decrease.

According to Figure 2-5 the compensation heater is the main dynamic of a Power Compensation reaction calorimeter as its temperature changes during a reaction measurement. The reactor wall has to be considered as a secondary dynamic element if q_{Flow} changes during a reaction. Similar to the Heat-Flow principle only the inner heat-flow balance shown in Figure 2-2 has to be considered for this type of calorimeter. The bound of the steady-state heat-flow balance is the inner reactor wall ($l=L$). The steady-state isothermal heat-flow balance can thus be expressed as follows:

$$q_{Stirr} + q_{Dos} + q_{tot} + q_{Comp} = q_{Flow} + q_{Lid} \quad (2-14)$$

Where q_{tot} [W] is the total heat release or uptake of the reaction mixture (Equation (2-1)). The heat flows q_{Dos} and q_{Stirr} were already explained in Equations (2-4) and (2-3), q_{Lid} is explained in Equation (2-13) and the same comments are valid as for the Heat Flow calorimeters (see Chapter 2.1.3.2).

The heat flow through the reactor wall q_{Flow} [W] does not have to be calculated explicitly because the compensation heater can be compared to a permanent calibration heater to determine q_{Flow} . However it should be noted that the overall heat-transfer coefficient U or the heat-transfer area A (see Equation (2-9)) generally change during the course of a reaction (see Chapter 2.1.3.1). This will cause an error in the measured q_{tot} . The dynamics of the heat transfer through the reactor wall is

generally neglected but will lead to an additional error in the measured q_{tot} especially if it is used to calculate kinetic informations.

The only new term in Equation (2-14) is the power of the compensation heater q_{Comp} :

$$q_{Comp} = U_{Comp} \cdot I_{Comp} \quad (2-15)$$

Where U_{Comp} is the voltage [V] and I_{Comp} the current [A] of the compensation heater. As the heat released by the compensation heater is directly measured in terms of electrical power, the temperature of the compensation heater (T_C) does not have to be known. Therefore changes of the heat-transfer coefficient on the compensation heater do not affect the steady-state heat-flow balance. But as shown above, in this case the heat transfer from the compensation heater to the reaction liquid will be dynamic. This could lead to errors if the measured q_{tot} will be used to get kinetic informations (see discussion in Chapters 2.1.4 and 2.1.5).

2.1.3.4 Steady-state isothermal heat-flow balance of a Heat-Balance reaction calorimeter

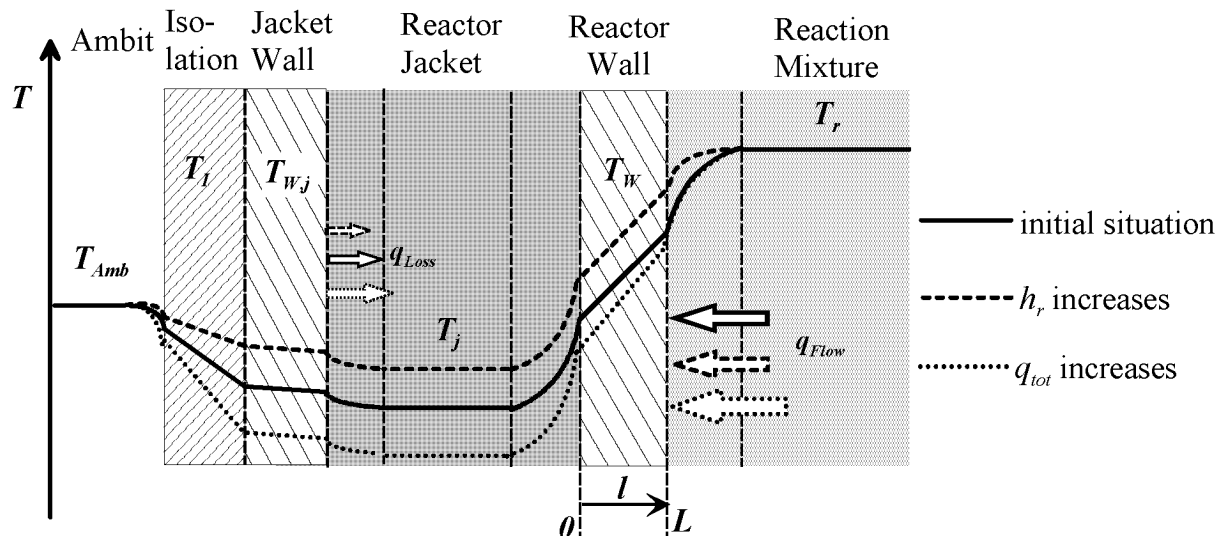


Figure 2-6: Steady-state temperature profile in Heat-Balance calorimeter when heat flows (q_{Flow}) from the reactor content ($T = T_r$) through the reactor wall ($T = T_W(l)$) into the jacket ($T = T_j$). The reactor temperature is controlled at isothermal conditions by varying T_j . An additional heat flow (q_{Loss}) from the ambient through the thermal insulation ($T = T_I$) and the jacket wall ($T = T_{W,j}$) into the cooling liquid is shown.

Figure 2-6 shows the steady-state temperature profile through the reactor wall as well as the jacket wall at different operating conditions. The straight black line represents the initial situation assuming e.g. $h_r = h_j = \lambda_W / L$, constant reaction heat release or uptake q_{tot} (Equation (2-1)) and therefore constant heat flow through the reactor wall (q_{Flow} , see Chapter 2.1.3.1). The temperature profiles shown in Figure 2-6 are identical to the temperature profiles shown in Figure 2-4 (Heat-Flow calorimeter Chapter 2.1.3.2). Additionally the ambient as well as the jacket wall temperatures

2 Theoretical Background

were considered. Therefore the comments to Figure 2-4 are also valid for the Heat-Balance calorimeter. The heat flow caused by the temperature difference between the cooling liquid T_j and the T_{Amb} is slightly changing for the three different situations shown in. The amount of this change depends strongly on the quality of the thermal insulation around the jacket wall.

According to Figure 2-6 the reactor wall, the jacket wall as well as the cooling liquid are the main dynamic elements, as they change their temperatures during a reaction measurement. The temperature of the cooling liquid T_j cannot be assumed to be homogeneous over the whole jacket as the flow rate of the cooling liquid has to be chosen low enough in order to be able to measure a temperature difference between inlet $T_{j,IN}$ and outlet temperature $T_{j,OUT}$ of the cooling liquid (see Figure 2-1). Therefore the temperature of the cooling liquid T_j , used in the following calculations, should be corrected on the basis of $T_{j,IN}$ and $T_{j,OUT}$ (e.g. [Landau 96], [RC1 Handbook]).

For the Heat-Flow as well as the Power-Compensation calorimeter only the inner heat-flow balance in Figure 2-2 was considered. For the Heat-Balance calorimeter ($q_{Comp} = 0$ W) both, the inner and the outer heat-flow balance, have to be taken into account. It should be noted that the outer heat-flow balance indicated in Figure 2-2 also contains the reactor cover. Depending on the calorimetric system the situation can differ from this ideal picture and thus part of the heat losses through the reactor cover will not be assessed by the outer heat-flow balance. However for the simplification ideal behavior is assumed and therefore the outer steady-state isothermal heat-flow balance can be expressed as follows ($q_{Comp} = 0$ W):

$$q_{Flow} + q_{Lid} + q_{Fluid,IN} = q_{Loss} + q_{Fluid,OUT} \quad (2-16)$$

Equation (2-12) and (2-16) can be combined to the final heat-flow balance of a Heat-Balance calorimeter:

$$q_{Stirr} + q_{Dos} + q_{tot} = q_{Loss} + q_{Fluid,OUT} - q_{Fluid,IN} \quad (2-17)$$

Where q_{tot} [W] is the total heat release or uptake of the reaction mixture (Equation (2-1)). The heat flows q_{Dos} and q_{Stirr} were already explained in Equations (2-4) and (2-3).

It is important to note that the problematic term q_{Flow} present in the heat-flow balances of the Power-Compensation and the Heat-Flow calorimeters (Equations (2-14) and (2-12)) could be eliminated by the outer heat-flow balance. But as shown above, the heat transfer through the reactor wall as well as the temperature of the jacket wall are clearly dynamic. This could lead to errors if q_{tot} , calculated by Equation (2-17), is used to get kinetic informations (see discussion in Chapter 2.1.4).

In Equation (2-17) a new heat loss term, q_{Loss} , is introduced. It describes all heat losses from the outer reactor wall to the environment. Similar to Equation (2-13) a general equation can be chosen to describe q_{Loss} :

$$q_{Loss} = k_{Loss} \cdot (T_j - T_{Amb}) \quad (2-18)$$

Where k_{Loss} is an empiric proportional coefficient [W/K] and T_{Amb} the ambient temperature [K]. In contrast to k_{Lid} , k_{Loss} does not depend on the conditions inside the reactor and should therefore be easier to calibrate.

The other two new heat flows in Equation (2-17) are the heat pumped by the cooling liquid, $q_{Fluid,IN}$ and $q_{Fluid,OUT}$:

$$q_{Fluid,OUT} - q_{Fluid,IN} = \dot{m} \cdot c_{P,Fluid} \cdot (T_{j,OUT} - T_{j,IN}) \quad (2-19)$$

Where \dot{m} is the mass flow of the cooling liquid [kg/s] and $c_{P,Fluid}$ the heat capacity [J/(kg·K)]. By Equation (2-19) the dynamics of the cooling liquid is taken into account.

2.1.4 Dynamics of an isothermal reaction calorimeter

If calorimetry is not only used to determine the total amount of heat released by a certain process, but also to provide information about the time flow of the heat release the dynamics of the measurement system should be considered [Becker 68], [Karlsen et. al. 87, b], [Cesari et. al. 81], [Hemminger et. al. 84], [Nilsson et. al. 82], and [Vincent et. al. 02].

If q_{tot} is still calculated based on a steady state isothermal heat-flow balances described in the previous Chapters 2.1.3.2, 2.1.3.3 and 2.1.3.4. The following error sources might cause deviations from ideal behavior and consequently a time distortion of q_{tot} :

Source A: Deviations from isothermal controlling:

If the total time constant of the apparatus is similar or even larger than the time constants of the chemical reactions investigated the control circuit (see Figure 2-7) will no more be able to control the reaction temperature at isothermal conditions. Consequently heat accumulation will take place in the reactor content and should be considered in the heat-flow balances.

Source B: Dynamic Elements:

Depending on the calorimetric principle applied, the constant temperature is maintained by different dynamic elements (reactor wall, compensation heater, Peltier elements (see Appendix A.1.2) or cooling liquid). In order to maintain an isothermal reactor temperature they will have to change their temperature and therefore heat accumulation inside of these elements will occur. The concept of this dynamic heat flow was already introduced and discussed in Chapter 2.1.3.1.

Source C: Time Constants of Temperature Sensors:

Temperature sensors have their own time constants. Additionally the heat conduction path from the site of the event to the measuring sensor can increase the observed time constant.

If q_{tot} is still calculated based on a steady state isothermal heat-flow balance (such as given in Chapters 2.1.3.2, 2.1.3.3 and 2.1.3.4) all the three sources will cause a time distortion of q_{tot} . The size of source A) is given by the overall dynamic behavior of the calorimetric device. Therefore the following paragraphs shall give a short introduction into the main elements in a control circuit of an isothermal reaction calorimeter. The basic setup is shown in **Figure 2-7**.

The reactor content produces a time-dependent heat flow $q_{tot}(t)$. This heat flow causes a temperature change inside the reactor content. This change will reach the sensor for the reactor temperature. The speed of the heat transport depends on the mixing and the properties of the reaction liquid.

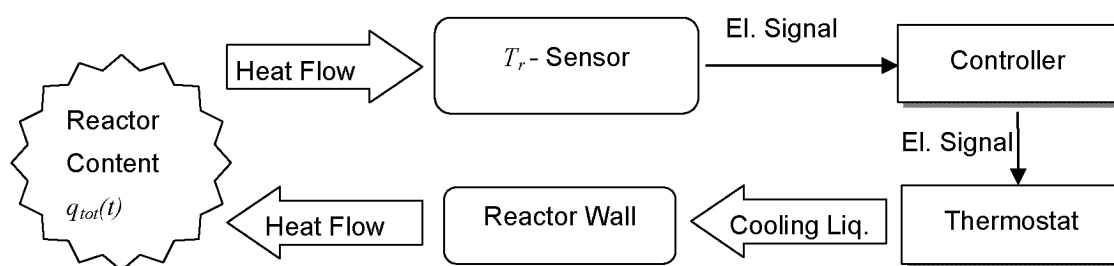
The temperature sensor for T_r , e.g. a thermocouple with a time constant of about 0.5s or a resistance sensor with a time constant of about 2s, will convert the temperature change into an electronic signal. The electric temperature signal is connected to the controller, e.g. a PID controller. Depending on the performance of the controller, the output will be varied slowly or fast in order to compensate the heat-flow change. Bad controller performance will lead to significant deviations of the reaction temperature from the desired isothermal set-point.

For a Heat-Balance or a Heat-Flow calorimeter the electrical output signal of the controller has to be converted by the thermostat into a change of the temperature of the cooling liquid T_j . This temperature change will cause a change of the temperature of the main dynamic element, in this case the reactor wall. All these three sources, thermostat, heat transport by the cooling liquid and the main dynamic element have their individual time constants that will contribute to the total dynamic behavior of the apparatus. For a BSC 81 reaction calorimeter, a precursor of the RC1 from [Mettler Toledo], [Karlsen et. al. 84] reported a time constant for the thermostat of about 50s.

For a Power-Compensation or Peltier calorimeter (see Appendix A.1.2) the output of the controller will be electrically amplified and then fed to the main dynamic element, the compensation heater or the Peltier elements. Generally the time constant of a compensation heater will be smaller than the time constant of a Peltier element because of its smaller thermal mass. However the compensation system as well as the Peltier system have much smaller time constants than the equivalent system of a Heat-Flow or Heat-Balance calorimeter as the temperature of the cooling liquid does not have to be changed.

The last step of the control circuit shown in Figure 2-7 is the heat transport from the main dynamic element to the reactor content.

Heat-Flow or Heat-Balance Calorimeter



Power-Compensation or Peltier Calorimeter (see Appendix A.1.2)

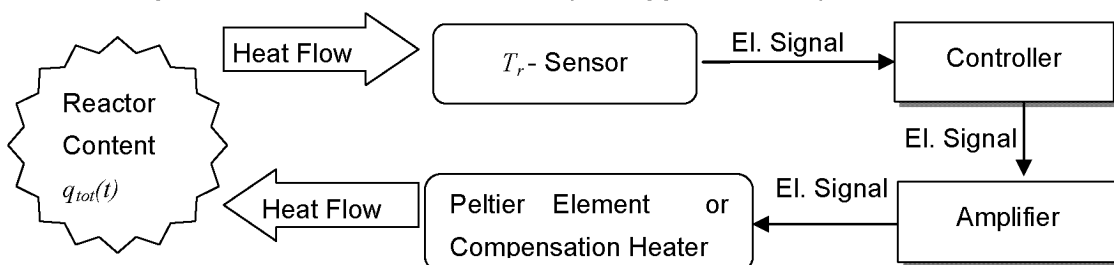


Figure 2-7: Control circuit of an isothermal reaction calorimeter.

Correction of a time-distorted calorimetric signal

Depending on the calorimetric signal a correction of the measured signals should be considered if the time constant of the measured chemical reaction is in the range of the time constant of the calorimeter.

Correction of source A)

If the heat capacity of the reaction mixture as well as the reactor inserts (stirrer, baffles, or sensors) is known, e.g. by calibration, a correction according to the measured reaction temperature change is easily possible (see also Chapters 3.2.1, 6.1.1, and 7.1.3).

Correction of sources B) and C)

Various black box methods were developed for an off-line time correction of the measured signals without using a dynamic heat-flow balance for the calorimeter or any other physical model [Cesari et. al. 81], and [Hemminger et. al. 84]. They are mostly applied for micro calorimetric systems where a correct physical model is quite complicated and the time constants of the measurement apparatus cannot be ignored. By these black box models the two sources B and C are corrected at the same time.

A correction method based on a physical model of the calorimeter was proposed by [Karlsen et. al. 87, b]. The model was applied to a Heat-Flow calorimeter and considered the dynamic heat flow through the reactor wall. The steady-state Equation (2-9) is replaced by a transient heat flux through the reactor wall because the reactor wall is the main dynamic element (see Chapters 2.1.3.1). No analogous approach was found for Heat-Balance or Power-Compensation calorimeters. [Nilsson et. al. 82] described a dynamic heat-flow balance for a Peltier calorimeter.

In this work a new black box time correction method will be described to correct the time distortion of the measured baseline signal (see Chapter 3.7.2).

2.1.5 Assessment of the three basic reaction calorimetric principles

The following section tries to give an overview on the most important topics related to the three different principles.

Heat Balance

The main advantage of this technique is that the determined signal q_{tot} is independent of changes of the heat transfer through the reactor wall during a reaction experiment. In contrast to all other techniques an additional calibration heater must be introduced if informations about the heat transfer on the reactor wall are also required, e.g. for later scale – up. The flow rate of the cooling liquid must meet two requirements that are difficult to accomplish simultaneously: On the one hand, the flow rate of the circulating fluid must be high enough to realize a fast heat transfer into the jacket in order to control the reaction temperature at a constant level. On the other hand, it should be low, to establish a temperature difference over the jacket large enough to be measured accurately. The influence of the ambient temperature on the finally determined q_{tot} signal is large compared to all other principles. Therefore good isolation of the reactor jacket is required.

Heat Flow

As in a Heat-Flow calorimeter the measured signal is the temperature difference between reactor content and reactor jacket, the flow rate of the cooling liquid can be chosen to be high without decreasing the quality of the signal. However the heat transfer through the reactor wall has to be calibrated with a calibration heater and changes during a reaction cannot be handled correctly in this standard setup. [Nilsson et. al. 82].

Power Compensation

From the technical point of view the Power-Compensation technique is the simplest technique to implement because the temperature of the cooling liquid T_j remains constant. Another advantage of this technique is the direct measurement of the electrical power required to maintain the temperature T_r at a constant level (however the noise of the measured signal is rather large [Hemminger et. Al 84]). The main drawbacks of this technique are the possible hot spots on the surface of the compensation heater. It is therefore crucial to check the ratio of reactor volume to heat-transfer surface of the system and that the compensation heater is optimally placed in the flow field of the stirrer. Another big drawback of this technique is that the constant heat flow through the reactor wall makes the measured signal more sensitive to a changing heat transfer (change of U or A in Equation (2-9)) than a Heat-Flow calorimeter [Singh 97] and [Pollard 01]. This is actually the reason why [Köhler et. al. 72] introduced an air gap between the reactor wall and the cooling liquid of the reactor jacket. This increases the fraction of the total heat-transfer resistance that originates from the external resistance. Other solutions to this problem are

reported in literature. They will be presented in the Appendix A.1. However if no measures are taken into account for a changing heat transfer through the reactor wall during a reaction, the determined heat release or uptake (q_{tot}) will be incorrect.

Dynamics of the three calorimeters

Apart from the general aspects discussed above, the dynamics (according to Chapter 2.1.4) of the three different principles differ significantly:

A) Quality of temperature control

A common feature for the Heat-Flow and especially Heat-Balance calorimeters is the fairly slow control of the jacket temperature [Regenass 83] because the main dynamic element is the reactor wall and the cooling liquid. Therefore even though the calorimeters are run in isothermal mode, heat accumulation in the reaction liquid has to be considered because the reaction temperature still varies in the range of some degrees Celsius [Karlsen et. al. 87, a]. The thermostatic units used to vary the temperature of the cooling liquid have to be fast and powerful [Riesen et. al. 85]. As will be shown in this work Power-Compensation calorimeters however can be tuned to control T_r very precisely even for fast and strongly exothermal reactions.

B) Dynamic Elements

As shown in Chapters 2.1.3.2, 2.1.3.3 and 2.1.3.4 isothermal calorimeters always require one or several dynamic elements in order to control the reactor temperature. Whenever temperatures are changing, heat accumulation takes place that will lead to a time distortion of the calculated q_{tot} . The concept of the dynamic heat flow was introduced in Chapter 2.1.3.1. It became clear that without enormous calculation effort, no accurate physical description can be found. Therefore most of the calculations are done on the basis of the steady-state approximations. This can lead to significant errors if the calorimetric data is used to determine kinetic informations. Therefore the three different principles shall be compared on the basis of the dynamic elements.

As shown above **Heat-Flow** and **Heat-Balance** calorimeters have two common dynamic elements: The reactor wall as well as the cooling liquid. As the flow rates of the cooling liquid are generally higher for a Heat-Flow calorimeter than for a Heat-Balance calorimeter the temperature changes, and thus the disturbance by the dynamic element, will be larger for the Heat-Balance calorimeter.

In **Power-Compensation** calorimeters the reactor wall is a dynamic element similar to the Heat-Flow and Heat-Balance calorimeters. However as shown in Figure 2-5 its temperature changes during a reaction measurement are generally much smaller compared to the other principles (Figure 2-4 and Figure 2-6). In a Power-Compensation calorimeter the heat flow through the reactor wall only changes if the reactor-side heat-transfer coefficient h_r or the heat-transfer area A changes during the measurement. These changes are generally much smaller than the changes caused e.g. by a chemical reaction. Furthermore the temperature of the reactor jacket is constant whereas T_j is varied for the Heat-Flow and Heat-Balance principle in order to control the reactor temperature T_r . Thus h_j will vary for the latter calorimeter types and the temperature change of the reactor wall can be very large. Further it should be considered that in a Heat-Flow or Heat-Balance calorimeter h_j will generally vary as a function of T_j leading to even larger temperature changes of the reactor wall. The main dynamic element in a Power-Compensation calorimeter is therefore the compensation heater. But the heat accumulation inside the heater element is generally much smaller compared to the heat accumulated in the wall of a Peltier (see Appendix A.1.2) or even Heat-Flow or Heat-Balance calorimeter. There are mainly two reasons:

- ❖ The heat capacity of a compensation heater is generally much smaller than the heat capacity of the reactor wall.
- ❖ There is no “jacket-side heat transfer” (h_j) in a compensation heater.

The total heat-transfer area of a compensation heater is generally smaller than the area of the reactor wall. Therefore bigger temperature changes of the compensation heater would be expected compared to temperature changes of the reactor wall in a Heat-Flow or Heat-Balance calorimeter. On the other hand the reactor-side heat-transfer coefficient h_r on a compensation heater is likely to be much higher than h_r on the reactor wall. This again would cause smaller temperature changes on the compensation heater.

Considering the different control principles (see Chapter 2.1.4) and dynamic elements, it becomes clear that q_{tot} determined based on Equations (2-12), (2-14), and (2-17) will be less time distorted for a well designed Power-Compensation calorimeter compared to a Heat-Flow or even Heat-Balance calorimeter. The Power-Compensation technique is therefore the method of choice if fast and strongly exothermal reactions have to be measured under isothermal conditions.

This will also be shown in this work (see Chapter 5.2 and Appendix E.4)

2.2 IR-ATR Spectroscopy

Infrared Spectroscopy

Vibrations and rotations of molecules generally absorb light in the infrared range (400 to 4000 cm^{-1}) as long as the dipole moment changes during the vibration or rotation. In liquid phase the rotations of the molecules are strongly influenced by molecular interactions. Therefore rotational stages cannot be resolved any more but will lead to broader absorption bands in the infrared spectrum. However the vibrations remain characteristic for specific functional groups of the molecules. Therefore infrared spectroscopy is often used for the purpose of substance characterization. In this work infrared spectroscopy will only be used to record relative changes of the absorption spectrum of a reaction mixture as a function of time. These changes origin in the chemical modification of the reaction compounds and therefore will give important informations about their concentration-time profiles.

ATR Spectroscopy

The focus of this work lies on the measurement of a time varying infrared spectra of a reaction experiment, in future referred to as reaction spectrum.

Conventionally infrared spectroscopy is carried out with transmission experiments, where the light passes through a sample cell with a defined thickness. There are two main disadvantages of this technique for the purpose of reaction analysis:

1. Either samples have to be taken or a flow-through cell has to be constructed.
2. Some solvents, like water, are strongly absorbing on a wide range of the infrared spectrum. Therefore the sample thickness should be very small otherwise a quantitative analysis will be very inaccurate. However in practice small sample thicknesses are difficult to achieve.

A general solution to both of these problems is the application of attenuated total reflectance (ATR) in combination with infrared spectroscopy. The theory of ATR Spectroscopy is well described in several Books and Articles [*Fringeli et. al. 02*], [*Harrick 67*] and [*Mirabella 93*].

As will be explained in Chapter 2.3.3 all evaluation methods of the measured reaction spectra are based on the law of Lambert Beer. It will be used in order to get informations about the concentration time profile of the absorbing components. It was derived for transmission spectroscopic experiments:

$$T = \frac{I}{I_0} = e^{-B} = e^{-\alpha \cdot d} = e^{-\kappa \cdot c \cdot d} = 10^{-A} = 10^{-a \cdot d} = 10^{-\epsilon \cdot c \cdot d} \quad (2-20)$$

Where T is the transmission at a certain wavelength [-], B and A the Napierian and decadic absorbance [-], α and a the Napierian and decadic absorption coefficient [m^{-1}], d the thickness of the sample [m], κ and ϵ the Napierian and decadic molar absorption coefficient [l/mol/m] and c the concentration of the absorbing component

in the sample [mol/l]. For transmission spectroscopy the molar absorption coefficients as well as the path length can be assumed to be constant during a reaction experiment. Therefore the linear relationship between absorbance and concentration of the absorbing species formulated in Equation (2-20) can be used to evaluate the measured reaction spectrum. **However ATR measurements are not transmission experiments** and therefore the applicability of the Lambert Beer's law has to be verified (see Appendix B.1).

Discussion of the IR-ATR approach

The technique of IR-ATR spectroscopy is easy to apply in reaction analysis as no sampling or flow-through cells are required. As most organic compounds are infrared active the technique should be useful for many reaction examples. However there are some aspects that should always be kept in mind if an ATR reaction spectrum is evaluated (see also Chapter 6.3.6):

- ❖ The **penetration depth** of the IR beam (see Appendix B.1) is in the range of some μm on top of the ATR crystal. Consequently the assumption, that the reaction observed in this surface layer equals the reaction in the bulk medium, must be verified. If **slurries** are measured only the liquid phase can be analyzed [*Furusjö et. al. 98, a*].
- ❖ Infrared spectra are generally **temperature dependent**, as the measured vibrations of the molecules in liquid phase depend on the temperature [*Furusjö et. al. 98, a*] and [*Furusjö et. al. 03*]. Additionally the effective thickness of the ATR "sample" (see Appendix B.1) depends on physical properties that may vary with temperature as well. Consequently IR-ATR measurements should be carried out at constant temperature.
- ❖ As explained in Appendix B.1 the **effective thickness** of the ATR "sample" depends on the absorption of the reaction mixture. As during a reaction measurement this absorption is changing the Lambert Beer's law might not be fulfilled any more. Generally these disturbances can be neglected [*Fringeli 03*] but care should be taken when strong absorption bands are evaluated.
- ❖ The technique might fail to identify components with **low concentrations** because their contribution to the total measured absorbance can no more be detected or disappears in the measurement noise [*Furusjö et. al. 00, a*].
- ❖ The ATR crystal also absorbs light. The ATR crystal used during this work is made of diamond. As **diamonds show strong absorbance** in the region of 1800 to 2400 cm^{-1} , this part of the infrared spectrum will not be available.
- ❖ In order to reduce the signal to noise ratio for a measured spectrum several spectra are typically recorded and averaged. The duration of a standard measurement is therefore in the range of **10 to 60 seconds**. The sampling time is thus restricted.

2.3 Evaluation of calorimetric and spectroscopic data

2.3.1 Overview and goal

As mentioned in the introduction, a crucial step of most analytical techniques is the evaluation of the measured data in order to extract the desired information. The analytical techniques applied in this work are reaction calorimetry and infrared spectroscopy. The measured data of a reaction experiment therefore consist of two different data sets: The **reaction power** (one dimensional vector in time) and a **reaction spectrum** (two dimensional matrix: time x wave number).

The aim of the evaluation is to identify unknown reaction parameters defined by a proposed reaction model based on these two data sets (see Chapter 1.2). Reaction parameters can be kinetic rate constants, activation energies, reaction orders, phase change rates, diffusion coefficients or reaction enthalpies.

It is important to note that this work does not focus on gathering qualitative information about concentration profiles, number of components in the reaction system or similar informations. It is assumed that a possible user will be skilled enough to suggest appropriate reaction models. As the selected analytical techniques will anyway not reveal deep mechanistic insight into the investigated reaction, the reaction models will be empirical, only describing the most important main and side reactions.

The following Chapter will give a short introduction into the evaluation methods applied for reaction spectra and calorimetric analysis. They can be separated into the following two groups: **Evaluation methods based on a reaction model** (hard modeling approaches) and **evaluation methods without reaction model** (soft modeling approaches). The first group of methods will directly reveal the desired reaction parameters whereas the second group mostly requires a subsequent evaluation based on a reaction model. Most of the soft modeling approaches will thus be rather useful to design an appropriate reaction model but not to determine the desired reaction parameters. The **model-free evaluation methods of the calorimetric data** are given in the following subchapters. **The model-free evaluation methods of the infrared data** however are presented in the Appendix B.2. In Appendix B.3 combinations and a comparison of soft and hard modeling approaches are given. *All evaluation techniques for the reaction spectrum discussed do not require any information about the pure spectra of the involved chemical components.*

For the evaluation of the reaction spectrum there would even be a third group of evaluation methods that require a calibration of the reaction system. As formulated in Chapter 1.2 the available time for the evaluation is restricted and therefore techniques based on calibrations are impeded in the context of early reaction optimization. Thus the following Chapters will not consider such techniques.

Only evaluation techniques for isothermal measurement data are considered because non-isothermal measurements are not suitable in the context of this work (see Chapters 1.3 and 2.2). If the behavior of the reaction at different temperatures has to be studied, several isothermal measurements at different temperatures have to be carried out. The results of the individual evaluations can then be plotted e.g. in an Arrhenius plot in order to calculate the activation energy or to check if the reaction mechanism did change between the different temperatures. Alternatively most of the proposed techniques also allow a simultaneous evaluation of isothermal measurements at different temperatures by including the Arrhenius law for the rate constants into the evaluation.

2.3.2 Evaluation methods for isothermal calorimetric reaction data

2.3.2.1 Evaluations not requiring a reaction model

As reaction calorimetry is a direct measure of the rate of reactions, most of the evaluation techniques are based on a more or less specific definition of a reaction model. There is actually only one model-free evaluation technique that still leads to a physically meaningful result: The integration of the measured reaction signal.

$$Q_{tot} = \int_{t=0}^{t=t_f} q_{tot} \cdot dt \quad (2-21)$$

Where q_{tot} is the measured power release or uptake [W] (Equation (2-1)), t_f the integration limit in time [s] and Q_{tot} the total measured heat released or consumed during a reaction measurement [J]. The total heat Q_{tot} is the sum of all thermally active physical or chemical processes measured. Some of the most important terms are given in the following equation:

$$Q_{tot} = \sum_{i=1..N_R} (-\Delta_r H_i) \cdot n_i + Q_{mix} + Q_{Phase} + Q_{Error} \quad (2-22)$$

Where $\Delta_r H_i$ is the enthalpy of the i 'th reaction [J/mol] (heat release or uptake by the reaction at constant pressure), n_i the number of moles of the i 'th reaction component [mol], Q_{mix} the heat of mixing [J], Q_{Phase} the heat revealed or consumed by phase change processes, and Q_{Error} the sum of all measurement errors [J]. It should be noted that the appropriate selection of the integration time limit has a significant influence on the calculated Q_{tot} .

2 Theoretical Background

For a further evaluation of Q_{tot} the following assumptions are generally made: Q_{mix} , Q_{Phase} , and Q_{Error} are assumed to be negligible, meaning that $q_{tot} = q_{React}$, and the reaction is assumed to perform in one single rate determining step. If these assumptions are fulfilled, the reaction enthalpy $\Delta_r H$ can thus be calculated directly by the following equation:

$$-\Delta_r H \approx -\Delta H = \frac{Q_{tot}}{n} \quad (2-23)$$

Where ΔH is the total enthalpy change [J/mol]. Thus model-free evaluation of the calorimetric signal for simple reactions will directly deliver one of the desired reaction parameters, the reaction enthalpy. However in real applications Q_{mix} , Q_{Phase} and Q_{Error} are generally not zero and will therefore be fully integrated into the reaction enthalpy.

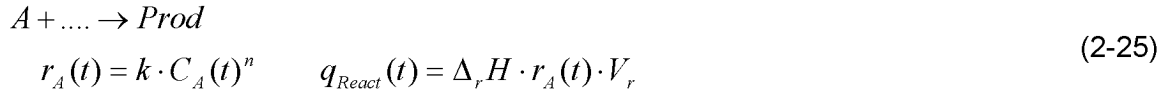
Once the reaction enthalpy is determined, it is possible to calculate the thermal conversion or fractional heat evolution of the reaction:

$$X_{thermal}(t) = \frac{\int_{\tau=0}^{\tau=t} q_{tot} \cdot d\tau}{Q_{tot}} \quad (2-24)$$

This thermal conversion can be compared to the chemical conversion of the investigated reaction as long as the assumptions mentioned above are fulfilled. However if the assumptions made are not fulfilled and/or informations about the rate constants of the investigated reactions are required, model-based approaches have to be chosen. Another drawback of model free evaluations is that all possible experimental errors such as base line drifts or control failures of the calorimetric device are integrated into the final result.

2.3.2.2 Model-based evaluation methods for simple single step n'th order batch reactions

Most of the model-based evaluations of the calorimetric signal are based on the assumption that the reaction performs in one single step of n'th order with only one rate determining component concentration. The reactions must be carried out in batch mode ($V_r = \text{constant}$) in order to simplify the evaluation. The general reaction model can therefore be written as follows:



Where C_A is the concentration of the rate-determining component A ([mol/l]), k the n'th order rate constant [(l/mol)ⁿ⁻¹/s], n the order of the reaction and r_A the reaction rate of component A [mol/(l·s)].

The task of the evaluation is to calculate the kinetic parameters k (and the Arrhenius activation energy E_A if measurements at different temperatures are evaluated) and possibly n as well as the thermodynamic parameter $\Delta_r H$. There are two different groups of evaluation methods:

Method I.A) Determination of the kinetic parameters based on the reaction enthalpy determined by prior integration of q_{tot} :

Assuming that Q_{mix} , Q_{phase} , and Q_{Error} in Equation (2-22) are negligible, r_A can be expressed based on Equations (2-24) and (2-25):

$$r_A(t) = \frac{q_{\text{tot}}(t)}{V_r \cdot \Delta_r H} = -k \cdot C_{A,0}^n \cdot (1 - X_{\text{thermal}}(t))^n \quad (2-26)$$

Where V_r is the reaction volume [l], q_{tot} the measured calorimetric power signal, $\Delta_r H$ the reaction enthalpy determined by prior integration (Equation (2-23)) and $C_{A,0}$ the initial concentration of component A.

[Litz 87], and [Hemminger et. al. 84] plotted $\log(r_A)$ versus $\log(1 - X_{\text{thermal}})$ and determined the reaction order n from the slope of the line and the rate constant k from the intersection (according to Equation (2-26)).

If the reaction order n of component A is known in advance, the reaction model (Equation (2-25)) can be integrated. Assuming e.g. a first-order reaction in component A ($n=1$), the rate constant k can then be determined by the following non-linear least-squares optimization ([Snee et. al. 93], [Pinto Machado e Silva et. al. 02], [Crevatin et. al. 99], [Ubrich et. al. 99] and [André et. al. 02]):

$$\min_k \sum_{i=1}^{N_t} \left[X_{\text{thermal}}(t_i) - (1 - e^{-k \cdot t_i}) \right]^2 \quad (2-27)$$

Where t_i is the i'th time sample of the calorimetric measurement and N_t the total number of samples.

A big drawback of these techniques, compared to the techniques described below, is that the errors and simplifications made in order to determine $\Delta_r H$ and $X_{thermal}$ (see Chapter 2.3.2.1) will also influence the determined rate constants k . Another problem is the appropriate selection of the final integration time, required for the calculation of $X_{thermal}$ (Equation (2-24)). Both problems were addressed by [Ubrich et. al. 99].

Method I.B) Separate determination of the rate constant k as well as the reaction enthalpy $\Delta_r H$ based on the reaction model

For first order reactions ($n=1$ in Equation (2-25)) the reaction model can be integrated and q_{tot} can be expressed as follows assuming that $q_{tot} = q_{React}$:

$$q_{tot}(t) = -V_r \cdot (-\Delta_r H) \cdot k \cdot C_{A,0} \cdot e^{-k \cdot t} \quad (2-28)$$

Therefore plotting $\log(q_{tot})$ versus time should result in a straight line with a slope equal to $-k$. Applications are reported by [Landau et. al. 94], [Regenass 83], and [Jansson et. al. 87] (The reaction enthalpy $\Delta_r H$ was calculated in an independent step by Equation (2-21) and (2-23)).

Any reaction period where the assumption $q_{tot} = q_{React}$ is not fulfilled will be visible in the plot as a deviation from the straight line. Such time periods can then be excluded from the determination of k . An example of such an application is the determination of the rate constant of the hydrolysis of acetic anhydride where a heat of mixing is released during the initial phase [Zogg et. al. 03] (see also Chapter 5.3), [Köhler et. al. 73] and [Litz 87].

For the same reaction [Köhler et. al. 73] and [Litz 87] determined the reaction enthalpy $\Delta_r H$ from the intercept of the line in the same plot ($\log(q_{tot})$ versus time, compare to Equation (2-28)). As the heat of mixing only takes place during the initial phase of the reaction, it does not influence the determination of $\Delta_r H$. [Walisch et. al. 65] and [Becker et. al. 65] described a similar calculation method for the same reaction in order to split the total measured heat Q_{tot} into the heat of mixing Q_{mix} and the enthalpy of reaction $\Delta_r H$. In contrast to method I.A this method represents another way to calculate $\Delta_r H$, alternative to the integration formulated in Equations (2-21) and (2-23). It should be more reliable in situations where the assumption $q_{tot} = q_{React}$ is not fulfilled and it is possible to extract e.g. a heat of mixing from the total measured heat Q_{tot} .

2.3.2.3 Model-based evaluation methods for more complex reactions

The evaluation methods I.A and I.B described in Chapter 2.3.2.2 can only be applied for single step reactions in batch mode with one single rate-determining component concentration. If the evaluation of the calorimetric signal should be extended to the general case of the semi-batch operation mode ($V_r = V_r(t)$) or to multiple reaction systems including eventual mass-transfer processes, these methods will fail. Therefore more general evaluation methods were developed.

The basis of these methods is a reaction model represented by a system of ordinary differential equations (compare to Equation (2-25)). However the reaction model can now include more than one chemical reaction as well as mass-transfer or dosing processes. Generally analytical solutions for such reaction models do not exist. Thus numerical differential equation solvers are used to integrate these models.

The task of the evaluation method is to calculate the unknown parameters of the reaction model. These reaction model parameters (in future indicated as $\theta_{1..N_p}$) can be rate constants, activation energies, reaction orders, or mass-transfer parameters. Additionally the reaction enthalpies of the different reaction steps have to be identified as the integration approach formulated by Equations (2-21) and (2-23) is not feasible any more.

There are two different groups of evaluation methods to solve this task:

Method II.A) Identification of either the reaction enthalpies or the reaction model parameters $\theta_{1..N_p}$ if the non-identified counterpart is known

If the reaction enthalpies of each reaction step would be known in advance, the reaction model parameters could be identified by the following non-linear least-squares optimization:

$$\min_{\theta_{1..N_p}} \sum_{i=1}^{N_t} \left[q_{tot}(t_i) - \sum_{j=1}^{N_R} V_r(t_i) \cdot (-\Delta_r H_j) \cdot r_j(t_i, \theta_{1..N_p}) \right]^2 \quad (2-29)$$

Where q_{tot} is the total measured heat release or uptake of the reaction [W], $\theta_{1..N_p}$ the unknown reaction model parameters, N_p the number of model parameters, N_t the number of samples, t_i the i 'th sample of the measurement, V_r the reactor volume [l], $\Delta_r H_j$ the j 'th reaction enthalpy [J/mol], N_R the number of reactions and r_j the j 'th reaction rate [mol/(l·s)]. The reaction rates are defined by the reaction model. Thus the reaction model has to be solved for all iterations during the optimization process. This method assumes that $q_{tot} = q_{React}$. However all thermal effects different to the reaction power influence the measured signal q_{tot} . Therefore these effects will still influence the result of the fitted model parameters $\theta_{1..N_p}$ but the influence will be smaller as compared to the evaluation method I.A given in Chapter 2.3.2.2 (see also Chapter 6.2) because the reaction model can act like a filter. If this assumption $q_{tot} =$

2 Theoretical Background

q_{React} is not fulfilled during certain time regions of the measurement (e.g. during the dosing), the corresponding measurement points can also be excluded from the summation in Equation (2-29).

Examples of this nonlinear parameter identification task, with known reaction enthalpies, are given by [Landau et. al. 95, b] who identified three rate constants of a consecutive catalytic hydrogenation with Excel, [Lunghi et. al. 02] who identified the reaction orders and the rate constant of a nitration with [BatchCAD] and [Sbirrazzuoli et. al. 00] who identified two rate constants and two reaction orders from a simulated parallel reaction system with the ForK program. All authors repeated the isothermal measurements at different temperatures and also identified the Arrhenius activation energy of the rate constants. [Landau et. al. 95, b] and [Sbirrazzuoli et. al. 00] included the Arrhenius parameters directly in the nonlinear parameter identification. [Lunghi et. al. 02] first evaluated the isothermal experiments individually and then calculated the Arrhenius activation energy from a subsequent Arrhenius plot.

However the crucial task is to find the appropriate reaction enthalpies. [Sbirrazzuoli et. al. 00] used pre-defined values for $\Delta_r H_j$ and [Lunghi et. al. 02] determined a single reaction enthalpy by integration of q_{tot} (Equation (2-21)). Only the approach of Landau et. al [Landau et. al. 95, b], to calculate the reaction enthalpies by a semi-empirical quantum mechanical program could be applied in a general case.

The method can also be applied the other way round: If the parameters $\theta_{1..Np}$ would be known in advance, the reaction enthalpies could be calculated according to the following linear least-squares optimization:

$$\min_{\Delta_r H} \sum_{i=1}^{N_I} \left[q_{tot}(t_i) - \sum_{j=1}^{N_R} V_r(t_i) \cdot (-\Delta_r H_j) \cdot r_j(t_i) \right]^2 \quad (2-30)$$

[Zogg et. al. 03] (see also Appendix E.2.4.1) initially determined the rate constant of the hydrolysis of acetic anhydride analogous to method I.B. The reaction enthalpy $\Delta_r H$ was then determined using Equation (2-31). The heat of mixing occurring during the dosing period was excluded from the summation in Equation (2-31).

Method II.B) Simultaneous identification of the reaction enthalpies and the reaction model parameters

If neither the reaction enthalpies nor the reaction model parameters ($\theta_{1..N_P}$) can be determined based on external informations or by any of the methods described so far, their determination must be carried out in a single step by the following non-linear least-squares optimization (combination of Equations (2-29) and (2-30):

$$\min_{\theta_{1..N_P}, \Delta_r H_{1..N_R}} \sum_{i=1}^{N_t} \left[q_{tot}(t_i) - \sum_{j=1}^{N_R} V_r(t_i) \cdot (-\Delta_r H_j) \cdot r_j(t_i, \theta_{1..N_P}) \right]^2 \quad (2-31)$$

All the comments made to method II.A are also valid for this evaluation method. Examples of this nonlinear parameter identification task, with unknown reaction enthalpies and reaction parameters, are presented by several authors: [Evans et al. 80] identified two rate constants, two reaction orders and two reaction enthalpies of a consecutive amination using an in-house program. The evaluation program TA-kin, described by [Anderson et al. 96], was used in several applications to identify rate constants, reaction enthalpies and activation energies in one step [Hinz et al. 98], [Heldt et al. 98], and [Willms et al. 98]. [Pastré et al. 01] used the ACSL optimization toolbox [ACSL] to identify the rate constant, reaction enthalpy and reaction orders of a one-step semi-batch reaction. [Dyer et al. 02] identified three rate constants, two reaction orders and three reaction enthalpies of a consecutive Vilsmeier reaction using an in-house program. [Balland et al. 00] presented a genetic optimization algorithm and identified two rate constants, three reaction orders and two reaction enthalpies of a saponification reaction. The heat of mixing was modeled and identified as well.

Commercial calculation packages that are able to carry out such a parameter identification task are [BatchReactor], [BatchCAD], and [ChemCAD].

*This Evaluation Method corresponds to the **separate calorimetric evaluation** described in Chapter 4 and applied in chapters 5.3 and 5.4.*

2.3.2.4 Evaluations based on a reaction model and supported by additional analytics

Method III.A) Identification of the reaction model parameters $\theta_{1..N_p}$ using additional concentration measurements obtained by a calibrated analytical technique

[Machado *et. al.* 96] investigated a complex parallel and consecutive reaction system. The enthalpies of reaction were determined in advance and finally two rate constants (including the activation energies) were fitted to the calorimetric data. The nonlinear optimization is similar to the one described by Equation (2-29) but additionally to the calorimetric power signal q_{tot} , concentration measurements were included into the objective function:

$$\min_{\theta_{1..N_p}} \left\{ \begin{array}{l} \sum_{i=1}^{N_t} W_Q \cdot \left[q_{tot}(t_i) - \sum_{j=1}^{N_R} V_r(t_i) \cdot (-\Delta_r H_j) \cdot r_j(t_i, \theta_{1..N_p}) \right]^2 \\ + \sum_{s=1}^{N_C} \sum_{i=1}^{N_{obs}} W_C \cdot \left[c_{measured,s}(t_i) - c_{calc,s}(t_i, \theta_{1..N_p}) \right]^2 \end{array} \right\} \quad (2-32)$$

Where W_Q and W_C are user defined weighting functions, N_C the number of measured components, N_{obs} the number of concentration observations, $c_{measured,s}$ the measured and $c_{calc,s}$ the calculated concentration (using the reaction model) of the s 'th component. All comments made to method II.A also apply to this evaluation method. The same evaluation principle was applied by [Fillion *et. al.* 02] to a more complex heterogeneous hydrogenation reaction with more than ten model parameters. Because the hydrogen-uptake rate was measured as well, the reaction enthalpies could be determined in an initial step.

In both examples several isothermal experiments were combined to one data set and evaluated at the same time. As the temperature was varied, the Arrhenius activation energies of the rate constants were calculated at the same time.

The combined evaluation of calorimetric and concentration data is also available in commercial software packages such as [BatchCAD], [BatchReactor], or [ChemCAD]. The application of this combined evaluation approach was also reported by [Dyer *et. al.* 02] but no details about the underlying mathematics were given.

It should be noted that any kind of concentration measurement carried out by e.g. HPLC, GC, or spectroscopic techniques, require a time consuming pre calibration of the analytical devices.

Method III.B) Identification of the reaction model parameters $\theta_{L,Np}$ using additional measurement of a gas production or uptake rate

The nonlinear optimization described in Equation (2-29) (method II.A) requires the knowledge of the reaction enthalpies. The overall optimization according to Equation (2-31) (method II.B) to estimate thermodynamic and kinetic reaction parameters at the same time might be difficult to solve in certain applications as the degrees of freedom of the non-linear optimization problem are rather large. Therefore the determination of the reaction enthalpies of the different reaction steps is often done in advance on the basis of the total measured heat Q_{tot} (Equation (2-21))

[Sempere et. al. 98] calculated the reaction enthalpies of the reaction steps during a complex N-oxidation reaction based on the knowledge of the oxygen production. It was measured additionally to the calorimetric signal q_{tot} . All other seven reaction model parameters were calculated by solving the optimization problem described by Equation (2-29).

[LeBlond et. al. 98] calculated the reaction enthalpies of the reaction steps during the hydrogenation of a nitro group based on the additionally measured hydrogen uptake. The rate constants of the reactions involved were then calculated on the basis of the infrared measurements and not on the basis of the calorimetric measurements.

2.3.3 Evaluation methods for isothermal spectroscopic reaction data

2.3.3.1 Lambert-Beer's law as the basis for all evaluation methods

The basis of all evaluation methods presented in the following sections is Lambert – Beer's law. All reaction spectra of any spectroscopic sensors can be used with these evaluation methods as long as Lambert – Beer's law is fulfilled. For a single wavelength and absorbing substance Lambert – Beer's law is given by Equation (2-20). For the case of a reaction spectrum with several wavelengths, chemical components and points in time, the following matrix form can be used:

$$A(N_t \times N_\lambda) = C(N_t \times N_C) \times E(N_C \times N_{\tilde{\nu}}) \quad (2-33)$$

$$\begin{bmatrix} a_{1,1} & \cdots & \cdots & \cdots & a_{1,N_{\tilde{\nu}}} \\ \cdots & \cdots & \mathbf{A} & \cdots & \cdots \\ a_{N_t,1} & \cdots & \cdots & \cdots & a_{N_t,N_{\tilde{\nu}}} \end{bmatrix} = \begin{bmatrix} c_{1,1} & \vdots & c_{1,N_C} \\ \vdots & \vdots & \vdots \\ \vdots & \mathbf{C} & \vdots \\ \vdots & \vdots & \vdots \\ c_{N_t,1} & \vdots & c_{N_t,N_C} \end{bmatrix} \times \begin{bmatrix} e_{1,1} & \cdots & \cdots & \cdots & e_{1,N_{\tilde{\nu}}} \\ \cdots & \cdots & \mathbf{E} & \cdots & \cdots \\ e_{N_C,1} & \cdots & \cdots & \cdots & e_{N_C,N_{\tilde{\nu}}} \end{bmatrix}$$

Where A is the measured reaction spectrum, N_t the number of measurement points in time, $N_{\tilde{\nu}}$ the number of wave numbers, C the concentration matrix with the concentration time profiles of each absorbing component in the columns, N_C the number of chemical components, E the pure spectra matrix with the pure spectra of each absorbing component in the rows. If a chemical component is not absorbing the corresponding pure spectrum will be a vector of zeros.

Spectroscopic techniques that are normally used in the context of reaction characterization are near/mid infrared, UV/VIS or Raman spectroscopy. As soon as the Lambert Beer's law is no more fulfilled (e.g. high absorptivities, or heterogeneous reaction mixtures) care has to be taken when the following evaluation methods are applied [Dyson *et. al.* 00].

It should be noted that by evaluating reaction spectra in order to estimate reaction model parameters (such as rate constants or activation energies) **a new set of unknown parameters is introduced: The pure spectra of the chemical components involved in the reaction (matrix E)**. The pure spectra can be compared to the reaction enthalpies that have to be identified additionally to the reaction model parameters when calorimetric data is evaluated (see Chapter 2.3.2). However the pure spectra of the chemical components are generally of no further interest in the context of reaction optimization. Therefore their identification has to be considered as a side product of the evolution methods described in this Chapter. **Methods that require the knowledge of the pure spectra are not mentioned.**

2.3.3.2 Special evaluation methods based on a reaction model: Single peak evaluation

The univariate evaluation technique mentioned in Appendix B.2 is also used in order to determine kinetic parameters of a given reaction model. Generally a single column of A , corresponding to the absorption profile a of a selected peak, is evaluated in order to determine kinetic parameters of the reaction system. It is assumed that only one chemical component of the reaction system is responsible for the absorption peak. The evaluation methods are the same as would be applied if the concentration profile of this component would be known. Examples are reported in [LeBlond *et. al.* 98] and [Pastré *et. al.* 01]. Univariate evaluation supported with calibration is reported by [Svensson *et. al.* 99] and [Ubrich *et. al.* 99].

2.3.3.3 General evaluation methods based on a reaction model: Multivariate evaluation

Generally, in the context of the evaluation of reaction spectra, the univariate evaluation technique of a single peak described in Chapter 2.3.3.2 will fail because pure spectral regions where only one single chemical component is absorbing cannot be assumed. Especially if several absorbing components are present in the reaction mixture. Therefore multivariate techniques, that allow peak overlapping, were developed. Most of them were developed for the evaluation of NIR reaction spectra where peak overlapping is a crucial problem. The same techniques can also be applied to evaluate mid infrared reaction spectra, however the spectra are more specific and peak overlapping less severe.

The task of these methods is to **fit a reaction model into the measured reaction spectrum** on the basis of Lambert-Beer's law (Equation (2-33)) and identify the kinetic parameters of the model. The general task can be described by the following nonlinear least-squares optimization:

$$\min_{\theta_{1..N_p}, \hat{E}} \|A - C_{calc}(\theta_{1..N_p}) \times \hat{E}\|_2^2 \quad \text{with } A(N_t \times N_\lambda), C_{calc}(N_t \times N_C), \hat{E}(N_C \times N_{\hat{v}}) \quad (2-34)$$

Where θ_k is the k 'th model parameter, N_p the number of model parameters, A the measured reaction spectrum. C_{calc} corresponds to C in Equation (2-33) and contains the calculated concentration profiles of the chemical components in the columns. The concentration profiles are simulated using a given reaction model and are therefore only depending on the model parameters $\theta_{1..N_p}$. Simple kinetic reaction models can be integrated analytically and C_{calc} is a direct function of $\theta_{1..N_p}$. If the reaction model chosen is too complex for analytical integration the ordinary differential equations of the reaction model have to be integrated numerically at each iteration step. Matrix \hat{E} corresponds to E in Equation (2-33) and contains the estimated pure spectra of each chemical component contained in C_{calc} . As already mentioned in Chapter 2.3.3.1 it should be noted that by the pure-spectra matrix E new unknown reaction parameters are introduced ($N_C \times N_{\hat{v}}$ values)!

The unknown reaction model parameters $\theta_{1..Np}$ as well as the unknown pure spectra matrix \hat{E} have to be identified by solving the given optimization problem in Equation (2-34). The direct solution of this nonlinear optimization is not feasible because far too many unknown parameters would have to be identified at one time. However the matrix elements of \hat{E} are linear whereas $\theta_{1..Np}$ are nonlinear parameters. Thus Equation (2-34) can be solved by separating the overall optimization into a linear optimization for \hat{E} and a nonlinear optimization for $\theta_{1..Np}$. Several solutions for this separation of linear and nonlinear parameters are reported in literature.

In the following section three different principles are shown. They are all explained on the basis of least squares as an objective function. Of course other ways of calculating the objective function are possible and sometimes suggested by the authors. However to keep the explanation as easy as possible only the least squares form will be discussed.

A) Direct solution using the complete spectral range (NLLS)

The easiest and most straightforward solution how to split the overall optimization problem of (2-34) into the linear and nonlinear parameters is to replace \hat{E} by its linear least-squares estimate:

$$\min_{\theta_{1..Np}} \left\| A - C_{calc}(\theta_{1..Np}) \times \hat{E} \right\|_2^2 \quad (\text{non-linear-least-squares}) \quad (2-35)$$

$$\text{where } \hat{E} \text{ is determined by } \min_{\hat{E}} \left\| A - C_{calc}(\theta_{1..Np}) \times \hat{E} \right\|_2^2 \quad (\text{linear-least-squares})$$

The linear least squares can be carried out with physical constraints for \hat{E} such as non-negativity. [Haario et. al. 98] applied the method to a reversible one-step reaction. [Bijlsma et. al. 01] used the method with non-negativity constraints for \hat{E} to evaluate a two-step consecutive reaction. In a later publication more alternatives to constrain the linear least-squares fit in Equation (2-35) were discussed [Bijlsma et. al. 02]. [Rivera et. al. 01] used the method to evaluate a heterogeneous reaction example, including binding and transport processes (no least-squares constraints were applied). [Taavitsainen et. al. 03] used the method with non-negativity and smoothness constraints for \hat{E} to evaluate a reversible esterification reaction.

B) Direct solution using a reduced spectral space (RNLLS)

In an initial step the measured reaction spectrum A is decomposed by PCA (principle component analysis [Malinowski 02], see Appendix B.2, Equation (B-8)) into C_{abs} and E_{abs} . Matrix A is then transformed into a new, reduced, reaction spectrum Matrix A' by the following equation:

$$A' = A \times E_{abs}^T = C_{calc} \times \hat{E} \times E_{abs}^T + R \times E_{abs}^T = C_{calc} \times \hat{E}' + R' \quad (2-36)$$

with $A' (N_t \times N_{PC}), \hat{E}' (N_C \times N_{PC}), R' (N_t \times N_{PC})$

Where N_{PC} is the number of principal components chosen during the PCA analysis and N_C the number of chemical components in C_{calc} . In Equation (2-34) A can now be replaced by the reduced reaction spectrum A' and \hat{E} can be replaced by the reduced pure-spectra matrix \hat{E}' :

$$\min_{\theta_{1..N_P}, \hat{E}'} \left\| A' - C_{calc}(\theta_{1..N_P}) \times \hat{E}' \right\|_2^2 \quad (2-37)$$

Thus the number of unknown linear parameters in Equation (2-34) can be reduced from $N_{\hat{v}} \times N_C$ to $N_{PC} \times N_C$. Generally N_{PC} is about 10 to 100 times smaller than the number of wave numbers in A and therefore the computation time for the linear optimization is significantly reduced. A side effect of the reduction of A and \hat{E} by PCA could be, that all information contained in A not modeled by the selected number of principal components, such as baseline drifts or measurement noise, does not affect the further calculation. Of course the selection of the appropriate N_{PC} is crucial and difficult to carry out in reality.

In a second step the linear and nonlinear parameters of Equation (2-37) have to be separated. Therefore \hat{E}' is replaced by its linear least-squares estimate (analogous to the solution A) but without any constraints):

$$\min_{\theta_{1..N_P}} \left\| A' - C_{calc} \times \left\{ \left[C_{calc}^T C_{calc} \right]^{-1} C_{calc}^T \times A' \right\} \right\|_2^2 \quad \text{with } C_{calc} = C_{calc}(\theta_{1..N_P}) \quad (2-38)$$

Equation (2-38) represents a nonlinear least-squares optimization with $\theta_{1..N_P}$ as unknown reaction model parameters. For the solution of the nonlinear optimization standard mathematical procedures are applied.

This method was first reported by [Maeder et. al. 90]. It was applied in several studies in order to estimate reaction rate constants of chemical reaction systems: Reversible one and two-step reactions at different temperatures [Bugnon et. al. 94], first-order one- step reaction [Bayada et. al. 95] and a reversible one-step reaction [Maeder et. al. 97].

C) Indirect solution based on target transformation (TTNLLS)

Similar to the approach of Maeder et al. the first step includes a PCA decomposition of the measured reaction spectrum A into C_{abs} and E_{abs} (see Appendix B.2, Equation (B-8)). The separation of the linear and nonlinear parameters is achieved by applying the principal of target transformation (see Appendix B.2, ITTFA method). According to Equation (B-10) a transformation vector T is introduced that rotates C_{abs} into physical meaningful values. T is calculated in a linear least-squares sense in order to transform C_{abs} as good as possible into the target C_{calc} :

$$\min_T \left\| C_{abs} T - C_{calc} \right\|_2^2 \quad \text{or} \quad T = (C_{abs}^T C_{abs})^{-1} C_{abs}^T \times C_{calc}(\theta_{1..N_P}) = C_{abs}^+ C_{calc} \quad (2-39)$$

$$T(N_{PC} \times N_C), C_{abs}(N_t \times N_{PC}), C_{calc}(N_t \times N_C)$$

In Equation (B-10) T must be a square matrix and therefore has the dimensions $N_{PC} \times N_{PC}$. Thus N_{PC} has to be equal to N_C , the number of chemical components in C_{calc} .

2 Theoretical Background

This restriction is not valid in Equation (2-39) as only the projection of C_{abs} into C_{calc} is considered. Thus T can have the dimensionality $N_{PC} \times N_C$. However in most applications of this evaluation method N_{PC} in Equation (2-39) is set equal to N_C . Only [Furusjö et. al. 00, a] suggested to use more principal components in C_{abs} than chemical components in C_{calc} if baseline drifts or other effects occur during the reaction that are not modeled by the reaction model.

The quality of the target transformation depends on how the parameters $\theta_{1..N_p}$ (required to calculate C_{calc}) are chosen. Therefore the residuals resulting from a target transformation can be used for the nonlinear optimization of the model parameters. Thus the desired separation of linear and nonlinear model parameters is achieved. However there are different ways to express the residuals of the target transformation. The following nonlinear optimization problems can be formulated on the basis of Equation (2-39) and (B-10):

$$\min_{\theta_{1..N_p}} \left\| C_{calc} - C_{abs} C_{abs}^+ C_{calc} \right\|_2^2 \quad \text{where} \quad C_{calc} = C_{calc}(\theta_{1..N_p}) \quad (2-40)$$

$$\min_{\theta_{1..N_p}} \left\| E_{calc} - E_{calc} E_{abs}^+ E_{abs} \right\|_2^2 \quad \text{where} \quad E_{calc} = C_{calc}(\theta_{1..N_p})^+ A \quad (2-41)$$

$$\min_{\theta_{1..N_p}} \left\| A - C_{calc} E_{calc} \right\|_2^2 \quad (2-42)$$

It is also possible to make the reverse transformation to Equation (2-39), to transform C_{calc} into C_{abs} by another transformation matrix T . This would result in the following optimization:

$$\min_{\theta_{1..N_p}} \left\| C_{abs} - C_{calc} C_{calc}^+ C_{abs} \right\|_2^2 \quad \text{where} \quad C_{calc} = C_{calc}(\theta_{1..N_p}) \quad (2-43)$$

Equations (2-40) to (2-43) represent the desired nonlinear least-squares optimizations with $\theta_{1..N_p}$ as unknown parameters. They can all be solved by standard mathematical procedures. The principle just explained was developed individually by several authors. [Tam et. al. 94] used an objective function similar to (2-40) and identified the rate constants of consecutive two- and three-steps first-order reactions. [Sans et. al. 97] combined Equations (2-40) to (2-42) to a single objective function; however no results of the algorithm were reported. In a successive publication [Nomen et. al. 01] Equation (2-43) was used to identify an equilibrium reaction. Alternatives to the sum of squares as objective function are discussed. [Bijlsma et. al. 98] and [Bijlsma et. al. 00] used an equation similar to (2-43) to identify the rate constants of a two-step first-order consecutive reaction. [Furusjö et. al. 98, b] used a combination of Equation (2-40) and (2-43) to identify rate constants of simulated reaction examples as well as a one-step reaction. In a later applications [Furusjö et. al. 00, a] and [Furusjö et. al. 03] it was shown that the technique can also be applied when baseline drifts or absorption shifts occur during the reaction measurement. However it was shown that selection of the appropriate number of principal

components N_{PC} in the initial PCA step is crucial and does not have to be equal to N_C . As reaction example a one-step reaction was used.

Matrix augmentation

Augmentation of the measured reaction spectrum A by concatenating several experiments into one single matrix A_{aug} , can also be applied for the model-based approaches discussed in this Chapter. The robustness of the nonlinear optimization will increase as more information is available (see also Appendix B.2).

Comparison of RNLLS and TTNLLS

[Furusjö et. al. 98, b] compared RNLLS with TTNLLS for a simple ideal reaction example and found no difference. However in later publications [Furusjö et. al. 00, a], [Furusjö et. al. 00, b], and [Furusjö et. al. 03] it was shown that the TTNLLS is superior in the case of baseline drifts or absorption shifts (see also B.3). This conclusion is correct as long as only Equations (2-40) or (2-43) are used as objective functions. As soon as the measured reaction matrix A is directly part of the objective function (Equations (2-41) and (2-42)) the result of the optimization will again be influenced by baseline drifts or absorption drifts, similar to the RNLLS approach.

2.3.4 Combined evaluation of spectroscopic and calorimetric data

Equation (2-34) represents the general, nonlinear optimization to evaluate spectroscopic measurement data, based on a reaction model:

$$\min_{\theta_{1..N_P}, \hat{E}} \left\| A - C_{calc}(\theta_{1..N_P}) \times \hat{E} \right\|_2^2 \quad (2-34)$$

Equation (2-31) (method II.B) represents the general, nonlinear optimization to evaluate the calorimetric measurement data, based on a reaction model:

$$\min_{\theta_{1..N_P}, \Delta_r H_{1..N_R}} \sum_{i=1}^{N_t} \left[q_{tot}(t_i) - \sum_{j=1}^{N_R} V_r(t_i) \cdot (-\Delta_r H_j) \cdot r_j(t_i, \theta_{1..N_P}) \right]^2 \quad (2-31)$$

Comparing Equation (2-34) to Equation (2-31) reveals that the nonlinear parameters $\theta_{1..N_P}$, defined by the reaction model, are common in both equations. Only the linear parameters in Equations (2-34) and (2-31) (\hat{E} and $\Delta_r H_{1..N_R}$) are different. As the linear parameters in Equations (2-34) and (2-31) can be replaced by linear least-squares estimates (see Chapters 2.3.2.3 and 2.3.3.3) the combination of the two nonlinear optimizations is actually straightforward and can be carried out in analogy to Equation (2-32) (see Chapter 2.3.2.4):

3 Theoretical Background

$$\min_{\theta_{1...N_P}} \left\{ \begin{array}{l} W_Q \cdot \min_{\Delta_r \hat{H}_{1...N_R}} \left(\sum_{i=1}^{N_t} \left[q_{tot}(t_i) - \sum_{j=1}^{N_R} V_r(t_i) \cdot (-\Delta_r \hat{H}_j) \cdot r_j(t_i, \theta_{1...N_P}) \right]^2 \right) \\ + W_{IR} \cdot \min_{\hat{E}} \left(\|A - C_{calc}(\theta_{1...N_P}) \times \hat{E}\|_2^2 \right) \end{array} \right\} \quad (2-44)$$

Amazingly no publication was found that takes advantage of Equation (2-44). In all publications, where reaction calorimetry and online spectroscopic measurements are carried out at the same time, the evaluations are carried out separately for each signal. Only the method described in 2.3.2.4 is a first step into the direction of a combined evaluation. But it still requires an initial, model-free step to convert the measured spectroscopic data into concentration profiles. The model-free conversion of the measured reaction spectrum into concentration profiles of the involved chemical components can be carried out in essentially two different ways: 1) By calibration of the spectroscopic signal using mixtures of known concentrations. 2) By applying SMCR techniques, described in Appendix B.2. As calibration requires too much time and SMCR techniques are less robust than the model-based evaluation methods (see discussion in B.3) it seems most reasonable to eliminate the conversion step of the reaction spectrum into concentration profiles. This elimination is achieved by Equation (2-44).

The potential of a combined evaluation of spectroscopic and calorimetric data was also mentioned by [Gemperline 02].

2.3.5 Model selection

A fundamental problem of reaction simulation is the choice of an appropriate reaction model. It is therefore essential that a model-based evaluation of measured reaction data supports the task of model selection. Generally the residuals of the modeled to the measured reaction data are taken as an indication for the quality of the underlying reaction model [Furusjö et. al. 98, b].

However the robustness of the model fit will generally decrease with the number of unknown reaction parameters (such as rate constants, activation energies, reaction enthalpies or pure spectra) that have to be identified. Therefore the robustness of the parameter identification should be a second indicator for the quality of the chosen reaction model. An optimal reaction model will have minimal residuals and maximal robustness of fit.

However no standard procedure was found in literature.

3 THE NEW CALORIMETER

3.1 Historical development

In this work a complete redesign of the **Power-Compensation calorimeter, that was developed by J. Pastré** ([Pastré 00] and [Pastré et. al. 01]) will be presented. The redesign with a sample volume of 25 - 45 ml implies a new measurement principle as well as improved mechanical properties of the reactor. Analogous to the first version it is still possible to measure IR-ATR spectra online during a reaction experiment.

A first prototype of the new calorimeter was tested during the diploma work of I. Zürcher [Zürcher 01]. This work clearly demonstrated the feasibility of the new approach (see Appendix E.5).

As will be shown the technical implementation is very different to existing calorimeters because a metal jacket is used instead of a double wall glass jacket with a circulation cooling liquid. The temperature of this metal jacket is separately controlled. It therefore represents an intermediate thermostat. Due to the simplicity of this new technique (compared to conventional implementations) and the additionally measured baseline signal, it is quite attractive for small reaction calorimeters. **The intermediate thermostat was therefore patented** [Zogg et. al. 00].

Based on the experience with this first prototype the construction, the signal acquisition as well as the control software, were **continuously improved**. At the same time manufactures of commercial reaction calorimeters were addressed in order to commercialize the system. The company Mettler Toledo decided to take a license of the above mentioned patent. An evaluation on commercializing this system is going on. **The following Chapter will describe the final version of the new reaction calorimeter** as it was used for most of the case studies described in Chapter 5. This final version as well as the basics of the measurement principle were also presented in a publication [Zogg et. al. 03].

3.2 Requirements for the new reaction calorimeter

As explained in Chapter 1.2 the goal of this project is to develop a small-scale reaction calorimeter. It should be appropriate for the purpose of kinetic and thermodynamic reaction screening in early phases of process development in the fine chemical and pharmaceutical industry. Based on this background the calorimeter has to meet the following requirements (*The requirements are formulated based on the general description of a reaction calorimeter (see Chapter 2.1)*):

Volume, pressure and temperature range

The sample volume should be in the range of 25 ... 45 ml, allowing semi-batch operations. The aim is to have a volume as small as possible but still all other requirements listed below have to be met. Therefore a further volume reduction was not realistic (see also discussion in Chapters 1.3 and 2.1).

Compared to conventional reaction calorimeters that meet all the requirements listed below, a volume reduction by a factor of 5 to 50 has been achieved. The consumption of required test substance per reaction experiment is therefore significantly reduced and the dynamic behavior of the sample mass is improved. However it should be kept in mind that by reducing the sample volume the amplitude of the measured calorimetric signal is reduced as well. Therefore all disturbances will have a larger relative influence on the final measured heat flow (see Chapter 3.2.1).

With the first version of the reaction calorimeter [*Pastré et. al. 01*] we encountered difficulties with evaporating solvents during long time reaction measurements [*Zogg 99*]. The evaporation resulted in a volume reduction and thus in reduction of the total heat-transfer area (see Chapter 2.1.3.1). Consequently the final measured heat flow showed a baseline drift due to evaporation. In order to avoid this effect the new reactor should be **completely closed and therefore pressure resistant up to 10 bar**. To meet this goal a metal jacket is appropriate and a magnetic coupled stirrer is required.

To meet the needs in fine chemical and pharmaceutical industry, the reactor should be **temperature resistant up to 200 °C**. The **lower temperature limit is mainly given by the capacity of the connected cryostat** and is therefore adaptable.

Simple technical implementation

The reactor should have realistic proportions, similar to a real production vessel (see Chapters 1.3 and 2.1). All components used should be easy and reproducible to manufacture.

8 different connections and sensors in the reactor cover

The reactor cover should have eight different connections. In a standard setup they should be used for the following purposes:

1. Pressure sensor
2. Over-pressure valve
3. Magnetic valve to open the reactor
4. Compensation heater
5. Temperature sensor for T_r
6. Feed tube 1, including a temperature sensor for measuring the dosing temperature T_{Dos} (see Equation (2-4)).
7. Feed tube 2
8. not used (endoscope as option)

No calibrations of the calorimeter – Online measurement of the baseline

In order to fulfill the goal set for this work (see Chapter 1.2), to develop a reaction calorimeter with short experiment times, the typical calibration step required to measure the overall heat-transfer coefficient U , the heat-transfer Area A (see Figure 2-2 and Chapter 2.1.3.1,) as well as the heat capacity of the reactor content (reaction mixture and inserts) $c_{p,tot}$ should be circumvented.

Additionally the new reaction calorimeter should be able to deal with applications, where U as well as A change during the course of an experiment, generally addressed as baseline changes. For standard reactions the behavior of the baseline could be guessed, e.g. to be proportional to the reactor volume, but it is well known that these assumptions will fail for many reaction examples. Difficulties were already encountered in the reaction example investigated by [Pastré 00] and [Zogg 99] that actually seems to behave ideal. As changing heat-transfer properties of the reaction mixture will also be a challenging problem in the later large-scale realization of the reaction step an accurate online estimation would be a big support. Therefore the new reaction calorimeter should be able to **measure the change of q_{Flow} online** (see also Chapter 2.1.5).

Additional online infrared, pressure and stirrer torque measurements

According to the goal set in Chapter 1.2 the device should be equipped with a standard IR-ATR-probe. The same probe as in the previous version [Pastré 00] was used. The pressure in the reactor should be monitored online as well as the current consumption of the stirrer. As the stirrer is run by a magnetic coupling relative changes of the current consumption could be used as an indicator for a changing viscosity in the reactor.

Optionally it should be possible to introduce an endoscope into the reactor lid in order to enable optical observations.

The calorimeter must be suited for parallelisation

As mentioned before, the aim of this work is to provide a reaction calorimeter which is fast in application. The time required for a single reaction calorimetric experiment is generally defined by the following terms:

1. Preparing the chemicals and the dosing.
2. Wait for thermal equilibrium of the whole calorimetric unit (jacket, reactor and cover) at the desired temperature. This time is mainly given by the total mass of a calorimetric device as well as the maximum cooling or heating power of the temperature controlling elements.
3. First calibration of the overall heat-transfer coefficient U , the heat-transfer area A as well as the heat capacity.
4. The reaction time.
5. Second calibration of the overall heat-transfer coefficient U , the heat-transfer area A as well as the heat capacity.
6. Cleaning of the reactor.

From the mentioned terms, the preparing, cleaning as well as the reaction step always remain constant in time and are not influenced by the measuring device. Whereas the calibration steps could be eliminated (see above). The time until thermal equilibrium is reached is more difficult to reduce and will always remain, especially if precise calorimetric measurements should be carried out.

Consequently there are two main, time consuming, steps left in the whole experimental procedure that do not need the interaction of a user: The reaction time as well as the time required to reach thermal equilibrium. It is clear that **only by running several reaction calorimetric experiments in parallel the total experiment time can be further reduced.**

The new reaction calorimeter should therefore be suitable for parallel applications. Thus **several of these devices could be connected to a single cryostat still maintaining their individual temperature levels.** The heat-flow balance of the calorimeter should thus include changes of the temperature of the cooling liquid.

Minimal requirements for the temperature range of the cooling liquid

The experience with the previous version of the reaction calorimeter [Pastré 00] clearly showed that the cooling liquid used in the reactor jacket, which is in direct contact with the reactor wall, would have to be adapted to the temperature range of the reaction experiments. The main reason is that there is no unique cooling liquid, with low viscosity and good heat-transfer properties, for the whole desired application range (reaching from temperatures below 0°C up to 200°C). Therefore the new calorimeter should also be designed to **minimize the final temperature range that has to be handled by the cooling liquid.**

Isothermal operation mode

As mentioned in Chapters 1.3 and 2.2 isothermal control of the reaction temperature is desired if thermodynamic and especially kinetic reaction parameters are to be measured. The main arguments are repeated:

- ❖ The infrared spectra recorded by the **ATR sensor are temperature dependent** (see Chapter 2.2).
- ❖ **Kinetic evaluation of non-isothermal** reaction runs implies more unknown parameters than isothermal evaluation. Industrial reactions can reach a complexity (several reaction paths and coupling of chemical reaction, transport and phase change processes) that impedes a meaningful interpretation of non-isothermal calorimetric data as the information density of a measured signal might be high [Karlsen et. al. 87, a].
- ❖ **Calorimetric evaluation of non-isothermal data presumes the exact knowledge of the dynamic behavior of the calorimeter.** This implies that steady-state heat-transfer models, suitable for isothermal reaction calorimeters, have to be replaced by much more complicated dynamic heat-transfer models (see Chapter 2.1.3.1). Additionally the heat capacity of the reactor components as well as the investigated reaction mixture must be calibrated. Both tasks are generally difficult to achieve and require more experimental time.

Therefore the new device should be running in isothermal operation mode.

3.2.1 Accuracy of the calorimeter

According to the discussion of the basic principles in Chapter 2.1 and the requirements formulated above, the following accuracy categories were defined. The requirement in each category is given. *The accuracy measures for the actual device were analyzed during the applications listed in Chapter 5 and will be given in Chapter 6.1.1.*

Detection limit [W/l]

As the absolute size of the heat flow measured is proportional to the reaction volume, the detection limit (smallest heat flow detectable by the device) must be given relative to the reaction volume. The **detection limit of the power compensation signal should be ≤ 3 W/l** (corresponds to 0.1W / 35 ml). This is about 5 % of the maximum reaction power released by a standard chemical reaction. Standard reaction calorimeters (liter scale) have a resolution of about 0.1 W/l [Marison et. al. 98] (the increase of the accuracy equals the increase of the sample volume). Standard DSC calorimeters are also in the range of 1..10 W/l [Mettler Toledo] and [Setaram]. The

detection limit of the small scale (20 ... 100 ml) Power-Compensation calorimeter Auto-mate was visually determined from the signals shown in [Simms et. al. 00] to be in the range of 1 ... 4 W/l. **The detection limit of 3 W/l is therefore a reasonable value in the context of reaction screening in early stages of process development.**

High precision reaction calorimeters reach resolutions down to 5 mW/l (modified RC1 [Marison et. al. 98]), 90 mW/l (CPA 200, 40 ... 180 ml reactor volume, [Chemisens]) and even about 0.5 mW/l (C80, 12.5 ml reactor volume, however with a large time constant of about 100 ... 250 s [Setaram]).

For calorimeters that determine the change of the heat transfer through the reactor wall independent from the main calorimetric signal the measured baseline signal must be characterized by a second detection limit.

Detection limit of the baseline measurement: ≤ 3 W/l

Maximum absolute temperature deviation [K/(kW/l)]

As mentioned before the reactor should maintain isothermal conditions in order to allow an isothermal evaluation of the reaction kinetics. However it should always be kept in mind that the strictly isothermal control of the reaction temperature is not realizable (see Chapter 2.1.4). A further requirement to isothermal control is therefore that the deviations from the isothermal set point are kept as small as possible and the time space of the deviation as short as possible.

As soon as the reaction temperature changes the reaction kinetics will change as well. A maximum change of the rate constant by 10% is tolerated. For a standard chemical reaction with an average activation energy of 60 kJ/mol at 300 K a temperature increase by only 1 K results in a 10 % increase of the rate constant.

According to this reflection the **maximum absolute temperature deviation for an isothermal calorimeter should be ≤ 0.5 K/(kW/l)**. Meaning that a maximum reaction power of 1 kW/l (most standard reactions don't even reach this reaction power) should cause a maximum temperature deviation of 0.5 K.

Maximum relative heat accumulation error [%]:

The standard heat-flow balances for isothermal reaction calorimeters, introduced in Chapter 2.1.3, do not consider heat accumulation terms. However as mentioned above a real isothermal reaction experiment cannot be carried out without any temperature change of the reaction temperature. A temperature change will result in heat accumulation that can be described by the following equation:

$$q_{\text{accu}} = m_{\text{tot}} \cdot c_{p,\text{tot}} \cdot \frac{dT_r}{dt} \quad (3-1)$$

Where q_{accu} is the heat accumulation [W], m_{tot} the total reaction mass [kg], $c_{p,\text{tot}}$ the overall heat capacity of the reactor content [J/kg/K], and T_r the reaction temperature [K]. The heat flow described by Equation (3-1) could only be considered if the overall heat capacity of the reactor content $c_{p,\text{tot}}$ would be well known. It depends on the

reactor inserts, such as stirrer, baffles and sensors, as well as on the heat capacity of the reaction mixture. Thus a calibration of the overall heat capacity would be required at the beginning and end of every measurement. Such a calibration generally requires a considerable amount of time and is thus in contradiction to the requirement formulated above (see also Chapter 7.1.3).

However an accurate temperature controlling will only result in small and short temperature deviations from the isothermal set point. Consequently the accumulation terms in the heat-flow balances with their ill-defined heat capacities can be neglected [Schlegel et. al. 97]. The instantaneous relative error made by neglecting the heat flow of accumulation can then be expressed by the following equation:

$$\Delta q_{accu,rel} = \frac{q_{accu}}{q_{tot}} \cdot 100\% = m_{tot} \cdot c_{p,tot} \cdot \frac{dT_r}{dt} \cdot \frac{1}{q_{tot}} \cdot 100\% \quad (3-2)$$

Where $\Delta q_{accu,rel}$ is the relative instantaneous heat accumulation error [%] and q_{tot} the total measured power signal (Equation (2-1)), determined by an isothermal heat-flow balance. Assuming a standard reaction example with $c_{p,tot}$ equal to the heat capacity of water (4.2kJ/kg/K) $\Delta q_{accu,rel}$ can be calculated for every measurement.

The maximum rel. instantaneous heat acc. error should be $\Delta q_{accu,rel} \leq 10\%$.

Additionally to the instantaneous heat accumulation the integrated heat accumulation should also be considered. It can be expressed as follows:

$$\Delta Q_{accu,rel} = \frac{Q_{accu}}{Q_{tot}} \cdot 100\% = m_{tot} \cdot c_{p,r} \cdot \frac{1}{Q_{tot}} \cdot \int_0^{t_f} \frac{dT_r}{dt} dt \cdot 100\% \quad (3-3)$$

The maximum rel. integrated heat acc. error should be $\Delta Q_{accu,rel} \leq 1\%$.

Relative error of the total measured heat [%]

The final and probably most important accuracy requirement is the relative error of the total measured heat from a known standard reaction example. It is defined by the following equation:

$$\Delta Q_{rel} = \frac{Q_{tot} - \Delta_r H \cdot n}{Q_{tot}} \cdot 100\% \quad Q_{tot} = \int_0^{t_f} q_{tot} dt \quad (3-4)$$

Where q_{tot} is the total measured power signal (Equation (2-1)), including eventual baseline corrections [W], $\Delta_r H$ the known reaction enthalpy of the investigated standard reaction [J/mol], t_f the final reaction time and n the number of moles used [mol].

The relative error of the total measured heat should be $\leq 10\%$.

The accuracy requirements for the actual device were analyzed during the applications listed in Chapter 5 and will be given in Chapter 6.1.1.

3.2.2 Time constants of the calorimetric signals

The time constant of a calorimetric power signal q [W] (such as q_{Comp} (see Chapter 2.1.3) or $q_{Cooling}$ (see Chapter 3.3.3)) is best determined by measuring the response of this signal (including the complete control circuit explained in Chapter 2.1.4) to a known heat-flow impulse of the following form:

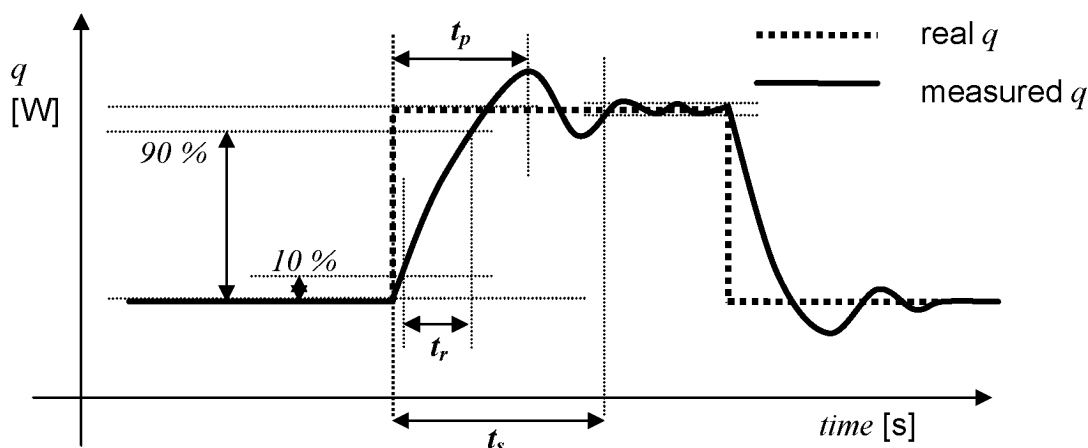


Figure 3-1: Heat flow q measured (solid line) by an isothermal reaction calorimeter when an impulse like heat flow (q real, dotted line) has to be compensated. The time delays required for the calculation of the time constant of the calorimeter are indicated.

The time constant τ of the measured calorimetric signal q could then be estimated according to the time delays t_r , t_p and t_s (see **Figure 3-1**) according to the following two equations [Franklin et. al. 02]:

$$\tau_1 = t_r / 1.8 \quad \tau_2 = t_p \sqrt{1 - \zeta^2} / \pi \quad \text{with } \zeta = 4.6 \cdot \tau_1 / t_s \quad (3-5)$$

The small volume of the new calorimeter makes it very well suited for the measurement of fast and strongly exothermal reactions. As one task of this work is to expand the applicability of reaction calorimetric measurements to such reactions (see Chapter 1.2), a fast responding control circuit is required. For standard reaction calorimeters (liter scale) time constants in the range of 50 s [Riesen et. al. 85] to 85 s [RC1 Handbook] are reported. The time constant of the whole reactor system, including the controller, might be even larger. For the CPA 200 (40 ... 180 ml, [Chemisens]) a time constant of about 25 ... 40 s is reported. The high precision calorimeter C80 (12.5 ml, [Setaram]) has a time constant of about 100 ... 250 s.

The time constant for the power compensation signal should thus be: $\tau \leq 10$ s. This is a reasonable value and corresponds to a five times faster device compared to commercial available reaction calorimeters.

The time constant for the baseline signal ($q_{Cooling}$, see below) should be: $\tau \leq 30$ s

The time constants for the actual device were analyzed during the applications listed in Chapter 5 and will be given in Chapter 6.1.1.

3.3 Concept for the realization

3.3.1 Selection of appropriate construction materials

Reaction calorimeters generally contain several glass parts because of their unique chemical resistance and transparency. However for applications in the required pressure range (up to 10 bar) glass parts should be avoided. Additionally it should be kept in mind that a reproducible production of glass parts is generally very difficult. Thus it was decided not to use any glass parts.

All materials that are in direct contact with the chemicals should be made of Hastelloy, Teflon or Kelef (better mechanical properties than Teflon). All these materials can be used up to 200 °C. For all other materials used in the calorimeter the chemical resistance is not important, only the temperature resistance is still required.

With this selection of materials the requirements in Chapter 3.2 are met.

3.3.2 Split fast and slow heat-flow changes by introducing an intermediate thermostat

To fulfill all the requirements formulated in Chapter 3.2 none of the three basic calorimetric principles explained in Chapter 2.1.1 are suited. Either they are too slow for strictly isothermal controlling of fast and strong reactions, require too much calibration time or are too sensitive to changes of the overall heat-transfer coefficient (see also discussion in Chapter 2.1.5). Another drawback of all principles is that the cooling liquid, required to finally remove all heat generated in the reactor, is in direct contact with the reactor wall (see Figure 2-1). This impedes the selection of an appropriate cooling liquid and makes it difficult that several devices can be connected to the same cryostat (see requirements Chapter 3.2).

In order to meet all requirements, the heat-flow changes taking place in a reaction calorimeter (see Chapter 2.1.3, Figure 2-2 and Equation (2-1)) were analyzed and then separated into the following two groups:

1) Fast and strong heat-flow changes ($\tau \leq 10$ s):

Fast heat-flow changes can be caused by the chemical reaction itself, especially if a reaction is carried out in batch operation. If e.g. the catalyst is dosed in order to initiate the reaction, a strong and nearly instant initial burst of the reaction power q_{React} (Equation (2-2)) will be observed.

A second process that will cause strong and instant heat-flow changes is caused by the start and the stop of the feed in semi-batch operation. Especially if the temperature difference between the feed T_{Dos} and the reaction mixture T_r is large (Equation (2-4)) the change of the dosing heat flow q_{Dos} will be large.

A third fast heat-flow change can be caused by a heat of mixing. Similar to q_{Dos} the fast changes will be at the beginning and end of the dosing period.

2) Slow and weak heat-flow changes ($\tau > 10$ s):

Most of the slower heat-flow changes are caused by the ongoing chemical reaction. Two heat flows will therefore change: 1) The reaction power q_{React} (Equation (2-2)) and 2) The heat flow through the reactor wall q_{Flow} (Equation (2-9)) if either the overall heat-transfer coefficient U or the heat-transfer area A change due to changing physical properties of the reaction mixture (density, heat capacity, viscosity or thermal conductivity (see Chapter 2.1.3.1)). As stated by [Karlsen et. al. 87, a] heat-flow changes due to changes of U are generally slower processes.

A second, generally slow heat-flow change is the change of q_{Flow} during the dosing of reactants due to an increasing heat-transfer area A . In contrast to the fast and instant processes related to the dosing described above, this change is not step like but generally corresponds to a linear increase spread over to the whole dosing period.

Although not all possible heat-flow changes were analyzed it can be concluded that, even when analyzing reactions that take half an hour or more to complete, fast and instant heat-flow changes can always occur. If reactions are measured with half-life times in the range of minutes, or even less, fast processes will be dominant. A good reaction calorimeter, fulfilling the requirements stated in Chapter 3.2 for the accuracy and the time constant, must therefore be able to compensate heat-flow changes as fast as possible. Also the requirement, that a calibration of the heat capacity of the reactor content should be avoided, can only be achieved if the control of the reaction temperature is fast and accurate. Otherwise heat accumulation in the reactor content would have to be considered requiring the knowledge of the heat capacity (see also Equation (3-1) in Chapter 3.2.1 and Chapter 7.1.3).

From all the different available techniques described in Chapter 2.1.1 and Appendix A.1 the most promising technique is therefore the Power-Compensation principle (see Chapter 2.1.3.3 and discussion in 2.1.5). Compared to other calorimetric principles, the Power-Compensation principle is very dynamic and easy to implement, as no fast responding thermostat for the cooling liquid is required. The experience made with the Power-Compensation principle during the former work by [Pastré 00] showed the feasibility of this technique. Thus the Power-Compensation principle was kept as the main calorimetric measurement principle, also for the new reaction calorimeter.

However as explained in Chapter 2.1.4 the Power-Compensation principle has two main disadvantages:

1. **Hot spots on the compensation heater** can occur due to the small heat-transfer area.
2. The final measured calorimetric signal q_{tot} is **highly sensitive to changes of the heat transfer through the reactor wall q_{Flow}** . This phenomenon is also known as “changing baseline”.

The subject of hot spots will be discussed in Chapter 3.3.4 and can be considered as not significant for this calorimeter. But the problem of the changing baseline, already encountered in the previous work ([Pastré 00] and [Zogg 99]), cannot be neglected. As argued in Chapter 3.2 it is even a requirement of the new reaction calorimeter to measure the change of q_{Flow} during a reaction. Considering also the requirements that the cooling liquid should be separated from the reactor jacket, that the reactor temperature should be independent from the temperature of the cooling liquid it was concluded that an intermediate thermostat has to be introduced between the reactor wall and the cooling liquid of a standard reaction calorimeter (compare with Figure 2-1).

3.3.2.1 Intermediate thermostat designed by Litz

The principle of an intermediate thermostat was first developed by [Litz 83] and is schematically shown in **Figure 3-2**.

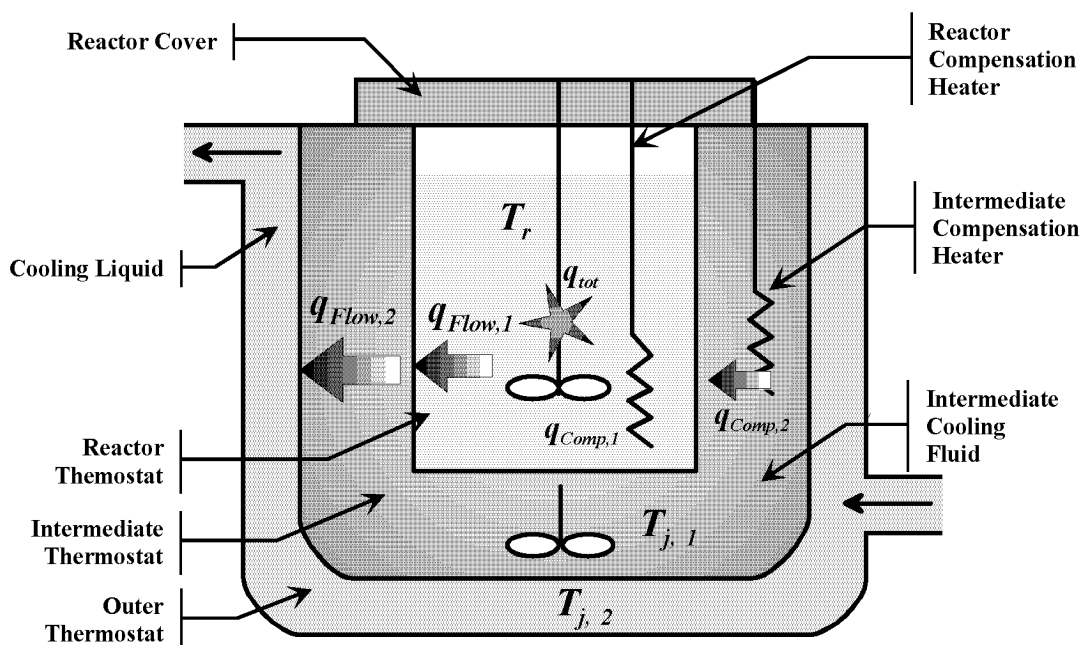


Figure 3-2: Picture of the reaction calorimeter designed by [Litz 83].

As shown in Figure 3-2, Litz designed the intermediate thermostat similar to the inner part of a Power-Compensation calorimeter. A second compensation heater is

maintaining a constant temperature $T_{j,1}$ of the cooling liquid in the intermediate thermostat. The only changing heat flow that has to be compensated by the intermediate compensation heater is $q_{Flow,1}$. The total heat production / consumption of the reaction mixture q_{tot} and all other fast heat-flow changes described above are already compensated by the inner compensation heater. Therefore in $q_{Flow,1}$ only the slow heat-flow changes described above remain. The temperature of the cooling liquid in the outer thermostat is kept at constant temperature $T_{j,2}$. Thus the heat flow from the intermediate thermostat into the cooling liquid of the outer thermostat $q_{Flow,2}$ can be assumed to be constant because $T_{j,2}$ as well as $T_{j,1}$ are both constant.

By introducing the intermediate thermostat the following goals are achieved at the same time:

- ❖ **A changing baseline during a reaction measurement can be measured online** by the power consumption change of the intermediate compensation heater (see requirements in Chapter 3.2).
- ❖ **The circulation cooling liquid is no more in direct contact with the reactor wall** (see requirements in 3.2).
- ❖ **The temperature of the reactor can be chosen more independently from the temperature of the cooling liquid** as $T_{j,1}$ can be adjusted as well (see requirements in Chapter 3.2).
- ❖ **Only slow heat-flow changes (see above) have to be handled by the intermediate thermostat.** The changes of q_{tot} are already compensated by the inner compensation heater and do not “flow out” into the intermediate thermostat.

3.3.2.2 Complete redesign of the intermediate thermostat proposed by Litz

Unfortunately there are two big drawbacks linked to the remarkable design concept proposed by Litz:

A) A more powerful cryostat is required

The temperature has to increase in the following order: $T_r > T_{j,1} > T_{j,2}$. Thus the temperature of the cooling liquid has to be chosen much lower compared to a standard Power-Compensation calorimeter. Additionally the cooling power of the cryostat, used to control the temperature $T_{j,2}$, does not only have to remove the power of the reactor compensation heater $q_{Comp,1}$ but also the power of intermediate compensation heater $q_{Comp,2}$:

$$q_{Flow,2} \approx q_{Comp,1} + q_{Comp,2} + q_{tot} \quad (3-6)$$

Consequently the cryostat has to remove more heat at a lower temperature level. Thus a much more powerful cryostat is required, compared to a standard Power-Compensation calorimeter.

B) Delicate construction of the intermediate thermostat

The intermediate thermostat again requires a cooling liquid and good circulation. This construction concept does not meet the requirement of an easy calorimeter manufacturing at all.

C) Difficult introduction of an IR-ATR probe

As discussed in Chapter 1.2 the developed reaction calorimeter should be combined with a standard IR-ATR probe. These probes are generally made of a Hastelloy tube with a diameter of about 16 mm. Such probe would have to be introduced from the side and would thus lead through the intermediate as well as the outer thermostat in Figure 3-2. This task would be difficult to achieve.

It was therefore decided to construct a completely new type of intermediate thermostat that meets the requirements formulated in Chapter 3.2 closer than the proposal of Litz does. The following changes were made:

- ❖ The **cooling liquid** of the intermediate thermostat was **replaced by a copper block**.
- ❖ The **intermediate compensation** heater was **replaced by Peltier elements**.
- ❖ The **IR-ATR probe was introduced** from the side to make a proper handling of the optical connections feasible.

The concept of the new intermediate thermostat was patented in [Zogg et. al. 00].

The new design is schematically shown in **Figure 3-3**.

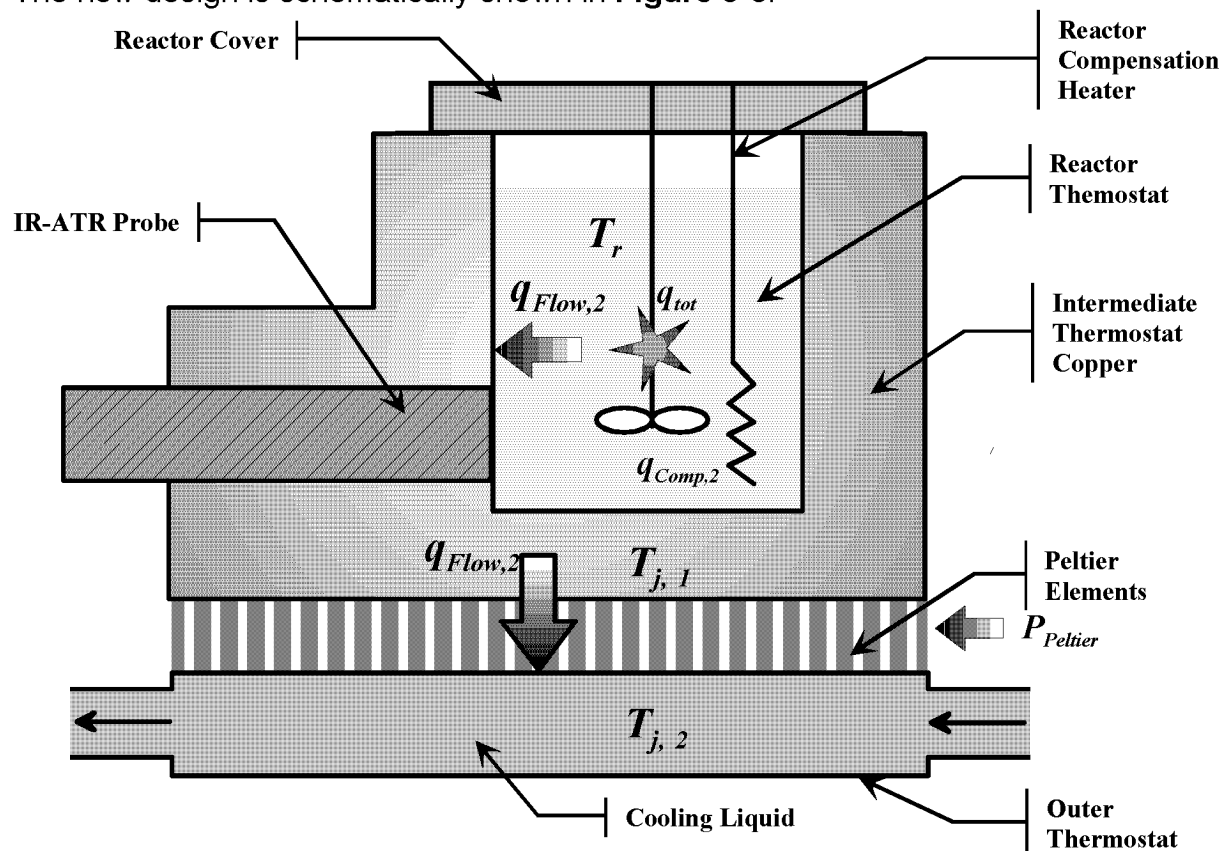


Figure 3-3: Schematical representation of the new intermediate thermostat using Peltier elements.

The drawbacks of the Litz design are circumvented in the following way:

A) A less powerful cryostat is required

By replacing the intermediate compensation heater with Peltier elements, the requirement that $T_{j,2} < T_{j,1}$ does not have to be fulfilled because Peltier elements can also act as cooling devices. The cooling potential of Peltier elements however is depending on the difference between $T_{j,2}$ and $T_{j,1}$. Generally the cooling potential is maximal if $T_{j,2} = T_{j,1}$ and zero if $T_{j,2} \approx T_{j,1} + 60 \text{ K}$ (a more detailed calculation example is given in Appendix C.7.2). Peltier elements can also act as conventional heating element if the direction of the current is reverted. No temperature restrictions exist in the heating mode except to the maximal operating temperature which is about 200°C .

Though $T_{j,2}$ is allowed to be higher than $T_{j,1}$ the total heat that has to be removed by the cryostat, used to control the temperature of the cooling fluid, is higher compared to a standard Power-Compensation calorimeter (compare to Equation (3-6)):

$$q_{Flow,2} \approx q_{Comp,1} + P_{Peltier} + q_{tot} \quad (3-7)$$

where $P_{Peltier}$ is the electrical power consumption of the Peltier elements ($= I_{Pelt} [\text{A}] \times U_{Pelt} [\text{V}]$). Thus more heat has to be pumped but at a higher temperature level. Compared to the design proposed by Litz a less powerful cryostat is required.

B) Simple intermediate thermostat

Compared to the intermediate thermostat suggested by Litz, the new design only contains solid materials with nearly temperature independent thermal conductivity properties. Therefore the manufacturing and application will be much simpler. A further benefit of this design is that eventual thermal simulations and characterizations of this metal jacket will be much easier because no fluid convection occurs inside the thermostat (see Chapter 7.1.3).

C) Introduction of the IR-ATR probe

As shown in Figure 3-3 a standard ATR-Probe can be introduced into the reactor. The tempering of the ATR-probe is achieved by the slightly asymmetric construction indicated in Figure 3-3.

Additionally the following improvement to the Litz design is achieved:

By using Peltier elements instead of a compensation heater, the jacket temperature $T_{j,1}$ can even be chosen more independently from $T_{j,2}$ because cooling is possible as well. Thus the requirements for parallelisation (see Chapter 3.2) are better met and it should be possible to connect several reactors to the same external cryostat. Also for applications at lower temperature this design will be superior.

There is also a drawback compared to the Litz design: Due to the slower heat conduction in the copper block compared to the stirred, liquid system of the Litz design and the bigger heat capacity of the main dynamic element (Peltier elements compared to compensation heater, compare to Chapter 2.1.4) a somewhat worse dynamic behavior of the new design can be expected. This problem will be addressed in Chapters 3.3.6, 3.7.2, and 6.1.4.

An additional drawback results from the ATR-Probe. Because it has to be introduced from the side, the Peltier elements are only covering the bottom of the copper jacket. This results in an inhomogeneous heat flow from the reactor wall to the Peltier elements (see Figure 3-9 in Chapter 3.4.2 and the redesign described in Chapter 7.1.1). Additionally there is more “passive” area, meaning that the main part of the copper jacket is not shielded from the ambient temperature. Therefore good thermal insulation is required for this type of thermostat and eventual corrections due to changes of the ambient temperature have to be considered (see Chapters 3.7.3 and 6.1.5). The same problem is encountered with standard Heat-Balance type calorimeters, without an intermediate thermostat (see Equation (2-18) in Chapter 2.1.3.4).

Finally it can be concluded that most of the requirements set in Chapter 3.2 are met by the presented new calorimeter design. The basic concept is to split fast and slow heat-flow changes and to control them separately by an inner- and intermediate thermostat.

3.3.3 Steady-state temperature profiles of the new calorimeter at different operating conditions

As an extension to the description of the operation principle of the Power-Compensation technique in Chapter 2.1.3.3 similar reflections can be carried out for the new calorimeter. This will be done according to the steady-state temperature profile that is schematically shown in **Figure 3-4** (compare Figure 2-5).

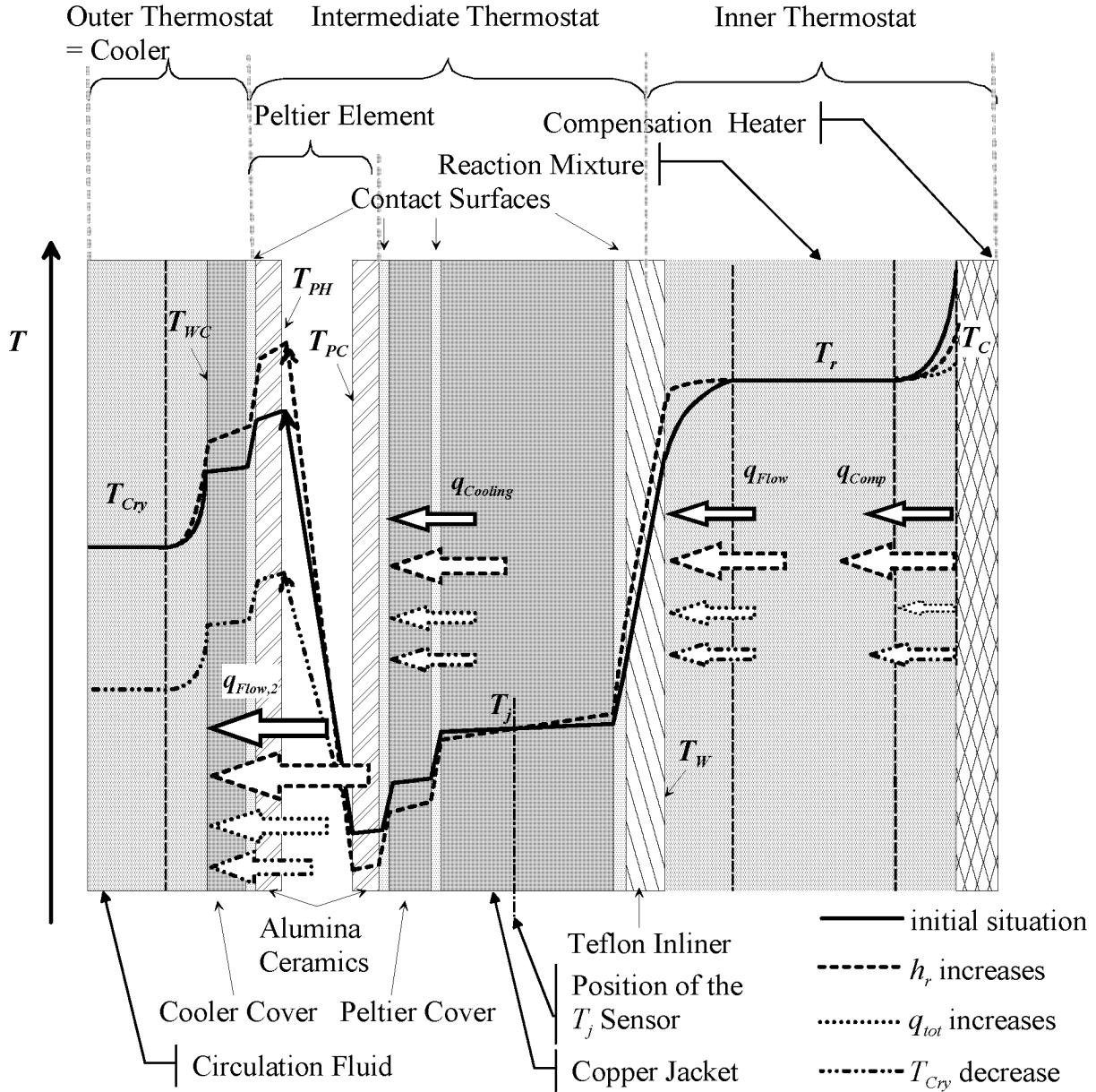


Figure 3-4: Steady-state temperature profile when heat flows from the reactor content ($T = T_r$) through the reactor wall into the copper jacket ($T = T_j$) and finally through the peltier elements into the cooler with the circulating fluid from the cryostat ($T = T_{Cry}$). T_r is controlled at isothermal conditions by varying q_{Comp} . T_j is controlled at isothermal conditions by varying $q_{Cooling}$.

Figure 3-4 shows more details (important for the discussion of the steady-state temperature profile) compared to Figure 3-3. However the asymmetric construction of the copper jacket is ignored for illustration purposes. Some names are adapted to fit the future nomenclature used for all further calculations. $T_{j,1}$ is replaced by T_j , $q_{Flow,1}$ by q_{Flow} and $T_{j,2}$ by T_{Cry} . **A new heat flow $q_{Cooling}$ is introduced and should not be confused with $q_{Flow,2}$. The heat flow $q_{Cooling}$ represents the total heat pumped by the Peltier elements on the reactor side.** According to Figure 3-3 $q_{Cooling}$ can be expressed as follows:

$$q_{Cooling} = q_{Flow,2} - P_{Peltier} \quad (3-8)$$

$P_{Peltier}$ ($= I_{Pelt} [A] \times U_{Pelt} [V]$) is not shown in Figure 3-4.

If heat flows from the compensation heater to the circulating fluid in the outer thermostat the following layers are passed (indicated in Figure 3-4):

1. Compensation heater
2. Reaction mixture
3. Teflon inliner that protects the copper jacket from corrosion.
4. Air gap between the Teflon inliner and the copper jacket (contact surface).
5. Copper jacket. Figure 3-4 is only a schematical picture as in reality the copper jacket has a three dimensional shape and the heat flow will not occur homogeneously as suggested by Figure 3-4.
6. Contact surface. In order to increase the thermal conductivity this connection is improved by the application of thermal grease (see Appendix C.7.1).
7. Peltier cover plate, made of copper. It is used to fix the Peltier elements onto the cooler.
8. Contact surface with thermal grease.
9. Alumina ceramics plate of the Peltier elements.
10. The semiconductor parts of the Peltier elements (not shown in Figure 3-4).
11. Alumina ceramics plate of the Peltier elements.
12. Contact surface with thermal grease.
13. Cover plate of the cooler, made of copper.
14. Circulating fluid inside the cooler.

The relative thicknesses of these layers shown in Figure 3-4 are not the same in reality but are of similar size (compare to construction Figure 3-6 and Figure 3-12).

The straight black temperature profile in Figure 3-4 represents the initial situation in which no reaction occurs ($q_{tot} = 0$, Equation (2-1)). Therefore the heat flow through the reactor wall (q_{Flow}), the power of the compensation heater (q_{Comp}), the total cooling flow of the peltier elements ($q_{Cooling}$) as well as $q_{Flow,2}$ are constant. The temperature profile inside the semiconductors of the Peltier elements does not have to be linear and is therefore indicated by an arrow. There are basically three different events that will cause a change of this situation:

1. A change of the reactor-side heat transfer, e.g. **an increase of h_r** (see Chapter 2.1.3.1). The resulting temperature profile is shown by the dashed line. q_{tot} does not change and the heat conductivities of all jacket materials are assumed to be independent of the temperature. Therefore the overall heat-transfer coefficient U (Equation (2-10) without h_j) will increase. As T_r and T_j are controlled at isothermal conditions q_{Flow} will increase (Equation (2-9) without h_j). The temperature difference $T_r - T_W$ has to decrease. An increased q_{Flow} is compensated by an **increased q_{Comp}** released by the compensation heater. Assuming identical heat-transfer conditions on the heater wall as on the reactor wall, the heat-transfer coefficient on the heater wall will increase as well. Thus the temperature of the compensation heater (T_C , see also Chapter 3.3.4) might decrease. The increase of q_{Flow} is propagating through the different jacket materials by heat conduction. Therefore all temperature gradients will increase. **Consequently $q_{Cooling}$ has to be increased by increasing $P_{Peltier}$** in order to keep T_j constant. As the measurement of T_j is done at a fixed position inside the copper jacket, the temperature at that point will always be constant. An increased $q_{Cooling}$ and $P_{Peltier}$ will result in an increased $q_{Flow,2}$ (Equation (3-8)). Assuming that the heat-transfer coefficient of the cooling liquid remains constant, the temperature difference $T_{Cry} - T_{WC}$ has to increase. This will result in a higher T_{PH} . On the reactor side of the Peltier elements T_{PC} is decreased. Therefore the Peltier elements have to overcome a bigger temperature difference $T_{PH} - T_{PC}$ resulting in a lower efficiency (see Appendix C.7.2).
2. A change of the total power release or uptake q_{tot} , e.g. an **increasing q_{tot}** . The resulting temperature profile is shown by the dotted line. In order to keep T_r constant **q_{Comp} is decreased**; h_r and the heat conductivities of the jacket materials do not change. Therefore q_{Flow} and the temperature profile through the rest of the reactor will not change. **This demonstrates that all fast heat-flow changes occurring in the reaction mixture will not disturb the intermediate and outer thermostat as they are already compensated by the inner thermostat** (compare to Chapter 3.3.2). As q_{Comp} is decreased and the heat transfer on the heater wall does not change, T_C will decrease.
3. Keeping in mind that the new reactor should be independent to changes of the temperature of the cooling liquid T_{Cry} (see Chapter 3.2) it is important to reflect the consequences of such a change. The temperature profile caused by a **decrease of T_{Cry}** is shown by a dash-dotted line. The temperature change is compensated by **decreasing $P_{Peltier}$** in order to keep T_j constant. However the **heat flows q_{tot} , q_{Flow} , $q_{Cooling}$, q_{Comp}** and the corresponding temperature profiles **remain constant**, but $q_{Flow,2}$ will decrease. Consequently $q_{Cooling}$ (see Chapter 3.7.2) must be used in the heat-flow balance of the calorimeter and not $q_{Flow,2}$. As the temperature difference $T_{PH} - T_{PC}$ decreases, the efficiency of the Peltier elements increases (see also Appendix C.7.2).

3.3.4 Hot spots on the surface of the compensation heater

An often mentioned drawback of the Power-Compensation principle is that due to the small size of the compensation heater local hot spots on the heater surface could occur (see also Chapter 2.1.5). In order to keep the temperature increase on the compensation heater as small as possible, the following two design principles have to be taken into account:

1. The **ratio of reactor volume to heater surface** should be kept as low as possible. This is either achieved by a small reactor volume or by a large compensation heater surface. However a large compensation heater will show undesirable slower dynamics unmaking one of the big advantages of this calorimetric principle (see Chapter 2.1.5). *The Power-Compensation technique should therefore only be used in combination with small reactor volumes.*
2. The compensation heater should be ideally placed in a well mixed zone in order to provide **optimal heat-transfer** conditions.

For the new calorimeter the surface of the chosen compensation heater is 6.3 cm^2 (coiled shape). For a standard experiment with 30 ml of reaction mixture, the ratio of heater surface to reaction volume is about 0.2 cm^{-1} . In a standard Heat-Flow, large-scale reaction calorimetric experiment using a 2 l reaction vessel, filled with 1l of reaction mixture the ratio of wet wall surface to reaction volume is about 0.5 cm^{-1} . **It can therefore be concluded that the temperature difference between the reaction mixture and the compensation heater is only about two times bigger than the temperature difference between the reactor wall and the reaction mixture in a large-scale heat-flow experiment.** However the reactor wall will be colder than the reaction mixture temperature whereas the compensation heater surface will be hotter (compare Figure 2-5 to Figure 2-4). This estimation is true as long as the reactor-side heat-transfer coefficient on the heater surface as well on the reactor wall of the large scale calorimeter are the same. Considering the placement of the compensation heater described below, it is likely that the heat-transfer conditions on the compensation heater of the new calorimeter are superior compared to the situation on the wall of a large scale vessel.

For the new calorimeter presented in this work, the compensation heater was rolled up in the form of a coil that was directly placed under the stirrer in order to provide optimal heat-transfer conditions. The stirrer was designed to push the reaction mixture down onto the compensation heater. This is schematically shown in **Figure 3-5** (left side). In order to determine the temperature increase towards the heater surface at different operating conditions three thermocouples were placed into the reactor according to Figure 3-5 (right side):

3 The new Calorimeter

1. T_r : The normal T_r sensor (thermocouple Type K, 1 mm diameter, 0.6 s time constant) used to control the reaction temperature in all experiments.
2. $T_{r,close}$: A second thermocouple (thermocouple Type K, 0.5 mm diameter, 0.2 s time constant) touches the compensation heater.
3. $T_{r,thin}$: The cover tube of a thermocouple was removed. Only the two very thin electrical wires, responsible for the temperature measurement, were wrapped around the compensation heater.

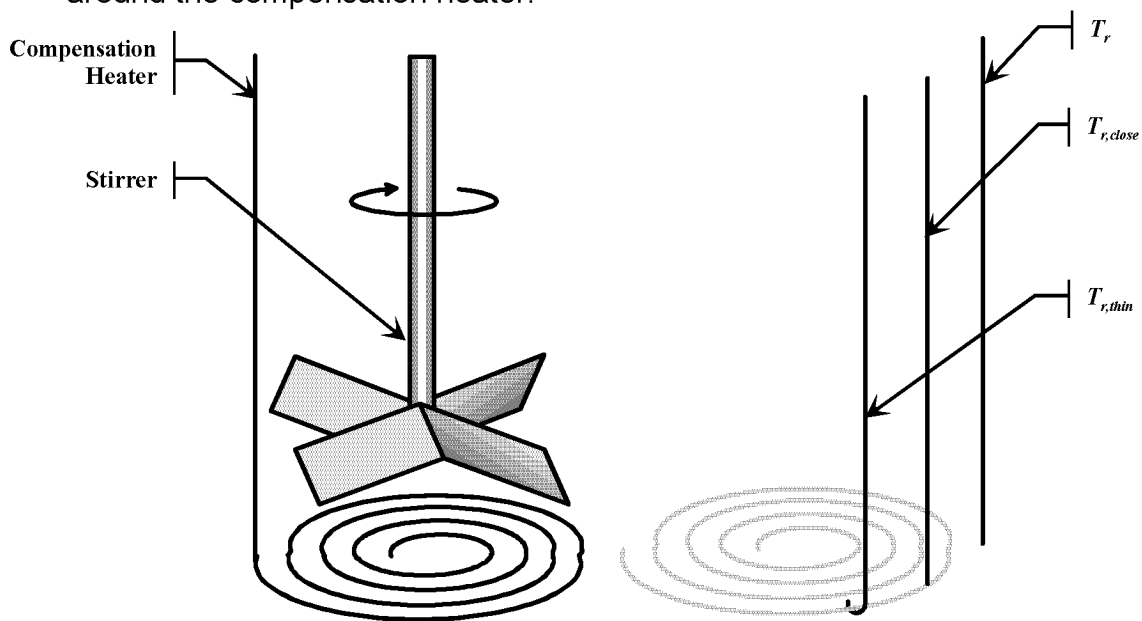


Figure 3-5: Left side: Design of the compensation heater and the stirrer. Right side: Temperature sensors used to determine the temperature increase on the heater surface.

The measurement results of this setup are summarized in **Table 3-1**. High compensation powers were applied and for better comparability they are given in kilo watts per volume of the reactor content.

The temperature increase is only about 15 K in a worst-case situation of highly viscous media, such as glycerin, and applying a compensation power of 2 kW/l. Thus for a standard application (q_{Comp} reaches a maximum of 0.5 kW/l) a temperature increase of only 4 K can be expected.

As between T_r^{close} and T_r no difference could be measured in any case, the temperature increase is supposed to take place in a small space around the heater.

Table 3-1: Measured range of the temperature increase towards the compensation heater surface at different operating conditions ($T_r = 20 \dots 60 \text{ }^\circ\text{C}$).

Reactor content	<i>Dyn. Viscosity at 18 °C [Römp]</i> [mPas]	q_{Comp} [kW/l]	$T_r^{thin} - T_r$ [K]	$T_r^{close} - T_r$ [K]
<i>Water</i>	1,056	1.3	4...10	0
<i>Water</i>	1,056	2	7...15	0
<i>Glycerin (87%)</i>	1600	1.3	10...12	0
<i>Glycerin (87%)</i>	1600	2	10...17	0

3.3.5 Calculation concept for the inner (reactor) thermostat

Considering the steady-state profiles at different operating conditions shown in Figure 3-4 the main dynamic elements of the reactor thermostat (see explanation in Chapter 2.1.5) are the compensation heater and a part of the Teflon inliner as they change their temperature during an isothermal experiment. However the temperature changes of the reactor wall (Teflon inliner) as well as the compensation heater are only small. Additionally the absolute heat capacity [J/K] of these dynamic elements is much smaller compared to the reaction mixture. Therefore these dynamic effects are neglected and thus the isothermal steady-state heat-flow balance for Power-Compensation calorimeters is used (see Chapter 2.1.3.3). However the temperature of the reaction mixture still changes during a reaction run. The errors made by using an isothermal heat-flow balance were mentioned in Chapter 3.2.1 and will be further discussed in Chapters 6.1.1 and 7.1.3.

3.3.6 Calculation concept for the intermediate (jacket) thermostat

Considering the steady-state profiles at different operating conditions shown in Figure 3-4 the main dynamic elements of the reactor thermostat are the different materials of the reactor jacket as well as the Peltier elements and even part of the cooler. However as discussed in Chapter 3.3.2 the intermediate thermostat does only have to deal with slower processes. Therefore to describe the intermediate thermostat a steady-state isothermal heat-flow balance is used as an initial approximation. In a second step a time correction of this steady-state heat-flow balance is applied in order to increase the accuracy. The time correction was carried out on the basis of a black-box model (detailed description in Chapter 3.7.2, further analysis of its importance in Chapter 6.1.4).

3.4 Design of the new calorimeter

3.4.1 Complete reactor and overview

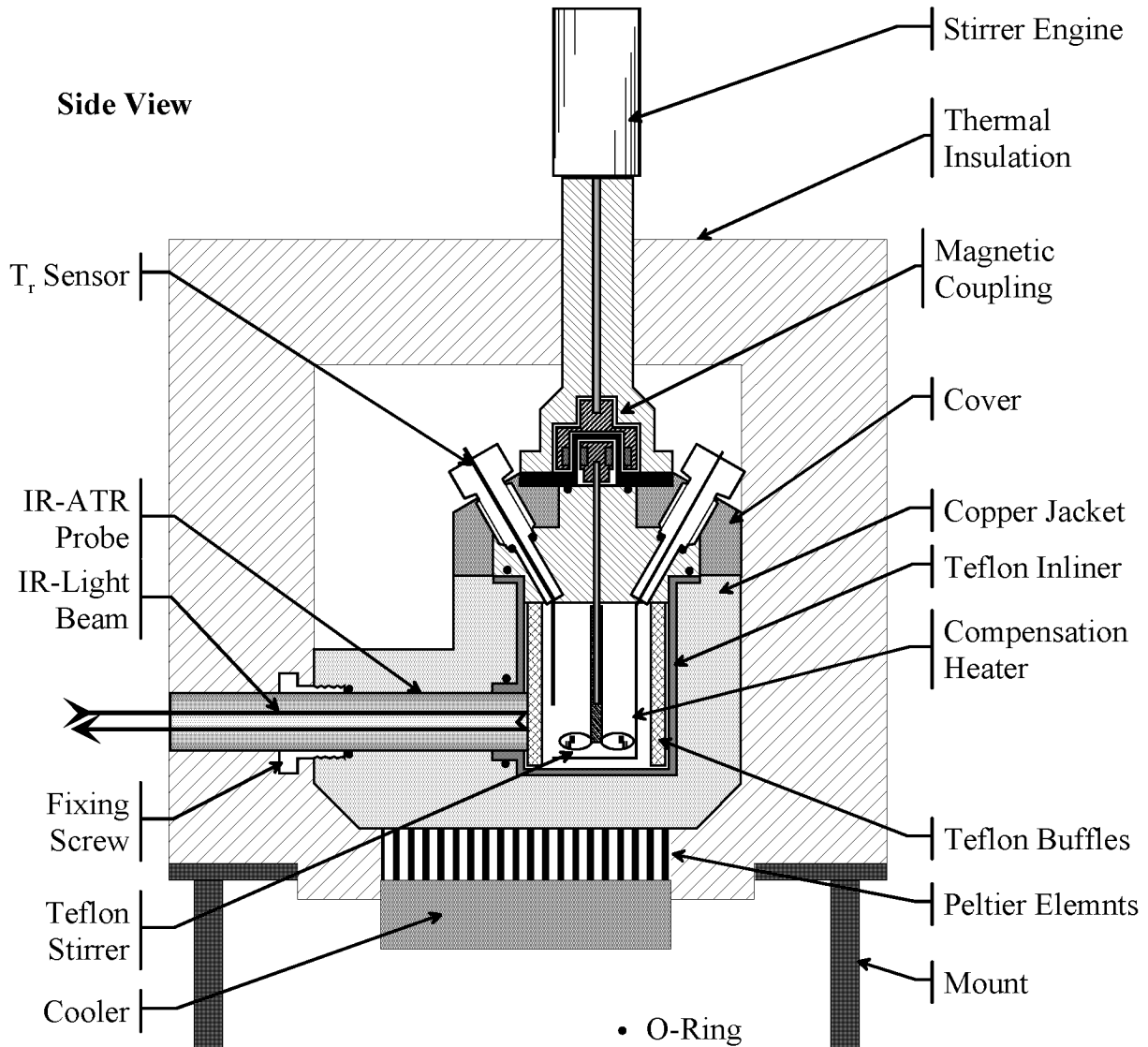


Figure 3-6: Design of the new calorimeter.

Table 3-2: Characteristic dimensions of the new calorimeter according to the description in [VDI Wärmeatlas].

Description	Size
Diameter of the reactor	40 mm
Height of the reactor	50 mm
Diameter of the stirrer	23 mm
Length of the stirrer blades	5.5 mm
Distance of the stirrer to the bottom of the reactor	6.5 mm
Angle of the stirrer blades	45°C
Number of stirrer blades	4
Width of the Buffles	4 mm

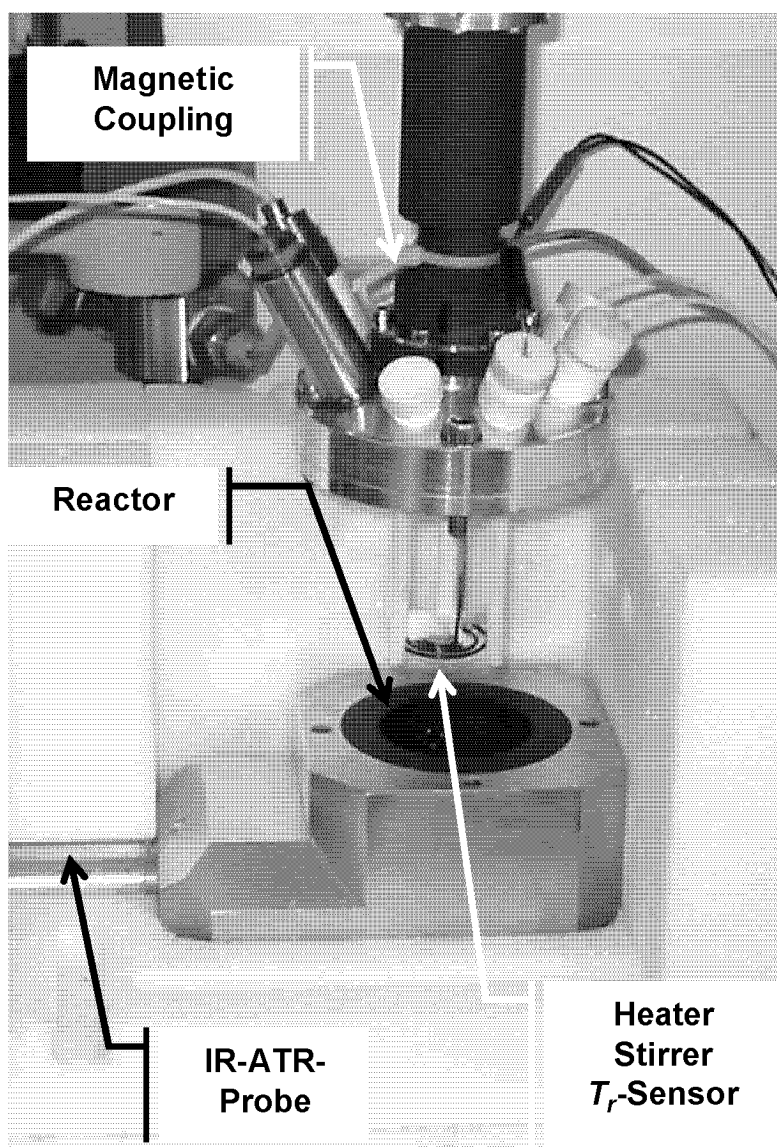


Figure 3-7: Main parts of the new calorimeter.

Figure 3-6 shows the cross section of the new calorimeter and Figure 3-7 a picture of the actual setup.

- ❖ The copper jacket is further described in Chapter 3.4.2.
- ❖ The cover as well as the connections in Chapter 3.4.3.
- ❖ The cooler, the Peltier elements and the T_{Pelt} sensors in Chapter 3.4.4.
- ❖ The compensation heater in Chapter 3.4.5.
- ❖ All the other parts shown in Figure 3-6 are explained in more details in Appendix C.1 to C.5.
- ❖ The exact position of the temperature sensors in the copper jacket in Appendix C.6.

3.4.2 Copper Jacket

The jacket of the calorimeter is the crucial part of the whole device. The jacket has several tasks to fulfill, which will lead the design and the choice of material:

- ❖ Heat conduction from the reactor wall to the Peltier elements should be as fast as possible keeping the reactor wall temperature as homogenous as possible.
- ❖ The IR-ATR probe has to be tempered to the jacket temperature T_j .
- ❖ The Teflon inliner has to be supported to reach the desired pressure resistance up to 10 bar.
- ❖ The IR-ATR probe must be fixed inside the jacket in order to resist to a maximal reactor pressure of 10 bar (see fixing screw in Figure 3-6).
- ❖ The reactor cover must be fixed to the reactor jacket to resist 10 bar reactor pressure (four screws are used (see Figure 3-10)).
- ❖ As soon as the cover is removed the reactor jacket might get in contact with chemicals and should therefore be resistant to chemicals.

First of all the **appropriate material** has to be selected. The material used must have maximal thermal conductivity in order to reduce temperature gradients inside the reactor as well as improving the dynamics of the jacket. The material should also have low heat capacity in order to improve the dynamics of the jacket. As the geometry and thus the total volume of the jacket will be rather dominated by other design constraints (see later) it is not useful to compare heat capacities in the standard units of [J/kg/K] but rather as volume specific heat capacities [J/m³/K]. For some important materials these two crucial properties are plotted in **Figure 3-8**. Last but not least the material should show reasonable strength in the whole temperature range (up to 200°C), especially for the threads of the different mounting screws. This last constraint clearly restricts the material choice to metals.

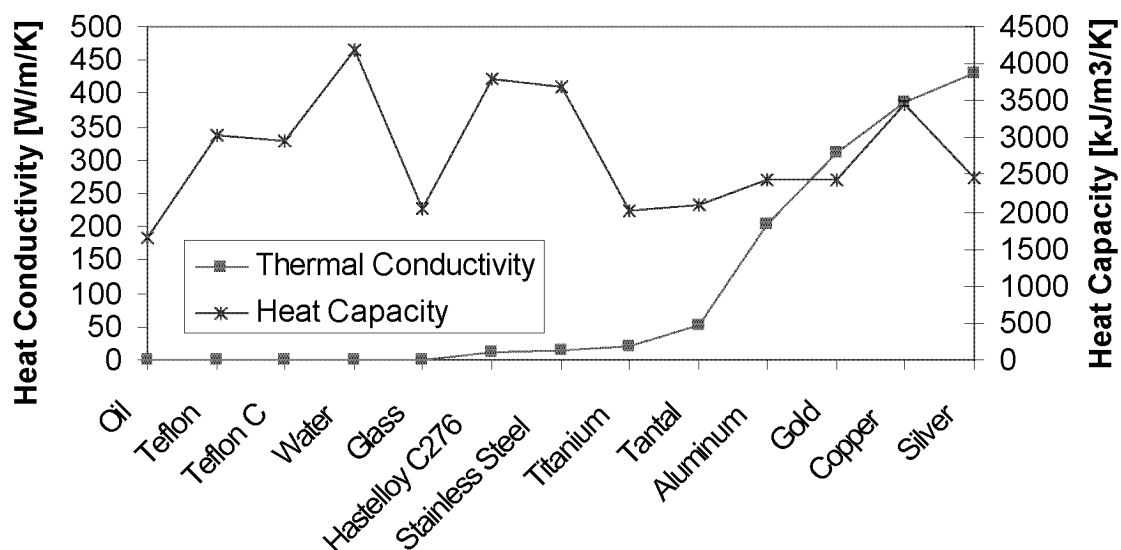


Figure 3-8: Comparison of the thermal conductivity and the heat capacity (volume specific) of important materials and substances [Melcor]. The materials are sorted by increasing thermal conductivity.

Considering the properties shown in Figure 3-8 it becomes clear that the volume specific heat capacity is only changing by a factor of 2 for all materials whereas the thermal conductivity shows a broad spectrum. Assuming equal influence of the two properties on the **dynamic behavior of the reactor jacket**, the material with the largest ratio of thermal conductivity to heat capacity has to be selected. The best materials are therefore silver (0.17), gold (0.13), copper (0.11) and aluminum (0.08). Because of the bad mechanic properties of gold and silver, copper was selected as jacket material. The absolute heat capacity of the copper block (as shown in Figure 3-6) is therefore about 1.6 kJ/K.

The second topic is the **optimal design of the reactor jacket**. Most of the geometry is given or restricted by the size of the reactor, Peltier elements, IR-ATR Probe as well as the mounting screws of the reactor cover. It is also clear that unnecessary right angle edges have to be removed (see also Figure C-2). However the wall thicknesses can still be varied. The arguments that lead to the actual design are therefore shortly explained.

- A) In order to have **small temperature gradients** inside the copper jacket and therefore a closely homogeneous reactor wall temperature the **heat-transfer area should be large** resulting in thick reactor walls.
- B) In order to have a **fast responding system** the reactor walls should be as thin as possible.
- C) **Heat conduction pathways are not homogenous** as shown in **Figure 3-9** and do even not always change homogeneously. The wall thickness on the side of the reactor as well as on the bottom of the reactor should therefore not be too small. Otherwise these inhomogeneities cannot be leveled out until the heat flow reaches the Peltier elements.

It is obvious that a compromise between the arguments A to C has to be found.

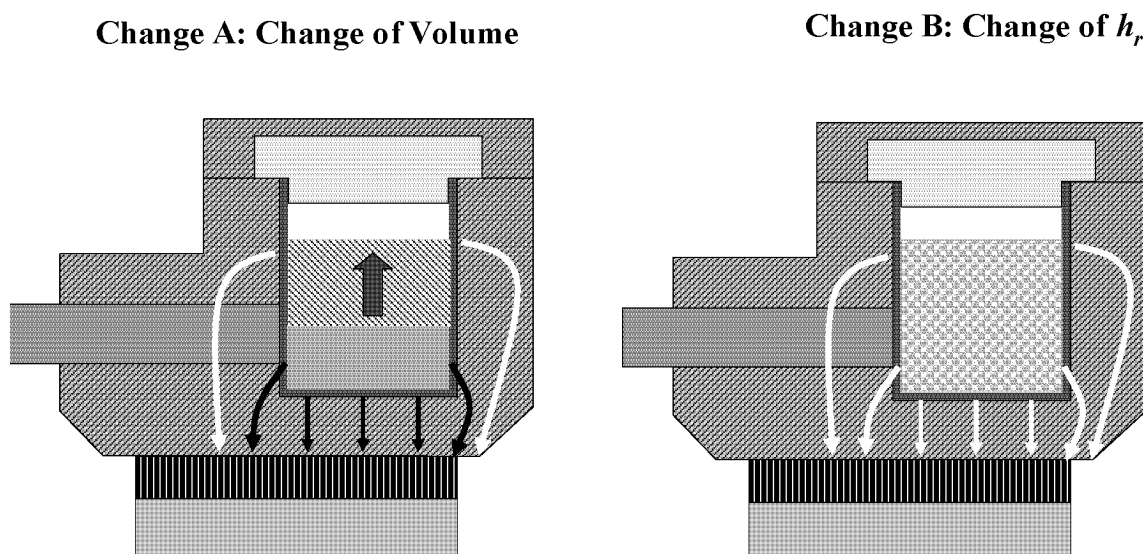


Figure 3-9: Schematic representation of the heat-flow changes inside the reactor jacket for two Situations: A) Change of the reactor volume and B) Change of the reactor-side heat-transfer coefficient h_r . Black arrows indicate that these heat flows do not change; white arrows indicate that these heat-flows change.

The last requirement for the reactor jacket mentioned above is chemical inertness. Therefore the whole copper block was coated with $5\mu\text{m}$ Nickel (chemically) and $5\mu\text{m}$ of Gold (galvanically). This protection would not be suitable for the reactor inside because gold could act as a catalyst in various reactions and the protection of the copper is not good enough. Therefore a **Teflon inliner** (see also comments in the Appendix C.1) is used to finally **protect the copper block from the reaction chemicals**.

3.4.3 Cover, connections and magnetic coupling

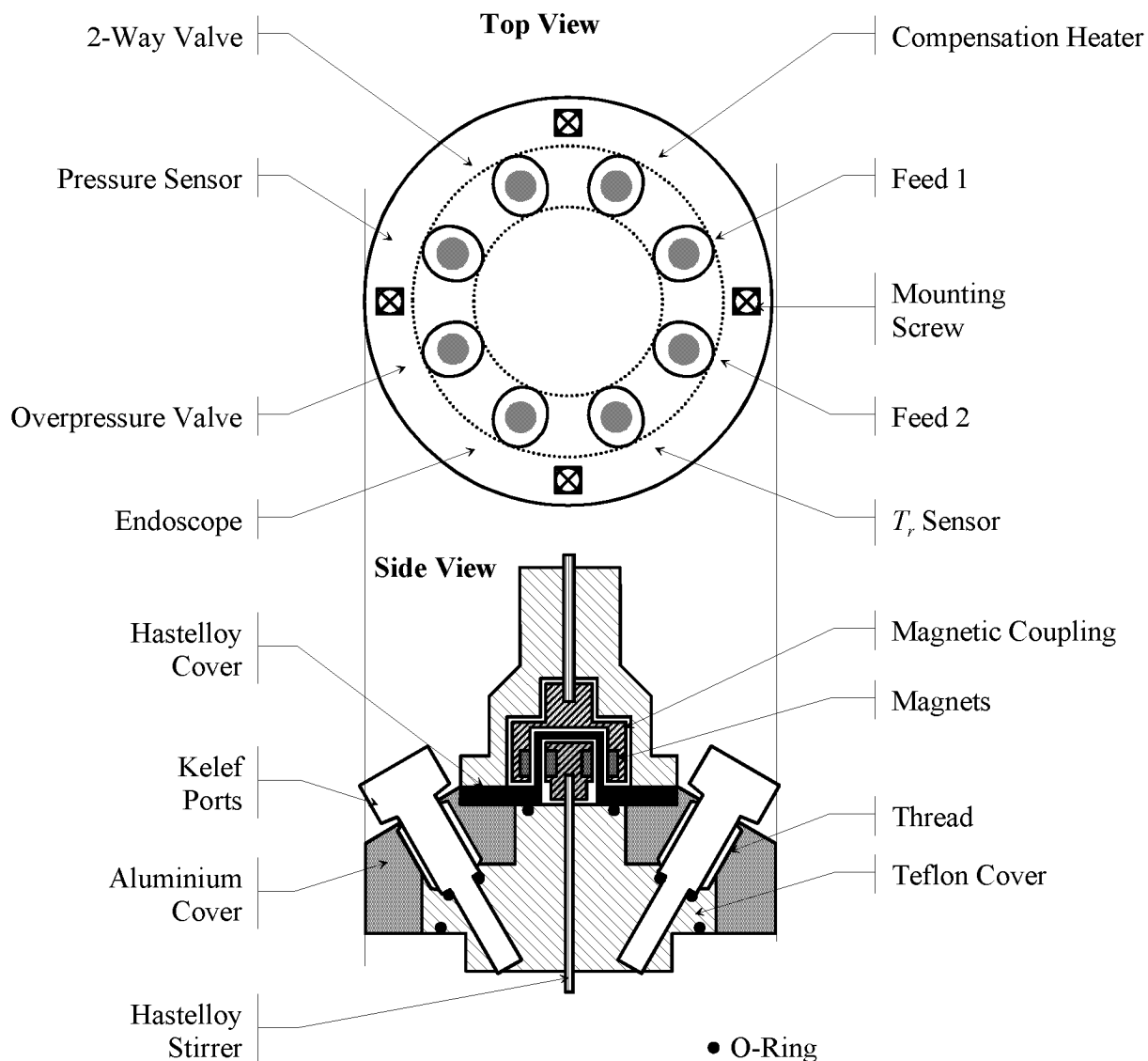


Figure 3-10: Detailed view of the reactor cover and the connections.

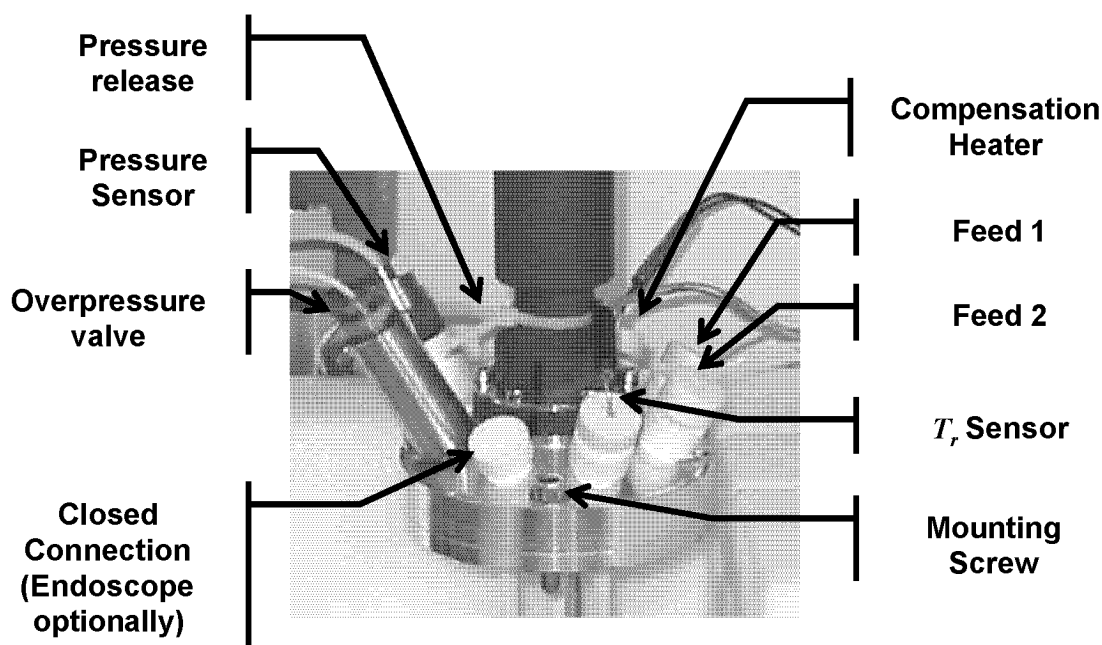


Figure 3-11: Connections and sensors in the reactor cover.

Figure 3-10 shows the cover of the reactor. Besides the problems caused by the miniaturization, the design of the reactor cover was also dominated by its later application in a calorimeter.

Basically the aim was to design a reactor cover that shows a **minimal absolute heat capacity** [J/K]. As the reactor will only be used at isothermal operating conditions the absolute heat capacity of the reactor cover should not influence the measured signals. However any reaction calorimetric experiment can only be started if the device has reached the desired temperature set point and is in thermal equilibrium. Therefore the basic design principle is minimal thermal mass.

Another general problem encountered in calorimetry is that the **reactor cover has a lower temperature than the reactor content**. Especially if the Power-Compensation principle is applied, the reaction temperature will always be higher than the than the temperature of the cover. As it would be quite complicate to implement a separately tempered reactor cover on this scale, the problem was solved by splitting the reactor cover into two parts (indicated in Figure 3-10): 1) An Aluminum cover for the mechanic stability and 2) A Teflon cover that should act as thermal insulation (low thermal conductivity). A second task of the inner Teflon cover is also to protect the aluminum cover from corrosion.

Consequently the eight ports (Figure 3-10 and **Figure 3-11**) were made of Kelef (similar to Teflon but better mechanical properties). Most of the materials, which are in direct contact with the reactor top space, have low thermal conductivities (see also Figure 3-8).

3.4.3.1 Magnetic coupling

The magnetic coupling (see Figure 3-6) was specifically designed for this small scale application. The commercial magnetic couplings are too large and would therefore increase the thermal mass of the cover. The magnetic coupling consists of the following main parts:

1. Outer magnets. As no chemicals will reach here no protection is required.
2. Cover part: This part will actually close the reactor. It is made of Hastelloy in order to meet the pressure requirements and chemical resistance.
3. The inner magnets: The inner magnets, connected to the stirrer shaft, are in direct contact with the chemicals and were therefore protected by a thin Hastelloy cover.

The strength of this magnetic coupling is sufficient to hold the complete stirrer in position. Therefore the Teflon part of the reactor cover can act as a bearing for the stirrer shaft.

3.4.3.2 Connections and Sensors

As shown in Figure 3-10 there are totally eight different connection possibilities. The different connections are also shown in Figure 3-11. The following connections are available in the actual setup:

- ❖ **Compensation heater** (2 mm diameter) (see Chapter 3.4.5).
- ❖ **Temperature sensor** to measure T_r : A thermocouple of type K (1 mm diameter, time constant 0.6 s) was used. The jacket material of the thermocouple is Inconel® Alloy 600, it was purchased from Thermocontrol.
- ❖ **Pressure sensor**: It is directly attached to the reactor cover as can be seen in Figure 3-11. The sensor was purchased from Kulite, HEM-375TM-10 bar A (made of Titanium)
- ❖ **Feed 1 and 2**: Teflon tubes (ID 0.8, OD 1.6 mm) are used for the dosing of the reactants. In one of the feed tubes a thin, Teflon coated thermocouple (Type T, 0.41 mm diameter, time constant 0.08 s) is introduced in order to allow an accurate measurement of the dosing temperature T_{Dos} (see Chapter 2.1.3.2, Equation (2-4)). The thermocouple was purchased from Physitemp (IT-21)
- ❖ **Over-pressure valve**: The over-pressure valve (stainless steel) shown in Figure 3-11 was specifically made for this reactor again keeping in mind that the total thermal mass of the reactor cover should be kept at a minimum.
- ❖ **Endoscope**: An endoscope with diameter 3.8 mm (see Appendix C.8.6) can be optionally connected to the reactor cover in order to have a look inside. It was only used for test measurements.
- ❖ **Pressure-release opening**: The last connection is used in order to safeguard the maximum pressure inside the reactor by a magnetic valve. A Teflon exhaust tube (ID 1.8, O.D. 3.2 mm) is connected to the magnetic valve outside of the thermal insulation.

3.4.4 Cooler, Peltier elements and T_{Pelt} sensors

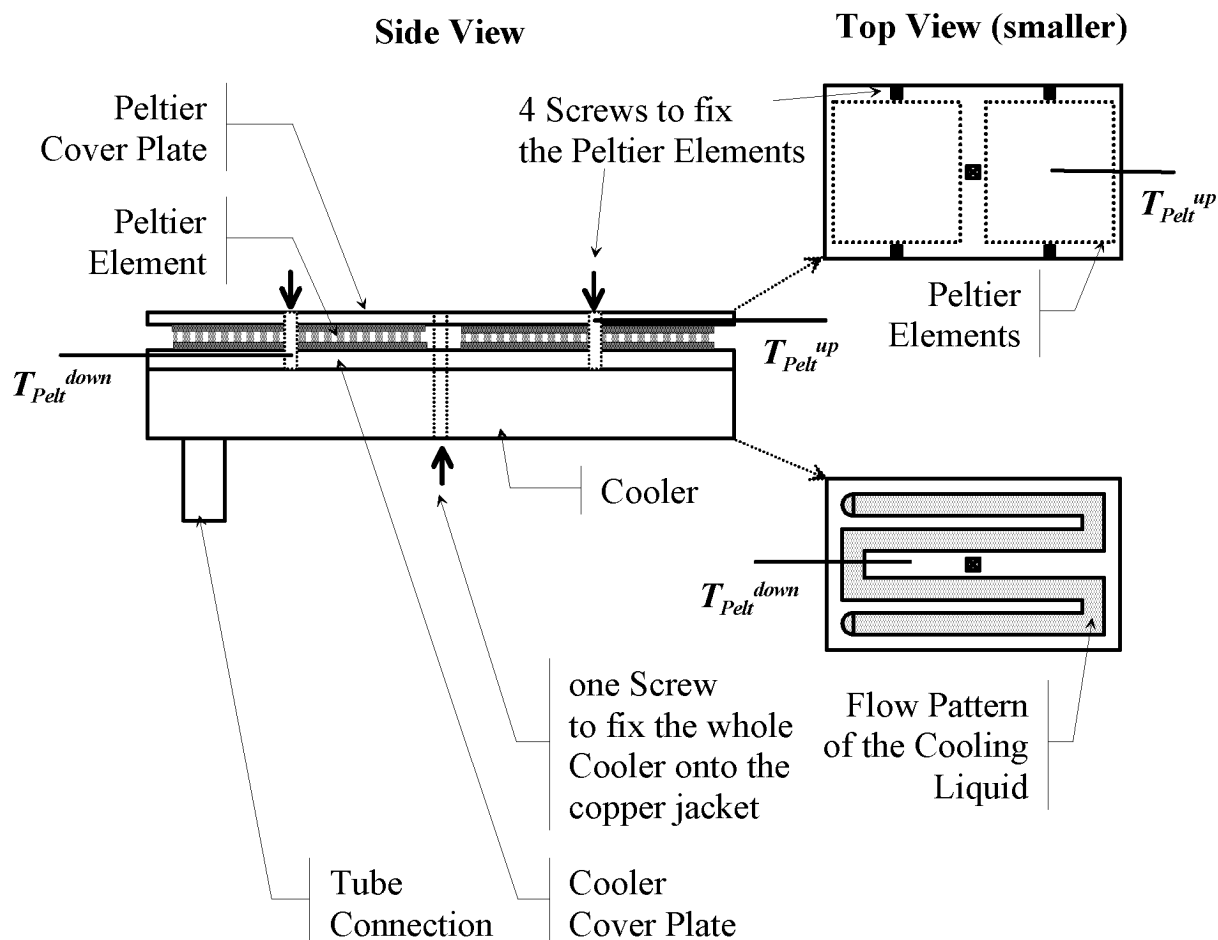


Figure 3-12: Detailed view of the cooler and the assembly of the Peltier elements. The position of the temperature sensors T_{Pelt}^{up} and T_{Pelt}^{down} is indicated as well.

The cooler and the mounted Peltier elements are shown in **Figure 3-12**. The different parts shown are discussed in details in Appendix C.7. The mounting procedure of the Peltier elements and the cooler is carried out as follows:

1. The two Peltier elements are treated with thermal grease and placed on the cover plate (copper) of the cooler (copper). Only as little thermal grease as possible was used. In order to improve the thermal contact, the Peltier elements were moved until they stuck to the cover plate.
2. The Peltier cover plate (copper, also treated with thermal grease) is put on top. It is screwed with four screws onto the cooler in order to fix the Peltier elements on it (see Figure 3-12). These four screws are thermal shortcuts as they will conduct heat from one side of the elements to the other (compare to Appendix D.1). In order to minimize this heat flow stainless steel screws with

low thermal conductivity were used and a hole was drilled into the screws to reduce the heat-transfer area.

3. The mounted Peltier elements were turned on for some time and then the mounting screws were tightened a second time.
4. The top side of the Peltier cover plate (treated with thermal grease) is then firmly pressed onto the bottom of the copper jacket. The whole cooler (including the Peltier elements) is finally fixed to the copper jacket with a single mounting screw (see Figure 3-12). Again a stainless steel screw was chosen and a hole was drilled in order to reduce the heat-transfer area.
5. Finally the cooler was connected to an outside cryostat by isolated tubes.
6. After running the device for some days, the main mounting screw was tightened a second time.

Crucial for the whole mounting procedure is the quality of the thermal contact of all contacting parts [Nagy et. al. 96]. As indicated in Figure 3-4 all these contact surfaces will cause temperature differences especially if air gaps remain. This will impair the dynamics of the whole cooler. Additionally changes over a long time period can be expected [Nagy et. al. 96]. It is therefore important to have a look at the available techniques for thermal contact.

Generally there are three different techniques to improve the thermal contact between different surfaces. They are described in Appendix C.7.1.

More technical details about the Peltier elements, the cooler, the cooling liquid as well as the temperature sensors T_{Pelt}^{up} and T_{Pelt}^{down} are also given in Appendix C.7.2 to C.7.4.

3.4.5 Compensation heater

The same type of compensation heater as used in the previous work [Pastré 00] was also applied here. The heater is manufactured by [Thermocoax]. As **Figure 3-13** shows, it mainly consists of two parts: 1) A cold part going out of the reaction mixture and 2) an active, hot part responsible for the heat flow q_{Comp} . This separation is important because otherwise hot spots on the part of the heater above the reaction mixture could occur. Additionally errors would be expected when the reaction volume and thus the heat-transfer area on the compensation heater would change during the dosing of reactants. The electric resistance of the heater is about 13 Ω .

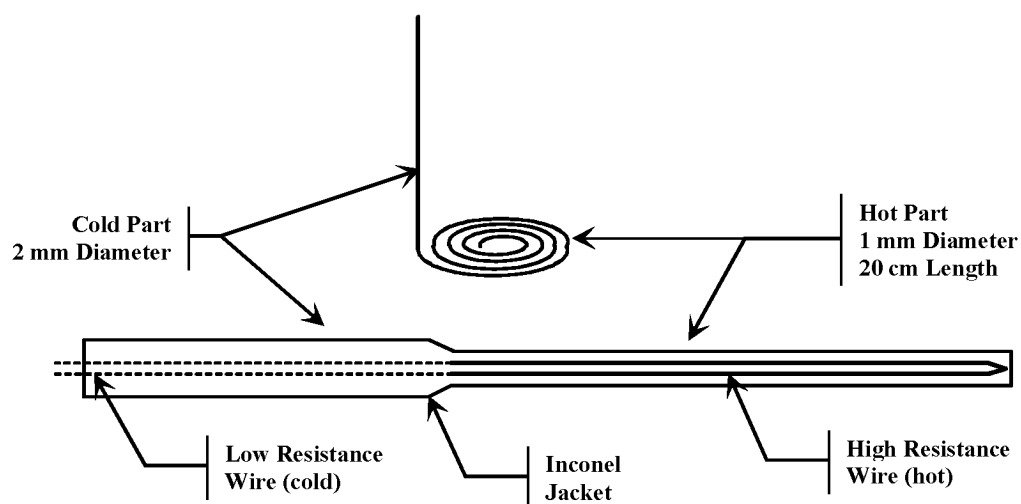


Figure 3-13: Construction of the compensation heater.

See also Chapter 3.3.4.

3.5 Setup and peripheral devices of the whole apparatus

The core of the new reaction calorimeter presented in this work was described in 3.4. This section will only describe the connections, peripheral devices and the software that was developed and used to run the calorimeter.

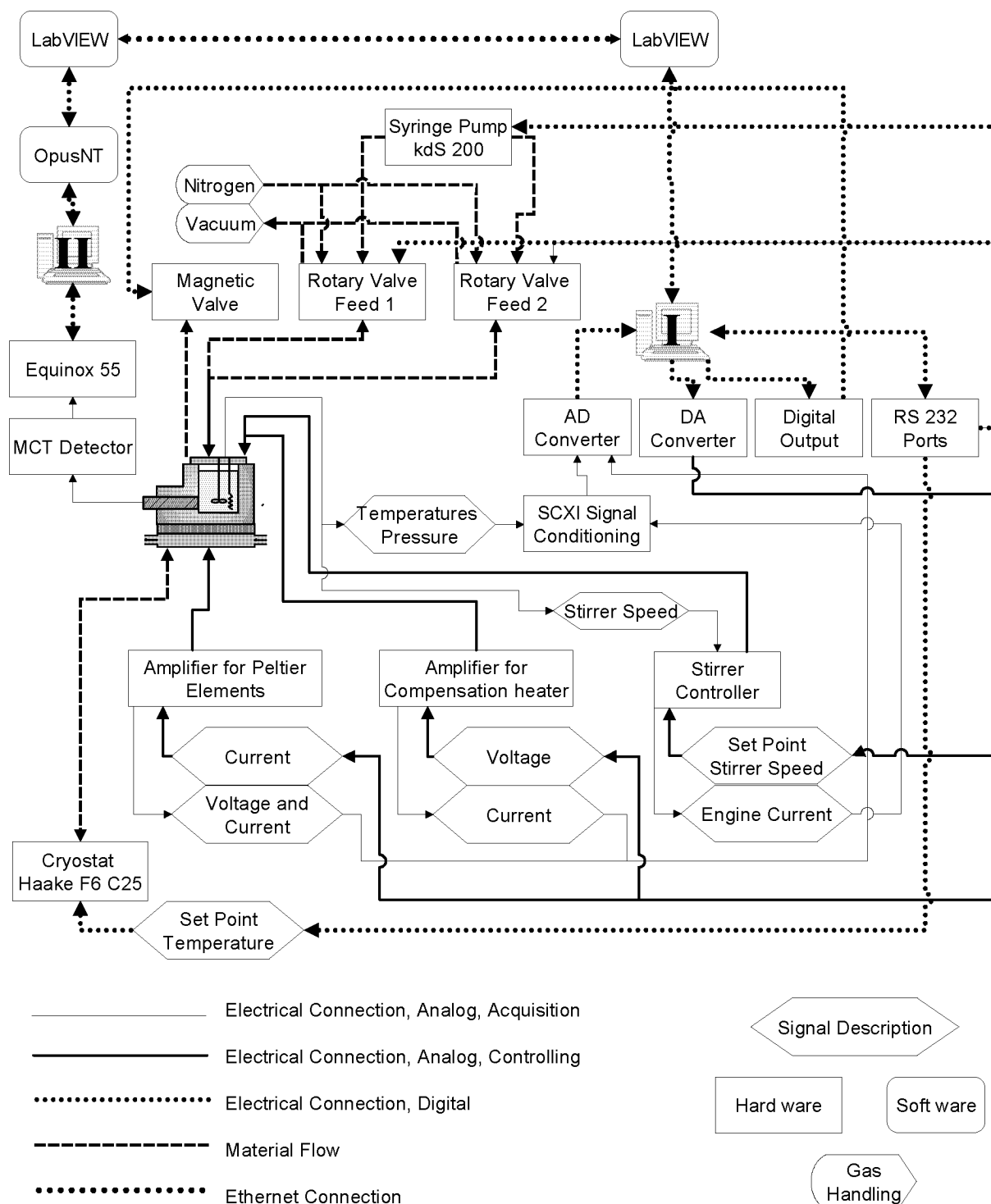


Figure 3-14: Picture of the whole calorimeter including all peripheral as well as infrared measurement devices. The whole application is controlled by a single LabVIEW program.

Figure 3-14 shows the whole setup of the calorimetric device. Most of the individual parts are explained in more details in the Appendix C.8. The different connections and sensors of the reactor cover were already described in Chapter 3.4.3.2. The temperature sensors in the copper jacket are described in Appendix C.6 and the temperature sensors in the cooler in Appendix C.7.4.

3.6 Software and controller

The whole application shown in Figure 3-14 is controlled by a single [LabVIEW] program running on computer I. The program was developed during this work. The infrared measurement, running on the remote computer II, is triggered by the same LabVIEW program (see also Appendix C.8.5). The program allows direct interaction to all devices connected to the system as well as automatic handling of a pre-defined recipe.

The main task of the LabVIEW program is to acquire the data of all sensors and devices (see Appendix C.8.4) as well as to control the reaction temperature T_r and the jacket temperature T_j at isothermal conditions. The program runs on a 1 GHz Intel Pentium with Windows 2000 as operating system. The sampling rate of the data acquisition and the subsequent update of the output channels is 10 Hz. The speed of the program is not triggered by the computer's system time but by the internal timer of the PCI-MIO card inserted into the computer (see Appendix C.8.4). The application is programmed using multithreading technique. This way the 10 Hz sampling rate can be maintained over a long measuring period (days) and eventual delays by the operating system can be handled.

The control algorithm, implemented in the LabVIEW program, will be described in the following section. It will only be explained for the inner thermostat (the power-compensation part) of the calorimeter. Exactly the same principle was applied for the intermediate thermostat (the tempering of the reactor jacket).

In order to fulfill the requirements formulated in Chapter 3.2.2 it was clear that a simple PID controller would not be appropriate. The reason is that the temperature measurement T_r using thermocouples contains a significant amount of noise. This noise will be amplified by the PID controller proportional to the value of the P parameter. Also the D part will strongly amplify the noise. Therefore the noise will also be present in the measured compensation power q_{Comp} and consequently in the calculated total power release or uptake q_{tot} (see Equation (2-14)). Unfortunately the frequency range of the noise of the T_r measurement is in the same range as the fast processes taking place inside the reaction mixture (described in Chapter 3.3.2). Therefore it cannot be simply filtered out. Selecting small values of the parameter P is neither possible because the response of the controller would get much too slow to compensate fast processes.

A solution for this control problem was found on the basis of the following observations:

- ❖ It was observed that the signal-to-noise ratio of q_{Comp} is small during the fast processes and increases as soon as the disturbance is compensated and the set-point for T_r is reestablished.
- ❖ As soon as the set point of the reaction temperature T_r is reached it is possible to switch the PID parameters of the PID controller without disturbing the control process. The reason is that when the deviation from the set-point is small, the P as well as the D part of the controller output are negligible. As the I part of the controller output is used as initial value for the controller with the new PID parameters, the switching will be smooth.
- ❖ As explained in Chapter 3.3.2 the points in time of all fast processes are well defined and for most of the reactions predictable: The start and the stop of the feed.

Based on these reflections the following control strategy was developed. It is shown in **Figure 3-15** and bases on three different sets of PID parameters (“slow”, “medium” and “fast”). They are determined in advance on experimental basis (for exact values see Table 3-3 and Table 3-4).

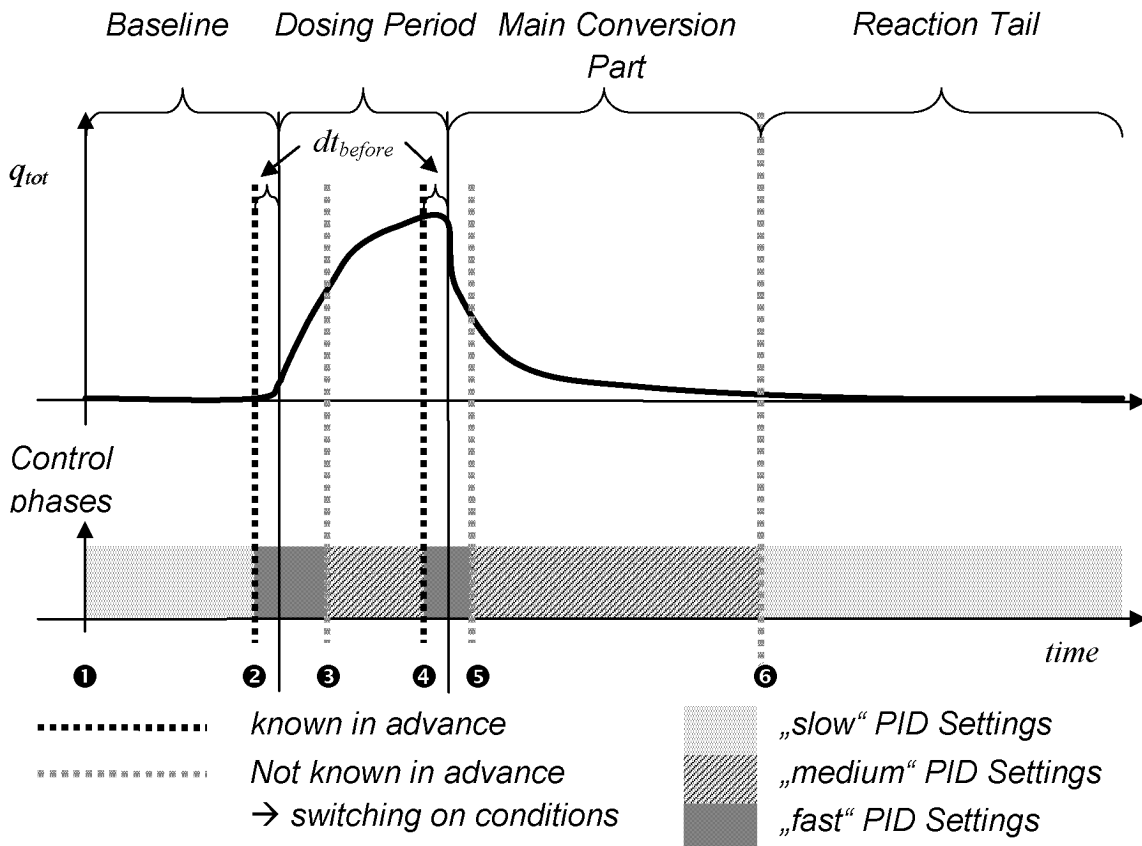


Figure 3-15: Typical reaction profile (q_{tot}) that can be expected for a standard chemical reaction. The control strategy to keep T_r isothermal is indicated (controlling of T_j is analogous).

Description to **Figure 3-15**:

- ❶ During the **baseline measurement** the “slow” set of PID parameters is used as no reaction is taking place.
- ❷ As the **dosing is automatically triggered by the LabVIEW** program the start point is known in advance. Thus dt_{before} seconds before the dosing starts, the “fast” PID parameter set is automatically selected because fast heat-flow changes are expected (see Chapter 3.3.2).
- ❸ As soon as the **three conditions** explained below are fulfilled, the “medium” PID parameter set is automatically selected.
- ❹ Similar to the start of the dosing, the **end of the dosing is known in advance** and fast heat-flow changes are expected. Therefore dt_{before} seconds before the dosing stops, the “fast” PID parameter set is automatically selected.
- ❺ Same as ❸.
- ❻ After a given time delay the “slow” PID parameter set is selected. This point in time is **supplied by the user** and does not have to be precise as the “slow” PID parameter set is **only selected if the three conditions described below** are fulfilled.

A schematic picture of the control algorithm able to deal with this control strategy is shown in **Figure 3-16**.

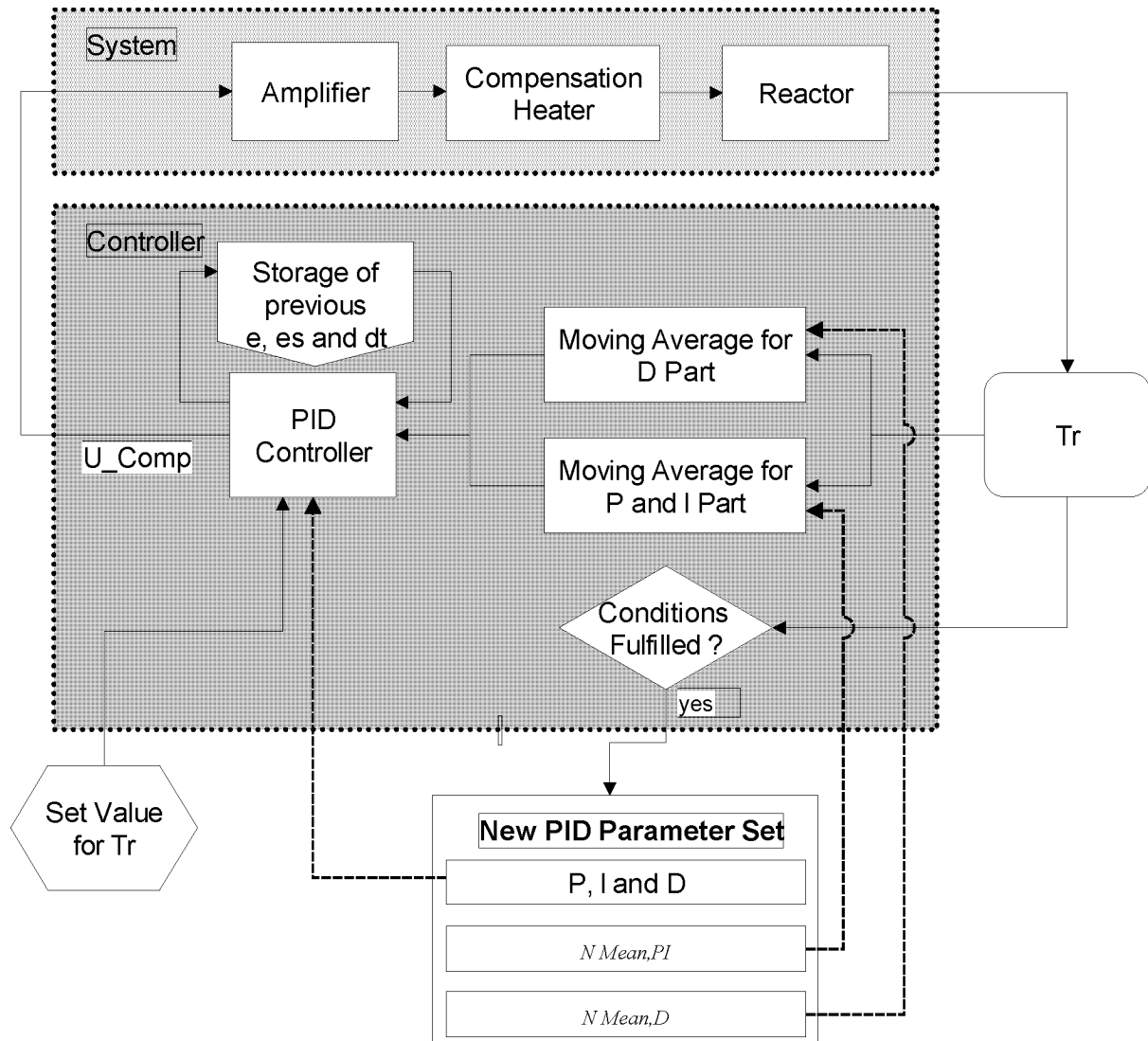


Figure 3-16: Structure of the control algorithm suitable for the control strategy shown in Figure 3-15. Parameter e is the deviation from T_r to the desired set point (used to calculate the P part of the controller output), es the error sum (used to calculate the I part of the controller output) and dt the sampling time (used to calculate the D part of the controller output). $N_{Mean,PI}$ and $N_{Mean,D}$ are the number of points used for the moving average filter of T_r .

The mentioned PID parameter sets “slow”, “medium” and “fast” are listed and described in **Table 3-3**. It is important to note that not only the P, I and D parameters are switched, but also the number of values used for the moving average filter of T_r (see Figure 3-16, $N_{Mean,PI}$ and $N_{Mean,D}$). Thus the filtering of the measured temperature signal can be adjusted to the actual situation.

Table 3-3: Description of the PID parameter sets required to control T_r (compare to the control algorithm shown in Figure 3-16). The loop frequency of the PID controller is 10 Hz.

Name of the PID Parameter Set	Slow	Medium	Fast
Control behavior	Slow	Medium	Fast
Amplification of noise in q_{Comp}	Low	Medium	High
Filtering	Strong	Medium	Weak
P, I, D used in this work	2.5, 0.025, 0	8, 0.3, 2	20, 1.7, 10
$N_{Mean,PI}, N_{Mean,D}$	40, -	20, 20	15, 20
Maximum U_{Comp} [V]	40	40	40

As mentioned (and indicated in Figure 3-15) switching conditions are required when the PID parameter set has to be changed from “fast” to “medium” (Ⓔ and Ⓕ in Figure 3-15) or from “medium” to “slow” (Ⓖ in Figure 3-15). The reason is that the time required by the controller to reestablish the desired temperature set point for T_r is unknown. If switching is done before the point is reached, the succeeding parameter set will not be able to deal with the fast process still going on. If switching is too late, the signal to noise in q_{Comp} will be unnecessarily increased.

In order to find the correct point of time to switch the parameter set, the following three conditions are applied:

Switching conditions:

1) Minimum waiting time: dt_{after} [s]

In order to make the subsequent evaluation possible a minimum time delay of dt_{after} [s] will pass anyway before switching to the next PID parameter set.

2) Maximal deviation from the set point: $Max_{\Delta T}$ [K]

The switching will only occur if the following condition is fulfilled:

$$|T_r - T_{r,set}| \leq Max_{\Delta T} \tag{3-9}$$

Where $T_{r,set}$ is the desired set point for T_r and $Max_{\Delta T}$ the maximum allowed deviation from the set point.

3) Maximal change of T_r versus time: Max_{dT} [K/s]

The switching will only occur if the following condition is fulfilled:

$$\frac{dT_r}{dt} \leq Max_{dT} \quad \frac{dT_r}{dt} \approx \frac{1}{N_{Mean}^{dt}} \cdot \sum_{i=1}^{N_{Mean}^{dt}} \frac{|T_{r,i} - T_{r,i-1}|}{\Delta t} \tag{3-10}$$

Where Max_{dT} is the maximum allowed change of T_r [K/s], $T_{r,i}$ the i 'th sample of T_r [K], N_{Mean}^{dt} the number of points used to calculate the moving average, and Δt the sampling time [s].

The motivation for this last condition is best demonstrated on the basis of a real example shown in **Figure 3-17**. The upper two plots show the control behavior during the initial phase of a reaction example without using this third condition. The controller switches at about 80 seconds from “fast” to “medium” control because condition (3-9) is fulfilled (❶ in Figure 3-17). However the set point is only reached for a very short time, then the subsequent (“medium”) controller reacts too slowly on the sudden decrease of q_{tot} and the subsequent temperature drop. This results in a maximum deviation of T_r to set point of about - 0.2 °C. Much better performance is achieved for the same reaction example when condition (3-10) is included into the controller. The two lower plots of Figure 3-17 show that the switching from “fast” to “medium” PID parameter set now occurs later, at about 220 seconds (❷ in Figure 3-17). The temperature set point is now reached smoothly as the derivative of T_r versus time is smaller as compared to ❶. The maximum deviation of T_r from the set point is now about -0.05 K.

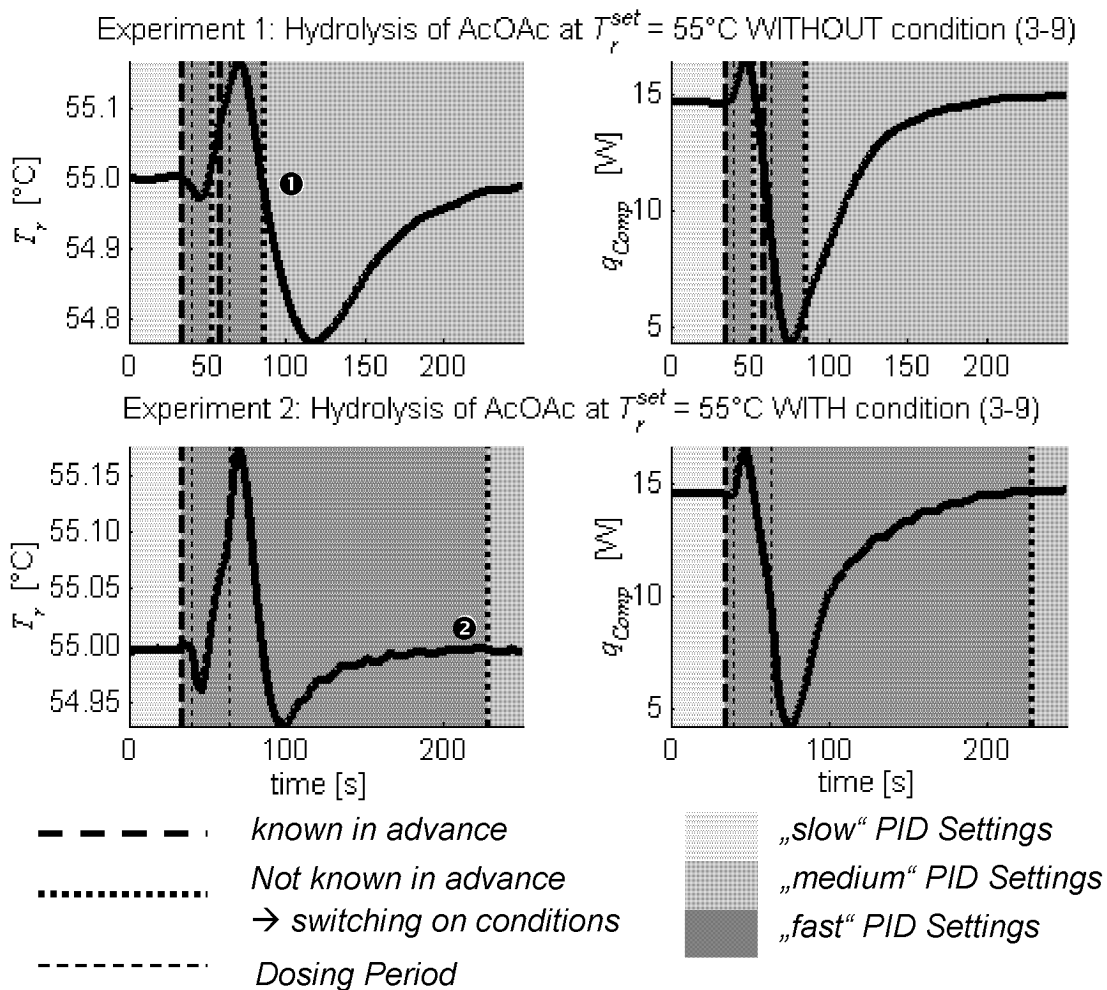


Figure 3-17: Control behavior of the controller using different switching conditions. The reaction example used is the hydrolysis of acetic anhydride (see Chapter 5.3).

3 The new Calorimeter

As the control strategy and algorithm explained above are able to deal with many different reaction examples, the same PID parameter were used for all experiments presented in this work. They are given in Table 3-3. They were determined “by hand” on the basis of the Ziegler-Nichols principle. Also unique values for dt_{before} , dt_{after} , $Max_{\Delta T}$, Max_{dT} , N_{Mean}^{dt} were found:

- ❖ $dt_{before} = 6 \text{ s}$
- ❖ $dt_{after} = 10 \text{ s}$
- ❖ $Max_{\Delta T} = 0.001 \text{ K}$
- ❖ $Max_{dT} = 0.001 \text{ K/s}$
- ❖ $N_{Mean}^{dt} = 30$

The switching of the parameters is therefore completely automatic and no user interaction is required at least for standard reactions. The only guess that has to be made is point ⑥ in Figure 3-15. However this is straightforward to do and it could also be automated in future.

As already mentioned the same control principle was applied for the control of T_j . However as there are no really fast processes to compensate by the intermediate thermostat (see Chapter 3.3.2) the control task is much easier to achieve. Therefore the same parameter set for “slow” and “medium” were used and no special filtering of the reaction temperature T_r for the D part (see Figure 3-16) was applied. The PID parameter sets used in this work are given in **Table 3-4**.

Table 3-4: Description of the PID parameter sets required to control T_j (compare to the control algorithm shown in Figure 3-16). The loop frequency of the PID controller is 10 Hz.

Name of the PID Parameter Set	<i>Slow</i>	<i>Medium</i>	<i>Fast</i>
P, I, D used in this work	2, 0.1, 0	2, 0.1, 0	4, 0.2, 0
$N_{Mean,PI}$	30	30	25
Minimum and Maximum I_{pelt} [A]	-4.5 / 4.5	-4.5 / 4.5	-4.5 / 4.5

3.7 From measured signals to calorimetric data

3.7.1 Calculation of q_{tot} by combination of the inner and outer heat-flow balance

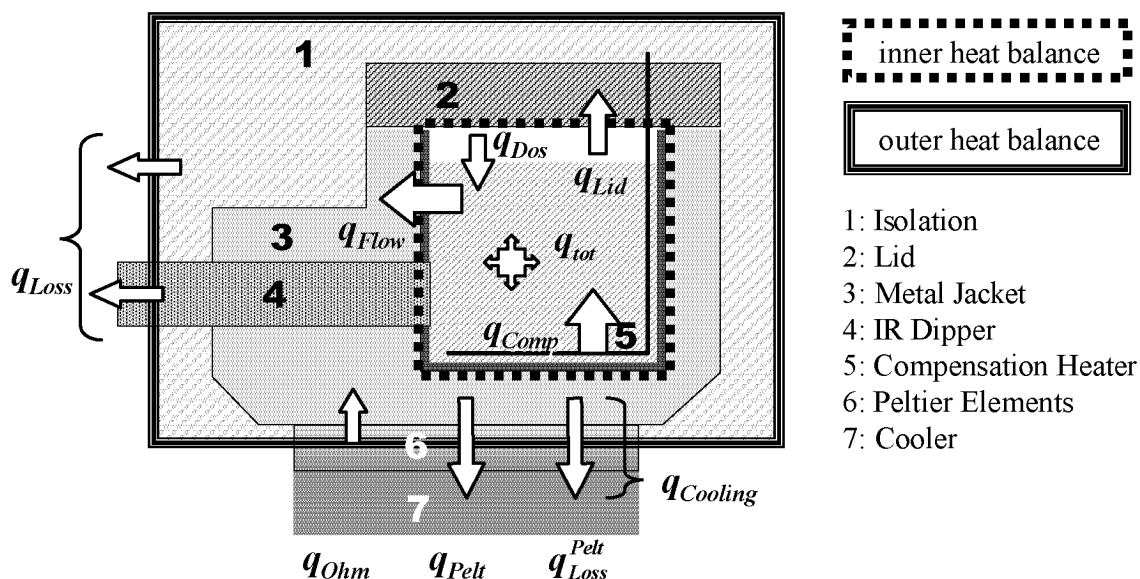


Figure 3-18: Steady-state isothermal heat-flow balance. The heat flow q_{Stirr} caused by the stirring is not shown here.

Figure 3-18 shows the two heat-flow balances that have to be considered in order to calculate the desired power release or uptake of the reaction mixture q_{tot} (see Equation (2-1)). The direction of the heat-flow arrows defines the positive value of the corresponding heat flow. The inner heat-flow balance, corresponding to the inner thermostat in Figure 3-3, equals Equation (2-14):

$$q_{tot} = q_{Flow} + q_{Lid} - q_{Stirr} - q_{Dos} - q_{Comp} \quad (2-14)$$

- ❖ q_{tot} [W] is the total power release or uptake during the reaction experiment (Equation (2-1)).
- ❖ q_{Dos} is the heat flow caused by the dosing of a reactant [W] (Equations (2-4)). T_{Dos} [K], the temperature of the dosing liquid, is measured by a small thermocouple inside the dosing tube (see Chapter 3.4.3.2).
- ❖ q_{Stirr} is the heat flow due to stirring [W] (Equation (2-3)). In all applications of this work this heat flow was assumed to be constant during a reaction measurement. See explanation in Chapter 3.7.3.
- ❖ q_{Comp} is the measured power of the compensation heater (Equation (2-15)) [W].
- ❖ q_{Lid} is the heat loss into the reactor lid (Equation (2-13)) [W].
- ❖ q_{Flow} is the heat flow through the reactor wall into the copper jacket [W] (Equation (2-9)).

3 The new Calorimeter

The outer heat-flow balance (corresponding to the intermediate thermostat in Figure 3-3) is given by the following equation:

$$q_{Cooling} + q_{Loss} = q_{Flow} + q_{Lid} \quad (3-11)$$

- ❖ $q_{Cooling}$ is the total heat pumped by the Peltier elements (see following description in Chapter 3.7.2) [W].
- ❖ q_{Loss} is the total heat loss of the reactor and the ATR-Probe through the thermal insulation into the environment (see following description in Chapter 3.7.3) [W].

The two heat-flow balances (2-14) and (3-11) can now be combined to the **final heat-flow balance of the new calorimeter**:

$$q_{tot} = q_{Cooling} + q_{Loss} - q_{Stirr} - q_{Dos} - q_{Comp} \quad (3-12)$$

Similar to the heat-flow balance of a Heat-Balance reaction calorimeter (see Chapter 2.1.3.4) it is important to note that the **problematic term** q_{Flow} still present in the inner and outer heat-flow balances **was eliminated** by the combination of the two heat-flow balances.

The heat flow through the reactor wall into the reactor jacket, q_{Flow} in Equations (2-14) and (3-11), could be expressed according to the discussion in Chapter 2.1.3.1 and the steady-state approximation (2-9):

$$q_{Flow} = U \cdot A \cdot (T_r - T_j) \quad (2-9)$$

where U is the total heat-transfer coefficient [W/(m²·K)], A the heat-transfer area [m²], T_r is the reaction temperature [K], and T_j is the temperature of the copper jacket [K]. However **U and A are usually unknown and can change during the course of a reaction**. Changes in A are mainly caused by dosing of a reactant or by density changes during the reaction. Changes in U are caused e.g. by viscosity changes during a reaction. These two parameters have to be calibrated in a conventional calorimeter. **Since in the new calorimeter Peltier elements are combined with the Power-Compensation principle these two variables do not have to be known.**

All remaining heat flows in Equation (3-12) can be calculated based on directly measured signals. By using **two independent control loops** and measuring two independent heat signals (q_{Comp} and $q_{Cooling}$) **changes of the baseline can be distinguished from the reaction power** (q_{React}) and neither a mathematical baseline correction **nor any calibration of the value $U \cdot A$** are required.

3.7.2 Calculation of the total heat pumped by the Peltier elements

$q_{Cooling}$

The total amount of heat pumped by the Peltier elements is represented by $q_{Cooling}$ [W] (see Figure 3-4). It can be calculated by splitting it into the three main heat flows (see Figure 3-18) that are taking place simultaneously:

$$q_{Cooling} = q_{Pelt} - q_{Ohm} + q_{Loss}^{Pelt} \quad (3-13)$$

Where q_{Pelt} is the heat pumped by the Peltier effect [W], q_{Ohm} the internal heat production due to the electrical resistance of the Peltier elements and q_{Loss}^{Pelt} the heat flow due to thermal conductivity of the Peltier elements and the mounting screws (see Chapter 3.4.4). The calculation of these three different heat flows is mostly done using the following steady-state (SS) approximations [Becker et. al. 65], [Nilsson et. al. 82], [Karlsen et. al. 87, a], and [Huang et. al. 00, a]:

$$q_{Pelt} \approx q_{Pelt,SS} = -S \cdot I_{Pelt} \cdot T_{Pelt}^{up} \quad (3-14)$$

$$q_{Ohm} \approx q_{Ohm,SS} = \frac{1}{2} \cdot R \cdot I_{Pelt}^2 \quad (3-15)$$

$$q_{Loss}^{Pelt} \approx q_{Loss,SS}^{Pelt} = \kappa \cdot (T_{Pelt}^{up} - T_{Pelt}^{down}) \quad (3-16)$$

Where S is the Seebeck coefficient [V/K], I_{Pelt} [A] is the current through the Peltier elements (cooling current is negative), T_{Pelt}^{up} and T_{Pelt}^{down} are the upper and lower temperature of the Peltier elements [K] (see Figure 3-12), R is the electrical resistance of the Peltier elements [Ω] and κ is the heat conduction coefficient through the Peltier elements [W/K].

The parameters S , κ and R are each a function of temperature [Huang et. al. 00, a], [Melcor], [Ferrotec] and have to be determined in advance (see Appendix D.1). The importance of the determination of accurate values for the Peltier parameters was tested by a sensitivity analysis described in Chapter 6.1.3.

[Huang et. al. 00, a] suggested a more complex model to describe $q_{Cooling}$. It requires even more unknown parameters that have to be identified and has therefore not been taken into consideration.

The steady-state Equation (3-11) can thus be rewritten:

$$q_{Cooling,SS} + q_{Loss} = q_{Flow} + q_{Lid} \quad q_{Cooling,SS} = q_{Pelt,SS} - q_{Ohm,SS} + q_{Loss,SS}^{Pelt} \quad (3-17)$$

Where $q_{Cooling,SS}$ is the $q_{Cooling}$ calculated on the bases of Equations (3-14) to (3-16). As can be seen from the different steady-state temperature profiles shown in Figure 3-4 the temperature of the Peltier elements will change during the course of an isothermal reaction experiment and thus steady-state approximations might be incorrect. This could lead to errors if q_{tot} , calculated on the basis of Equations (3-14) to (3-16), is used to get kinetic informations (see discussion in Chapter 2.1.4). [Nilsson *et. al.* 82] therefore included the heat capacity of the Peltier elements into the heat-flow balance but Equations (3-14) and (3-15) were still used. [Huang *et. al.* 00, b] developed a detailed dynamic model for Peltier coolers.

However considering Figure 3-4 makes clear that not only the dynamic behavior of the Peltier elements but also the whole copper jacket and part of the Teflon inliner would have to be included into a correct dynamic model for the calculation of $q_{Cooling}$. Additionally it should be kept in mind that the steady-state Equation (3-11) is not valid for the dynamic situation as q_{Flow} and $q_{Cooling}$ are separated by the thermal mass of the reactor jacket. However as discussed in Chapter 3.3.2 the intermediate thermostat, and thus the Peltier elements, do only have to deal with slow heat-flow changes as all fast changes are already compensated by the compensation heater (this is not the case for the Peltier calorimeters presented by [Nilsson *et. al.* 82] and [Becker *et. al.* 65]). Therefore Equations (3-14) to (3-16) have been used as the basis to calculate $q_{Cooling,SS}$. Based on two test experiments a mathematical “black box” time correction was then established and applied to the calculated steady-state $q_{Cooling,SS}$. The two test experiments are shortly described below:

1) Change of the stirrer speed

25 ml of water were filled into the reactor. T_j was controlled at 0 °C ($T_{Cry} = 5$ °C) and T_r at 25 °C. The stirrer speed was then instantly changed from 300 to 400, 200, 400 and back to 300 rpm. By this step-wise change of the stirrer speed the reactor-side heat-transfer coefficient should instantly change. This can be verified in **Figure 3-19** (left side) showing the power of the compensation heater q_{Comp} during this experiment. It can be seen that immediately after changing the stirrer speed, q_{Comp} changes due to the change of q_{Flow} . The measured $q_{Cooling,SS}$ (black line, calculated by Equations (3-14) to (3-16)) as well as the real, expected $q_{Cooling,exp}$ are also plotted (dotted black line). The height of the steps was normalized to one prior to the system identification (see **Figure 3-20** left side).

It is concluded that for such a fast heat-flow change the steady-state calculation of $q_{Cooling}$ is not accurate enough.

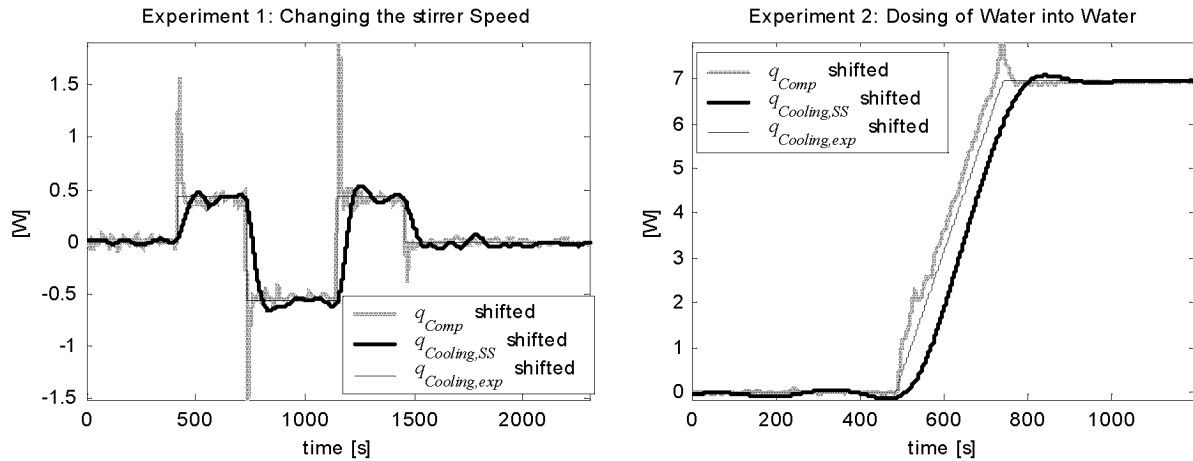


Figure 3-19: Measurement data of the two test experiments used to identify the dynamic behavior of the $q_{Cooling}$ heat flow. All signals are shifted to be zero at the beginning in order to allow a comparison. The expected $q_{Cooling,exp}$ is also shown.

2) Dosing

After the stirrer change, 15 ml of water were dosed into the reactor with constant dosing rate (3.5 ml/min). Because water is dosed into water, the physical properties of the reaction mixture remain constant and no heat of mixing (q_{mix}) occurs. Therefore q_{Flow} (Equation (2-9)) should change linear in time as the value $U \times A$ (see Equation (2-9)) will change proportional to the volume increase. This assumption can also be verified in **Figure 3-19** (right side) showing the power consumption q_{Comp} of the compensation heater during this experiment. It raises proportional to time and that means proportional to the volume increase. The real, expected $q_{Cooling,exp}$ is plotted as well (dotted black line). The small difference between q_{Comp} and $q_{Cooling,exp}$ might be caused by the heat flow q_{Dos} (Equation (2-4)) as T_r (25 °C) is slightly higher than T_{Dos} (22 °C). The measured $q_{Cooling,SS}$, based on Equations (3-14) to (3-16), is also plotted in Figure 3-19 (black line).

It is also concluded that even for this slower heat-flow change the steady-state calculation is not accurate enough.

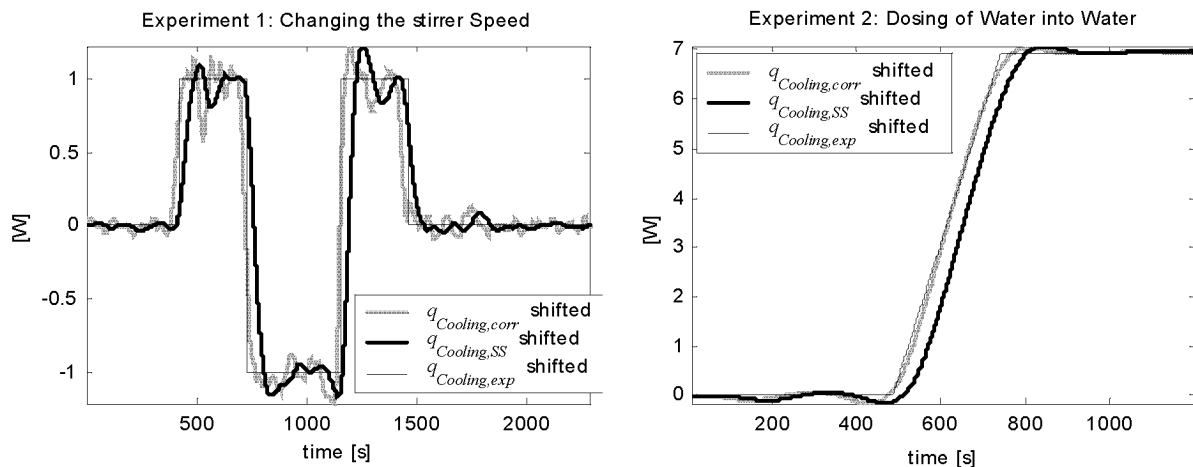


Figure 3-20: Result of the mathematical time correction based on the two test experiments.

Based on these two experiments a mathematical time correction was established. The idea is shown in **Figure 3-21**. In an initial step a linear system has to be identified based on the experiments described above and shown in Figure 3-19. The heat flow $q_{Cooling,exp}$ is used as input and $q_{Cooling,SS}$ as output from the system (schematically shown in Figure 3-21). In a next step an appropriate model has to be selected. The models Auto Regressive (ARX), Output Error (OE) and Box-Jenkins (BJ) are shown in Figure 3-21, where q is the time-shift operator. Thus the OE model could also be written in explicit form:

$$y(t_i) + f_1 y(t_{i-1}) + \dots + f_{nf} y(t_{1-nf}) = b_1 u(t_{i-nk}) + \dots + b_{nb} u(t_{i-nb+1-nk}) + y(t_i) + f_1 e(t_{i-1}) + \dots + f_{nf} e(t_{1-nf}) \quad (3-18)$$

Where t_i is the i 'th sample of the signal, y the output, u the input, e the error (white noise), nk the number of delays from input to output (dead time), f_k the elements of vector F (size nf), b_k the elements of vector B (size nb). The explicit definition of the ARX and BJ models could also be done according to (3-18). Once a model type and the corresponding orders (e.g. nf , nb and nk for the OE model) are selected, the unknown vector elements (parameters of the model) have to be identified. If nk is chosen to be zero (no dead time correction) the models can be inverted. The inverted model can then be used to perform the desired task: To convert the $q_{Cooling,SS}$ (calculated based on steady-state assumptions) into a time corrected $q_{Cooling,corr}$. In Equation (3-11) $q_{Cooling}$ can now be replaced by $q_{Cooling,corr}$ resulting in the following outer heat-flow balance:

$$q_{Cooling,corr} + q_{Loss} = q_{Flow} + q_{Lid} \quad q_{Cooling,corr} = correction(q_{Cooling,SS}) \quad (3-19)$$

In contrast to Equations (3-11) and (3-17), Equation (3-19) is also valid in dynamic situations when $q_{Cooling}$ is changing as a function of time.

As mentioned, various linear models and model orders were tested (60 different models) but only a few of them showed good performance after model inversion. The model with the lowest orders and best performance was the output error (OE) model with $nk = 0$, $nb = 1$ and $nf = 3$ (Equation (3-18)). The inverted model is given by the following equation (compare to Figure 3-21):

$$y'(t_i) = 3.253e6 \cdot u'(t_i) - 9.687e6 \cdot u'(t_{i-1}) + 9.615e6 \cdot u'(t_{i-2}) - 3.181e6 \cdot u'(t_{i-3}) + e'(t_i) \quad (3-20)$$

The corrected $q_{Cooling,corr}$ calculated by Equation (3-20) are shown in Figure 3-20. It can be **concluded that for both test experiments the mathematical time correction was successful and approximates $q_{Cooling,exp}$ very well**. However the noise of the signal is amplified. *The importance of this time correction was tested by a sensitivity analysis described in Chapter 6.1.4.*

For all future calculations shown in Chapter 5 Equation (3-19) will be used instead of the steady-state approximation (3-11) ($q_{Cooling,corr}$ is always calculated on the basis of the measured $q_{Cooling,SS}$ and the mathematical time-correction method shown above). For all calculations the same model was used that was identified based on the two test experiments described above. **In the following the term $q_{Cooling}$ will be used instead of $q_{Cooling,corr}$ in order to make the formulas simpler.** The whole calculation was carried out using the System Identification Toolbox from Matlab [Matlab Ident].

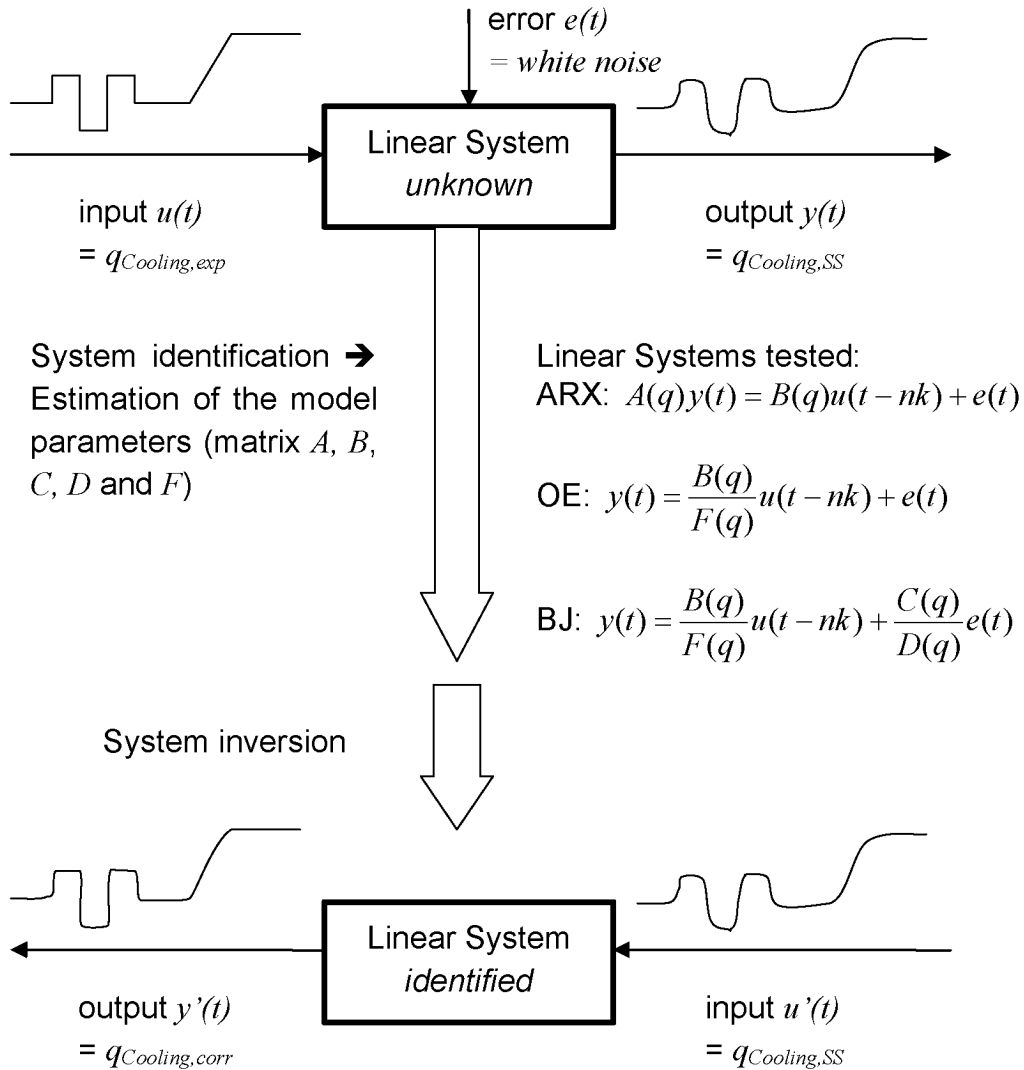


Figure 3-21: Schematic representation of the calculation of the time corrected $q_{Cooling,corr}$ based on the steady-state approximation $q_{Cooling,SS}$ and the expected ideal $q_{Cooling,exp}$. The symbol q represents a time shift operator.

3.7.3 Calculation of q_{Stirr} and q_{Loss}

The only unknown heat flows that remain in the combined heat-flow balance (3-12) are q_{Stirr} and q_{Loss} .

The heat flow q_{Stirr} can be calculated according to Equation (2-3). In all experiments carried out during this work the current consumption of the stirrer engine (I_{Stirr}) was measured as a function of time. As no changes could be measured in most applications q_{Stirr} was assumed to be constant for all reaction experiments of this work.

The heat flow q_{Loss} [W] represents the heat loss through the thermal insulation into the surroundings, similar to a Heat-Balance calorimeter (see Chapter 2.1.3.4). Because q_{Loss} is independent of the reactor content it is much easier to describe than q_{Flow} and the heat flow into the reactor lid (q_{Lid}). As the reactor is insulated (see Figure 3-6) the heat loss to the surroundings could be assumed to be constant during a reaction. This assumption is feasible as long as the ambient temperature (T_{Amb}) does not change significantly. However it is more accurate to include T_{Amb} into the heat-flow balance as it is anyway measured during the whole experiment. The ambient temperature was measured at three different positions as shown in **Figure 3-22**.

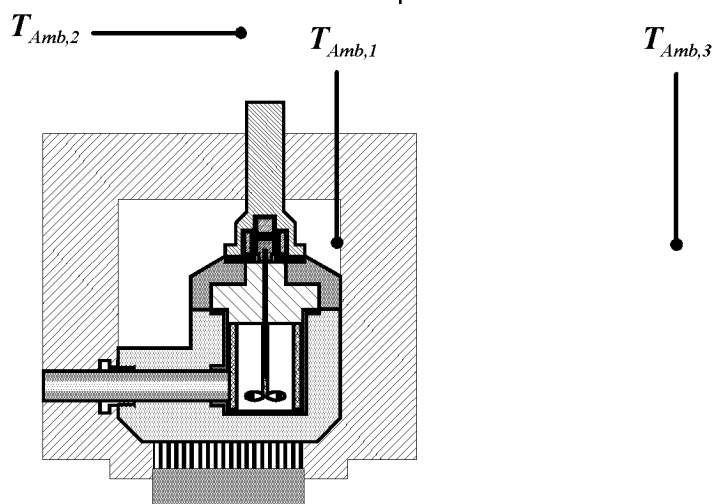


Figure 3-22: Position of the sensors for the ambient temperature.

Sensor $T_{Amb,1}$ is located inside the thermal insulation, $T_{Amb,2}$ close to the whole reactor and $T_{Amb,3}$ far away on the back wall of the fume hood. $T_{Amb,3}$ was best suited for the following correction as it is less sensitive to short time changes of the ambient temperature due to opening or closing of the cover of the fume hood. As the change of the ambient temperature is a slow process (normally in the range of 2-5 °C a day) $T_{Amb,3}$ was strongly filtered (see Table 3-5) prior to the evaluation shown below.

Both terms q_{Stirr} and q_{Loss} are calculated in one step using the following equation (derivation see below):

$$\Delta q = q_{Loss} - q_{Stirr} = q_{Comp,0} - q_{Cooling,0} + k_{Loss} \cdot \left(|T_j - T_{Amb}| - |T_{j,0} - T_{Amb,0}| \right) \quad (3-21)$$

All terms with the index $_0$ are determined before the reaction is started. For the calculation a mean value over a range of minimum 4 minutes was used. For the jacket temperature (T_j) the sensor T_{TI} was used (Figure C-2) as it is most exposed to the ambient temperature. The parameter k_{Loss} is a device specific constant [W/K] that has to be determined in advance (see Appendix D.2). In contrast to k_{Lid} (used to describe q_{Lid} in Equation (2-13)) k_{Loss} does not depend on the conditions inside the reactor and can therefore be estimated once, similar to the Peltier parameters S , R and κ , and then be used for any reaction experiment.

The first term in Equation (3-21) ($q_{Comp,0} - q_{Cooling,0}$) eliminates the offset between $q_{Cooling}$ and q_{Comp} before the start of the reaction. This offset will be called Δq_0 . It is derived from Equation (3-12) by setting q_{tot} and q_{Dos} to zero (no reaction and no dosing):

$$\Delta q_0 = q_{Comp,0} - q_{Cooling,0} = q_{Loss,0} - q_{Stirr,0} \quad (3-22)$$

Δq_0 was determined for the hydrolysis and epoxidation experiments (see Chapters 5.3, 5.4). **Figure 3-23** shows a plot of Δq_0 versus the temperature difference $T_{j,0} - T_{Amb,0}$.

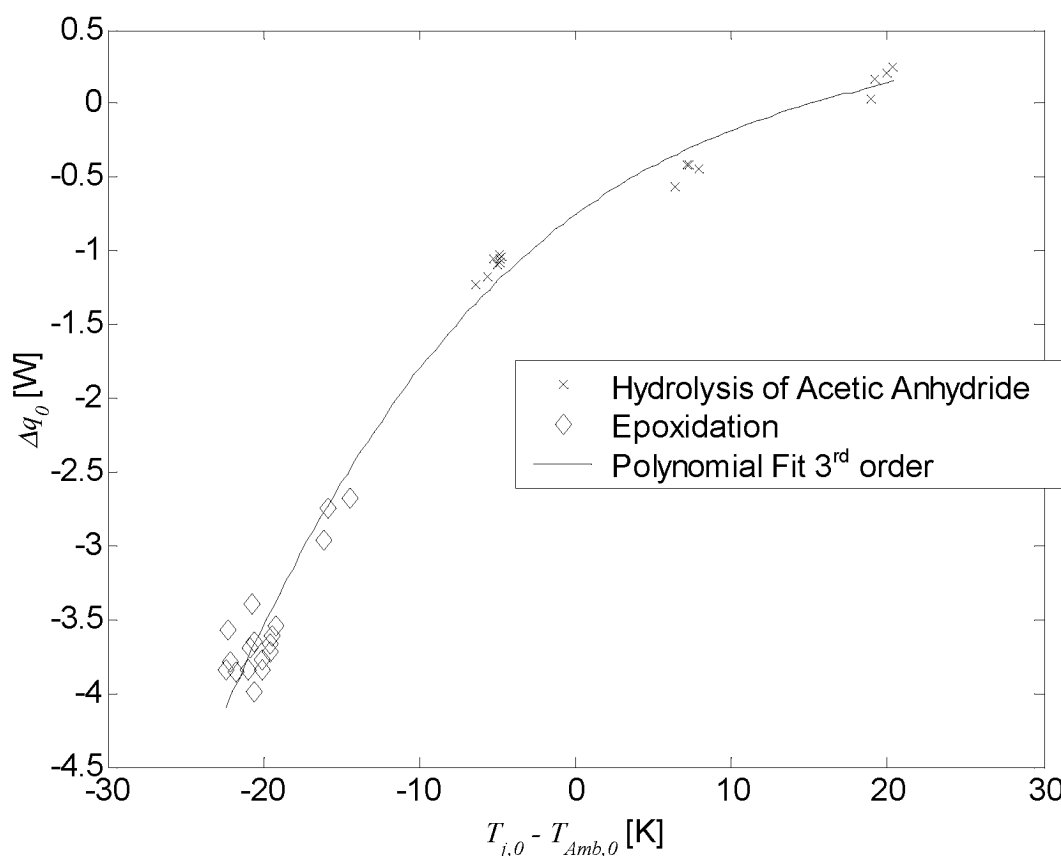


Figure 3-23: Δq_0 plotted versus $T_{j,0} - T_{Amb,0}$ (data is taken from the epoxidation and hydrolysis experiments described in Chapters 5.3 and 5.4).

From Figure 3-23 the following two observations can be made:

1) Δq_0 is obviously not proportional to $T_{j,0} - T_{Amb,0}$ in the whole temperature range studied. However the change of T_{Amb} during a reaction measurement is much smaller (2 to 4°C) and thus Equation (3-21) could still be used but k_{Loss} must be a function of the temperature difference $T_{j,0} - T_{Amb,0}$.

2) Δq_0 is not zero when $T_{j,0} - T_{Amb,0}$ and consequently $q_{Loss,0}$ are zero. According to Equation (3-22) $q_{Stirr,0}$ would thus be in the range of 1 W. This unreasonable high value can be explained by considering the fact that Δq_0 also contains different error sources that can lead to a shift of $q_{Cooling}$ or q_{Comp} :

- ❖ Shift of $q_{Cooling}$ due to errors in the determined Peltier parameter sets A and B (see Appendix D.1)
- ❖ Shift of q_{Comp} due to errors in the measured U_{Comp} (see Appendix C.8.3).

It was therefore concluded that Δq_0 must be part of the total heat-flow balance (3-12) by including it into Equation (3-21). Thus any heat flows or calculation errors that remain constant during a reaction measurement are eliminated.

The second term in Equation (3-21) describes the change of q_{Loss} during the reaction experiment. As $q_{Loss,0}$ is already compensated by Δq_0 only the change of $T_j - T_{Amb}$ relative to the initial temperature difference is important and thus included in Equation (3-21).

The determination of the k_{Loss} value by precalibration is described in the Appendix D.2. The importance of this ambient temperature correction was tested by a sensitivity analysis described in Chapter 6.1.5.

3.7.4 Final calculation formula for q_{tot} and filtering of the required measurement signals

The combined heat-flow balance required to calculate the total power release or uptake by the reaction mixture (q_{tot}) is given by Equation (3-12). Inserting Equation (2-4) for q_{Dos} , Equation (2-15) for q_{Comp} , Equations (3-13) to (3-16) for $q_{Cooling}$, Equation (3-21) for q_{Stirr} and q_{Loss} the following formula for the calculation of q_{tot} results (to keep the formula small, $q_{Cooling,0}$ and $q_{Comp,0}$ were not replaced by the corresponding equations):

$$q_{tot} = correction \left[-S \cdot I_{Pelt} \cdot T_{Pelt}^{up} - \frac{1}{2} \cdot R \cdot I_{Pelt}^2 + \kappa \cdot (T_{Pelt}^{up} - T_{Pelt}^{down}) \right] \\ + q_{Cooling,0} - q_{Cooling,0} + k_{Loss} \cdot (|T_j - T_{Amb}| - |T_{j,0} - T_{Amb,0}|) \\ - f \cdot c_{p,Dos} \cdot (T_{Dos} - T_r) - U_{Comp} \cdot I_{Comp} \quad (3-23)$$

Equation (3-23) is the final and complete calculation formula for q_{tot} used in this work. It can be calculated based on directly measured signals from the calorimeter, the device specific calibration constants S , R , κ (see Appendix D.1), and k_{Loss} (see Appendix D.2) as well as the time correction on the basis of an identified and inverted OE model (see Chapter 3.7.2).

The measured signals required are filtered with a Butterworth filter [*Matlab Signal*] prior to the calculation. Three different filters are used for the faster signals from the inner thermostat, the slower signals from the intermediate thermostat and the ambient temperature. The filter settings are summarized in **Table 3-5**. The same settings were used for all experiments shown in this work. Finally the calculated q_{tot} was filtered again using the filter settings of the inner thermostat signals.

Table 3-5: Filter settings for the required measurement signals of the new reaction calorimeter to calculate q_{tot} . ¹⁾ Calculated based on the overall heat-flow balance.

	Order of the filter	Cut off frequency of the filter	Description of the signal
I_{Pelt} [A]	4	0.001	Appendix C.8.4
T_{Pelt}^{up} [K]	4	0.001	Appendix C.7.4
T_{Pelt}^{down} [K]	4	0.001	Appendix C.7.4
T_j [K]	4	0.001	Appendix C.6 (Equation (C-1))
T_{Amb} [K]	2	0.0001	Chapter 3.7.3
T_{Dos} [K]	2	0.02	Chapter 3.4.3.2
T_r [K]	2	0.02	3.4.3.2
U_{Comp} [V]	2	0.02	C.8.4
I_{Comp} [A]	2	0.02	C.8.4
q_{tot} [W] ¹⁾	2	0.02	Equation (3-23)

4 EVALUATION OF THE CALORIMETRIC AND SPECTROSCOPIC DATA, A NEW COMBINED APPROACH

4.1 Historical background

A first version of a combined evaluation algorithm was successfully applied during the diploma thesis of I. Zürcher [Zürcher 01]. The final version, used for all calculations shown in this work, will be explained in details in this Chapter. It was presented at the AIChE Meeting 2002 [Zogg et. al. 02].

4.2 Requirements

Model-based identification of kinetic and thermodynamic reaction parameters based on a combined data set

From a single reaction experiment, the new reaction calorimeter, described in Chapter 3, will deliver two different sets of measurement data: Calorimetric and infrared data. Both contain information about the individual reaction steps as well as the chemical components involved in the experiment. This is shown in **Figure 4-1**.

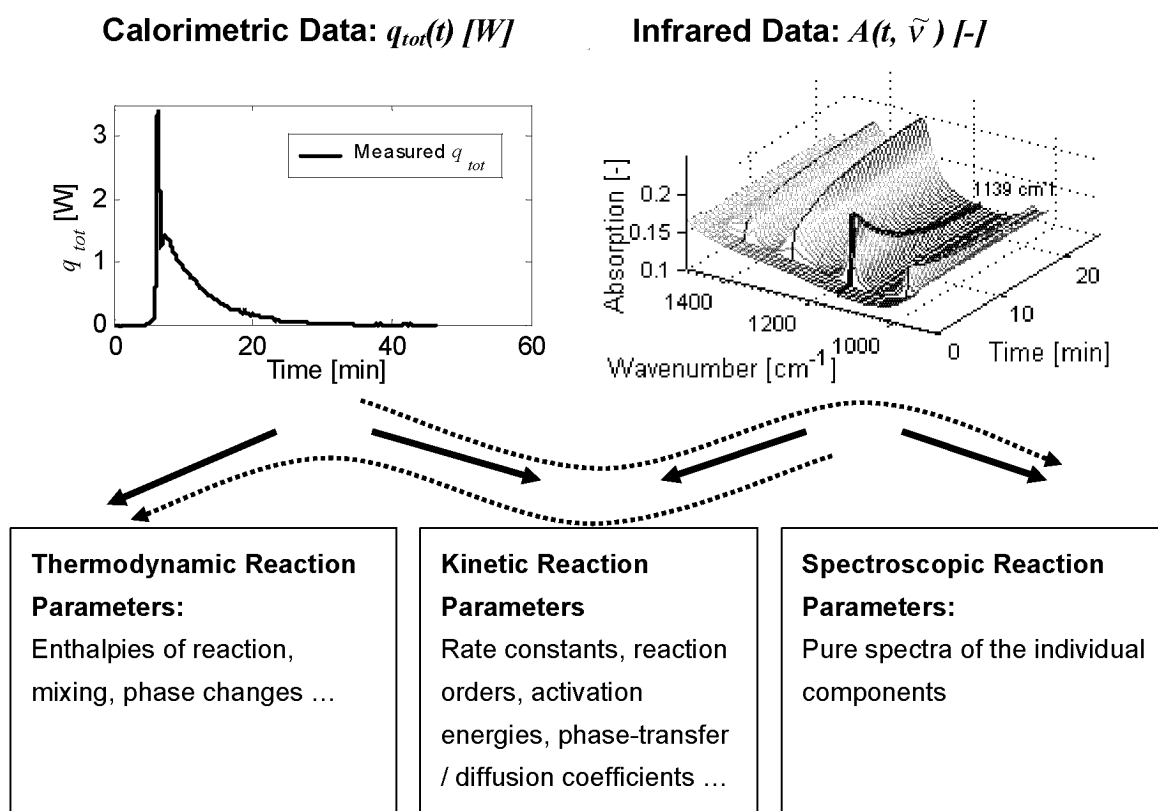


Figure 4-1: Information content of the different data measured by the new reaction calorimeter (t =time [min], $\tilde{\nu}$ = wave number [cm^{-1}], A = reaction spectrum in absorbance units [-]).

As explained in Chapters 2.3.2 and 2.3.3, for both data sets many different separate evaluation methods were developed. However the overlapping information content indicated in Figure 4-1 and Table 1-1 has not yet been used in a combined evaluation (see Chapter 2.3.4). In a combined evaluation the infrared data would also support the evaluation of the calorimetric data in order to identify thermodynamic reaction parameters and vice versa. This is schematically shown by the dotted lines in Figure 4-1. Additionally it can be assumed that the identification of the kinetic reaction parameters will be more robust as they have to suit the two individual data sets at the same time.

Therefore the main requirement for the new evaluation algorithm is to allow a combined and simultaneous evaluation of calorimetric and spectroscopic data.

According to the goal of the thesis (see Chapters 1.2), the evaluation method should be able to identify the following reaction parameters simultaneously

- ❖ **Thermodynamic reaction** parameters, such as reaction enthalpies.
- ❖ **Kinetic reaction parameters**, such as rate constants, activation energies, reaction orders, or phase change / diffusion coefficients.

*The determination of **pure spectra** (spectroscopic reaction parameters) is **not the focus of this work**. However they will be a side product of the combined evaluation as they are primarily assumed to be unknown.*

It should be noted that such an evaluation of the calorimetric data stays in contrast to the evaluation methods I.A and II.A presented in Chapters 2.3.2.2 and 2.3.2.3 that require a determination of the reaction enthalpy prior to the kinetic evaluation. The benefits of the simultaneous evaluation of thermodynamic and kinetic reaction parameters were already discussed in these Chapters.

The reaction parameters that have to be identified are to be defined in advance based on an empirical kinetic model of the reaction (see Chapter 1.2).

Fast application

The whole evaluation procedure should be fast in application (according to Chapter 1.2). Therefore **any calibrations** of the infrared data are not allowed and **any additional information** from chromatographic experiments should **not be required**. Additionally the parameter identification should run completely automatic, meaning that **the user should not have to spend time for the adjustment of the objective function, weighting functions or other optimization parameters**.

Inclusion of external information

As mentioned in Chapter 1.2 the algorithm should be **designed to be applied by adequately educated people** and not for people without any chemical background. Therefore the algorithm should be able to include external knowledge and information about the investigated reaction:

- ❖ **Chemical knowledge** about possible reaction mechanisms, mean products (e.g. gathered by other analytical techniques or by model free evaluation methods (see Appendix B.2)) should be included in the form of an empirical reaction model. The **reaction model** has to be described in terms of differential equations. The integration has to be carried out numerically during the evaluation of the data. Thus the complexity of the model is not restricted.
- ❖ If **pure infrared spectra** of some substances are available, it should be possible to include them into the evaluation. However the evaluation should also work if no pure spectra are available (compare to discussion in 6.3.5).
- ❖ If **enthalpies of reaction** or other thermodynamic parameters are known (e.g. from heats of formation, quantum mechanical calculations (see also [Zogg *et. al.* 03, submitted]) or group contribution methods) they should be included into the evaluation.
- ❖ If some **physical constraints for the reaction parameters**, such as non-negativity, temperature independency, are available, they should be included into the evaluation.
- ❖ If **certain time regions** of one of the data sets cannot be correctly described by the reaction model (e.g. if the assumption $q_{tot} = q_{React}$ is not fulfilled, see also Chapter 2.3), it should be possible to **exclude** it from the evaluation.

Augmentation of the measured data

The evaluation algorithm should be able to **treat the measured data sets from different experiments** (e.g. with different concentration conditions or at different temperatures) **simultaneously**.

Model selection

As mentioned above the evaluation is based on a reaction model that has to be suggested in advance. However in most cases several reaction models will seem equally feasible for the investigated reaction. **The algorithm should therefore support the final step of model selection**. Therefore the algorithm has to answer the following two main questions:

1. **How well** can the reaction model be fitted into the measured data?
2. **How robust** is the identification of the unknown parameters of the corresponding reaction model?

Once the answer to these two questions is known the optimal model can be easily chosen by the user.

4.3 Concept of the evaluation method

4.3.1 Combined evaluation algorithm

As explained in Chapter 2.3 there are basically two different ways to evaluate calorimetric as well as infrared data in order to identify the desired reaction parameters:

1. **Model-free** evaluation as an initial step (Chapter 2.3.2.1 and Appendix B.2) followed by a subsequent fitting of the reaction model into the determined conversion and concentration profiles.
2. Direct **model-based** evaluation of both data sets (Chapters 2.3.2.2, 2.3.2.3, 2.3.3.2 and 2.3.3.3).

For the combined evaluation of calorimetric and infrared data the second approach was chosen mainly because of the following two reasons:

1. As discussed in Chapter 2.3.4 the **model-based evaluations are supposed to show better performance** for the separate evaluation of calorimetric and spectroscopic data sets.
2. A model-based combined evaluation of both data sets is straightforward (see Chapter 2.3.4 and Figure 4-1) **whereas a model-free combined evaluation is probably difficult to achieve or even impossible**.

It was therefore decided to use a model-based evaluation approach, according to Equation (2-44) in Chapter 2.3.4:

$$\min_{\theta_{1..N_P}} \{ f(err_Q, err_{IR}) \}$$

$$err_Q = \min_{\Delta_r \hat{H}_{1..N_R}} \left(\sum_{i=1}^{N_t} \left[q_{tot}(t_i) - \sum_{j=1}^{N_R} V_r(t_i) \cdot (-\Delta_r \hat{H}_j) \cdot r_j(t_i, \theta_{1..N_P}) \right]^2 \right) \quad (4-1)$$

$$err_A = \min_{\hat{E}} \left(\left\| A - C_{calc}(\theta_{1..N_P}) \times \hat{E} \right\|_2^2 \right)$$

Equation (4-1) represents a nonlinear least-squares optimization of a combined calorimetric and spectroscopic objective function. The combination of the objective function is done using a combination function f . Inside the nonlinear optimization, two linear least-squares problems are to be solved in order to determine estimates for the reaction enthalpies $\Delta_r \hat{H}_{1..N_R}$ (thermodynamic reaction parameters) and pure component spectra \hat{E} (spectroscopic reaction parameters). The kinetic reaction parameters defined by the chosen reaction model are indicated by $\theta_{1..N_P}$. As already discussed in Chapter 2.3 it is assumed that $q_{tot} = q_{React}$.

As mentioned in Chapter 2.3.4 the formulation of Equation (4-1) is straightforward. However the crucial and most difficult point is the appropriate selection the combination function f . Of course this could be left to the user of the evaluation algorithm. But then the benefits of a combined evaluation would be compensated by

a complicated and time consuming determination of appropriate weighting factors and a combination functions (such as W_Q and W_{IR} in Equation (2-44)). Therefore an automatic determination of an appropriate combination function f was developed and will be described separately in Chapter 4.5.

Using Equation (4-1) as the basis for the evaluation, the following three physical models will automatically be included in the calculation (see **Figure 4-2** for an example):

- ❖ Reaction model, containing the **kinetic model** equations. By integration of the reaction model the reaction rates as well as the concentration profiles can be calculated.
- ❖ Sensor model for the calorimetric data to calculate q_{React} (Equation ((2-2)) on the bases of the reaction rates ($q_{tot} = q_{React}$ is assumed).
- ❖ Sensor model for the infrared data to calculate the reaction spectra A on the bases of the concentration profiles.

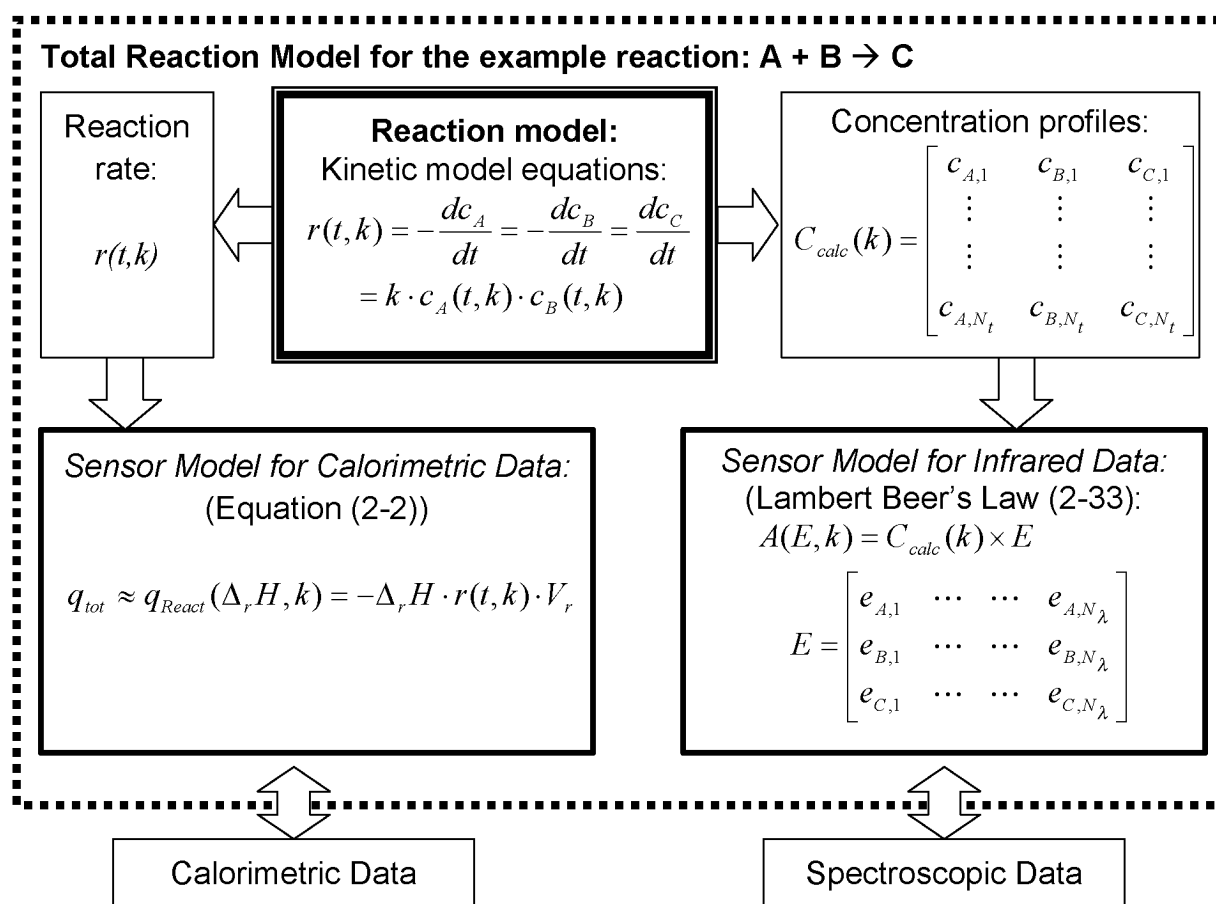


Figure 4-2: Schematic representation of the total reaction model consisting of the kinetic and the two sensor models. The model equations are given for the example reaction A + B → C. The rate constant k is the kinetic (θ_t), $\Delta_r H$ the thermodynamic, and E (the matrix of pure spectra) the spectroscopic reaction parameter.

By using the approach expressed by Equation (4-1) the remaining requirements in formulated in Chapter 4.2 can be easily fulfilled:

- ❖ The **nonlinear optimization** will be carried out using boundary constraints for $\theta_{1..Np}$. In this way physical constraints on the values of $\theta_{1..Np}$ can be included.
- ❖ The **two linear optimizations** will also be carried out using boundary constraints for $\Delta_r \hat{H}_{1..NR}$ and \hat{E} . Eventual known pure spectra can therefore be included by generating an upper and lower bound for the corresponding row in \hat{E} . Analogous upper and lower bounds can be introduced for an element of $\Delta_r \hat{H}_{1..NR}$ if a value is known in advance.

If several experiments at different conditions are carried out, the measured data is concatenated along the time axis into a single vector q_{Data} (calorimetric data) and a single matrix A_{Data} (infrared data):

$$q_{Data} = \begin{bmatrix} q_{React,1} & \cdots & \cdots & q_{React,N_{exp}} \end{bmatrix} \quad A_{Data} = \begin{bmatrix} A_1 \\ \vdots \\ \vdots \\ A_{N_{exp}} \end{bmatrix} \quad (4-2)$$

Where $q_{React,i}$ and A_i are the calorimetric and infrared data from the i 'th reaction experiment. The evaluation of all concatenated experiments will then be carried out in one single step. If reactions are combined that were measured at different temperatures, the Arrhenius law for the calculation of the kinetic rate constants will be used. Consequently a rate constant will be described by a rate constant at a certain reference temperature and the Arrhenius activation energy (Equation (4-5)). Additionally the pure spectra matrix E will be identified for each temperature as it must be assumed that the pure component spectra are depending on the temperature.

4.3.2 Model selection

The task of model selection (see requirements in 4.2) is splitted into two parts:

1) How well can the reaction model be fitted into the measured data?

After the nonlinear optimization task of Equation (4-1) is solved, the remaining sum of squares will be used as an indicator for the fit quality.

2) How robust is the identification of the unknown parameters of the corresponding reaction model?

In order to answer this question it is important to note that the mathematical step of nonlinear optimization, required to calculate the unknown model parameters by Equation (4-1), is generally difficult to solve. Many different nonlinear optimization techniques are reported in literature such as Gauss-Newton, Simplex, Levenberg-Marquardt, Simulated Annealing, Genetic Algorithm, Monte Carlo, Tabu Search. However none of them can guarantee to find the global optimal parameters $\theta_{I..Np}$ that minimize the objective function given by Equation (4-1). They will all stop after some time and might deliver only a locally optimal solution. The performance of these algorithms can be roughly summarized as follows: The closer the local optimum, found by the optimization algorithm, is to the global optimum, the more computing time was required. Thus allowing indefinite calculation time, the probability to find the global optimum will be close to one for some of the mentioned algorithms. However in practical applications the calculation time is restricted to minutes. **Therefore any solution found by any optimization algorithm will generally depend on the initial values suggested for the model parameters $\theta_{I..Np}$.**

Based on these reflections it was concluded that the best way to calculate the robustness of the parameter identification is to **use 10 random start values for the model parameters $\theta_{I..Np}$.** From the 10 solutions obtained by the nonlinear optimization, the ones with identical parameters $\theta_{I..Np}$ (within 5 %) and minimal value of the objective function are counted. This number will be called "number of hits". If all ten solutions are identical it can be concluded that the identification is robust and the model parameters are reliable. If all ten solutions are different it must be concluded that the identification is not robust, actually resulting in a random solution for the reaction parameters $\theta_{I..Np}$.

Another approach, widely applied in literature, is to calculate a standard deviation for the determined reaction parameters based on a sensitivity analysis around the corresponding optimum. However this method will only characterize the shape of the objective function and not the whole problem of nonlinear parameter optimization. It is therefore not used in this work.

If several models are evaluated 10 times, using random start values for the model parameters, the best model will have a minimal value of the final objective functions err_q and err_A in Equation (4-1) and a maximal "number of hits".

4.3.3 Step by step evaluation procedure

In order to extract a maximum amount of information from the two measured data sets (infrared and calorimetry) the combined evaluation described above should only be one part of an overall evaluation procedure. The complete step by step evaluation procedure that was elaborated and applied in this work is shown in **Figure 4-3**.

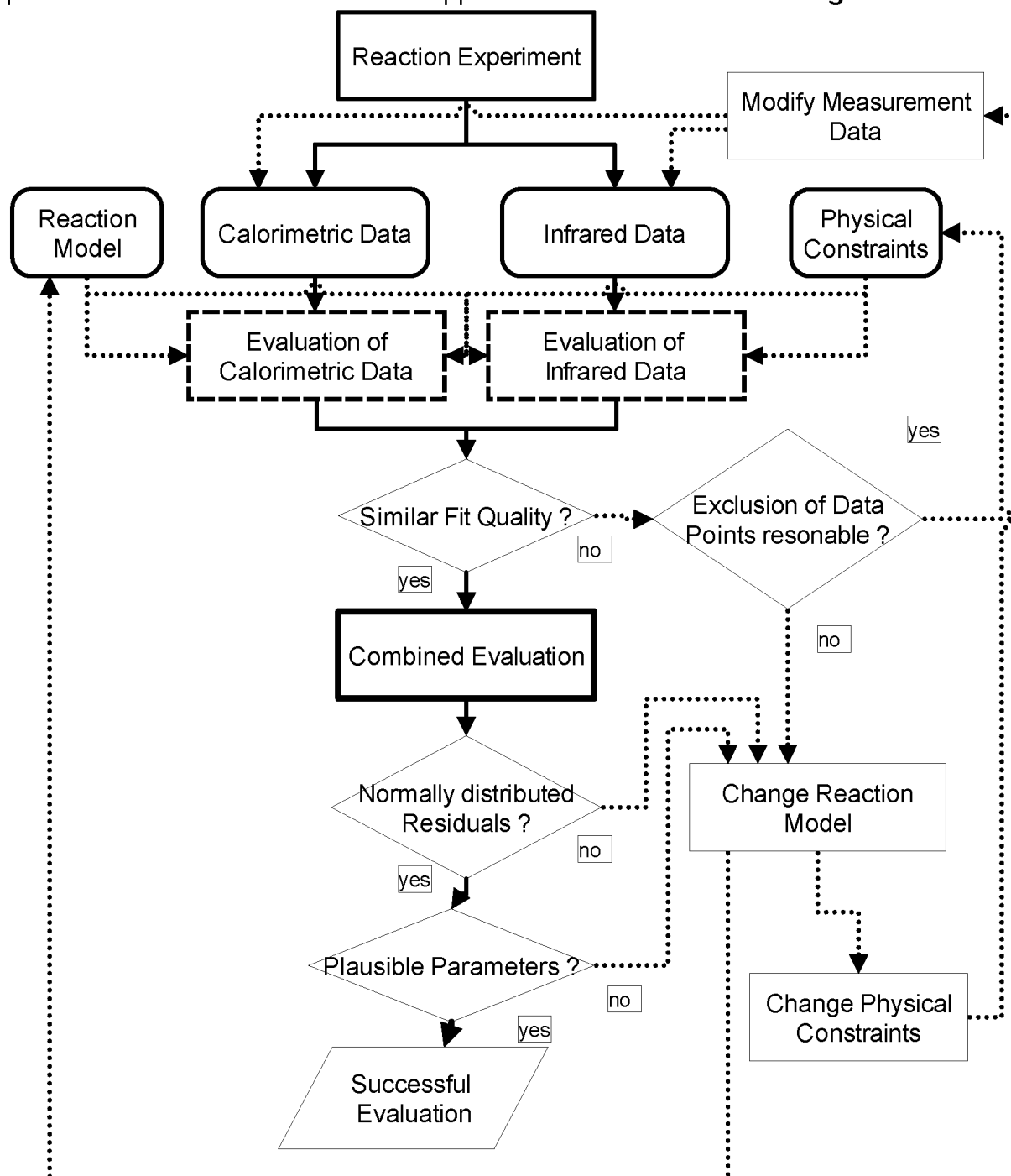


Figure 4-3: Flow sheet of the overall evaluation procedure of the measured data.

The evaluation procedure consists in the following steps:

- 1 The measured calorimetric and infrared data are first **evaluated separately**. This is achieved by only considering err_q (evaluation of the calorimetric data) or err_A (evaluation of the infrared data) in Equation (4-1). This corresponds to Equations (2-31) and (2-34).
- 2 The focus of the first, separate evaluation is not the determined reaction parameters, but the **quality of the model fit**. If both (spectroscopic as well as calorimetric) model-fit residuals do not show a similar behavior, it can be concluded that in one of the data sets more physical or chemical processes were measured than described by the reaction model. E.g. it could be that the reaction shows a heat of mixing (the assumption $q_{tot} = q_{React}$ is not fulfilled). This will only affect the calorimetric measurement whereas the infrared data will be unaffected. If the chosen reaction model does not model the heat of mixing, the quality of the calorimetric model fit will be worse than the quality of the infrared model fit.
 - 2.1 If the qualities of the separate model fits are different, it might be reasonable to **exclude some data points** of the linear least-squares optimizations in Equation (4-1). E.g. in the calorimetric data set all data points measured during the dosing period could be excluded if a heat of mixing is present. The calculation is then restarted with the modified data set.
If the exclusion of data points is unreasonable, the **reaction model has to be improved** in order to explain the observed difference to the measured data.
- 3 As soon as the reaction model can be equally well fitted to the two data sets, the **combined evaluation** can be carried out.
- 4 If the reaction model chosen and the identified reaction parameters can explain all variance in the data except the measurement noise (white noise), the remaining residuals of the combined evaluation will be normally distributed. Of course in practical applications this will never be the case. However if **no significant deviation from the normal distribution is present, the combined identification of the reaction parameters was successful**.
 - 4.1 If on the other hand the residuals of the combined evaluation show significant deviations from the normal distribution, it must be concluded that the underlying reaction model is not able to accurately explain the measured data sets. Thus **the reaction model must be modified** and the calculation repeated.
- 5 At the end of the evaluation the **plausibility of the identified reaction parameters must be verified based on chemical and physical knowledge**. If unreasonable reaction parameters were identified either the reaction model or the physical constraints can be changed and the evaluation must be repeated. Otherwise the evaluation is **finished**.

4.4 Mathematical formulation of the combined evaluation algorithm

4.4.1 Pre-treatment of the infrared data

4.4.1.1 Baseline Correction

The proposed combined evaluation algorithm determines the best model and parameter values to describe all variance in the measurement data. It assumes that all systematic variance in the data can be explained by the reaction model. Thus, if a varying baseline is present in the infrared data (caused by an instrument drift) it will disturb the results using the proposed evaluation method and the estimated reaction parameters might be erroneous (see also discussions in Chapter 2.3.3.3).

The following baseline correction was therefore applied to all measured infrared data prior to the evaluation (application examples are given in Appendix E.2.2 and E.3.2):

1. All wave numbers in the reaction spectrum A with locally minimal absorption, or where no absorbance change due to the reaction is expected, were determined.
2. The absorbance time profiles (columns of A) at these wave numbers were then compared to each other. All similar absorbance time profiles were then averaged to a unique baseline profile. If a wave number is chosen where absorptions are changing due to the reaction, the corresponding absorbance profile deviates from the other profiles and is therefore not included in the calculation of the baseline profile.
3. The calculated baseline profile is then subtracted from the reaction spectrum A at each wave number. It is assumed that the baseline drift changes with time but is constant for all wave numbers.

4.4.1.2 Selection of the spectral evaluation region

In order to reduce the calculation time not all wave numbers of the measured reaction spectrum were used for the evaluation. Only those spectral regions, where absorption changes occur during the reaction were selected for the evaluation.

All spectral regions where deviations from the Lambert Beer's law are expected (see Chapter 2.2) were excluded from the calculation.

4.4.1.3 Resampling and exclusion of data points

In order to reduce calculation time and memory consumption or to exclude certain time ranges of the experiment (see Chapter 4.3.3) the user can freely choose the data points that will be used for the evaluation. The points in time, where an infrared spectrum is available, do not have to be equal to the points in time with available calorimetric signal.

4.4.2 Pre-treatment of the calorimetric Data

4.4.2.1 Resampling and exclusion of data points

In order to reduce the calculation time and memory consumption or to exclude certain time ranges of the experiment (see Chapter 4.3.3) the user can freely choose the data points that will be used for the evaluation. The points in time, where a calorimetric signal is available, do not have to be equal to the points in time with available infrared spectrum.

In contrast to the infrared measurement the sampling frequency of the measured power release or uptake q_{tot} is very fast (10 Hz). Therefore data reduction is crucial in order to enable reasonable calculation times.

4.4.3 Step by step explanation

The functionality of the algorithm is explained on the basis of the following chemical reaction example:



The corresponding reaction model for a batch operation is shown in Figure 4-2. Additionally it is now assumed that the component B is dosed during the reaction. Therefore the reaction model has to be extended as the reaction volume V_r is no more constant. It can be expressed by the following differential equations:

$$\begin{aligned} \frac{dn_A}{dt} &= -r(t, k) \cdot V_r(t) & \frac{dn_B}{dt} &= -r(t, k) \cdot V_r(t) + v_{dos} \cdot c_{dos} \\ \frac{dn_C}{dt} &= r(t, k) \cdot V_r(t) & r(t, k) &= k \cdot \frac{n_A(t)}{V_r(t)} \cdot \frac{n_B(t)}{V_r(t)} & \frac{dV_r}{dt} &= v_{dos} \end{aligned} \quad (4-3)$$

Where n_A , n_B and n_C are the moles of the corresponding components [mol], v_{dos} the dosing rate [l/s] and c_{dos} the dosing concentration of B [mol/l]. k is the unknown rate constant (kinetic reaction parameter, compare Figure 4-1)) and therefore the only unknown parameter of the reaction model. Further the reaction enthalpy ($\Delta_r H$ [J/mol]) as well as the pure component spectra of the three components are assumed to be unknown. Equation (4-1) can be rewritten as follows:

$$\min_k \left[f \left\{ \min_{\Delta_r H} \left(\| q_{Data} - V_r \cdot (-\Delta_r H) \cdot r(k) \| \right), \min_E \left(\| A_{Data} - C_{calc}(k) \times E \| \right) \right\} \right] \quad (4-4)$$

Where f is any combination function, q_{Data} the measured and pre-treated calorimetric data [W] (vector of length $N_{t,Q}$, see Chapter 4.4.1), $N_{t,Q}$ the number of calorimetric time samples, A_{Data} the measured and pre-treated infrared spectra [-] (matrix of dimension $N_{t,IR} \times N_{\bar{\nu}}$, see Chapter 4.4.2), $N_{t,IR}$ the number of infrared time samples and $N_{\bar{\nu}}$ the number of wave numbers in the reaction spectrum. In contrast to Equation (4-1) V_r and r are now both vectors of length $N_{t,Q}$. The matrix C_{calc} contains the concentration time profiles of the three components calculated by integration of the reaction model (dimension $N_{t,Q} \times N_C$, N_C the number of chemical components in the reaction model).

Matrix E contains the unknown pure component spectra (dimension $N_C \times N_{\nu}$). If several experiments are carried out they can be evaluated in one single step by concatenating the measured data according to Equation (4-2) to an augmented q_{Data} vector and A_{Data} matrix. If several experiments are evaluated at the same time the following additions have to be considered:

- ❖ A unique reaction enthalpy $\Delta_r H$ is used for all experiments.
- ❖ If experiments at different temperatures are combined, different pure spectra matrices will be identified. Thus $E = E(T_r)$.
- ❖ If experiments at different temperatures are combined, the rate constant k will be replaced by the following Arrhenius approximation:

$$k(T_r) = k(T_{ref}) \cdot \exp\left\{-\frac{E_A}{R} \left(\frac{1}{T_r} - \frac{1}{T_{ref}}\right)\right\} \quad (4-5)$$

Where E_A is the activation energy [J/mol], R the ideal gas constant [J/mol/K], T_{ref} the reference temperature [K], and T_r the reaction temperature of the experiment [K]. Instead of a single rate constant k the activation energy E_A as well as the reference rate constant $k(T_{ref})$ have to be identified by the nonlinear optimization.

The structure of the evaluation is divided into an outer nonlinear least-squares optimization to identify the reaction rate k (kinetic reaction parameter) and two inner linear least-squares optimizations to identify the enthalpy of reaction $\Delta_r H$ (thermodynamic reaction parameter) and the pure spectra matrix E (spectroscopic reaction parameter). Compare to Figure 4-1.

The calculation, based on Equation (4-4), will now be explained step by step.

1. The calculation starts with an **initial value** k_0 for the rate constant which is the initial value for the nonlinear optimization algorithm (see below). As explained in Chapter 4.3.1 ten different start values will be chosen randomly in a user-defined range. The nonlinear optimization algorithm will use the same range as boundary conditions for k . If more than one unknown parameter has to be identified they will be scaled to one according to their initial values.
2. The optimization algorithm will **suggest a new estimate** \hat{k} for the unknown rate constant k (k_0 at the first iteration).
3. Based on \hat{k} the **reaction model** (Equation (4-3)), system of ordinary nonlinear differential equations) **is numerically integrated** and results in the mole profiles $n_A(t)$, $n_B(t)$ and $n_C(t)$ and the reaction volume $V_r(t)$. The integration requires the

knowledge of the initial mole numbers of these components and the initial reaction volume. For the numerical calculation the C version of the LSODA (Livermore solver for Ordinary Differential Equations) algorithm is used [Tam 91]. If several experiments are evaluated at the same time, this integration step is carried out for each experiment using different initial conditions. Eventually Equation (4-5) is used to calculate k . The resulting mole and volume profiles are concatenated to single vectors.

4. Based on the mole profiles, $V_r(t)$ and the reaction model (Equation (4-3)) the **concentration profiles $c_A(k)$, $c_B(k)$, $c_C(k)$ as well as the reaction rate $r(k)$ can be calculated** (vectors of length $N_{t,Q}$). c_A , c_B , and c_C are the columns of matrix C_{calc} .
5. The following **linear least-squares optimization** is carried out in order to calculate an **estimate $\Delta_r\hat{H}$ of the reaction enthalpy Δ_rH** :

$$\Delta Q(k) = \min_{\Delta_r H} \left(\sum_{i=1}^{N_{t,Q}} [q_{Data}(i) - r(i,k) \cdot V_r(i) \cdot (-\Delta_r H)]^2 \right) \quad (4-6)$$

Where $N_{t,Q}$ is the total number of calorimetric samples in q_{Data} (all experiments, all selected points in time), and ΔQ the remaining error (sum of squares) for the optimal estimation $\Delta_r\hat{H}$. The linear least-squares optimization is bound constrained. The upper and lower bounds are user defined (see requirements in Chapter 4.2). The BVLS (Bounded Variable Least Squares) algorithm [Parker et. al. 90] originally written in FORTRAN was converted to C and implemented in the evaluation algorithm.

6. The following **linear least-squares optimization** is carried out for each wave number in A_{Data} in order to calculate an **estimate \hat{E} of the pure spectra matrix E** (pure spectra of the components A, B and C as rows (compare to (2-33)):

$$\Delta A_n(k) = \min_{e_n} \left(\sum_{i=1}^{N_{t,IR}} [A_{Data}(i, \tilde{\nu}_n) - A_{calc,n}(i, k)]^2 \right) \quad A_{calc,n} = C_{calc}(k) \times e_n \quad (4-7)$$

$$C_{calc}(k) = [c_A(k), c_B(k), c_C(k)] \quad E = \begin{bmatrix} e_A \\ e_B \\ e_C \end{bmatrix} = [e_1 \cdots e_n \cdots e_{N_{\tilde{\nu}}}]$$

Where $N_{t,IR}$ is the total number of infrared samples (all experiments, all selected points in time), ΔA_k the remaining error (sum of squares) for the optimal estimation \hat{e}_k , e_k the pure spectra of each component at the k 'th wave number and $N_{\tilde{\nu}}$ the number of selected wave numbers in A_{Data} . The linear least-squares optimization is bound constrained. Thus it is possible, **but not necessary**, to include known pure spectra into the evaluation. This is achieved by defining upper and lower bounds for the corresponding row in E according to the measured spectra (e.g.

maximum deviation of 10%). The bounds thus allow the algorithm to deviate from the pure spectra measured. The upper and lower bounds are user defined and are not requisite. The C version of the BVLS algorithm is used for the calculation. In a next step all the remaining errors ΔA_k (at each wave number) are combined to a single sum of squares for all wave numbers:

$$\Delta A(k) = \sum_{n=1}^{N_{\tilde{\nu}}} \Delta A_n(k) \quad (4-8)$$

7. It is now possible to **calculate the combined objective function** ($\Delta Comb$ [-]) that has to be minimized by the outer, nonlinear optimization algorithm:

$$\Delta Comb(k) = f(\Delta Q(k), \Delta A(k)) \quad (4-9)$$

This combination is the crucial step in the whole combined evaluation (usually called **multi-objective optimization**). The exact calculation of the combination function f will be explained in Chapter 4.5.

8. The combined error ($\Delta Comb$) is then given to the outer optimization loop of the **nonlinear optimization algorithm** (see below). The calculation restarts with a different estimate of the rate constant \hat{k} at step number two until a minimal $\Delta Comb$ is found.

The time consuming part of the evaluation algorithm (steps three to seven) are written in C and included into Matlab® as a Dynamic Link Library. The outer optimization loop is running in Matlab®

Nonlinear optimization algorithm

For the nonlinear optimization problem that has to be solved during the combined evaluation of the calorimetric and infrared data several different algorithms were tested:

- ❖ Unconstrained Nelder-Mead **simplex algorithm** (included in the `fminsearch` function of the Matlab Optimization Toolbox [*Matlab Optim*]).
- ❖ General constrained nonlinear optimization function **fmincon** [*Matlab Optim*]. Sequential Quadratic Programming (SQP) method. The QP sub problem is solved using an active set strategy.
- ❖ Constrained **Levenberg-Marquardt and Gauss-Newton** non linear least squares algorithms implemented in the `lsqnonlin` function [*Matlab Optim*].
- ❖ **Simulated Annealing** (translated from FORTRAN [*Goffe 94*] to Matlab).

The fmincon function showed the best performance for this problem and was thus used for all calculations shown in this work. The other algorithms either required too much calculation time or did only find reaction parameters close to the initial guesses.

4.5 Automatic calculation of the combined objective function $\Delta Comb$

The crucial step in the combined evaluation algorithm described in Chapter 4.4.3 is the calculation of the combined objective function $\Delta Comb$ [-] in order to identify the unknown kinetic parameters of the reaction model (see Figure 4-2) by nonlinear optimization:

$$\min_{\theta_{1..N_p}} (\Delta Comb(\theta_{1..N_p})) \quad \Delta Comb(\theta_{1..N_p}) = f_Q(\Delta Q(\theta_{1..N_p})) + f_A(\Delta A(\theta_{1..N_p})) \quad (4-10)$$

Where $\theta_{1..N_p}$ are the unknown kinetic model parameters, and f_Q as well as f_A any mathematical function that scales ΔQ and ΔA . **Such a mathematical problem is usually called multi-objective optimization.** The common problem in multi-objective optimization is that none of the single objectives can be reached without accepting trade-offs in the other objectives. In this application, the two objectives could be described as follows:

1. **Calorimetric objective function $\Delta Q(\theta_{1..N_p})$ [W^2]:**

To minimize the sum of squared errors between the measured reaction power (calorimetric data) and the simulated reaction power (Equation (4-6)) by varying the reaction model parameters $\theta_{1..N_p}$.

2. **Infrared objective function $\Delta A(\theta_{1..N_p})$ [-]:**

To minimize the sum of squared errors between the measured reaction spectrum (infrared data) and the simulated reaction spectrum (Equation (4-8)) by varying the reaction model parameters $\theta_{1..N_p}$.

A common way to deal with such a problem is to use normalized objective functions and to combine them using an arbitrary weighting factor α [-]:

$$\Delta Comb(\theta_{1..N_p}) = \Delta Q_{norm}(\theta_{1..N_p}) + \alpha \cdot \Delta A_{norm}(\theta_{1..N_p})$$

$$\text{with } \Delta Q_{norm}(\theta_{1..N_p}) = \sum_1^{N_{t,Q}} \left[\frac{q_{Data,measured} - q_{Data,calculated}(\theta_{1..N_p})}{q_{Data,measured}} \right] \quad (4-11)$$

$$\text{and } \Delta A_{norm}(\theta_{1..N_p}) = \sum_1^{N_{t,IR}} \sum_1^{N_{\bar{\nu}}} \left[\frac{A_{Data,measured} - A_{Data,calculated}(\theta_{1..N_p})}{A_{Data,measured}} \right]$$

The parameter α could be elaborated for each application to a new data set. This could only be done by **“trial and error”** and would cause unacceptable time consumption for the user. If the calculation time required for an optimization with a given value for α is low enough, a more systematic way is to show the mentioned trade-offs by plotting a **Pareto optimal curve** of the single objective functions (varying α from 0 to ∞) see example in Chapter 5.4.4). Based on such a plot the selection of the appropriate α is more systematic but still requires user interaction. However the approach based on Equation (4-11) was not satisfying due to the following reasons:

- ❖ As ΔQ and ΔA are **completely different in magnitude** (different units, different measurement equipment, different measured properties, different number of data points, different preceding linear least-squares problem, ...) the **normalization described in Equation (4-11) is not sufficient in order to make the two objective functions comparable**. Additionally this normalization is not reasonable if the measurement errors are absolute as it is the case for both signals.
- ❖ As long as the two objective functions are not comparable the **interpretation of the Pareto-optimal curve is misleading**.

Therefore in this work an automatic and systematic combining procedure was developed and will be explained in this Chapter. In the context of reaction-parameter identification **the focus lies rather on the determined reaction parameters** than on the two objective functions (calorimetric and infrared). The basic idea of the proposed combined objective function is therefore to scale them in order to equalize their influence on the determined reaction parameters $\theta_{1..Np}$. This goal can be formulated in the following way:

With given scaling functions f_Q and f_A (compare to Equation (4-10)) the nonlinear optimization of $\Delta Comb$ will result in a certain set of reaction-model parameters $\theta_{1..Np}$. If the reaction model parameters are slightly varied from their determined this will cause a change in ΔQ as well as in ΔA and consequently a change of $f_Q(\Delta Q) = \Delta_{f_Q}$ and a change of $f_A(\Delta A) = \Delta_{f_A}$. **The aim of the automatic scaling procedure is to automatically determine the functions f_Q and f_A that will deliver identical Δ_{f_Q} and Δ_{f_A} if the reaction parameters are varied. In this way the influence of the calorimetric and infrared measurement data on the final estimated reaction model parameters $\theta_{1..Np}$ is equalized.**

The proposed scaling can still be changed by the user based on external knowledge (e.g. if it was known that the Lambert Beer's law will only poorly be fulfilled during an experiment the influence of ΔA on the final results should be weaker compared to the calorimetric data). Such a scaling can never be performed automatically. However as long as ΔQ and ΔA are not yet pre-scaled by an appropriate f_Q and f_A , it will be difficult. Once this pre-scaling is done, it will be easy for the user to add his "personal" weighting to the evaluation.

Based on the aim described above, the mathematical procedure will now be explained in detail:

Figure 4-4 (first plot) shows possible shapes of the two objective / error functions ΔA (fat gray line) and ΔQ (fat black line) for the reaction example selected in Chapter 4.3.3 (one kinetic model parameter k). The minima of the two functions are marked. These two minima can be expressed according to the following separate nonlinear optimizations:

$$\Delta Q_{\min} = \min_{\theta_{1..N_P}} [\Delta Q(\theta_{1..N_P})] \rightarrow \text{estimated parameters: } \theta_{Q,1..N_P} \quad (4-12)$$

$$\Delta A_{\min} = \min_{\theta_{1..N_P}} [\Delta A(\theta_{1..N_P})] \rightarrow \text{estimated parameters: } \theta_{IR,1..N_P} \quad (4-13)$$

Independent from the optimal reaction parameters that were identified in these separate evaluations, ΔQ_{\min} [W²] and ΔA_{\min} [-] will always be a good estimate of the minimal remaining error if the selected reaction model has to be fitted into the corresponding data set. The values will generally depend on the following parameters:

- ❖ Measurement error.
- ❖ Number of measurement points.
- ❖ Model error.
- ❖ Absolute value of the measured signal.

It should be noted that ΔQ_{\min} and ΔA_{\min} only describe ΔQ and ΔA at their minima. They do not contain any information about the shape of ΔQ and ΔA . However it is assumed that the optimal model parameters found by the later combined optimization will be close to the parameters found by the separate optimization.

According to these reflections it was concluded that ΔQ_{\min} and ΔA_{\min} can be useful to transform ΔQ and ΔA to a similar range. This is achieved in the following way:

$$\Delta Q'(\theta_{1..N_P}) = \Delta Q(\theta_{1..N_P}) - \Delta Q_{\min} \quad \Delta A'(\theta_{1..N_P}) = \Delta A(\theta_{1..N_P}) - \Delta A_{\min} \quad (4-14)$$

The easiest way to combine ΔQ and ΔA is by simply adding $\Delta Q'$ to $\Delta A'$:

$$\begin{aligned} \Delta Comb^*(\theta_{1..N_P}) &= \Delta Q(\theta_{1..N_P}) - \Delta Q_{\min} + \Delta A(\theta_{1..N_P}) - \Delta A_{\min} \\ \Delta Comb^*_{\min} &= \min_{\theta_{1..N_P}} (\Delta Comb^*(\theta_{1..N_P})) \end{aligned} \quad (4-15)$$

This combined objective function is shown in **Figure 4-4** (first plot). However the minima of the combined objective ($\Delta Comb^*_{\min}$) function is more or less at the same value for k as ΔQ_{\min} . The reason for this behavior is that the sensitivity of $\Delta Q'$ with respect to k is much higher than the corresponding sensitivity of $\Delta A'$. Therefore a

combination according to Equation (4-15) will always favor the more sensitive data set (see example in Appendix E.3.8).

It is important to note that the two sensitivities of $\Delta Q'$ and $\Delta A'$ cannot be compared to each other as they have completely different sources:

- ❖ Different preceding linear least-squares optimization (Equations (4-8) and (4-9)) with different number of unknowns.
- ❖ Different signal sources (reaction rates vs. component concentration).
- ❖ Different measurement equipment and consequently measurement error.

It was therefore concluded that the following scaling factors have to be added to Equation (4-15):

$$\begin{aligned} \Delta Comb(\theta_{1..N_p}) &= S_{IR} (\Delta A(\theta_{1..N_p}) - \Delta A_{\min}) + S_Q (\Delta Q(\theta_{1..N_p}) - \Delta Q_{\min}) \\ \Delta Comb_{\min} &= \min_{\theta_{1..N_p}} (\Delta Comb(\theta_{1..N_p})) \end{aligned} \quad (4-16)$$

With the scaling factors S_{IR} [-] and S_Q [W^2] it is possible to influence the sensitivity of $\Delta A'$ and $\Delta Q'$ with respect to the reaction model parameters $\theta_{1..N_p}$. This is shown in Figure 4-4 (second plot). By choosing different scaling factors ($S_{IR} = 3$ and $S_Q = 0.5$ as example values) the position of the combined minimum $\Delta Comb_{\min}$ is significantly moved compared to the first plot.

Thus the remaining task is to determine the correct values of S_{IR} and S_Q automatically. Equation (4-16) can then be applied to any optimization problem. It was used for all calculations shown in this work.

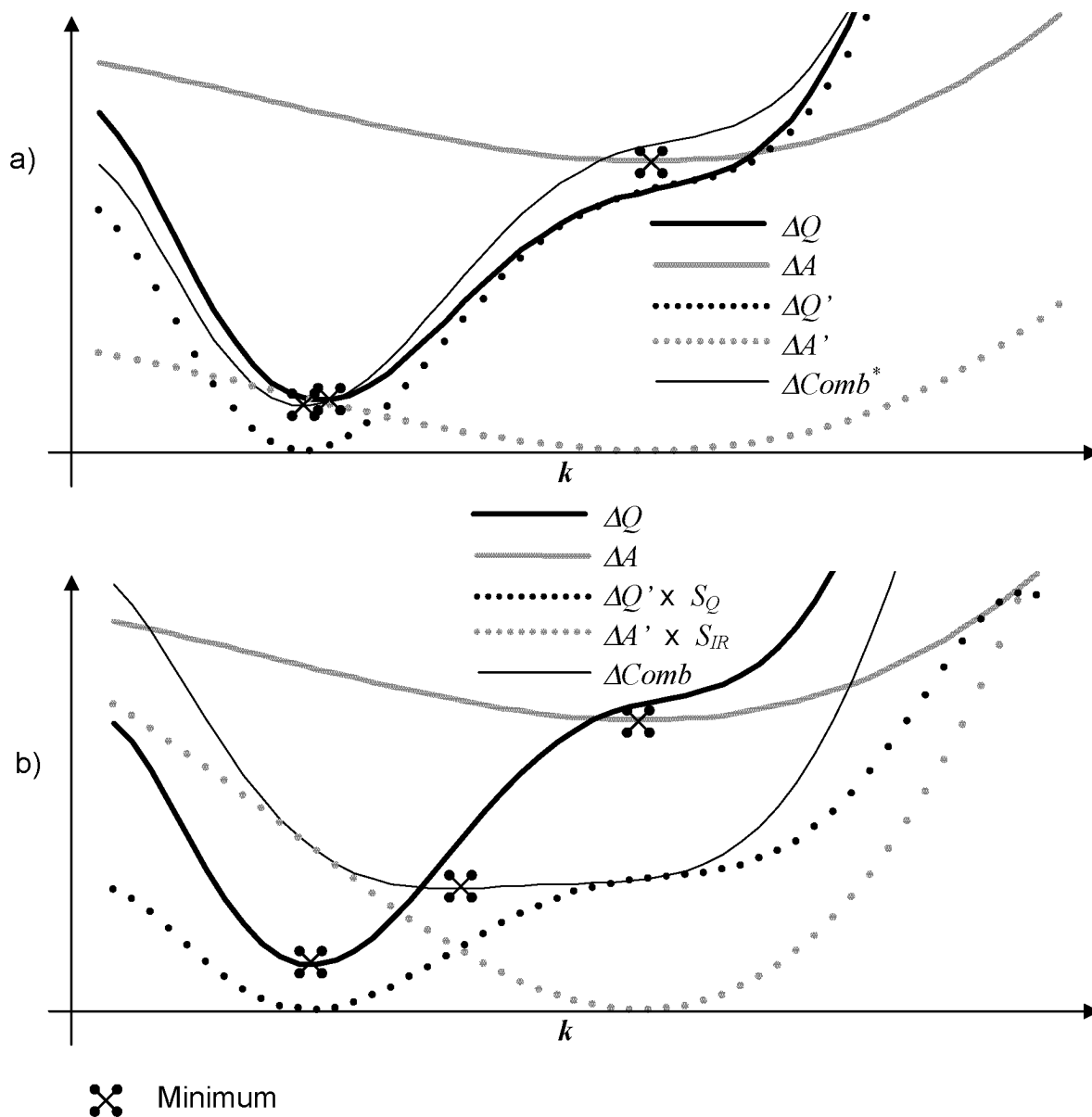


Figure 4-4: Possible shape of the different objective functions. a) Unscaled separate objective functions ΔQ and ΔA . b) Scaled separate objective functions ΔQ and ΔA with arbitrary values ($S_Q = 0.5$ and $S_{IR} = 3$).

The aim of the combination method is to guarantee that ΔA and ΔQ have equal influence to the finally determined reaction model parameters $\theta_{1..Np}$. It is therefore necessary to perform a sensitivity analysis in order to determine appropriate values for S_Q and S_{IR} :

$$S_Q = S_{Q,1} = \frac{2 \cdot N_P}{\sum_{i=1}^{N_P} |\Delta Q(\theta_{Q,i} + \Delta\theta_i) - \Delta Q_{\min}| + \sum_{i=1}^{N_P} |\Delta Q(\theta_{Q,i} - \Delta\theta_i) - \Delta Q_{\min}|} \quad (4-17)$$

$$S_{IR} = S_{IR,1} = \frac{2 \cdot N_P}{\sum_{i=1}^{N_P} |\Delta A(\theta_{IR,i} + \Delta\theta_i) - \Delta A_{\min}| + \sum_{i=1}^{N_P} |\Delta A(\theta_{IR,i} - \Delta\theta_i) - \Delta A_{\min}|} \quad (4-18)$$

Where N_P is the number of kinetic model parameters that have to be identified, $\theta_{Q,i}$ the optimal i 'th model parameter determined by the separate optimization (4-12), $\theta_{A,i}$ the optimal i 'th model parameter determined by the separate optimization (4-13) and $\Delta\theta_i$ the sensitivity range of the i 'th parameter. The magnitude of these sensitivity ranges is crucial. A small magnitude will only give informations about the shape of ΔQ and ΔA close to their individual minima; a large range will probably result in an arbitrary scaling factor. It was concluded that the most reasonable range for the sensitivity analysis is the range defined by the separate optimizations of ΔQ and ΔA :

$$\Delta\theta_i = \theta_{Q,i} - \theta_{IR,i} \quad (4-19)$$

A **first combined optimization** according to Equations, (4-12), (4-13), and (4-16) to (4-19) can now be carried out (compare to **Figure 4-5**).

However the sensitivity analyses of ΔQ and ΔA were not performed at the same values for the model parameters but at the optimal values of the separate optimizations (Equations (4-12) and (4-13)). Therefore the **calculation of the scaling factors is repeated** after the first combined optimization:

$$S_Q = S_{Q,2} = \frac{2 \cdot N_P}{\sum_{i=1}^{N_P} |\Delta Q(\theta_{Comb_1,i} + \Delta\theta_i) - \Delta Q_{\min}| + \sum_{i=1}^{N_P} |\Delta Q(\theta_{Comb_1,i} - \Delta\theta_i) - \Delta Q_{\min}|} \quad (4-20)$$

$$S_{IR} = S_{IR,2} = \frac{2 \cdot N_P}{\sum_{i=1}^{N_P} |\Delta A(\theta_{Comb_1,i} + \Delta\theta_i) - \Delta A_{\min}| + \sum_{i=1}^{N_P} |\Delta A(\theta_{Comb_1,i} - \Delta\theta_i) - \Delta A_{\min}|} \quad (4-21)$$

Where $\theta_{Comb_1,i}$ is the optimal i 'th model parameter determined by the first combined optimization (Equations, (4-12), (4-13), and (4-16) to (4-19)).

Applying Equations (4-12), (4-13), and (4-18) to (4-21) it is now possible to perform a **second combined optimization** of the calorimetric and infrared data according to the objective function defined by Equation (4-16) (compare to Figure 4-5)). However in none of the applications shown in this work, a significant change between the first and second combined evaluation could be observed. **Therefore in Chapter 5 only the result of the second combined optimization will be considered.**

The whole calculation performs completely **automatic and systematic**. The influence of the error functions ΔA and ΔQ at the combined optimum onto the combined objective function $\Delta Comb$ (and thus to the finally determined reaction model parameters $\theta_{1..Np}$) is equalized by the following two modifications:

1. The **absolute values of $\Delta A(\theta_{1..Np})$ and $\Delta Q(\theta_{1..Np})$** at the combined optimum are **equalized** by shifting them by the values ΔA_{min} and ΔQ_{min} .
2. The **sensitivity of $\Delta A(\theta_{1..Np})$ and $\Delta Q(\theta_{1..Np})$** with respect to the model parameters $\theta_{1..Np}$ at the combined optimum are **equalized** by the scaling factors $S_{IR,2}$ and $S_{Q,2}$.

The aim formulated above is thus met. The whole calculation flow sheet is summarized in Figure 4-5. As explained in Chapter 4.3.3 the separate evaluation of the calorimetric and infrared data is anyway required for a systematic evaluation. The results can thus be used directly for the succeeding combined evaluation.

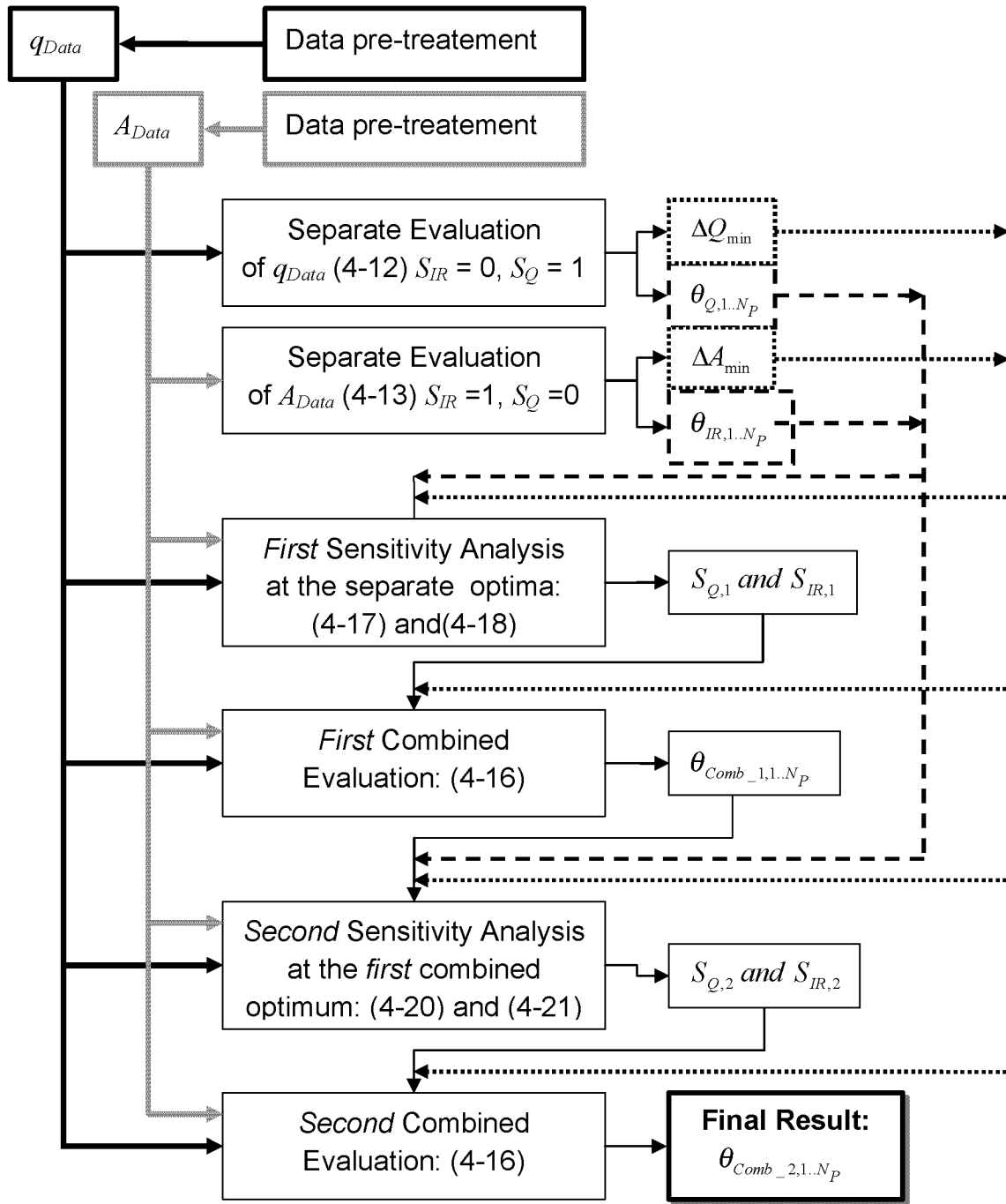


Figure 4-5: Flow sheet of the combined evaluation algorithm. The combined objective function $\Delta Comb$ is calculated automatically not requiring any weighting functions.

5 APPLICATIONS AND RESULTS

5.1 Overview

The following reaction examples were carried out with the new reaction calorimeter combined with an IR-ATR probe (described in Chapter 3). Some of them were then evaluated using the new evaluation algorithm (described in Chapter 4).

Neutralization of NaOH with H₂SO₄ (Chapter 5.2)

This experiment was chosen because reference data about the heat of neutralization is available from different sources. Based on this reaction the capability of the new reaction calorimeter to deal with fast and highly exothermal reactions can be shown. The measured calorimetric data was evaluated based on classical methods.

Single step reaction: Hydrolysis of acetic anhydride (Chapter 5.3)

This reaction was chosen because many reference data about the reaction enthalpy as well as the kinetics are available from different sources. This reaction represents the “standard reference” reaction within the field of reaction calorimetry. The measured infrared and calorimetric data was evaluated separately based on classical methods (Chapter E.2.4 and [Zogg *et. al.* 03]) as well as with the new developed combined approach (Chapters 5.3.1 and 5.3.2).

Consecutive reaction: Epoxidation of 2,5-di-tert-butyl-1,4-benzoquinone (Chapter 5.4)

This reaction was chosen as it represents one of the few appropriate consecutive reaction examples where reference data from different sources is available. However as described in Chapter E.3.6 their reliability turned out to be rather low. Based on this more complex reaction the performance of the combined evaluation of calorimetric and infrared data can be discussed (see Chapters 5.4.1 to 5.4.4 and some more results in [Zogg *et. al.* 03, submitted]).

Industrial reaction examples (Appendix E.4)

Two industrial reaction examples demonstrated that new reaction calorimeter is able to deal with reactions relevant in practice and not only with “ideal” model reactions. It was shown that the calorimeter is able to deal with fast and highly exothermal reactions due to the significant improvement of the dynamics compared to a standard reaction calorimeter. Both reaction examples show strong and unpredictable baseline changes that could be measured with the new reaction calorimeter.

Heterogeneous reaction example (Appendix E.5)

This last reaction example was chosen in order to investigate the behavior of the new reaction calorimeter as well as the IR-ATR probe, if a heterogeneous (solid – liquid) reaction system is investigated.

5.2 Neutralization of NaOH with H₂SO₄

5.2.1 Evaluation of the calorimetric data

Experimental conditions are given in Appendix E.1.1. The measurement results of the neutralization of NaOH with H₂SO₄ are shown in **Figure 5-1**. The heat flow from the reactor into the jacket (q_{Flow} , (2-9)) is changing. The main reason is a change of the heat-transfer area A . The large change is caused by the dosing of 14.4 ml of H₂SO₄ into 26 ml of NaOH. A shift of the power-compensation signal (q_{Comp} , ((2-15))) can be observed from about 20 to 26 W. The change of the q_{Comp} signal is compensated by a change of the total cooling power ($q_{Cooling}$ ((3-13))) of the Peltier elements of the intermediate thermostat. By applying Equation (3-23) the total heat production of the neutralization reaction q_{tot} can be calculated without any calibrations of the heat-transfer coefficient and is shown in the second plot of Figure 5-1.

Figure 5-1 further shows the precision of the temperature controlling. As the neutralization reaction is an extremely fast reaction (dosing controlled), the true heat production profile q_{tot} should be a step like function. In other words, the reaction power of about 15 W / 26 ml is present as soon as the dosing starts and disappears right after the end of the dosing. Although a maximum reaction power of about 550 W/l has to be removed instantly, the temperature of the reactor content is only changing by 0.3 K over a period of about 30 seconds.

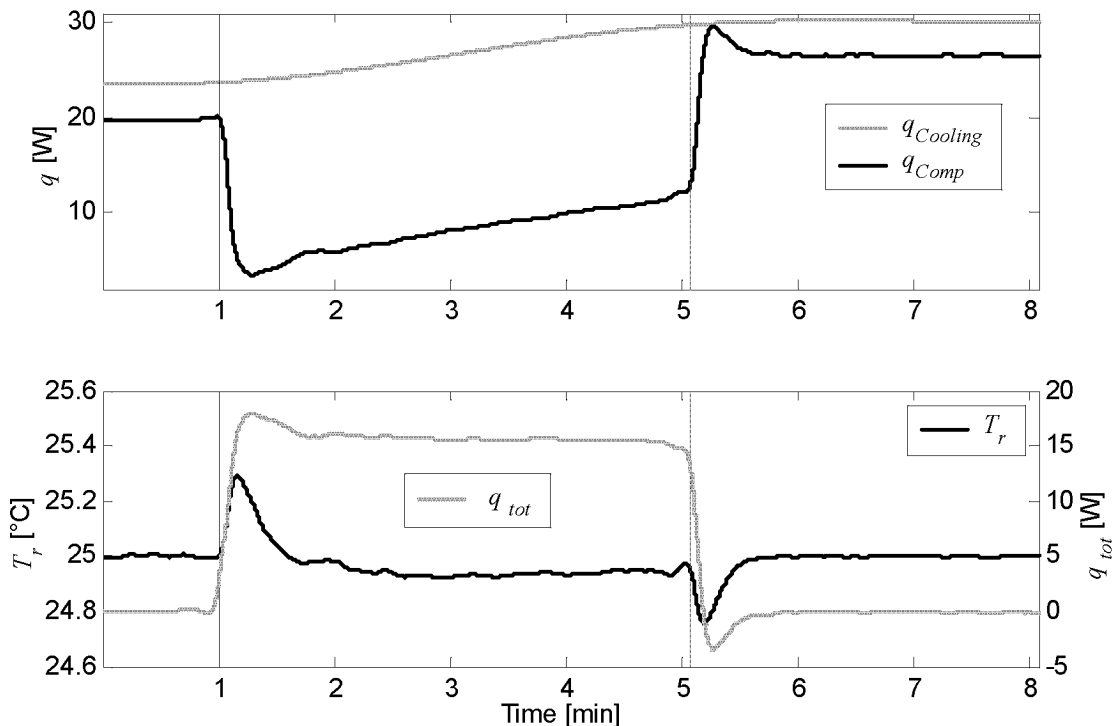


Figure 5-1: Neutralization experiment of 26 ml of NaOH (2.77N) with 14.4 ml of H₂SO₄ (4N, Feed) at 25 °C. The maximum reaction power equals 550 W/l. The dosing period of H₂SO₄ is indicated with dashed lines.

The measured baseline can be expressed as follows (according to Equation (3-12) and (3-21)):

$$q_{Baseline}^{measured} = q_{Cooling} + \Delta q - [q_{Cooling}(t=0) + \Delta q(t=0)] \quad (5-1)$$

Figure 5-2 (second plot, straight line) shows the measured baseline. If only the power-compensation signal would be available, as is the case for conventional calorimeters, the observed baseline change would have to be compensated mathematically by supposing a linear change of the heat-transfer area (according to (D-12) with $bl(t) = V_r(t)$):

$$q_{Baseline}^{mathematical} = \frac{V_r(t) - V_r(t=0)}{V_r(t=end) - V_r(t=0)} \cdot (q_{Comp}(t=end) - q_{Comp}(t=0)) \quad (5-2)$$

Where V_r is the reaction volume [l]. This compensation is accurate as long as the density of the mixture is changing linearly as well and the heat-transfer coefficient U in q_{Flow} (Equation (2-9)) remains constant. The mathematical baseline calculated by Equation (5-2) is also shown in Figure 5-2 (second plot, dotted line) and is similar to the measured baseline (straight line).

The heat production q_{tot} calculated using this mathematical baseline is also shown in Figure 5-2 (first plot, dotted line) and is similar to the measured q_{tot} (straight line). The integration of the q_{tot} curves gives an enthalpy of -134 ± 1 kJ/mol using the measured baseline and -136 ± 2 kJ/mol using the mathematical baseline. The two values deviate only by 1% and are close to the literature values of -139.1 kJ/mol [Schildknecht 81] and -132 kJ/mol [Landolt-Börnstein, a].

Figure 5-2 further shows the power consumption of the stirrer engine. No change can be observed during the reaction.

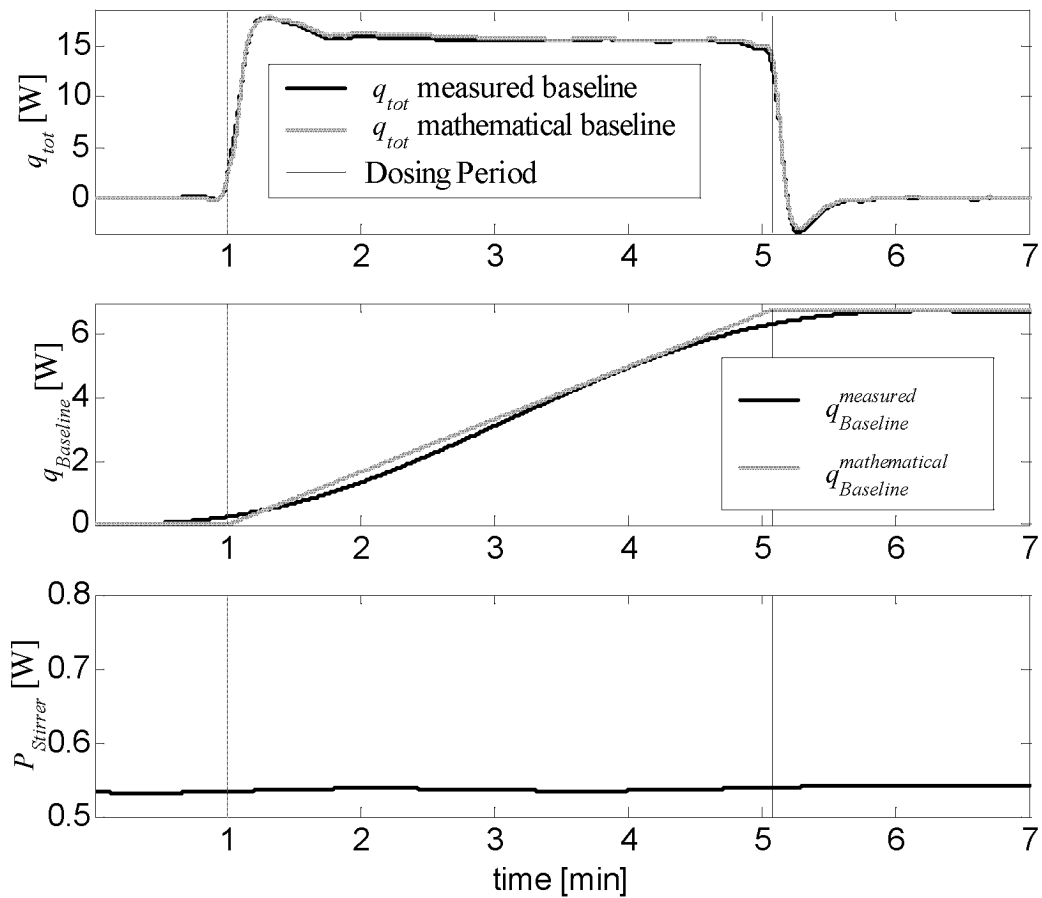


Figure 5-2: Comparison of the mathematical and measured baseline for the neutralization experiment of NaOH with H₂SO₄ at 25 °C. The dosing period of H₂SO₄ is indicated with dashed lines. The changing baseline is mainly caused by the change of the heat-transfer area due to the volume increase.

5.3 Hydrolysis of acetic anhydride

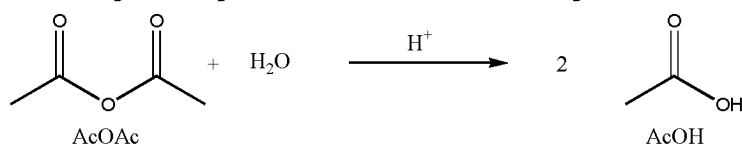


Figure 5-3: Hydrolysis of acetic anhydride with water. The acetic anhydride was fed together with acetic acid in order to increase the solubility of acetic anhydride in water.

The experimental conditions are given in Appendix E.2.1. The evaluations described in the following subchapters use pre treated measurement data. This data pre treatment required for the calorimetric as well as the infrared data is given in Appendix E.2.2 and E.2.3. The algorithm required for the evaluations is described in Chapter 4.

A separate evaluation of the calorimetric and infrared data based on classical evaluation methods is given Chapter E.2.4. All literature references are also given in this Appendix.

5.3.1 Combined evaluation of the infrared and calorimetric data

In the following the total power release or uptake measured by the calorimeter (q_{tot}) mainly contains two different heat flows: 1) the reaction power (q_{React}) and the heat of mixing (q_{mix}) during the dosing period. q_{tot} is calculated based on the measured data using Equation (3-23).

Pretreated infrared and calorimetric data (see Appendix E.2.2 and E.2.3) were used for all the calculations performed in this section. The evaluation method applied is described in Chapter 4. All measurements, carried out at the same temperature, were concatenated into a single measurement vector (q_{Data}) and matrix (A_{Data}) (according to Equation (4-2)). The evaluation of all the measured data at one temperature is thus carried out in a single step. The evaluation is then repeated for each measured temperature (25, 40 and 55 °C).

In order to allow a visual comparison of the measured and calculated reaction spectrum A only one wave number of A will be shown throughout this section (see Figure E-4). However it should be noted that the whole reaction spectrum is evaluated and that overlapping of different components at the same wave number is allowed (see description of the evaluation algorithm in Chapter 4.4.3).

The reaction model was formulated according to the discussion in Appendix E.2.4.1. It is the basis for all evaluations (compare to Figure 4-2) and implemented in form of the following differential equations:

$$\begin{aligned}
 \frac{dn_{AcOAc}}{dt} &= -r(k,t) \cdot V_r(t) + v_{dos} \cdot c_{dos,AcOAc} \\
 \frac{dn_{H_2O}}{dt} &= -r(k,t) \cdot V_r(t) \\
 \frac{dn_{AcOH}}{dt} &= 2 \cdot r(k,t) \cdot V_r(t) + v_{dos} \cdot c_{dos,AcOH} \\
 \frac{dV_r}{dt} &= v_{dos} \\
 r(t,k) &= k \cdot \frac{n_{AcOAc}(t)}{V_r(t)}
 \end{aligned}
 \tag{5-3}$$

Where V_r is the reaction volume [l], n the number of moles of the corresponding component [mol], v_{dos} is the dosing rate [l/s], $c_{dos,AcOAc}$ the concentration of acetic anhydride in the feed, $c_{dos,AcOH}$ the concentration of acetic acid in the feed. The only kinetic reaction model parameter is the rate constant k [s^{-1}]. All three chemical components defined by the reaction model (water, acetic anhydride and acetic acid) are considered as absorbing species in the calculation of the reaction spectrum. No measured pure spectra were used as constraints. The reaction parameters that have to be identified are listed in **Table 5-1** together with their bounds.

Table 5-1: Reaction parameters (and their bounds) required for the evaluation of the acetic anhydride measurements and their bounds.

	Lower bound	Upper bound
Rate constant k [s^{-1}] (at each temperature).	1e-4	0.1
Absorption coefficients at each wave number of the reaction Spectrum A and for all three chemical components [-]. (For each temperature new absorption coefficients were calculated.)	0	5
Heat of reaction $\Delta_r H$ [kJ/mol] (at each temperature).	0	-1000

The whole evaluation will be carried out according to the flow sheet presented in Chapter 4.3.3 (Figure 4-3). Therefore in a first step the complete time range of both measurement data (calorimetric and infrared) was evaluated separately (evaluation set II Table E-4 and Table E-6). The result is shown in **Figure 5-4**.

The left plot of Figure 5-4 shows the total measured calorimetric data (fat gray line), the selected measurement points for the evaluation (triangles, see Appendix E.2.3) and the simulated calorimetric signal (thin black line, best fit according to Equation (4-12)). It is obvious that the reaction model (5-3) could not be fitted into the whole time range of the measurement data.

However the same reaction model could be fitted into the infrared data. This is shown in the lower left plot of Figure 5-4: The measured absorbance time curve at 1139 cm^{-1} (points, compare to Figure E-4, only one wave number is chosen in order to simplify the illustration) fits well into the simulated absorbance profile (thin black line, best fit according to Equation (4-13)).

It is assumed that the difference of the two separate evaluations is due to the heat of mixing occurring during the dosing of acetic anhydride. They do only affect the calorimetric signal. Therefore it is possible to exclude the calorimetric data, measured during the dosing phase, from the evaluation.

Figure 5-5 shows the analogous plots to Figure 5-4 (left) but now the points during the dosing phase as well as 1 minute after and 0.5 minutes before, are excluded from the separate calorimetric evaluation (evaluation set I, Table E-5). The model agrees now quite well.

The hypothesis made, that the heat of mixing are responsible for the disturbance of the calorimetric signal during the dosing phase, can finally be tested by carrying out a combined evaluation of the infrared and calorimetric data.

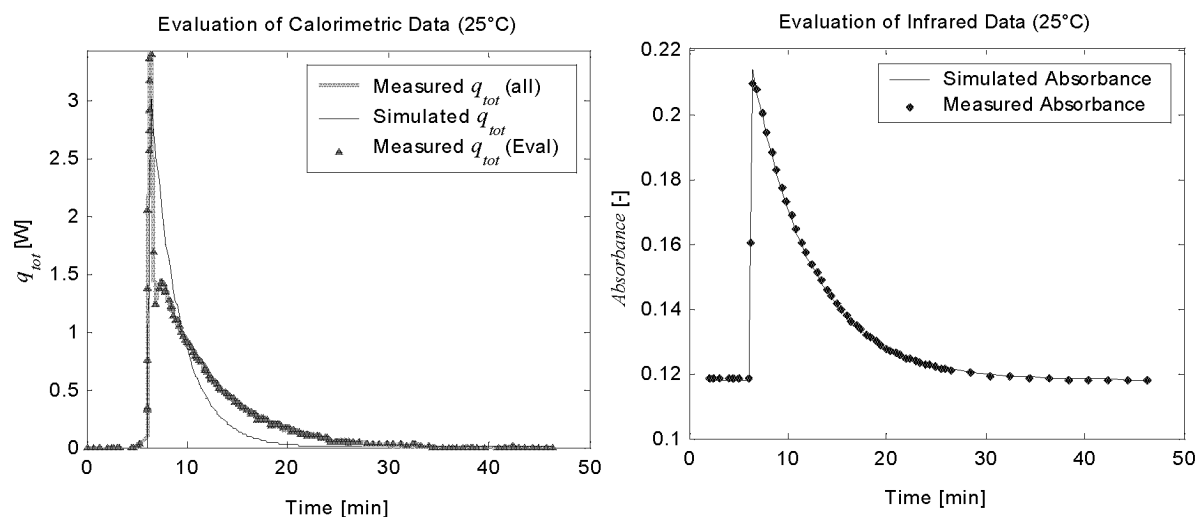


Figure 5-4: Hydrolysis of acetic anhydride. Separate evaluation of the calorimetric (left) and infrared (right) data of the full time range (evaluation set II). In both plots a mean value of all reaction experiments at 25 °C is displayed. Only one wave number (1139 cm^{-1} , see Figure E-4) of the reaction spectrum is shown in the right plot. The reaction starts with the dosing of acetic anhydride / acetic acid mixture (only 24 s).

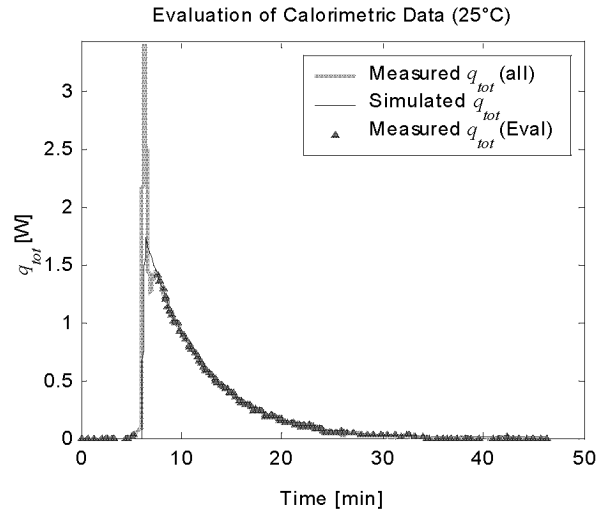


Figure 5-5: Hydrolysis of acetic anhydride. Separate evaluation of the calorimetric data. The measurement points during and shortly before / after the dosing period are excluded (evaluation set I). A mean value of all reaction experiments at 25 °C displayed. The reaction starts with the dosing of acetic anhydride / acetic acid mixture (only 24 s).

The results of the combined evaluation (see Equation (4-16) and Figure 4-5) are shown in **Figure 5-6** (25, 40 and 55 °C). As the differences between the model and the measured data (calorimetric as well as infrared) are not significant it can be concluded that the reaction model (5-3) is now able to describe both data sets simultaneously.

The independently determined rate constants k at the three different temperatures are plotted in an Arrhenius plot (upper right plot in Figure 5-6). First of all, the separate as well as the combined evaluation resulted in similar values for k . It can be concluded that the reaction model (5-3) is now able to describe both measurement data (calorimetry and infrared) well. Further it should be noted that the independently determined k at each temperature all lay on a straight line in the Arrhenius plot. This fact further indicates a proper choice of the reaction model.

5 Applications and Results

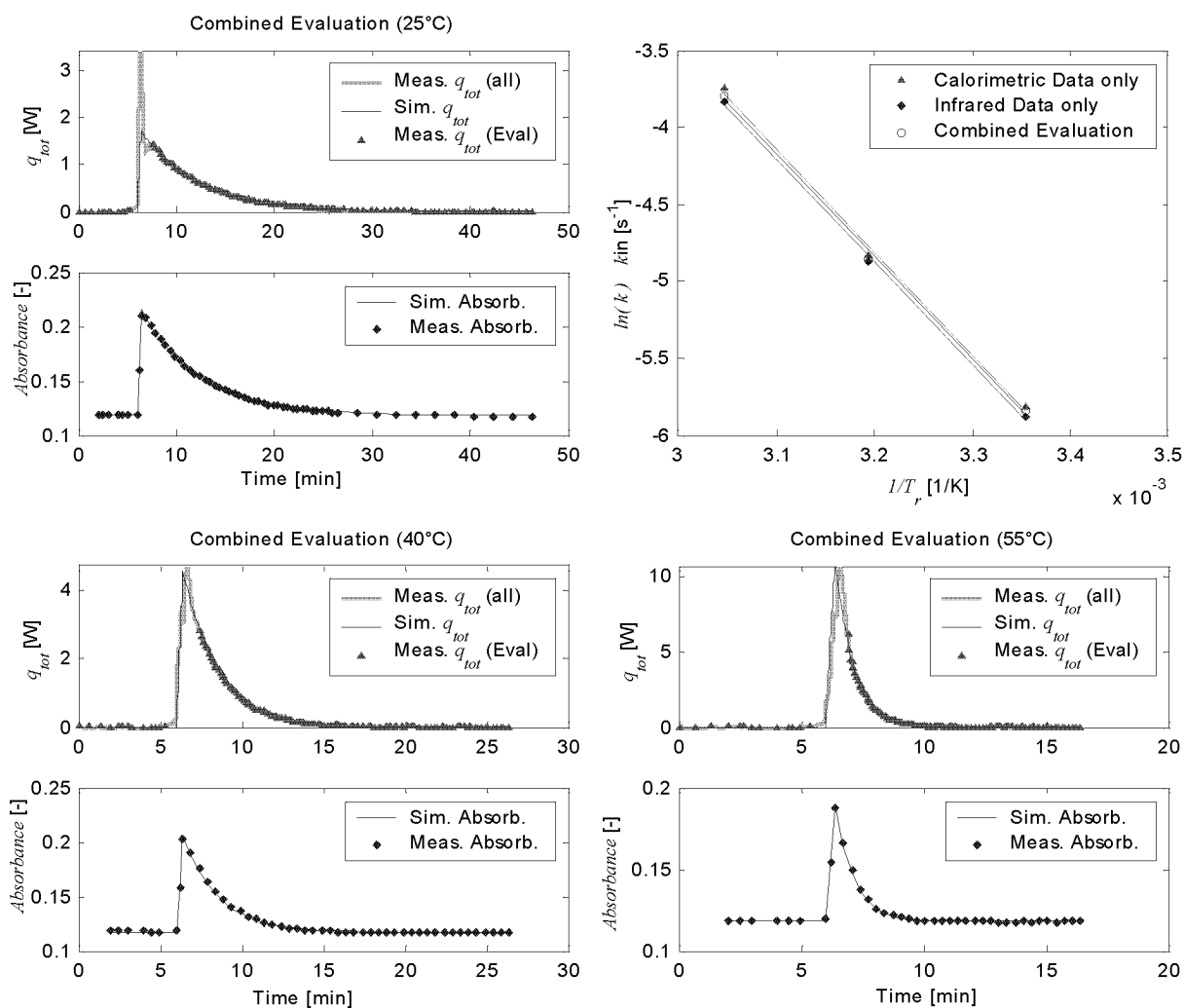


Figure 5-6: Hydrolysis of acetic anhydride. Results of the combined evaluation. The model-fit results are shown for all experiments (mean values at each temperature) at all temperatures.

All the results obtained by the separate as well as the combined evaluation (see Figure 4-5) are listed in **Table 5-3** and compared to the corresponding results of the classical evaluation (Appendix E.2.4, Table E-7) as well as the literature references. Obviously any kind of evaluation method applied, results in basically the same values for the desired reaction parameters $\Delta_r H$, k and E_A .

The generally suggested flow-sheet (see Figure 4-3) for the evaluation of calorimetric and infrared data proved to be useful. Even for this simple application, the heat of mixing, occurring during the dosing phase of the acetic anhydride, was successfully identified and excluded from the calculation (see also discussion in Appendix E.2.4).

As mentioned in Chapter 4.2 the determination of the pure spectra of the involved chemical component is not the focus of the developed evaluation method. However these spectroscopic reaction parameters (see Figure 4-2) have to be identified during the evaluation and are therefore a side product of the whole calculation. The

calculated pure spectra are shown in **Figure 5-7** and are compared to measured pure spectra. Although no prior information about the pure spectra was used (see bounds of the pure spectra matrix in Table 5-1), the calculated and measured pure spectra are quite similar. No significant difference between the calculated pure spectra at different temperatures can be seen. However the deviations of the relative peak intensities as well as the spectral position of the peaks is significant.

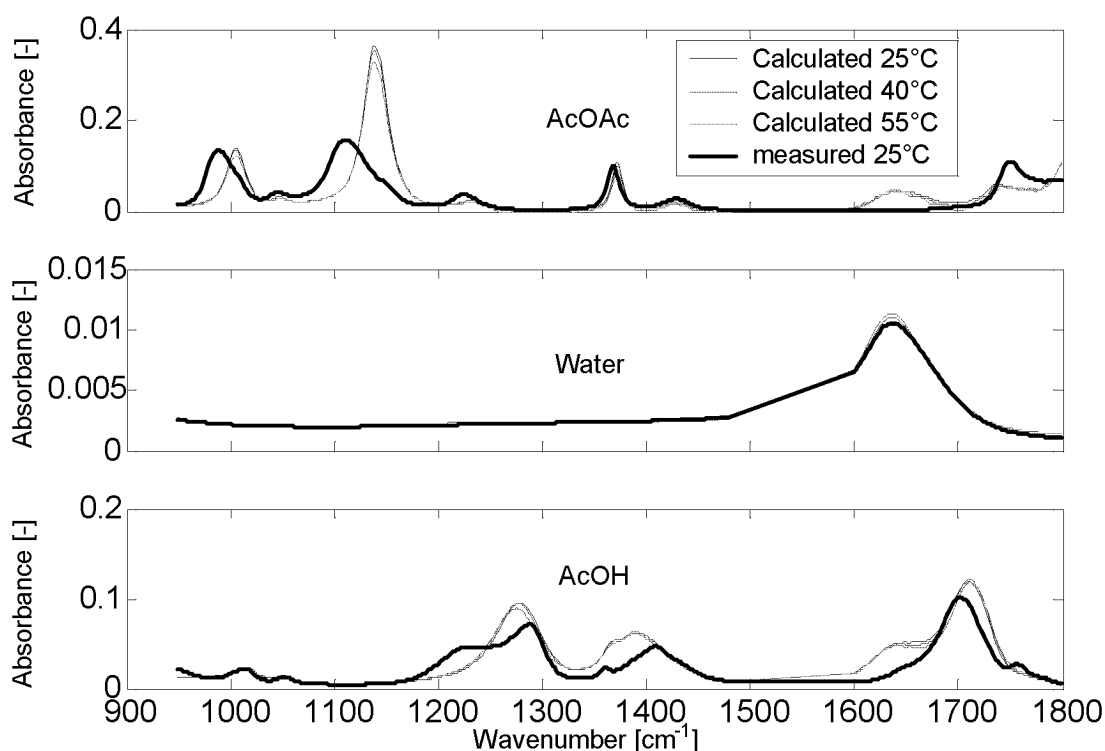


Figure 5-7: Hydrolysis of acetic anhydride. Calculated pure spectra by the combined evaluation (data set I). They are compared to measured pure spectra.

In **Figure 5-8** (first and second plot) the error functions ΔA and ΔQ (Equations (4-8) and (4-6)) are shown for each evaluation step (compare to Figure 4-5). As mentioned, the experiments at different temperatures were evaluated separately. Therefore the values are given for each temperature. As would be expected the lowest infrared model-fit error ΔA was found by the separate evaluation of the infrared data, the highest by the separate evaluation of the calorimetric data. The analogous behavior is found for the model-fit error ΔQ . The sums of ΔQ and ΔA over all measurement temperatures are shown in Table 5-3.

As all evaluations were carried out using ten different random start values, the quality of the identification can be measured by counting the number of equal and best solutions found (see Chapter 4.3.2). This “number of hits” is shown in the third plot of Figure 5-8. It can be concluded that all identifications were very robust as all “number of hits” are close to the maximum of 10. The mean value over all measurement temperatures is given in Table 5-3.

The automatically calculated scaling factors S_{IR} and S_Q (see Chapter 4.5, Equations (4-16) to (4-20) and Figure 4-5) are shown in the last two plots of Figure 5-8.

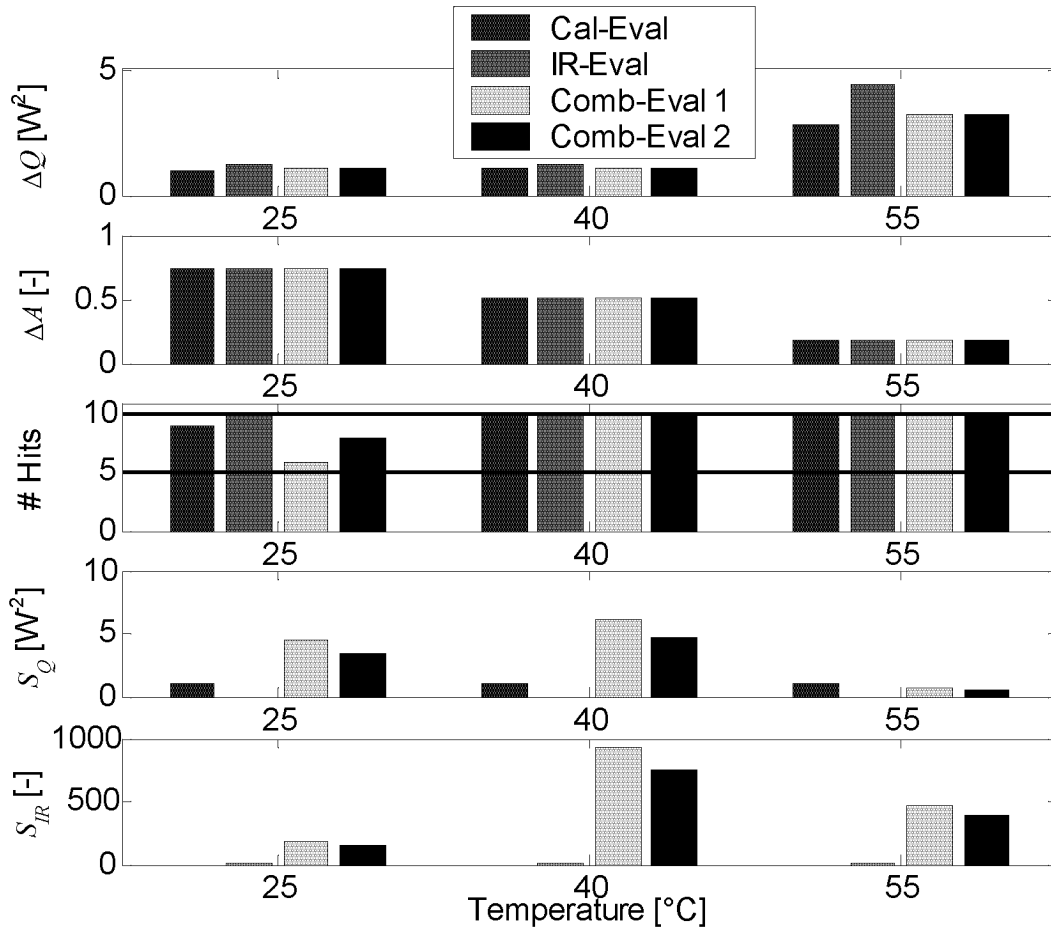


Figure 5-8: Hydrolysis of acetic anhydride. First and second plot: Final error functions ΔA and ΔQ . Third plot: Number of hits (maximum 10). Last two plots: S_{IR} and S_Q (see Equation (4-16)).

5.3.2 Simultaneous evaluation of all measurements at all temperatures

As explained in Chapter 4.4.3 it is also possible to evaluate several measurements at different temperatures in one single step. This was done using the evaluation data set I (Table E-4 and Table E-5, all measurements at all temperatures). In contrast to the individual evaluation at each temperature (see Chapter 5.3.1) only one reaction enthalpy $\Delta_r H$ for all temperatures had to be identified. The pure spectra of the three components (matrix E) were still assumed to be temperature dependent and thus three sets of E were identified. The rate constant k was replaced by the Arrhenius Equation (4-5). The reaction parameters that were identified by the combined evaluation algorithm are summarized in **Table 5-2**.

Table 5-2: All reaction parameters (and their bounds) required for the evaluation of the acetic anhydride measurements at all temperatures.

	<i>Lower bound</i>	<i>Upper bound</i>
Rate constant k at 25 °C [s^{-1}]	1e-4	0.1
Activation energy E_A [kJ/mol]	10	100
Absorption coefficients at each wave number of the reaction Spectrum A and for all three chemical components [-]. (<i>For each temperature new absorption coefficients were calculated.</i>)	0	5
Heat of reaction $\Delta_r H$ [kJ/mol]	0	-1000

The results of this overall evaluation are shown in **Table 5-3** (shaded in gray). Similar to the discussion in 5.3.1 it can be concluded that the separate calorimetric and infrared as well as the combined evaluation gave the same results. They are in good agreement with the results of the individual evaluations at each temperature. The identification of the pure spectra E was also possible (similar to Figure 5-7). The differences between the pure spectra at different temperatures were negligible. The robustness of the evaluation was high as the “number of hits” was at the maximum of 10 for each evaluation (compare to Figure 5-8).

5.3.3 Summary of all results

Table 5-3: *Hydrolysis of acetic anhydride*. Final results of the separate and combined evaluations using the new evaluation algorithm (see 4). The main results from the classic evaluation as well as the literature reference are also listed (for details see Table E-7). ¹⁾ Average value of the three temperatures. ²⁾ The separate evaluation was carried out by setting $S_Q = 0$ in (4-16) but still both data sets were evaluated. Therefore $\Delta_r H$ can also be identified from the separate evaluation of the infrared data. ^{3, 4)} Data set I, with excluded dosing period in the calorimetric data. ³⁾ Each temperature was evaluated separately (see Chapter 5.3.1). The activation energy E_A was calculated in a succeeding Arrhenius plot. ⁴⁾ All measurements at all temperatures were evaluated at the same time (see Chapter 5.3.2). ⁵⁾ Calculated based on the identified activation energy E_A and the rate constant at 25°C. ⁶⁾ Classic evaluation of the calorimetric data (see Appendix E.2.4.1). ⁷⁾ Classic evaluation of the calorimetric data (see Appendix E.2.4.3). ⁸⁾ Calorimetric and infrared error function at the determined optimum (Equations (4-8) and (4-6)). Sum over all temperatures. ⁹⁾ Number of hits (see Chapter 4.3.2), maximum 10 (mean value over all temperatures). ¹⁰⁾ A detailed list of literature references is given in Chapter E.2.4.1, Table E-7.

	Comb Eval ³⁾	Cal Eval ³⁾	IR Eval ³⁾	Comb Eval ⁴⁾	Cal Eval ⁴⁾	IR Eval ⁴⁾	Classic Cal Eval ⁶⁾	Classic IR Eval ⁷⁾	Ref. ¹⁰⁾
$\Delta_r H$ 25°C [kJ/mol]	-57	-57	-58 ²⁾	-	-	-	-57 ± 1	-	-57
$\Delta_r H$ 40°C [kJ/mol]	-60	-60	-60 ²⁾	-	-	-	-62 ± 2	-	
$\Delta_r H$ 55°C [kJ/mol]	-59	-60	-58 ²⁾	-	-	-	-60 ± 1	-	
$\Delta_r H$ av. ¹⁾ [kJ/mol]	-59 ± 1	- 59 ± 2	- 58 ± 1	-59	-59	-58 ²⁾	-60 ± 3	-	
E_A [kJ/mol]	56	56	55	56	57	54	57	57	57
k 25°C [10 ⁻³ s ⁻¹]	2.9	3	2.8	2.8	2.8	2.8	3 ± 0.2	2.8 ± 0.2	2.76
k 40°C [10 ⁻³ s ⁻¹]	7.8	8	7.6	8.2 ⁵⁾	8.4 ⁵⁾	7.9 ⁵⁾	8.5 ± 0.6	7.8 ± 0.3	
k 55°C [10 ⁻³ s ⁻¹]	22.5	23.5	21.5	21.9 ⁵⁾	23.2 ⁵⁾	20.6 ⁵⁾	23.5 ± 0.8	22.2 ± 0.5	
ΔQ ⁸⁾ [W ²]	5.4	4.9	6.9	6.5	5.6	9.1			
ΔA ⁸⁾ [-]	1.425	1.431	1.423	1.425	1.429	1.424			
# Hits ⁹⁾ [-]	9.3	9.7	10	10	10	10			

5.4 Epoxidation of 2,5-di-tert-butyl-1,4-benzoquinone

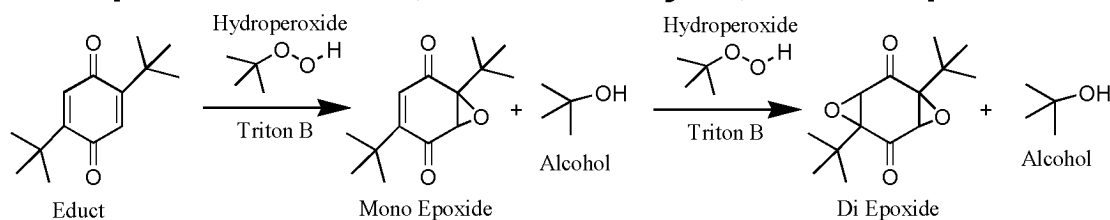


Figure 5-9: Consecutive epoxidation of 2,5-di-tert-butyl-1,4-benzoquinone with tert-butyl-hydroperoxide. The catalyst was dosed into the reaction mixture in order to initiate the reaction.

The experimental conditions are given in Appendix E.3.1. The evaluations described in the following subchapters use pre treated measurement data. This data pre treatment required for the calorimetric as well as the infrared data is given in Appendix E.3.2 and E.3.3.

A separate evaluation of the calorimetric data based on classical evaluation methods is given Chapter E.3.4. Literature data on the reaction enthalpy are also discussed in this Chapter. Literature references that describe the kinetics of the reaction are discussed in Appendix E.3.6. Special observations made during these experiments that will not be mentioned in the following subchapters are summarized in Appendix E.3.5. The behavior of the measured baseline $q_{Cooling}$ is also shown Appendix E.3.5.

The reaction experiments were carried out at four different temperatures. In a first step the measurement data were evaluated using the new combined evaluation algorithm (described in Chapter 4) using different reaction enthalpies for each temperature (see Chapter 5.4.1). Then different possible reaction models were evaluated based on the same measurement data but also using measurement data of additional experiments at different concentrations (see Chapter 5.4.2). In third step the evaluation all experiments at all temperatures was carried out using the same reaction enthalpies for each temperature (see Chapter 5.4.3).

Finally the performance of the automatic scaling method described in (Chapter 4.5), which was used for all the three steps mentioned above, was analyzed in a Pareto plot (Chapter 5.4.4).

One more different way to evaluate the measured data (setting $\Delta_r H_1 = \Delta_r H_2$) will be presented in [Zogg et. al. 03, submitted] and the results will be compared to semi empirical quantum mechanical calculations.

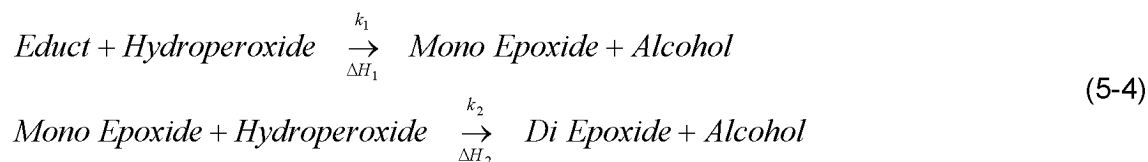
5.4.1 Combined evaluation of the infrared and calorimetric data

In the following the total power release or uptake measured by the calorimeter (q_{tot}) mainly contains one heat flow, the reaction power (q_{React}). q_{tot} is always calculated based on the measured data using Equation (3-23).

Pretreated infrared and calorimetric data (see Appendix E.3.2 and E.3.3) were used for the calculations shown in this section. The evaluation method applied is described in Chapter 4. All measurements, carried out at the same temperature, were concatenated into a single measurement vector (q_{Data}) and matrix (A_{Data}) (according to Equation (4-2)). The evaluation of all measurements at one temperature is thus carried out in a single step. The evaluation is then repeated for each measured temperature (17, 24, 30 and 36 °C).

In order to allow a visual comparison of the measured and calculated reaction spectrum A only one wave number of A will be shown throughout this section (see Figure E-12). However it should be noted that the whole reaction spectrum is evaluated and that overlapping of different components at the same wave number is allowed (see description of the evaluation algorithm in Chapter 4.4.3).

Two main reaction steps are involved during the epoxidation. These can be expressed as follows (according to Figure 5-9):



The reaction is initiated by rapid addition (24s) of the catalyst solution (Triton B in Methanol). The kinetics of the reaction was investigated under similar conditions by several people [Hairfield et. al. 85], [Bijlsma et. al. 98], and [Mayes et. al. 92]. All applied a large excess of the tert-butyl hydroperoxide compared to the educt (2,5-di-tert-butyl-1,4-benzoquinone). The two reaction steps were therefore assumed to be pseudo first order in the concentration of the educt (mono Epoxid). As only a small amount of catalyst was dosed during a very short time, all authors evaluated the measured data as batch experiments. The reaction mechanism is further discussed by [Moore 67] and [House 72].

According to these literature references the reaction model was implemented in form of the following differential equations. It is the basis for all evaluations (compare Figure 4-2):

$$\begin{aligned}
\frac{dn_{\text{Educt}}}{dt} &= -r_1(t, k_1) \cdot V_r(t) \\
\frac{dn_{\text{Hydroperoxide}}}{dt} &= \{-r_1(t, k_1) - r_2(t, k_2)\} \cdot V_r(t) \\
\frac{dn_{\text{Mono Epoxide}}}{dt} &= \{r_1(t, k_1) - r_2(t, k_2)\} \cdot V_r(t) \\
\frac{dn_{\text{Di Epoxide}}}{dt} &= r_2(t, k_2) \cdot V_r(t) \\
\frac{dn_{\text{Alcohol}}}{dt} &= \{r_1(t, k_1) + r_2(t, k_2)\} \cdot V_r(t) \\
\frac{dn_{\text{Solvent}}}{dt} &= 0 \quad \frac{dn_{\text{Methanol}}}{dt} = v_{\text{dos}} \cdot c_{\text{dos, Methanol}} \quad \frac{dn_{\text{TritonB}}}{dt} = v_{\text{dos}} \cdot c_{\text{dos, TritonB}} \\
\frac{dV_r}{dt} &= v_{\text{dos}} \\
r_1(t, k_1) &= k_1 \cdot \frac{n_{\text{Educt}}(t)}{V_r(t)} \cdot \frac{n_{\text{TritonB}}(t)}{V_r(t)} \cdot c_{\text{Hydroperoxide}, 0} \\
r_2(t, k_2) &= k_2 \cdot \frac{n_{\text{Mono Epoxide}}(t)}{V_r(t)} \cdot \frac{n_{\text{TritonB}}(t)}{V_r(t)} \cdot c_{\text{Hydroperoxide}, 0}
\end{aligned} \tag{5-5}$$

where V_r is the reaction volume [l], n the number of moles of the corresponding component [mol], v_{dos} is the dosing rate [l/s], $c_{\text{dos, Methanol}}$ the concentration of methanol in the feed, $c_{\text{dos, TritonB}}$ the concentration of the catalyst (Triton B). The only kinetic reaction model parameters are the two rate constants k_1 and k_2 [l/(mol·s)]. The concentration of the catalyst is included in r_1 and r_2 . However it is only varying during the short addition phase (24 s) and remains constant during the rest of the experiment.

All eight chemical components defined by the reaction model (educt (2,5-di-tert-butyl-1,4-benzoquinone), hydroperoxide (tert-butyl hydroperoxide), mono Epoxid, alcohol (tert-Butanol), di Epoxid, solvent (ethanol and Dioxan), methanol and Triton B) are considered as absorbing species in the calculation of the reaction spectrum. No measured pure spectra were used as constraints. All the reaction parameters (including their bounds) that have to be identified are listed in **Table 5-4**.

Table 5-4: All reaction parameters (with bounds) required for the evaluation of the epoxidation measurements.

	<i>Lower bound</i>	<i>Upper bound</i>
Rate constant k_1 and k_2 [l/(mol·s)] (at each temperature).	0	1
Absorption coefficients at each wave number of the reaction Spectrum A and for all eight chemical components [-]. (For each temperature new absorption coefficients were calculated.)	0	5
Heat of reaction $\Delta_r H_1$ and $\Delta_r H_2$ [kJ/mol] (at each temperature).	0	-1000

The whole evaluation will be carried out according to the flow sheet presented in Chapter 4.3.3 (Figure 4-3). Therefore in a first step the complete time range of both measurement data (calorimetric and infrared) was evaluated separately (evaluation data set I Table E-9 and Table E-10). The results of the experiments at 30 and 17 °C are shown in **Figure 5-10** and **Figure 5-11**.

The left plots show the total measured calorimetric data (fat gray line), the selected measurement points for the evaluation (triangles, see Appendix E.3.3) and the simulated calorimetric signal (thin black line, best fit according to Equation (4-12)). It is obvious that the reaction model (5-5) could be fitted into the whole time range of the measurement data. Only slight deviations can be seen for the data measured at 17 °C.

The same reaction model was also fitted into the infrared data. This is shown in the right plots of Figure 5-10 and Figure 5-11: The measured absorbance time curves at 1687 cm^{-1} (points, compare to Figure E-12, only one wave number is chosen in order to simplify the illustration) fit well into the simulated absorbance profiles (thin black line, best fit according to Equation (4-13)). The slight deviations, observed at the calorimetric evaluation, are not visible in the infrared data.

It was concluded that the fit quality of two separate evaluations does not differ significantly. The slight deviations of the calorimetric data at 17 °C are too weak to argue a different model or exclude data points. Therefore the combined evaluation was carried out using the same data set I and the same reaction model.

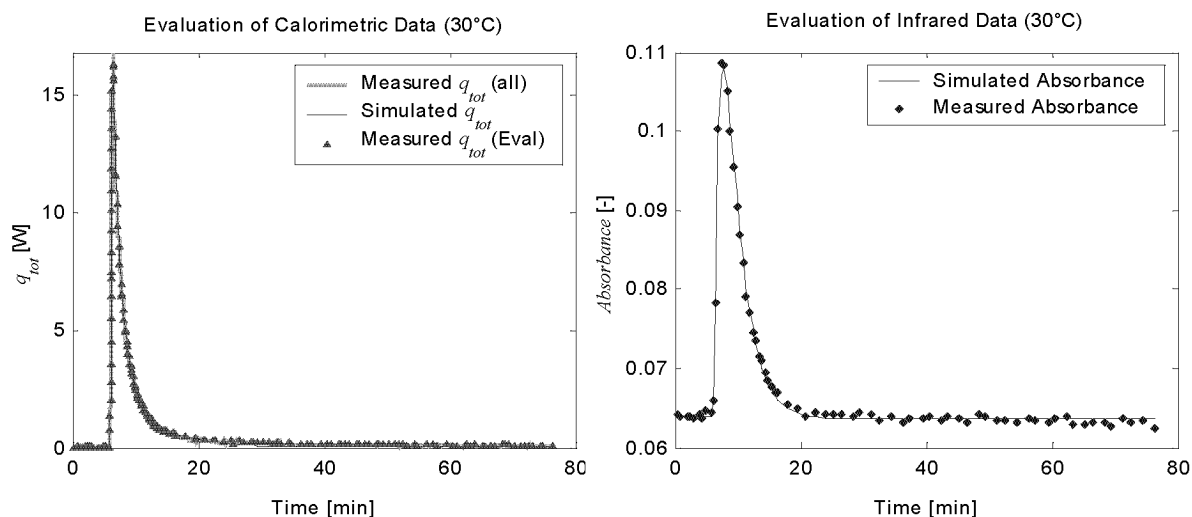


Figure 5-10: Epoxidation of 2,5-di-tert-butyl-1,4-benzoquinone. Separate evaluation of the calorimetric (left) and infrared (right) data of the full time range (evaluation data set I). A mean value of all reaction experiments at 30 °C is shown in the two plots. Only one wave number (1687 cm^{-1} , see Figure E-12) of the reaction spectrum is shown on the right side. The reaction is initiated by the dosing of the catalyst Triton B (only 24 s).

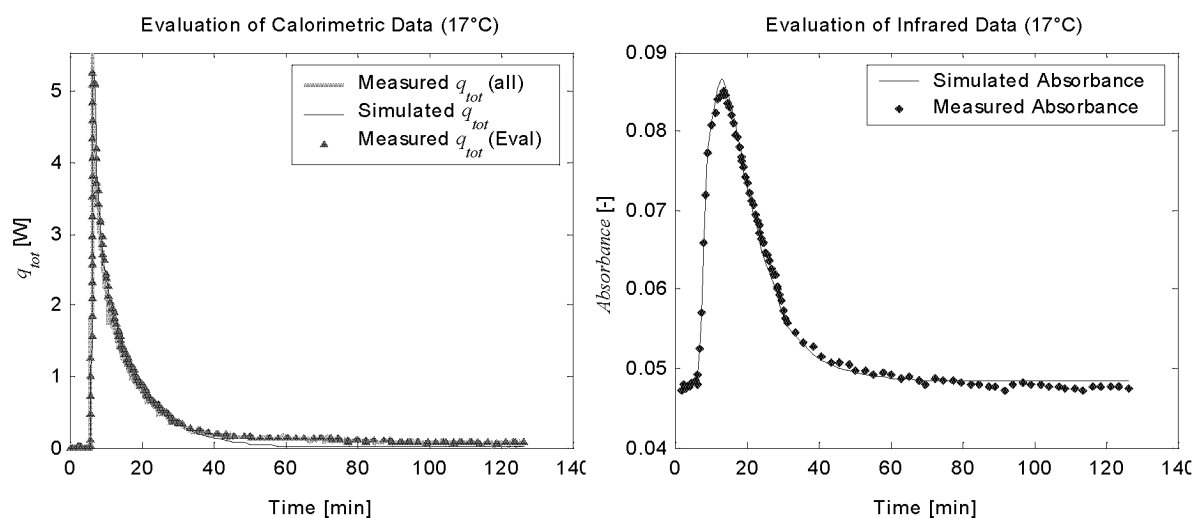


Figure 5-11: Epoxidation of 2,5-di-tert-butyl-1,4-benzoquinone. Separate evaluation of the calorimetric (left) and infrared (right) data at 17 °C. Explanations see Figure 5-10. The reaction is initiated by the dosing of the catalyst Triton B (only 24 s).

The results of the combined evaluation (Equation (4-16) and Figure 4-5) are shown in **Figure 5-12**. The mean values of all measurements at each temperature and the corresponding model fit are shown. Generally the model-fit quality is similar to the quality of the separate evaluation.

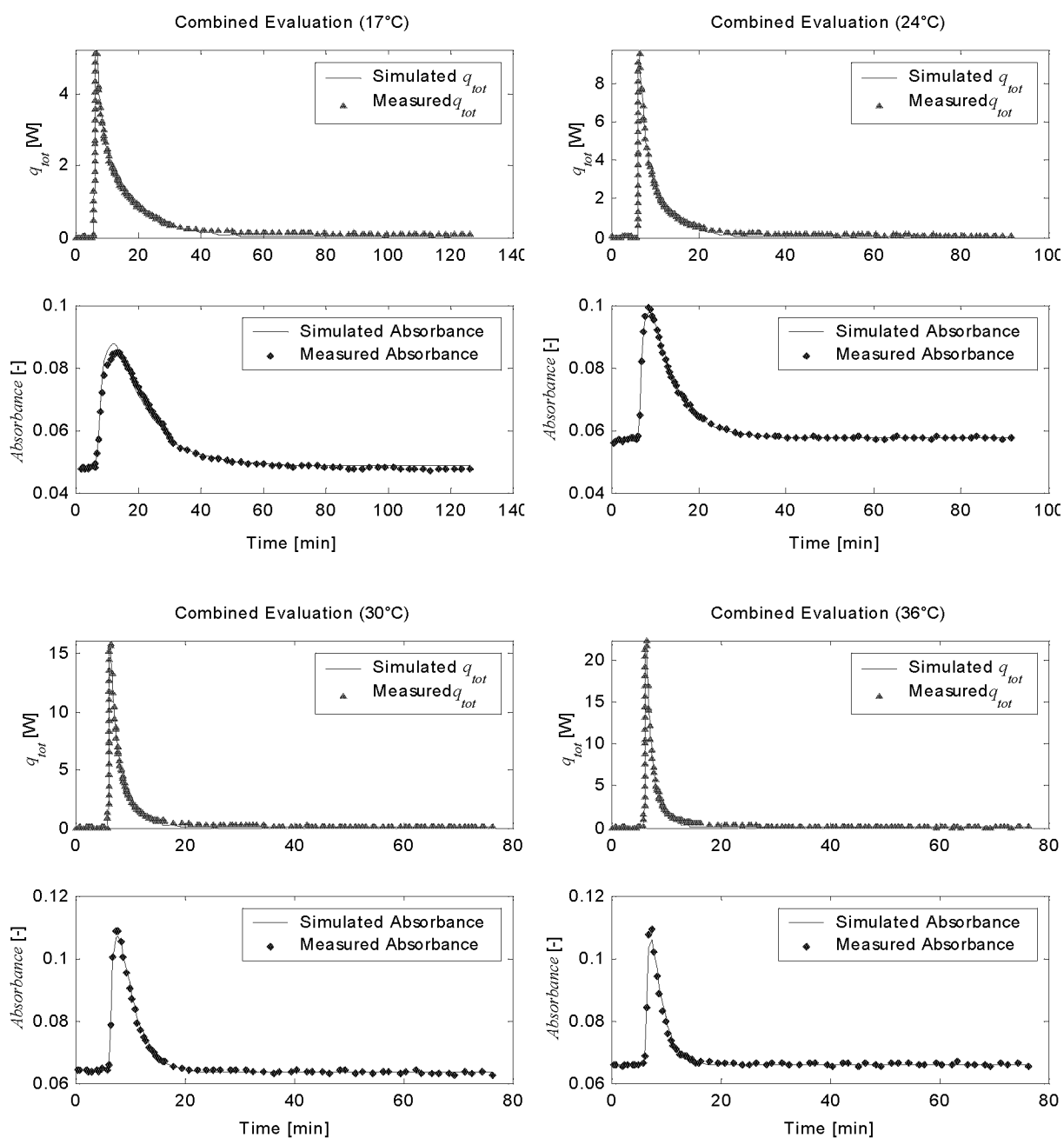


Figure 5-12: Epoxidation of 2,5-di-tert-butyl-1,4-benzoquinone. Combined evaluation of the calorimetric and infrared data (evaluation data set I). A mean value of all reaction experiments at each temperature is shown. Only one wave number (1687 cm^{-1} , see Figure E-12) of the reaction spectrum is shown.

The combined as well as the separate evaluations were carried out for each temperature (17, 24, 30 and 36 °C). The independently determined rate constants k_1 and k_2 at the four different temperatures are plotted in an Arrhenius plot in **Figure 5-13**. First of all it becomes clear that the separate as well as the combined evaluation did not result in the same values for k_1 and k_2 . The independently determined k_1 and k_2 values all lay on a straight line for the combined as well as the separate infrared evaluation. However the deviations from the straight line are significantly higher for the separate calorimetric evaluation. This fact indicates that a proper reaction model was chosen but that the separate calorimetric evaluation was difficult.

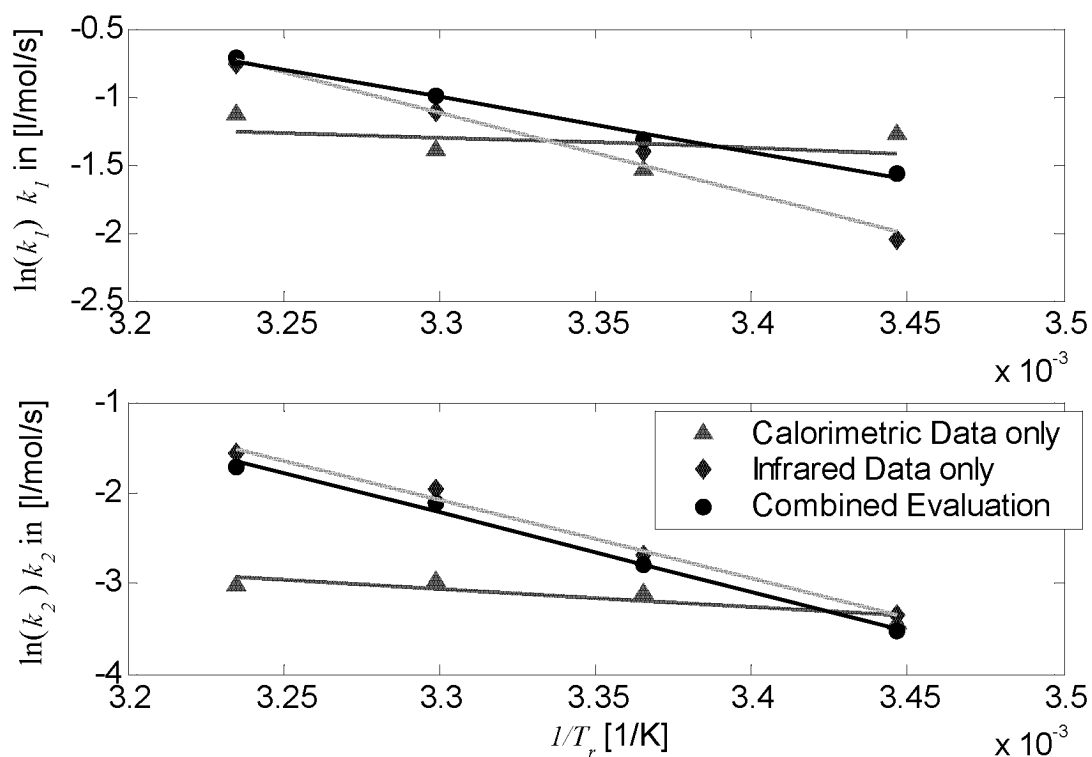


Figure 5-13: Epoxidation of 2,5-di-tert-butyl-1,4-benzoquinone. Arrhenius plot of the two rate constants k_1 and k_2 determined by the separate and combined evaluations.

The results obtained by the separate as well as the combined evaluation of the calorimetric and infrared data (compare to Figure 4-5) are listed in **Table 5-5** (first three columns) and compared to the corresponding results of the classical, separate evaluation (7th column, for details see Appendix E.3.4 and Table E-12) as well as to an overall evaluation of all measurements at all temperatures (4th to 6th column, for details see Chapter 5.4.3). In the last column only links to literature references for the thermodynamic as well as kinetic reaction parameters are listed as the quality of the reference data is bad.

Table 5-5: Epoxidation of 2,5-di-tert-butyl-1,4-benzoquinone. Final results of the separate and combined evaluations (data set I) based on reaction model (5-5). The main results from the classic evaluation are also listed (for details see Appendix E.3.4). $\Delta_r H_1$ / $\Delta_r H_2$ / $E_{A,1}$ / $E_{A,2}$ as well as k_1 / k_2 are listed in the same field on top of each other. ¹⁾ Sum of $\Delta_r H_1$ and $\Delta_r H_2$. ²⁾ The separate evaluation of the infrared data was carried out by setting $S_Q = 0$ in Equation (4-16) but still both data sets were evaluated. Therefore $\Delta_r H$ can still be identified. ³⁾ All measurements are evaluated separately at each temperature. ⁴⁾ All measurements at all temperatures are evaluated simultaneously (Chapter 5.4.3). ⁵⁾ Average values of the evaluations at the different temperatures or directly identified values. ⁶⁾ Calculated based on the rate constants determined at 30°C and the activation energies $E_{A,1}$ / $E_{A,2}$. ⁷⁾ Calorimetric and infrared error function at the determined optimum (Equations (4-8) and (4-6)). Sum over all temperatures. ⁸⁾ Number of hits (see Chapter 4.3.2, mean value over all temperatures), maximum 10.

	Comb. Eval. ³⁾	Cal. Eval. ³⁾	IR Eval. ³⁾	Comb. Eval. ⁴⁾	Cal. Eval. ⁴⁾	IR Eval. ⁴⁾	Cal. Classic	Ref.
$\Delta_r H$ 17 °C [kJ/mol]	-100	-70	-150 ²⁾	-	-	-	-	-
	-270	-290	-190	-	-	-	-	-
	-370 ¹⁾	-360 ¹⁾	-340 ¹⁾	-	-	-	-440±50	-
$\Delta_r H$ 25 °C [kJ/mol]	-140	-180	-150 ²⁾	-	-	-	-	-
	-210	-200	-190	-	-	-	-	-
	-350 ¹⁾	-370 ¹⁾	-340 ¹⁾	-	-	-	-440±20	-
$\Delta_r H$ 30 °C [kJ/mol]	-180	-260	-200 ²⁾	-	-	-	-	-
	-180	-140	-150	-	-	-	-	-
	-360 ¹⁾	-400 ¹⁾	-350 ¹⁾	-	-	-	-480±30	-
$\Delta_r H$ 36 °C [kJ/mol]	-190	-290	-200 ²⁾	-	-	-	-	-
	-170	-130	-150	-	-	-	-	-
	-360 ¹⁾	-410 ¹⁾	-350 ¹⁾	-	-	-	-440±10	-
$\Delta_r H$ ⁵⁾ [kJ/mol]	-150 ± 40	-200±100	-170±30	-160	-240	-180	-	-
	-210 ± 50	-190±70	-170±20	-200	-150	-170	-	-
	-360 ± 10	-390 ± 20	-350 ± 4	-360	-390	-350	-450±10	E.3.4
E_A [kJ/mol]	34	6	50	60	61	53	-	E.3.6
	72	17	72	70	76	73	-	E.3.6
k 17°C [l/mol/s]	0.21	0.28	0.13	0.13 ⁶⁾	0.09 ⁶⁾	0.13 ⁶⁾	-	E.3.6
	0.030	0.032	0.035	0.033	0.015	0.035	-	E.3.6
k 24°C [l/mol/s]	0.27	0.21	0.24	0.24 ⁶⁾	0.16 ⁶⁾	0.22 ⁶⁾	-	-
	0.062	0.045	0.068	0.065	0.031	0.071	-	-
K 30°C [l/mol/s]	0.37	0.25	0.33	0.38	0.25	0.34	-	E.3.6
	0.121	0.051	0.139	0.155	0.057	0.127	-	E.3.6
k 36°C [l/mol/s]	0.49	0.33	0.47	0.61 ⁶⁾	0.41 ⁶⁾	0.51 ⁶⁾	-	-
	0.179	0.049	0.210	0.196	0.103	0.222	-	-
ΔQ ⁷⁾ [W ²]	125	86	168	201	173	294	-	-
ΔA ⁷⁾ [-]	2.541	2.637	2.527	2.529	2.685	2.528	-	-
#Hits ⁸⁾ [-]	4.25	7	3.25	8	10	6	-	-

Table 5-5 first of all shows that the reaction parameters identified by the combined and the separate evaluations disagree. The same conclusion was already drawn from the Arrhenius plot Figure 5-13. The only values in Table 5-5 that are similar for all evaluations are the sums of $\Delta_r H_1$ and $\Delta_r H_2$. $E_{A,1}$ and $E_{A,2}$ are similar for the combined and the infrared evaluation but differ to the calorimetric evaluation. The activation energies calculated based on the separate calorimetric evaluation are physically unreasonable.

Also common to all evaluations is a decreasing $\Delta_r H_1$ (more exothermal) and an increasing $\Delta_r H_2$ (less exothermal) as a function of temperature. The changes of the reaction enthalpies are in the range of 100% for a temperature increase of only 19 K. The largest temperature change can be observed at the separate calorimetric evaluation. Therefore the average values of $\Delta_r H_1$ and $\Delta_r H_2$ over all temperatures show the highest standard deviations for the separate calorimetric evaluation. No reasonable physical or chemical explanation can be given for this behavior.

Another doubtful result is the large difference of the two activation energies $E_{A,1}$ and $E_{A,2}$. $E_{A,1}$ obtained by the combined as well as calorimetric evaluation is only about half of the size of $E_{A,2}$. From a mechanistic point of view this is quite surprising. In the first epoxidation the conjugation of the whole benzoquinone system has to be broken. In the second epoxidation only a smaller conjugated system has to be broken, but the steric hindering of the epoxidation will probably be bigger. However such a large difference of the activation energies cannot be expected.

As mentioned the comparison to literature data turned out to quite difficult. The only hard fact that could be extracted from the literature data is that the large difference of $E_{A,1}$ and $E_{A,2}$ was not observed. For details and literature references see Appendix E.3.6.

The large temperature change of $\Delta_r H_1$ and $\Delta_r H_2$, the unrealistic small activation energies $E_{A,1}$ and $E_{A,2}$ as well as the bad quality of the Arrhenius regression (see Figure 5-13, deviations from the straight line) are hints that the results from the separate calorimetric evaluation are less reliable compared to the infrared and combined evaluation.

In **Figure 5-14** (first and second plot) the error functions ΔA and ΔQ (Equations (4-8) and (4-6)) are shown for each evaluation step (compare to Figure 4-5). As mentioned the experiments at different temperatures were evaluated separately, therefore the values are given for each temperature. As would be expected the lowest infrared model-fit error ΔA was found for the separate evaluation of the infrared data, the highest for the separate evaluation of the calorimetric data. The analogous behavior is found for the model-fit error ΔQ . The sums of ΔQ and ΔA over all measurement temperatures are given in Table 5-5.

As all evaluations were carried out using ten different random start values, the quality of the identification can be measured by counting the number of equal and best solutions found (see 4.3.2). This “number of hits” is shown in the third plot of Figure E-15. It can be concluded that the separate calorimetric evaluation was most robust, followed by the combined evaluation. The separate evaluation of the infrared data was most difficult from that point of view. The mean value over the evaluations at each temperature is given in Table 5-5.

The automatically calculated scaling factors S_{IR} and S_Q (see 4.5, Equations (4-16) to (4-20) and Figure 4-5) are shown in the last two plots of Figure E-15.

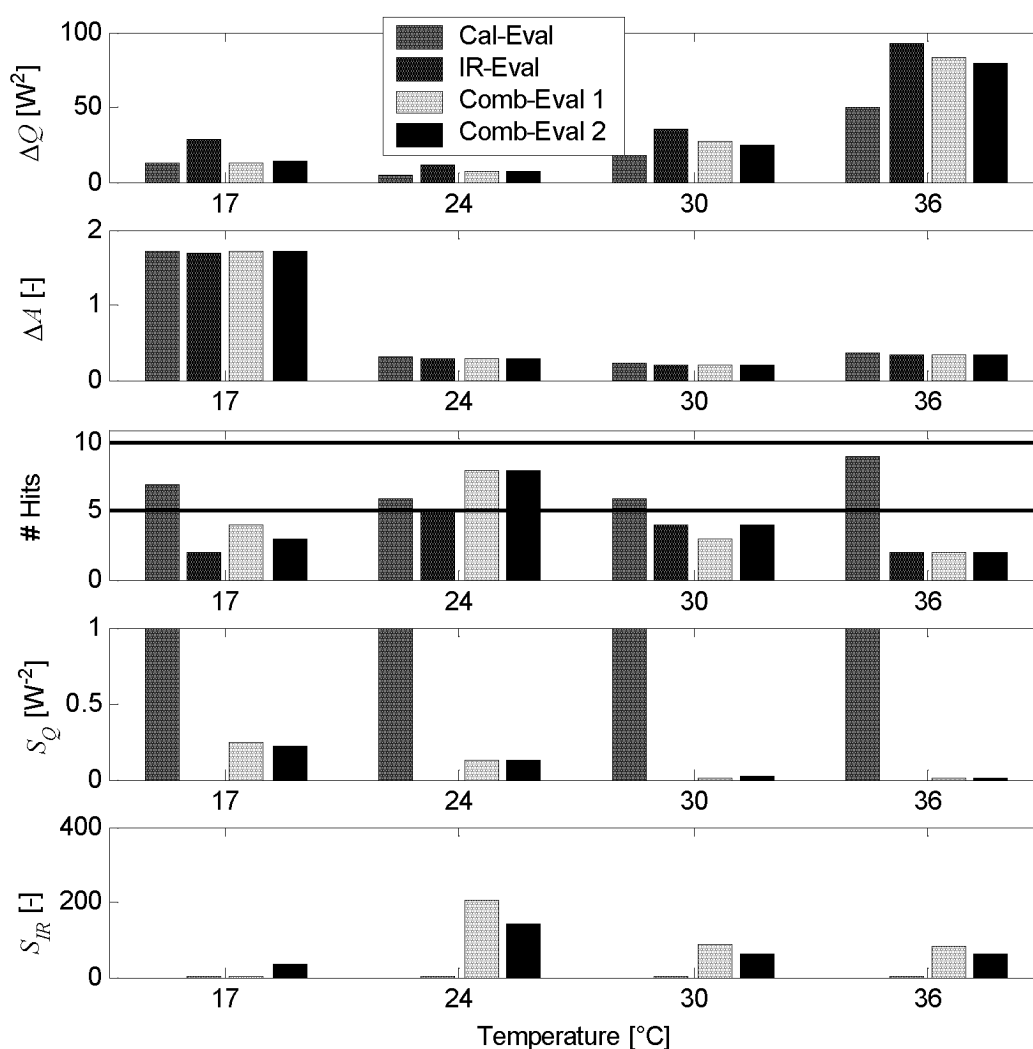


Figure 5-14: Epoxidation of 2,5-di-tert-butyl-1,4-benzoquinone. First and second plot: Final error functions ΔA and ΔQ . Third plot: Number of hits (maximum 10). Last two plots: S_{IR} and S_Q (see Equation (4-16)).

The discussion of the different evaluations is summarized in **Table 5-6**. The combined evaluation is the most reliable but still leads to some unreasonable results.

Table 5-6: Epoxidation of 2,5-di-tert-butyl-1,4-benzoquinone. Summary of the discussion of the different evaluations.

	Combined Evaluation	Calorimetric Evaluation	Infrared Evaluation
Robustness (see Figure 5-14)	Medium	Best	Worst
Arrhenius plot k_1	Best	Worst	Medium
Arrhenius plot k_2	Best	Worst	Best
Temperature change of $\Delta_r H_1$ and $\Delta_r H_2$	medium	largest	smallest
Activation energies $E_{A,1}$ and $E_{A,2}$	large difference	large difference and very small values	most reasonable

As mentioned in Chapter 4.2 the determination of the pure spectra of the involved chemical component is not the focus of the presented evaluation method. However, these spectroscopic reaction parameters (see Figure 4-2) have to be identified during the evaluation and are therefore a side product of the calculation. The calculated pure spectra (combined evaluation only) are shown in the Appendix Figure E-15. No prior information about the pure spectra was used for all evaluations (see bounds of the pure spectra matrix in Table 5-4). It was not possible to extract physically meaningful pure spectra. However this is not surprising as the rank of the concentration matrix C_{calc} (calculated based on the reaction model (5-3), see Equation (4-1)), is equal to five. Therefore a maximum of five pure spectra could be identified as all the other concentration profiles are linear dependent (see Appendix B.2). Because eight absorbing components were assumed (all components in the reaction model (5-3)) these linear dependencies can be seen in the calculated pure spectra. It is important to note that they do not influence the estimation of the other reaction parameters (k_1 , k_2 , $\Delta_r H_1$ and $\Delta_r H_2$) as they have no effect on the size of ΔA .

Based on chemical and physical knowledge it must be concluded that the evaluation shown in this Chapter did not reveal plausible reaction parameters. According to the flow sheet shown in Figure 4-3 two modifications of the evaluation are possible and will be discussed in the following Chapters:

1. *Testing a different reaction model. See Chapter 5.4.2.*
2. *Applying more physical constraints. See Chapter 5.4.3.*

5.4.2 Testing different reaction models

As discussed in Chapter 5.4.1 the evaluation of the measured data, based on the reaction model (5-5), did not lead to reasonable results (large temperature dependency of $\Delta_r H_1$ and $\Delta_r H_2$ as well as large difference of $E_{A,1}$ and $E_{A,2}$). A possible reason could be that the reaction model is not correct. Therefore different reaction models were tested, using the same evaluation method and settings as described in Chapter 5.4.1. The aim is to show that it is possible to distinguish between different reaction models but also to see whether another reaction model suits better into the measured data.

The reaction models are basically equal to model (5-5) they only differ in the formulation of the two reaction rates r_1 and r_2 . The different models and the corresponding reaction model parameters that have to be identified additionally to the pure spectra matrix E are shown in **Table 5-8**. The bounds applied for the reaction parameters are given in **Table 5-7**. It should be noted that for the reaction model 9 the lower bound of the reaction order of tert-butyl hydroperoxide was set to -3. This is on purpose as a strange concentration dependency of the reaction rates to the concentration of tert-butyl hydroperoxide was observed (see discussion below).

The models were evaluated based on the evaluation data set I (see Appendix Table E-9 and Table E-10). In order to get more informations about the reaction order of tert-butyl hydroperoxide three more measurements at 30 °C were carried out with decreased concentration on tert-butyl hydroperoxide (see Table E-9). The models were thus evaluated a second time based on the evaluation data set II (see Table E-9 and Table E-10) that includes these three measurements at different concentrations.

Table 5-7: All reaction parameters defined in Table 5-8 and their bounds. The bounds were equal for the evaluation data set I and II.

	<i>Lower bound</i>	<i>Upper bound</i>
Rate constant k or k_1 and k_2 [...] (at each temperature).	0	1
Reaction orders ord_C , $ord_{C,1}$, $ord_{C,2}$ [-] (at each temperature)	0	3
Reaction order ord_P [-] (at each temperature)	-3	3
Absorption coefficients at each wave number of the reaction Spectrum A and for all eight chemical components [-]. (For each temperature new absorption coefficients were calculated.)	0	5
Heat of reaction $\Delta_r H$ or $\Delta_r H_1$ and $\Delta_r H_2$ [kJ/mol] (at each temperature).	0	-1000

Table 5-8: Different reaction models that were tested. The reaction models are identical to Equation (5-5) except for the definition of the reaction rates r_1 and r_2 . The reaction parameters that have to be identified are listed on the right side. ^{a)} Internal model number. ^{b)} Model used for the calculations shown in Chapters 5.4.1 and 5.4.3.

	r_1	r_2	Rate Const.	Reaction Enthalpies	Reaction Orders
1 (7) ^{a)}	$k \cdot c_{Ed} \cdot c_{Cat}$	0	k	$\Delta_r H$	-
2 (8) ^{a)}	$k \cdot c_{Ed} \cdot c_{Cat} \cdot c_{Peroxide}$	0	k	$\Delta_r H$	-
3 (5) ^{a)}	$k \cdot 2 \cdot c_{Ed} \cdot c_{Cat}$	$k \cdot c_{mEpoxide} \cdot c_{Cat}$	k	$\Delta_r H_1, \Delta_r H_2$	-
4 (6) ^{a)}	$k \cdot 2 \cdot c_{Ed} \cdot c_{Cat} \cdot c_{Peroxide}$	$k \cdot c_{mEpoxide} \cdot c_{Cat} \cdot c_{Peroxide}$	k	$\Delta_r H_1, \Delta_r H_2$	-
5 ^{b)} (1) ^{a)}	$k_1 \cdot c_{Ed} \cdot c_{Cat}$	$k_2 \cdot c_{mEpoxide} \cdot c_{Cat}$	k_1, k_2	$\Delta_r H_1, \Delta_r H_2$	-
6 (2) ^{a)}	$k_1 \cdot c_{Ed} \cdot c_{Cat} \cdot c_{Peroxide}$	$k_2 \cdot c_{mEpoxide} \cdot c_{Cat} \cdot c_{Peroxide}$	k_1, k_2	$\Delta_r H_1, \Delta_r H_2$	-
7 (3) ^{a)}	$k_1 \cdot c_{Ed} \cdot c_{Cat}^{ord_C}$	$k_2 \cdot c_{mEpoxide} \cdot c_{Cat}^{ord_C}$	k_1, k_2	$\Delta_r H_1, \Delta_r H_2$	ord_C
8 (4) ^{a)}	$k_1 \cdot c_{Ed} \cdot c_{Cat}^{ord_C} \cdot c_{Peroxide}$	$k_2 \cdot c_{mEpoxide} \cdot c_{Cat}^{ord_C} \cdot c_{Peroxide}$	k_1, k_2	$\Delta_r H_1, \Delta_r H_2$	ord_C
9 (11) ^{a)}	$k_1 \cdot c_{Ed} \cdot c_{Cat}^{ord_C} \cdot c_{Peroxide}^{ord_P}$	$k_2 \cdot c_{mEpoxide} \cdot c_{Cat}^{ord_C} \cdot c_{Peroxide}^{ord_P}$	k_1, k_2	$\Delta_r H_1, \Delta_r H_2$	ord_C ord_P
10 (9) ^{a)}	$k_1 \cdot c_{Ed} \cdot c_{Cat}^{ord_{C,1}}$	$k_2 \cdot c_{mEpoxide} \cdot c_{Cat}^{ord_{C,2}}$	k_1, k_2	$\Delta_r H_1, \Delta_r H_2$	$ord_{C,1}$ $ord_{C,2}$
11 (10) ^{a)}	$k_1 \cdot c_{Ed} \cdot c_{Cat}^{ord_{C,1}} \cdot c_{Peroxide}$	$k_2 \cdot c_{mEpoxide} \cdot c_{Cat}^{ord_{C,2}} \cdot c_{Peroxide}$	k_1, k_2	$\Delta_r H_1, \Delta_r H_2$	$ord_{C,1}$ $ord_{C,2}$

In order to be able to discriminate between different reaction models the concept described in Chapter 4.3.2 was applied (quality and robustness of the model fit as indicators). However it is not possible to compare the models based on the combined objective function $\Delta Comb$ (Equation (4-16)) as the scaling factors S_{IR} and S_Q (see Equations (4-18) and (4-17)) depend on the sensitivity analysis of the unknown reaction model parameters ($\theta_{I..NP}$). As shown in Table 5-8 the reaction model parameters are different for different models. Therefore the quality of the model fit has to be judged based on the unscaled calorimetric and infrared fit errors ΔQ and ΔA (Equations (4-6) and (4-8)).

The results of the combined evaluation (infrared and calorimetric data) of the evaluation data sets I and II are shown in **Figure 5-15** (ΔQ and ΔA are normalized between 0...1). Only the results at 30 °C are shown. The results at 17, 24 and 36 °C (only evaluation data set I) are similar.

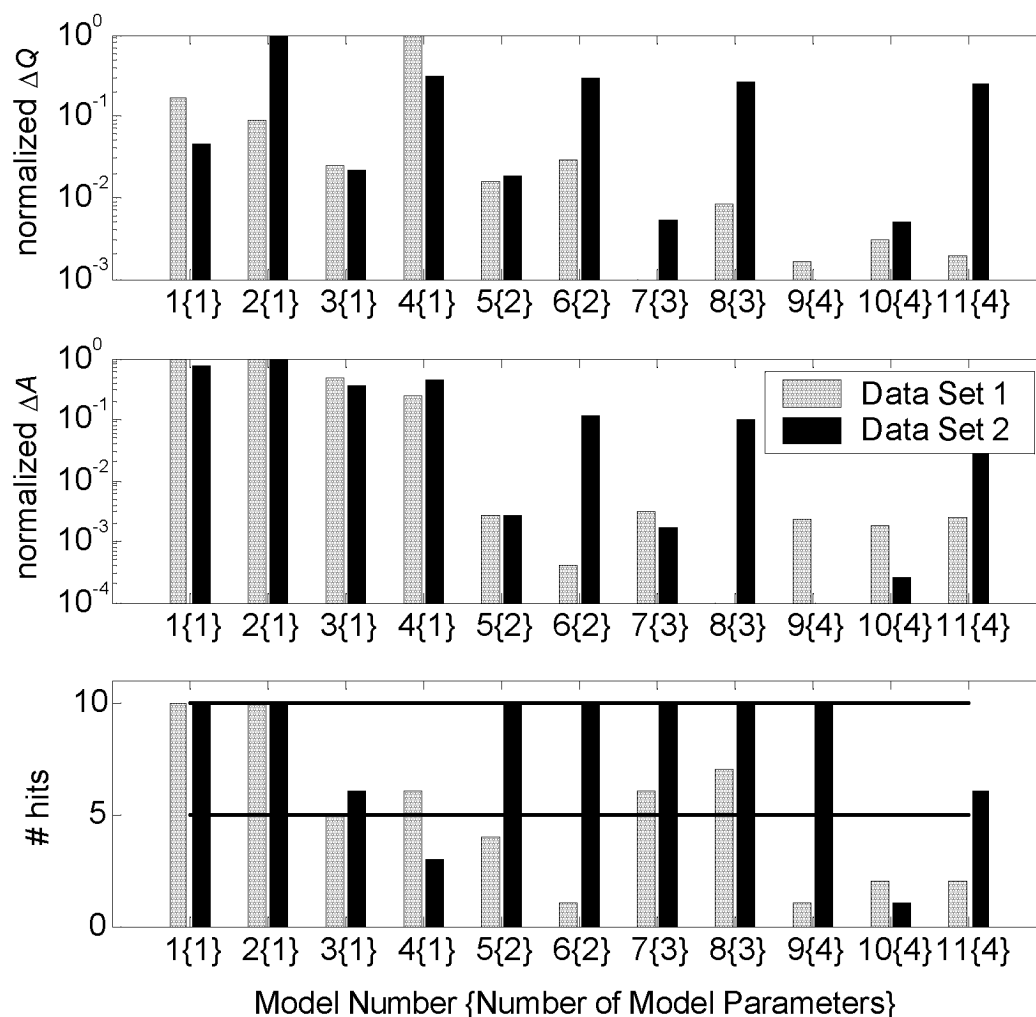


Figure 5-15: Epoxidation of 2,5-di-tert-butyl-1,4-benzoquinone. Results of the combined evaluation of the epoxidation experiments (evaluation data set I and II) at 30 °C. The minimal ΔQ and ΔA are not visible in the plot.

Based on the results of evaluation data set I it becomes clear that the identification of models with only a few model parameters ($\theta_{1..Np}$) is generally robust (number of hits > 5) but the model-fit errors ΔQ and ΔA are high. Models with four parameters were difficult to identify (number of hits < 2) but show small ΔQ and ΔA .

The best model for evaluation data set I would therefore be model number 7 as the identification was robust (number of hits > 5) and the errors ΔQ and ΔA are both small. Although the reaction order, that was additionally fitted in model 7, does only influence the reaction measurement during the dosing phase (catalyst concentration constant after dosing) it influences the quality of the model fit.

It should be noted that model 7 is not the one suggested by the literature (model number 5) and used in Chapters 5.4.1 and 5.4.3. Further results of the evaluation of model 7 are shown in the **Figure 5-16** and **Table 5-9**.

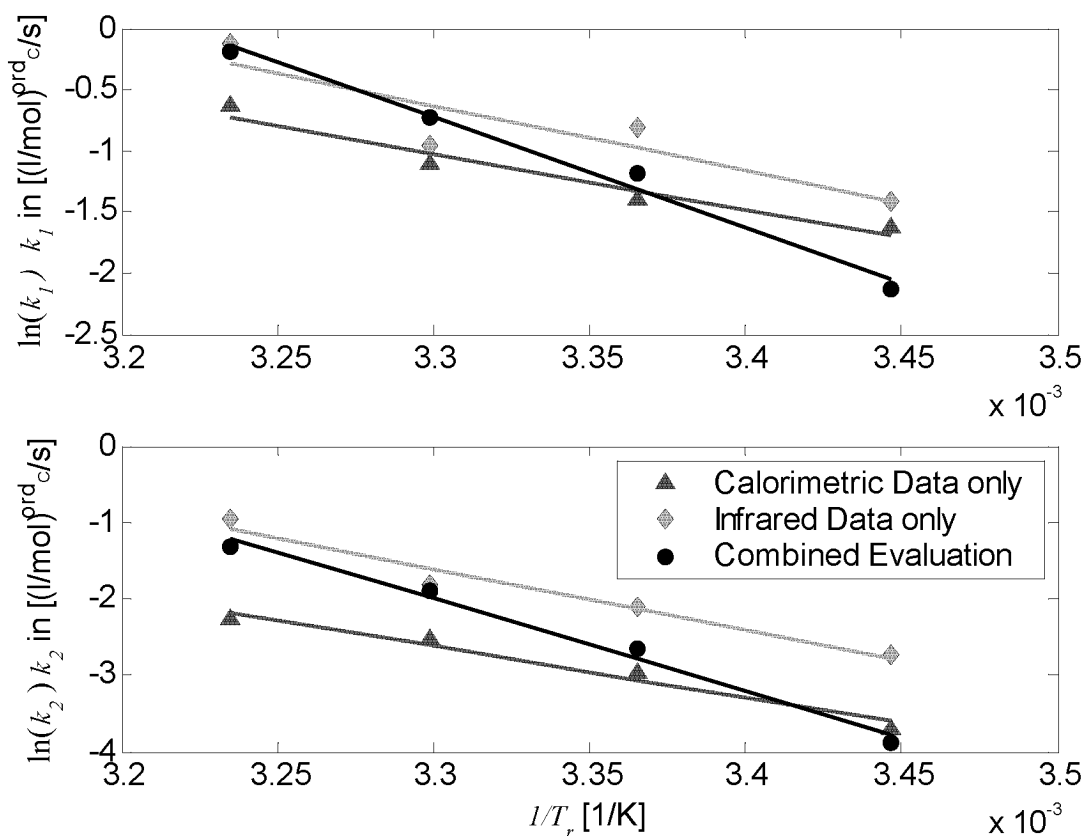


Figure 5-16: Epoxidation of 2,5-di-tert-butyl-1,4-benzoquinone. Arrhenius plot of the rate constants determined by the calorimetric, infrared and combined evaluation of the epoxidation measurements (evaluation data set I, reaction model 7).

The reaction order identified is close to one for all three evaluations (calorimetric, infrared and combined) and does not show a significant temperature dependency.

Similar to the results shown in Chapter 5.4.1, the three evaluations do not give the same values for all the other reaction parameters. The temperature dependency of $\Delta_r H_1$ and $\Delta_r H_2$ remains and is largest for the separate calorimetric evaluation. The difference of the activation energy $E_{A,1}$ and $E_{A,2}$ is decreased but is still in an unreasonable range.

It should be noted that the separate evaluation of the infrared data was unstable as the “number of hits” is close to one (see Table 5-9). Similar to 5.4.1 the separate calorimetric evaluation was the most robust.

It was concluded that the combined evaluation of reaction model 7 is the most reliable but still leads to some unreasonable results. According to the flow sheet shown in Figure 4-3 the calculation should be repeated applying more physical constraints (see Chapter 5.4.3)

Table 5-9: Epoxidation of 2,5-di-tert-butyl-1,4-benzoquinone. Final results of the separate and combined evaluations (evaluation data set I) based on reaction model 7. $\Delta_r H_1$ / $\Delta_r H_2$, $E_{A,1}$ / $E_{A,2}$ as well as k_1 / k_2 are listed in the same field on top of each other. ¹⁾ Sum of $\Delta_r H_1$ and $\Delta_r H_2$. ²⁾ The separate evaluation was carried out by setting $S_Q = 0$ in Equation (4-16) but still both data sets were evaluated. Therefore $\Delta_r H$ can also be identified from the separate evaluation of the infrared data. ³⁾ All measurements are evaluated separately at each temperature. ⁵⁾ Average values of the evaluations at the different temperatures. ⁶⁾ Calculated based on the rate constant determined at 30°C and the activation energy E_A . ⁷⁾ Calorimetric and infrared error function at the determined optimum (Equations (4-8) and (4-6)). Sum of over all temperatures. ⁸⁾ Number of hits (see Chapter 4.3.2, mean value over all temperatures), maximum 10. ⁹⁾ [(l/mol)^{ord_C}/s]

	Combined Evaluation ³⁾		Calorimetric Evaluation ³⁾		Infrared Evaluation ³⁾	
$\Delta_r H$ 17 °C [kJ/mol]	-110 -140	-370 ¹⁾	-80 -280	-370 ¹⁾	-150 ²⁾ -190	-340 ¹⁾
$\Delta_r H$ 25 °C [kJ/mol]	-140 -210	-350 ¹⁾	-170 -200	-370 ¹⁾	-160 ²⁾ -180	-340 ¹⁾
$\Delta_r H$ 30 °C [kJ/mol]	-170 -180	-360 ¹⁾	-240 -140	-380 ¹⁾	-200 ²⁾ -150	-350 ¹⁾
$\Delta_r H$ 36 °C [kJ/mol]	-180 -180	-360 ¹⁾	-260 -130	-400 ¹⁾	-210 ²⁾ -140	-350 ¹⁾
$\Delta_r H$ ⁵⁾ [kJ/mol]	-150 ± 30 -210 ± 30	-360 ± 10	-190±80 -190±70	-380 ± 10	-180±30 -160±20	-350 ± 3
E_A [kJ/mol]	75 100		38 56		44 66	
k 17°C [...] ⁹⁾	0.12 0.021		0.2 0.025		0.24 0.065	
k 24°C [...] ⁹⁾	0.31 0.070		0.25 0.051		0.44 0.123	
k 30°C [...] ⁹⁾	0.48 0.151		0.33 0.079		0.39 0.161	
k 36°C [...] ⁹⁾	0.83 0.265		0.53 0.103		0.89 0.386	
ord_C 17°C [-]	0.88		0.93		1.21	
ord_C 24°C [-]	1.04		1.03		1.20	
ord_C 30°C [-]	1.08		1.06		1.05	
ord_C 36°C [-]	1.14		1.12		1.20	
ord_C ⁵⁾ [-]	1.0 ± 0.1		1.0 ± 0.1		1.2 ± 0.1	
ΔQ ⁷⁾ [W ²]	89		61		183	
ΔA ⁷⁾ [-]	2.53		2.60		2.53	
# Hits ⁸⁾ [-]	7		9.5		1.5	

The results of the evaluation of data set II (only at 30 °C, including three measurements with lower concentration of tert - butyl hydroperoxide) show that generally the robustness of the identification increases compared to evaluation data set I (see Figure 5-15). This is reasonable as more information is now present in order to estimate the reaction parameters.

Comparing the model-fit error ΔQ and ΔA of the models 1, 3, 5, 7, 10 (concentration of tert-butyl hydroperoxide not included in the reaction model) to the models 2, 4, 6, 8, 11 (concentration of tert-butyl hydroperoxide included in the reaction model as first-order) it is obvious that the latter group shows worse fit quality. This can only be explained by the fact that actually the reaction rate is increasing when the concentration of tert-butyl hydroperoxide is decreased.

The model selection based on evaluation data set II is trivial: The identification of Model 9 is very robust (number of hits = 10) and shows the lowest ΔA and the lowest ΔQ (therefore not visible in Figure 5-15). Further results of the evaluation of model 9 are shown in **Table 5-10**. According to the discussion above, the reaction order of the tert-butyl hydroperoxide concentration was identified to be negative. The negative reaction orders determined for the hydroperoxide concentration (ord_p) represent the fact that the reaction experiments carried out using less hydroperoxide proceeded faster compared to the other experiments. However a negative reaction order does not make sense from a mechanistic point of view and indicates that the empirical reaction model 9 does not accurately describe the epoxidation reaction. A more appropriate guess for a reaction model, able to describe such a situation, is given in **Figure 5-17**: In a fast preliminary equilibrium the hydroperoxide is deprotonated. Assuming that at equilibrium the catalyst is nearly completely protonated it can be concluded that the concentration of the active epoxidation agent (*Hydroperoxide_dep*) increases if the amount of hydroperoxide is decreased due to the total volume decrease. This would explain the observed and identified negative reaction order with respect to the total hydroperoxide concentration. Such a reaction model, that was found based on the application of the new evaluation algorithm, is also supported by mechanistic considerations [Moore 67], [House 72].

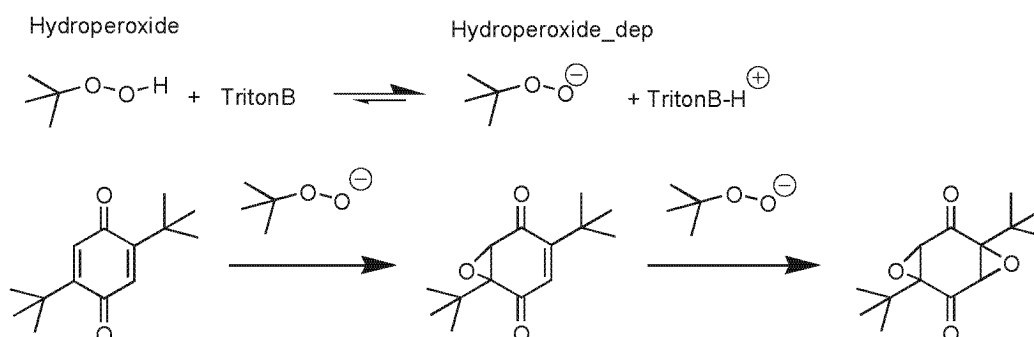


Figure 5-17: Guess for a modified reaction model for the epoxidation reaction.

Again it should be noted that the separate evaluation of the infrared data was unstable as the “number of hits” is only one. The reaction order of the catalyst concentration determined is close to one and thus similar to the evaluation of reaction model 7. The large difference of the reaction enthalpies identified by the separate calorimetric evaluation (see Table 5-10) is unreasonable based on mechanistic considerations, whereas the combined evaluation results in the most reasonable values.

Finally it can be concluded that the proposed evaluation algorithm is also a valuable tool to distinguish between different reaction models. However for this reaction example the evaluation of data set II clearly showed that the reaction mechanism is much more complex than suggested by any of the chosen empirical reaction models. For a comprehensive analysis, more measurements at different concentrations would be required. However it was possible to establish a new reaction model, based on the evaluation results that resembles the reported mechanism of the reaction.

Care should be taken if any kinetic parameters, determined at different concentration conditions, are compared to each other (compare to Appendix E.3.6).

Table 5-10: Epoxidation of 2,5-di-tert-butyl-1,4-benzoquinone. Final results of the separate and combined evaluations (data set II, only 30°C) based on reaction model 9 (see Table 5-8). $\Delta_r H_1$ / $\Delta_r H_2$ as well as k_1 / k_2 are listed in the same field on top of each other. ¹⁾ Sum of $\Delta_r H_1$ and $\Delta_r H_2$. ²⁾ The separate evaluation was carried out by setting $S_Q = 0$ in Equation (4-16) but still both data sets were evaluated. Therefore $\Delta_r H$ can also be identified from the separate evaluation of the infrared data. ⁵⁾ Average values of the evaluations at the different temperatures or directly estimated value. ⁷⁾ Calorimetric and infrared error function at the determined optimum (Equations (4-8) and (4-6)). ⁸⁾ Number of hits (see Chapter 4.3.2), maximum 10.

30 °C	Combined Evaluation	Calorimetric Evaluation	Infrared Evaluation
$\Delta_r H_1, \Delta_r H_2, \Sigma \Delta_r H_i$ [kJ/mol]	-180 -180 -360 ¹⁾	-240 -140 - 380 ¹⁾	-200 ²⁾ -140 -340 ¹⁾
k [(l/mol) ^(ord_C + ord_P) /s]	0.61 0.185	0.42 0.097	0.66 0.260
ord_C [-]	1.13	1.12	1.20
ord_P [-]	-0.16	-0.15	-0.18
ΔQ ⁷⁾ [W ²]	58	45	104
ΔA ⁷⁾ [-]	0.284	0.326	0.282
# Hits ⁸⁾ [-]	10	10	1

5.4.3 Simultaneous evaluation of all experiments at all temperatures

As discussed in Chapter 5.4.1 the evaluation of the measured data, based on the reaction model (5-5) as well as on any other tested reaction modes (see Chapter 5.4.2), did not lead to reasonable results (large temperature dependency of $\Delta_r H_1$ and $\Delta_r H_2$ as well as large difference of $E_{A,1}$ and $E_{A,2}$). According to the general evaluation flow sheet presented in Figure 4-3, in such a situation more physical constraints should be applied. The aim of this Chapter is therefore to check whether it is still possible to model the measured data using the additional physical constraint that $\Delta_r H_1$ as well as $\Delta_r H_2$ should be constant in the temperature range of 17 to 36 °C.

As explained in Chapter 4.4.3 it is possible to evaluate several measurements at different temperatures in one single step. This was done using the evaluation data set I (Appendix Table E-9 and Table E-10, all measurements at all temperatures). In contrast to the individual evaluation at each temperature (see Chapters 5.4.1 and 5.4.2) only one set of reaction enthalpies ($\Delta_r H_1$ and $\Delta_r H_2$) for all temperatures has to be identified.

The pure spectra of the eight involved chemical components (matrix E) were still assumed to be temperature depending and thus four sets of E were identified. An attempt to use the same matrix of pure spectra E for all temperatures failed. This is an indication that the pure spectra of the chemical components involved in this reaction example are temperature depending. This was not the case for the hydrolysis of acetic anhydride (see Figure 5-7).

The same reaction model as was used for the individual evaluation of all temperatures was chosen (Equation (5-5), 5.4.1). The rate constants k_1 and k_2 were replaced by the Arrhenius Equation (4-5). The reaction parameters that were identified by the combined evaluation algorithm are summarized in **Table 5-11**.

Table 5-11: All reaction parameters (with bounds) required for the evaluation of the epoxidation measurements.

	<i>Lower bound</i>	<i>Upper bound</i>
Rate constant k_1 and k_2 at 30 °C [l/(mol·s)]	0	1
Activation energy $E_{A,1}$ and $E_{A,2}$ [kJ/mol]	10	150
Absorption coefficients at each wave number of the reaction Spectrum A and for all three chemical components [-]. (For each temperature new absorption coefficients were calculated.)	0	5
Heat of reaction $\Delta_r H_1$ and $\Delta_r H_2$ [kJ/mol]	0	-1000

The results of the overall evaluation are shown in Table 5-5 (shaded in gray) and in **Figure 5-18**. They are compared to the results obtained by the individual combined evaluation of each temperature (Chapter 5.4.1).

Generally it can be concluded that the overall evaluation was successful and that the quality of the model fit is still satisfying (see **Figure 5-19**). However the error functions ΔA and especially ΔQ are both increased compared to the individual evaluation for single temperatures (see Table 5-5).

The results of the three evaluations (calorimetric, infrared and combined) are still different but the differences are much smaller as compared to the individual evaluations of the temperatures.

In contrast to the results obtained in Chapters 5.4.1 and 5.4.2 the activation energies $E_{A,1}$ and $E_{A,2}$ determined are all reasonable and in a relatively small range (compare to Figure 5-18).

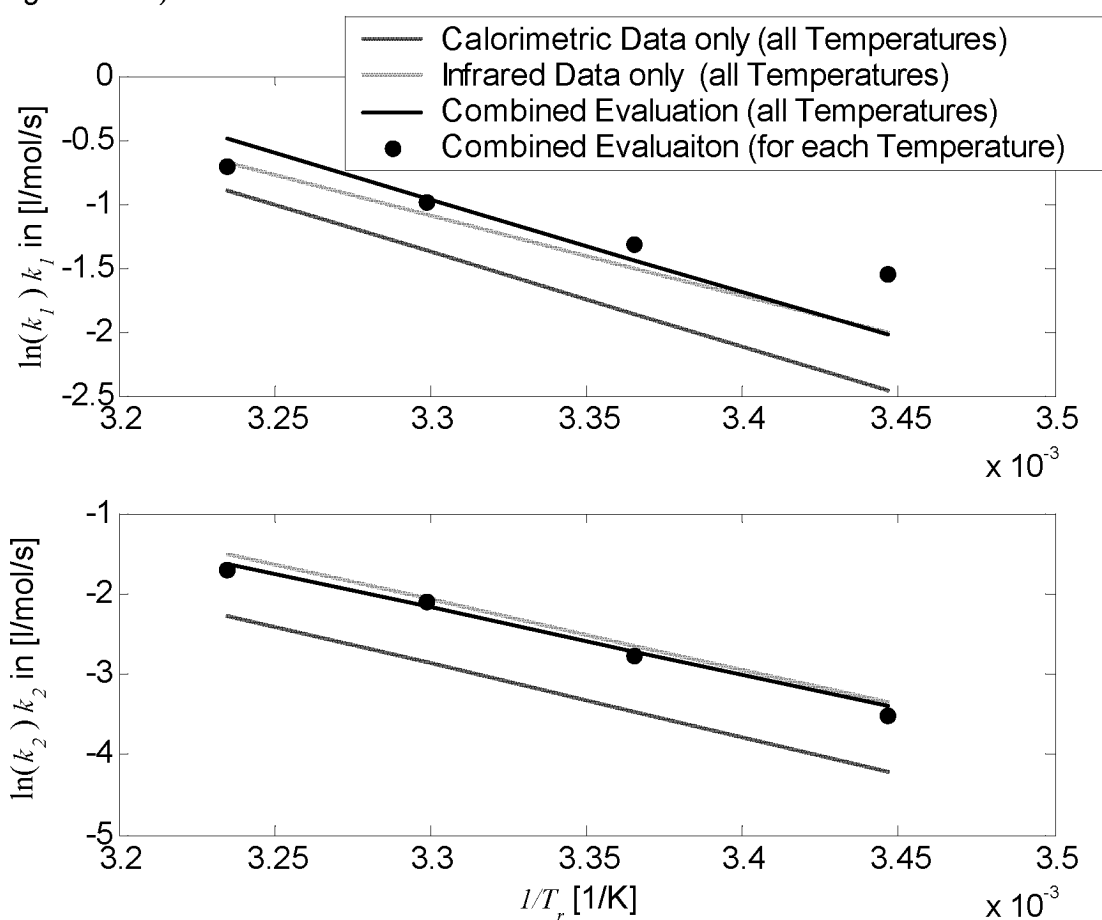


Figure 5-18: Epoxidation of 2,5-di-tert-butyl-1,4-benzoquinone. Arrhenius plot of the rate constants and activation energies determined by the calorimetric, infrared and combined evaluation of the measurements at all temperatures (data set I, reaction model 5, Equation (5-5)). Additionally the rate constants determined by the combined evaluation of each single temperature is shown (reaction model 5, Chapter 5.4.1).

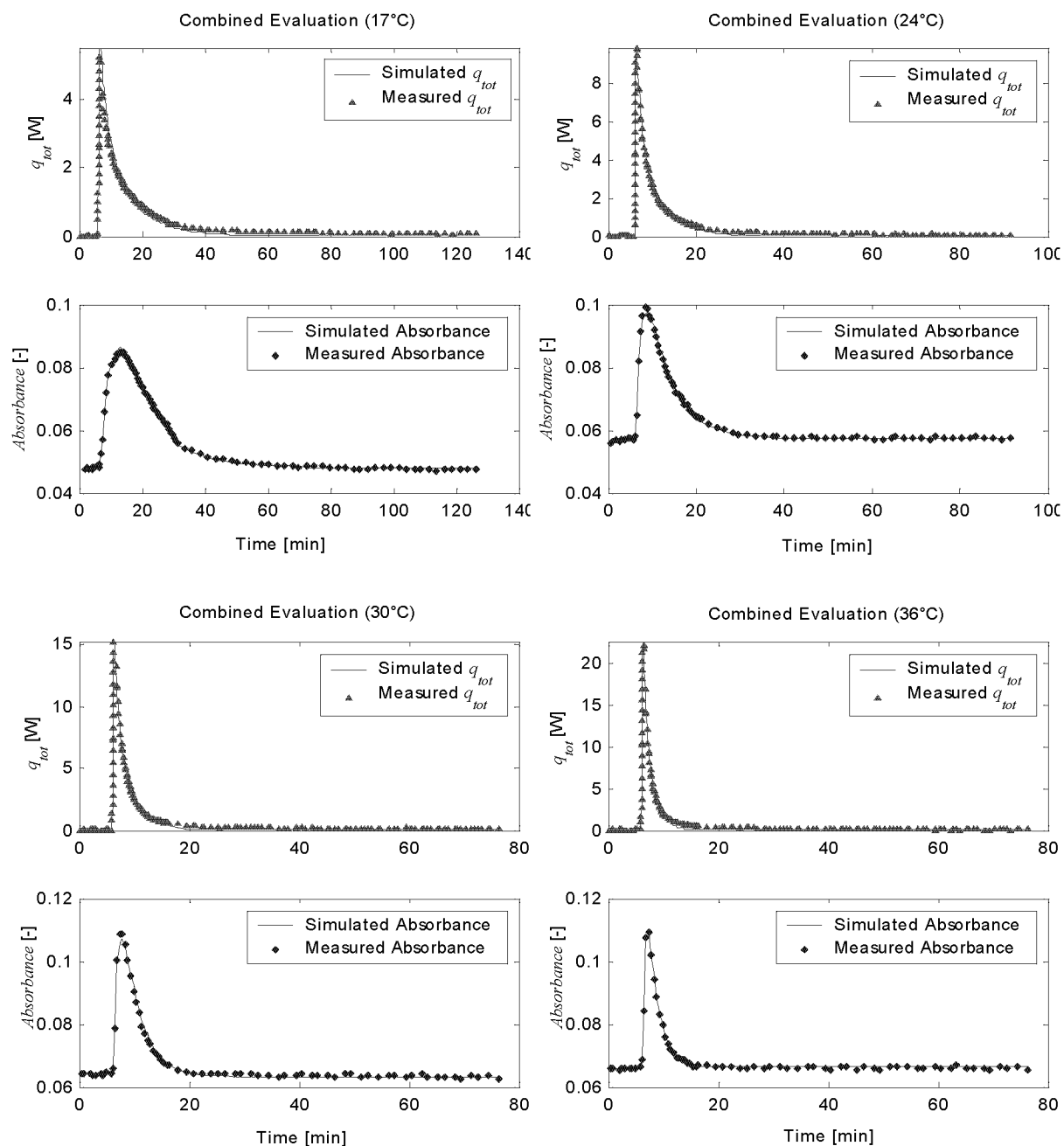


Figure 5-19: Epoxidation of 2,5-di-tert-butyl-1,4-benzoquinone. Combined evaluation of the calorimetric and infrared data. All experiments at all temperatures were evaluated simultaneously (evaluation set I, reaction model 7). A mean value of all reaction experiments at each temperature is shown. Only one wave number (1687 cm^{-1} , see Appendix Figure E-12) of the reaction spectrum is shown.

The reaction enthalpies $\Delta_r H_1$ and $\Delta_r H_2$ still differ significantly between the different evaluations. The largest difference of $\Delta_r H_1$ and $\Delta_r H_2$ was obtained by the separate calorimetric evaluation (90 kJ/mol), a medium difference by the combined evaluation (40 kJ/mol) and a very small difference by the infrared evaluation (10 kJ/mol). Based on mechanistic considerations such a large difference cannot be argued. Semi-empirical quantum mechanical calculations were carried out to estimate the heat of formation of the involved compounds. Cache and HyperChem as well as four different Hamiltonians (AM1, PM3, PM5, MNDO) were used. In most of the calculations, the first epoxidation step turned out to be slightly more exothermal than the second step. However the estimated difference is not significant (see also [Zogg *et. al* 03, submitted]). The **large difference suggested by the separate calorimetric evaluation of $\Delta_r H_1$ and $\Delta_r H_2$ is thus unreasonable**. On the other hand the **large difference of $E_{A,1}$ and $E_{A,2}$ (20 kJ/mol) suggested by the separate infrared evaluation is unreasonable** considering the literature data given in Appendix E.3.6.

The robustness of all three evaluations (see Table 5-5) is quite high (number of hits > 5). The calorimetric evaluation is again the most robust (number of hits = 10) and the infrared evaluation the less robust (number of hits = 6).

*Finally it can be concluded that the results of the **combined evaluation** are most reliable as the identification was robust (number of hits = 8) and as they do not contain any physically or chemically unreasonable information:*

- ❖ Difference of $\Delta_r H_1$ and $\Delta_r H_2$ is only 25 %
- ❖ $E_{A,1} \approx E_{A,2}$ (17 % difference).

The obtained thermodynamic and kinetic reaction parameters are quite close to reference values reported in literature (see Appendix E.3.4 and E.3.6).

Thus the introduction of the additionally physical constraint, that the heats of reaction ($\Delta_r H_1$ and $\Delta_r H_2$) should be constant as a function of the reaction temperature, was successful. It can be concluded that in both evaluations without this constraint (Chapters 5.4.1 to 5.4.2) the degrees of freedom were too high and therefore unreasonable temperature dependencies of $\Delta_r H_1$ and $\Delta_r H_2$ as well as an unreasonable large difference of $E_{A,1}$ and $E_{A,2}$ were obtained.

*This example further shows that a critical analysis of the obtained reaction parameters based on chemical and physical knowledge will always be necessary. Otherwise mathematical artifacts might lead to misinterpretation of the final results. This critical analysis is also indicated in the general evaluation flow sheet shown in Figure 4-3. A third evaluation introducing the constraint $\Delta_r H_1 = \Delta_r H_2$ will be presented in [Zogg *et. al.* 03, submitted].*

5.4.4 Analysis of the automatic scaling method

The basis for all combined evaluation results shown in the previous Chapters (5.3.1 and 5.3.2 as well as 5.4.1 to 5.4.3) is the automatic scaling method developed during this work. It was explained in details in Chapter 4.5. The analysis of the epoxidation experiments (see previous Chapters) clearly showed that the separate evaluation of the infrared and the calorimetric data did not result in the same values for the reaction parameters. This example is therefore interesting to analyze the relationship between the two objective error functions $\Delta Q(\theta_{1..N_p})$ and $\Delta A(\theta_{1..N_p})$ (see Equations (4-6) and (4-8)).

The dependency of the two error functions is best shown by repeating the combined optimization of the infrared and calorimetric data using a varying scaling factor. This was done using the following definition for the combined objective function (compare to Equation (4-16)):

$$\Delta Comb_{\alpha}(\theta_{1..N_p}) = \alpha \cdot (\Delta A(\theta_{1..N_p}) - \Delta A_{min}) + (\Delta Q(\theta_{1..N_p}) - \Delta Q_{min})$$

$$\alpha = 0 \rightarrow \infty [W^2] \quad (5-6)$$

The optimization, based on the combined objective function $\Delta Comb_{\alpha}$, was carried out for the overall evaluation of all epoxidation experiments at all temperatures (compare to Chapter 5.4.3 and the results in Table 5-5). The parameter α was varied from 0 to $1e6 [W^2]$. The remaining calorimetric and infrared error (ΔQ and ΔA) are shown in a Pareto plot (upper plot of **Figure 5-20**). The lower plot of Figure 5-20 shows the logarithm of the parameter α that was used to carry out the combined evaluation according to Equation (5-6).

In both plots the results of the separate infrared ($\alpha = \infty$, $\Delta A = \Delta A_{min}$) as well as the separate calorimetric ($\alpha = 0$, $\Delta Q = \Delta Q_{min}$) evaluation are indicated. Also the results of the combined evaluation using the automatic scaling procedure (see Chapter 4.5, Figure 4-5 and Equation (4-16)) are shown. The parameter alpha was calculated as $\alpha = S_{IR} / S_Q$ (see lower plot of Figure 5-20).

According to the upper plot of Figure 5-20 the infrared error ΔA only shows significant deviations from its minimal value ΔA_{min} as long as ΔQ is smaller than $220 W^2$. This asymmetric shape of the Pareto curve indicates that the internal linear least squares, required to calculate ΔA (see Equations (4-8) and (4-7)), is less sensitive to changes of the reaction model parameters $\theta_{1..N_p}$ (two rate constants and two activation energies in this case) compared to the linear least squares required to calculate ΔQ (Equation (4-6)). *A reasonable combined optimum should therefore show a ΔQ in the range of 173 to $220 W^2$. The solution proposed by the combined evaluation, using the automatic scaling procedure, lies in this region where the changes of ΔA start to become significant. From the Pareto plot it can thus be concluded that the automatic scaling performs well.*

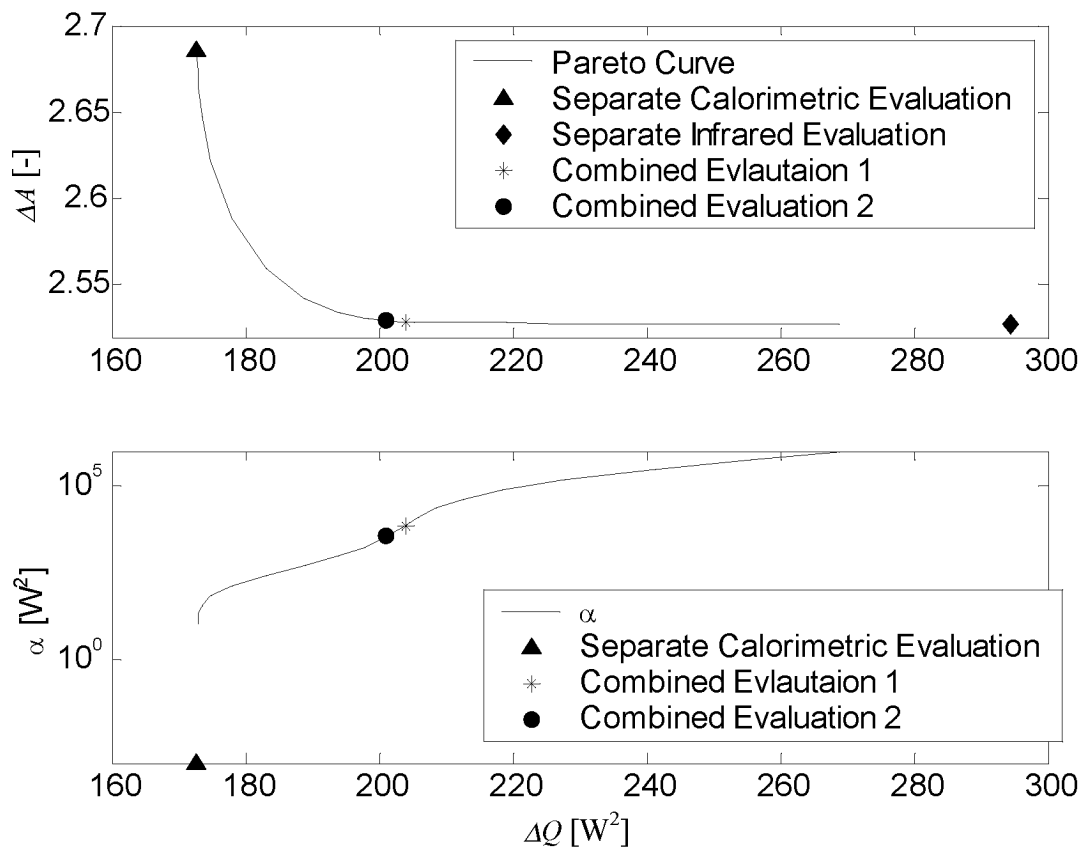


Figure 5-20: Upper plot: Infrared error ΔA as a function of the calorimetric error ΔQ (Pareto curve) calculated based on Equation (5-6) with increasing α . The parameter α is that was used for the calculation of the Pareto curve is shown in the lower plot as a function of ΔQ .

It should be noted that the Pareto curve plotted in Figure 5-20 only shows the remaining model-fit errors. However the focus of the combined evaluation is to determine the reaction model parameters and not to minimize the model-fit error as it contains all kinds of measurement errors. Therefore in **Figure 5-21** all identified reaction parameters (two rate constants, two activation energies and two reaction enthalpies, see Chapter 5.4.3) that were identified based on Equation (5-6) are plotted as a function of ΔQ . Again the results of the separate and the automatic combined evaluation (compare to Table 5-5) are indicated.

Figure 5-21 shows that the identified reaction parameters show a nonlinear dependency on the chosen scaling parameter α . *Further it clearly shows that the parameters identified by a combined optimization can also lay outside of the range defined by the separate calorimetric and infrared evaluation.*

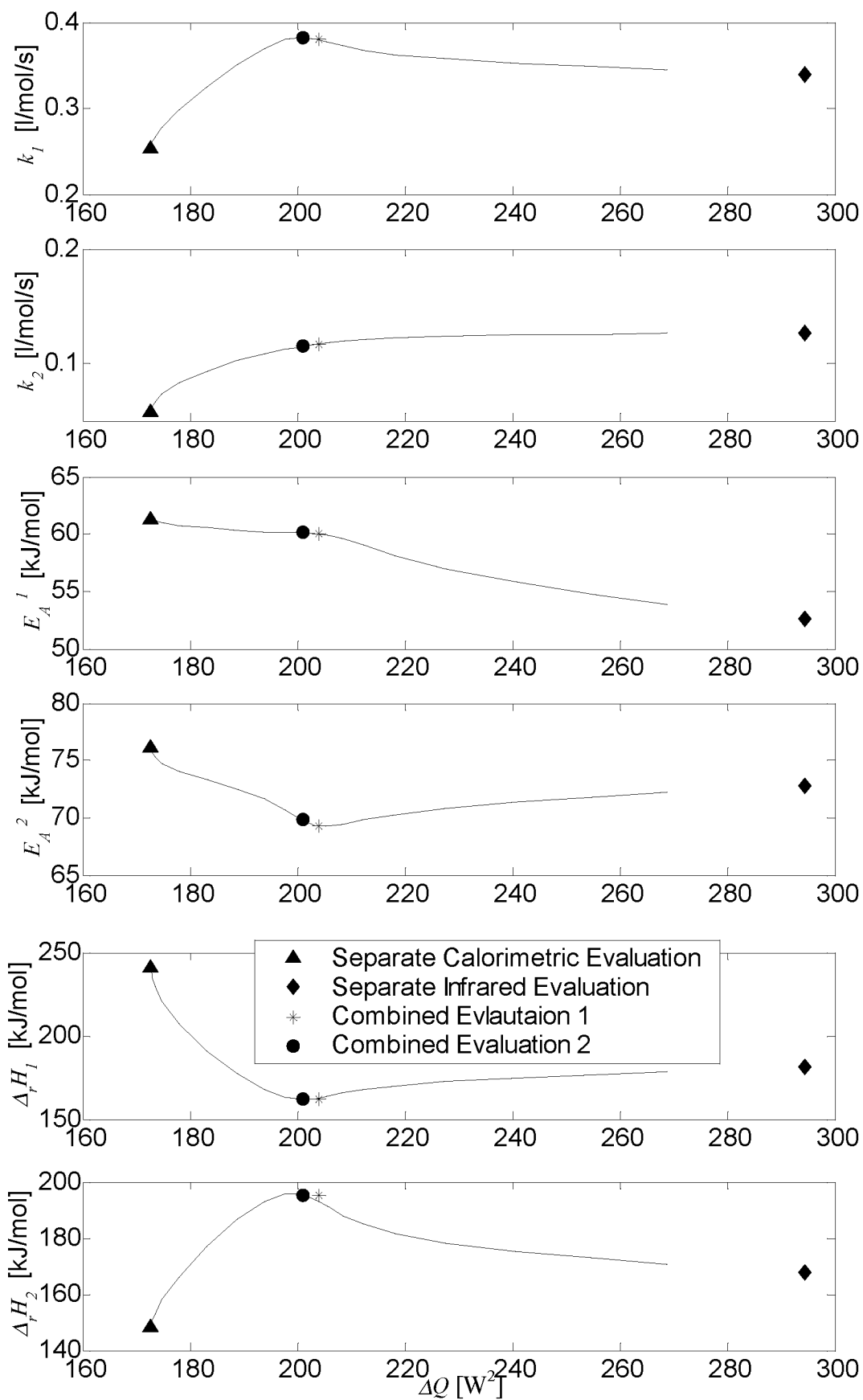


Figure 5-21: Identified reaction parameters, on the basis of the combined objective function (Equation (5-6)), as a function of the calorimetric error ΔQ . Compare to Figure 5-20.

6 FINAL DISCUSSION AND CONCLUSIONS

6.1 New reaction calorimeter

During this work a new, small-scale reaction calorimeter was developed. It is combined with a standard IR-ATR probe to measure additional infrared spectra online. The development was carried out according to the goals formulated in Chapter 1.2: The calorimeter should be small in volume in order to **decrease the consumption of test substance and the application should be as little time consuming as possible**. The measurement principle as well as the construction is described in Chapter 3. The applicability of the calorimeter was verified by carrying out several test reactions, described in Chapter 5.

First of all it can be concluded that the requirements for the new reaction calorimeter (see Chapter 3.2) are widely fulfilled. The calorimeter has a **sample volume of 25 to 45 ml**, is pressure **resistant up to 10 bar**, and temperature resistant up to **200 °C**.

The calorimeter is basically a **Power-Compensation** calorimeter (see Chapter 2.1.1). The combination of a small reactor volume, the fast responding Power-Compensation principle, and a sophisticated control algorithm (see Chapter 3.6) makes this reaction calorimeter **well suited for measurements of fast and highly exothermal reactions**. Several of such reaction examples were carried out (see Chapter 5.2 and Appendix E.4) and despite the **high reaction powers of up to 2.5 kW/l** the reaction temperature T_r could be controlled at isothermal conditions (maximum temperature deviation of 4 °C), so far unrivaled. This allows an easy evaluation of the measured data compared to the case when the reaction temperature would deviate from the set point. **The accuracy of the new reaction calorimeter is high and by far sufficient for the purpose of kinetic and thermodynamic reaction screening**. An overview on the accuracy and the time constants of the new reaction calorimeter is given in Subchapter 6.1.1.

The double wall reactor jacket with a circulating cooling liquid, that represents the basis of most conventional reaction calorimeters, was replaced by an **intermediate thermostat**. This intermediate thermostat basically consists of a copper block as heat-transfer medium and **Peltier elements** as dynamic cooling and heating elements. By the introduction of this intermediate thermostat the following advantages are achieved:

- ✓ It is possible to control the jacket T_j as well as the reactor temperature T_r independent from the temperature of the outside thermostat. It was shown that the determined calorimetric signal q_{tot} **is independent to changes of the temperature of the cooling liquid** (provided by the outside thermostat, see Appendix D.1, Figure D-3). The new reaction calorimeter is therefore **well suited for parallelisation**.
- ✓ **No more calibrations** (for each experiment) of the heat-transfer coefficient, the heat-transfer area or the heat capacity are required. The time required to carry out a single experiment is therefore clearly reduced.
- ✓ **A changing heat flow through the reactor wall** (e.g. due to volume changes or changes of the physical properties of the reaction mixture) can be **measured online**. The benefit of such a measured baseline will be discussed separately in Subchapter 6.1.2.

During the development of this new reaction calorimeter the following three main topics turned out to be important for the accuracy of the measured baseline. They will also be relevant for a potential commercial application.

- ✗ The **Peltier elements** of the intermediate thermostat have to be **precalibrated** (only once and not for each experiment). The developed calibration method (see Chapter 3.7.2 and Appendix D.1) turned out to be useful for the purpose of this work but would have to be replaced by a more practicable method for a commercial application (see outlook 7.1.2). The accuracy as well as the influence of the developed calibration method on the determined reaction parameters is further discussed in Subchapter 6.1.3.
- ✗ The **dynamics of the intermediate thermostat has to be corrected**. The correction method developed (see Chapter 3.7.2) is useful. However other correction methods are possible and should be compared to the chosen method (see outlook 7.1.2). The accuracy as well as the influence of the developed time-correction method on the determined reaction parameters is further discussed in Subchapter 6.1.4.
- ✗ The **influence of the ambient temperature on the measured baseline cannot be neglected**. Therefore a corresponding correction method was developed (see Chapter 3.7.3 and Appendix D.2) during this work and applied to all measurements. It requires a precalibration of the reaction calorimeter, similar of the precalibration of the Peltier elements. A better solution of this problem will be presented in outlook 7.1.1. The accuracy as well as the influence of the correction method on the determined reaction parameters is further discussed in Subchapter 6.1.5.

The **mechanical design** of the new calorimeter proved to be well suited to all industrial and standard reaction examples investigated. The only component that needs further improvements is the **sealing of the IR-ATR probe** (see Appendix C.1) as the applied principle still showed some leakage and would not be applicable in a commercial version. A completely new solution will therefore be presented in the outlook 7.1.1.

6.1.1 Accuracy and time constants of the new calorimeter

The accuracy requirements were specified in Chapter 3.2.1 (and also related to commercial available reaction calorimeters). The actual accuracy of the presented reaction calorimeter is described below.

Relative error of the measured total heat \approx 5% (integration of q_{tot})

This accuracy specification was determined by two well documented reference reactions and a special dosing experiment:

- ❖ Total enthalpy of reaction of the **hydrolysis of acetic anhydride**, determined by direct integration of the measured signal q_{tot} (see Appendix E.2.4.1): -60 ± 5 kJ/mol; reference: -63 ± 2 kJ/mol \rightarrow **relative error: \approx 5 %**.
The reproducibility of the acetic anhydride measurements was \approx 10 %.
- ❖ Total enthalpy of reaction of the **neutralization of NaOH with H₂SO₄**, determined by direct integration of the measured q_{tot} signal (see Chapter 5.2.1): -134 ± 1 kJ/mol; reference: -136 ± 5 kJ/mol \rightarrow **relative error: \approx 1 %**.
- ❖ The accuracy of the measurement of the heat flow q_{Dos} was determined during the hydrolysis experiments of acetic anhydride (see Appendix E.2.4.2). The errors made by the correction of this heat flow were in the **range of 4% compared to the total integrated signal q_{tot}** .

The requirement of maximum 10 % error is therefore met in all cases.

Relative error of the measured baseline \approx 2%

Only for the **neutralization of NaOH with H₂SO₄** it was possible to guess an accurate mathematical baseline (see Chapter 5.2.1). The determined enthalpy of reaction deviates by **2%** from the enthalpy determined with the measured baseline.

The requirement of maximum 10 % error is therefore met.

Detection limit of the power-compensation signal \approx 2 W/l

The detection limit of the q_{Comp} was determined based on the experiments described in Chapters 5.2 to 5.4 and Appendix E.4.1 to be \approx **2 W/l**. **The requirement of 3 W/l is met**. The precision of the presented calorimeter is thus about twenty times smaller compared to a conventional device (for details see Chapter 3.2.1). *This accuracy decrease corresponds to the decrease of the sample volume.*

Detection limit of the baseline signal ≈ 5 W/l

The highest detection limit of $q_{Cooling}$ was determined based on the industrial reaction example described in Appendix E.4.1 to be about 20 W/l. As shown the baseline change is quite strong and the total cooling power of the Peltier elements is close to the maximum. This resulted in an offset error of the measured baseline in the range of 20 W/l at the end of the reaction. The requirement of 3 W/l is therefore not met in this case. However **for standard applications, as described in Chapters 5.2 to 5.4, the detection limit of the baseline signal is ≈ 5 W/l and close to the requirement of 3 W/l.**

Maximum absolute temperature deviation ≈ 0.5 °K/(kW/l)

It was determined by a linear regression of the maximum temperature deviation to the maximum reaction power measured during the reaction applications described in Chapters 5.2 to 5.4 as well as Appendix E.4.1 and E.4.2 (slow dosing rate). **The requirement of a maximal deviation of 0.5 K for a standard reaction example is therefore met.** The reaction example described in Appendix E.4.2 (fast dosing rate) however clearly demonstrates the limits of the actual device: The maximum deviation of the reaction temperature was about 4 K and thus outside of the desired range.

Maximum relative heat accumulation error: $\Delta q_{accu,rel} \approx 20$ %, $\Delta Q_{accu,rel} \approx 1$ %

$\Delta q_{accu,rel}$ as well as $\Delta Q_{accu,rel}$ were determined for the measurements described in Chapters 5.2 to 5.4 and Appendix E.4.1. The heat capacity was assumed to be equal to the heat capacity of water (4.2kJ/kg/K). The instantaneous heat accumulation $\Delta q_{accu,rel}$ is quite high (in the range of 80%) at the start point of the dosing because the measured power consumption / production q_{tot} is close to zero. **During the dosing $\Delta q_{accu,rel}$ reaches maximum values of up to about 20%. The requirement of ≤ 10 % is therefore not met.** After the dosing the instantaneous heat accumulation is close to zero as the reaction temperature is always well controlled. The integrated accumulation error $\Delta Q_{accu,rel}$ **was smaller than 1% for all experiments. The requirement is thus met.**

However especially the accuracy of the measured baseline decreases with increasing reaction power. The closer the cooling power of the Peltier elements is to the maximum possible cooling power, the larger will be the **offset error of the baseline correction**. This problem is addressed in the redesign of the presented reaction calorimeter (see outlook 7.1.1).

In the actual setup of the new calorimeter a **maximum reaction power of about 2 kW/l can be handled**. Reactions with higher reaction powers will cause temperature deviations > 1 K from the set point. If even more powerful reactions have to be investigated, the number of Peltier elements would have to be increased (see outlook 7.1.1).

Time constants

The requirements and the definition for the time constants were specified in Chapter 3.2.2 (and also related to commercial available reaction calorimeters). The actual time constants of the presented reaction calorimeter are given below.

Time constant of the power-compensation signal: $\tau \approx 4$ s

This time constant of q_{Comp} was determined by a step wise change of the stirrer speed (see Chapter 3.7.2) and based on the neutralization experiments of NaOH (see Chapter 5.2). The **requirement of 10s is met**. It should be noted that in this time constant the controlling is already included. The time constant of the sensor and the power supply system is about 1s. **The time constant of the presented calorimeter is thus more than ten times smaller compared to a conventional device** (for details see Chapter 3.2.1).

Time constant of the baseline signal: $\tau \approx 40$ s

This time constant of the $q_{Cooling}$ signal was determined by a step wise change of the stirrer speed (see Chapter 3.7.2). The **requirement of ≤ 30 s is not met. Therefore a time correction of the $q_{Cooling}$ signal was developed (see Chapter 3.7.2) and applied for all evaluations.**

6.1.2 Comparison mathematical – measured baseline

The following table gives an overview on the experiments carried out with the new reaction calorimeter. It specifies whether a baseline change occurred and if it would be possible to guess a mathematical baseline. If a mathematical baseline can be guessed the difference to the measured baseline is given.

Table 6-1: Baseline changes of all the experiments carried out with the new reaction calorimeter. ¹⁾ It is assumed that the baseline change is proportional to the volume change of the reaction mixture. ²⁾ Difference between the total reaction enthalpy ΔH determined by integration of q_{tot} using either the mathematical or the measured baseline.

<i>Experiment</i>	<i>Described in</i>	<i>Baseline Change Occurred</i>	<i>Math. Correction reasonable</i>	<i>Difference of the integrated q_{tot} signals ²⁾</i>
Change of the Stirrer Speed	3.7.2, Figure 3-19	yes	no	-
Neutralization of NaOH	5.2, Figure 5-2	yes	yes ¹⁾	2 %
Hydrolysis of Acetic Anhydride	5.3	yes (small)	yes ¹⁾	6 %
Epoxidation	5.4, Figure E-14	yes (small)	yes ¹⁾	7 %
Industrial Example A	E.4.1, Figure E-18	yes	no	-
Industrial Example B	E.4.2 Figure E-19	yes	no	-

As mentioned in 2.1.5 the **Power-Compensation principle is quite sensitive to changes of the heat flow through the reactor jacket**. This is clearly visible in **Table 6-1** as baseline changes occurred in all reaction experiments. Especially the industrial applications showed strong baseline changes that are difficult to handle if the baseline is not measured online. But also the relatively small baseline changes during the hydrolysis and epoxidation experiments caused significant deviations in the calculated reaction enthalpy if the mathematical is replaced by the measured baseline. The reaction enthalpy was calculated by integration of the measured heat production signal q_{tot} (Equations (3-23) and (2-21)) using either the mathematical or the measured baseline. **Of the three mathematical baselines (hydrolysis, epoxidation and neutralization experiments) used to calculate Table 6-1 only the baseline for the neutralization experiment is acceptable (deviation \approx 2%).**

It can therefore be concluded that an **online measured baseline is crucial and significantly improves the accuracy as well as the information content** of the measured calorimetric data.

6.1.3 Calibration of the Peltier elements

First of all it can be concluded that using the developed calibration procedure (see Chapter 3.7.2) it was possible to determine the Peltier parameters (S , R , and κ .) as a function of the temperature. As the Peltier elements were replaced during this work, two Parameter sets were used for the evaluation of all reaction experiments shown. No significant difference between the calibrated Peltier parameters at the beginning and at the end of a reaction experiment could be measured. Thus for standard reaction experiments constant Peltier parameters can be assumed during a reaction measurement.

In order to get an estimation for the importance of the calibration of the Peltier parameters (see Chapter 3.7.2) the classical evaluation of the calorimetric data of the neutralization and hydrolysis experiments (compare to Chapter 5.2.1 and Appendix E.2.4.1) was repeated using manufacturer values [*Melcor*] for the three Peltier parameters S , R and κ . The relative deviations from the corresponding results given in Chapter 5.2.1 and Table E-7 are summarized in **Table 6-2**.

Table 6-2: Sensitivity of determined reaction enthalpies and rate constants on the Peltier parameters. Relative changes to the corresponding reaction parameters reported in Chapters 5.2.1 (neutralization of NaOH) and Chapter E.2.4.1 (hydrolysis of acetic anhydride, Table E-7) are listed.

<i>Reaction parameter</i>	<i>Neutralization of NaOH</i>	<i>Hydrolysis of Acetic Anhydride</i>
ΔH (model free, integrated)	5 %	9 % 25 °C 16 % 40 °C 25 % 55 °C
$\Delta_r H$ (model based, pseudo first order)		3 % 25 °C 0 % 40 °C 1 % 55 °C
k (pseudo first order)		4 % 25 °C 7 % 40 °C 3 % 55 °C

Table 6-2 clearly shows that the final results of the chosen reaction examples significantly depend on the chosen values for the Peltier parameters. **An accurate determination of these three parameters is thus crucial** for the accuracy of the calculation of $q_{Cooling}$. To improve the accuracy, the cooler (including the Peltier elements) should be calibrated in a separate device similar to the method reported by [*Huang et. al. 00, a*]. Especially the measurement of T_{Pelt}^{up} and T_{Pelt}^{down} could be improved by using several thermocouples on each side of the cooler instead of just one in order to determine a correct mean temperature (see also outlook 7.1)

Further Table 6-2 clearly shows that the sensitivity of the reaction enthalpy determined by integration is much higher compared to the model-based evaluation. This is a hint that the **model-based evaluation is more reliable** because the reaction model acts like a “filter” (compare to compare to the following Chapter 6.2).

6.1.4 Time correction of the baseline signal ($q_{Cooling}$)

The time-correction method for the $q_{Cooling}$ signal (total cooling power of the Peltier elements) developed during this work (see Chapter 3.7.2) was successful for the investigated reaction examples.

In order to get an estimation of the importance of the time correction of the $q_{Cooling}$ signal the classical evaluation of the calorimetric data of the neutralization and hydrolysis experiments (compare to Chapter 5.2.1 and Appendix E.2.4.1) was repeated without time-correction. The relative deviations from the corresponding results given in Chapter 5.2.1 and Table E-7 are summarized in **Table 6-3**.

Table 6-3: Sensitivity of determined reaction enthalpies and rate constants on the time-correction method. Relative changes to the corresponding reaction parameters reported in Chapters 5.2.1 (neutralization of NaOH) and Chapter E.2.4.1 (hydrolysis of acetic anhydride, Table E-7) are listed.

<i>Reaction parameter</i>	<i>Neutralization of NaOH</i>	<i>Hydrolysis of Acetic Anhydride</i>	
ΔH (model free, integrated)	6 %	3 %	25 °C
		3 %	40 °C
		6 %	55 °C
$\Delta_r H$ (model based, pseudo first order)		1 %	25 °C
		1 %	40 °C
		3 %	55 °C
k (pseudo first order)		2 %	25 °C
		3 %	40 °C
		4 %	55 °C

Table 6-3 shows that the **final results of the chosen reaction examples depend on the time-correction**. However the **sensitivity on the time correction is generally smaller than the sensitivity on the Peltier parameters** (see Chapter 6.1.3). An accurate time correction is important for the accuracy of the calculation of $q_{Cooling}$. To improve the accuracy other time-correction methods or a more dynamic reactor jacket would have to be developed (see also outlook 7.1).

Further Table 6-3 shows that the sensitivity of the reaction enthalpy determined by integration is higher compared to the model-based evaluation. This is an additional hint that the **model-based evaluation is more reliable** because the reaction model acts like a “filter” (compare to the following Chapter 6.2).

6.1.5 Influence of the ambient temperature

The developed correction method during this work to take changes of the ambient temperature into account (see Chapter 3.7.3) was successful for the investigated reaction examples. Unique values for $k_{Loss,a}$ and $k_{Loss,b}$ were obtained.

In order to get an estimation of the importance of the ambient-temperature correction of the $q_{Cooling}$ signal, the classical evaluation of the calorimetric data of the neutralization and hydrolysis experiments (compare to Chapter 5.2.1 and Appendix E.2.4.1) was repeated without ambient-temperature correction. The relative deviations from the corresponding results given in Chapter 5.2.1 and Table E-7 are summarized in **Table 6-4**.

Table 6-4: Sensitivity of determined reaction enthalpies and rate constants on the ambient-temperature correction. Relative changes to the corresponding reaction parameters reported in Chapters 5.2.1 (neutralization of NaOH) and Chapter E.2.4.1 (hydrolysis of acetic anhydride, Table E-7) are listed.

<i>Reaction parameter</i>	<i>Neutralization of NaOH</i>	<i>Hydrolysis of Acetic Anhydride</i>	
ΔH (model free, integrated)	0 %	6 % 25 °C	2 % 40 °C
		11 % 55 °C	
$\Delta_r H$ (model based, pseudo first order)		1 % 25 °C	0 % 40 °C
		0 % 55 °C	
k (pseudo first order)		3 % 25 °C	1 % 40 °C
		1 % 55 °C	

Table 6-4 shows that the **final results of the chosen reaction examples depend on the ambient-temperature correction**. However the **sensitivity on the ambient-temperature correction is generally smaller than the sensitivity on the Peltier parameters** (see Chapter 6.1.3). An accurate ambient-temperature correction is important for the accuracy of the calculation of $q_{Cooling}$. To improve the accuracy the reactor should be better isolated, the total area of passive jacket surface should be decreased and the infrared probe should be made of a less heat conductive material (see also outlook 7.1.1).

Further Table 6-4 clearly shows that the sensitivity of the reaction enthalpy determined by integration is much higher compared to the model-based evaluation. This is a third hint that **the model-based evaluation is more reliable** because the reaction model acts like a “filter” (compare to the following Chapter 6.2).

6.2 Evaluation of the calorimetric data

In order to get thermodynamical reaction parameters (such as reaction enthalpies), the evaluation of the measured calorimetric signal q_{tot} (Equation (3-23)) **on the basis of a reaction model** (see Chapters 2.3.2.2 and 2.3.2.3) is clearly advantageous to the **classical, model-free** evaluation based on integration of the measured signal (see Chapter 2.3.2.1) due to the following reasons:

- ❖ All thermal effects that are not related to the physical and chemical processes described by the reaction model can be excluded from the evaluation. Whereas all these effects (heat of mixing, heat of phase change) will be integrated using the classical approach. Of course exclusion of measurement data is only possible as long as the remaining measurement time still allows the identification of the desired reaction parameters (compare to Chapter 5.3.1).
- ❖ The influence of any measurement errors (e.g. base line drifts) or errors in device specific parameters (see Chapters 6.1.3 to 6.1.5) to the finally determined reaction enthalpy is smaller because the reaction model acts like a filter.

The difference of the two approaches in calculating the reaction enthalpy can also be shown for the hydrolysis experiments of acetic anhydride (see Chapter 5.3) and the epoxidation experiments (Chapter 5.4). The results are summarized in **Table 6-5**.

Table 6-5: Difference of the reaction enthalpy determined on the basis of a reaction model ($\Delta_r H$) and by integration (ΔH). ¹⁾ ΔH determined by integration of q_{tot} (Chapter E.2.4.1). ²⁾ $\Delta H_1 + \Delta H_2$ determined by integration of q_{tot} (Chapter E.3.4). ³⁾ Average of the values at 17 ... 36 °C. ⁴⁾ $\Delta_r H$ determined by the separate calorimetric evaluation (Chapter 5.3.1). ⁵⁾ $\Delta_r H_1 + \Delta_r H_2$ determined by the separate calorimetric evaluation (Chapter 5.4.1). ⁶⁾ Result of the overall evaluation of all experiments at all temperatures (separate calorimetric evaluation, Chapter 5.4.3).

	ΔH [kJ/mol] model free	$\Delta_r H$ [kJ/mol] model based	Difference
Acetic Anhydride 25 °C	-60 ¹⁾	-57 ⁴⁾	5 %
Acetic Anhydride 40 °C	-59 ¹⁾	-60 ⁴⁾	2 %
Acetic Anhydride 55 °C	-57 ¹⁾	-60 ⁴⁾	5 %
Epoxidation 17 °C	-440 ²⁾	-360 ⁵⁾	20 %
Epoxidation 24 °C	-440 ²⁾	-370 ⁵⁾	20 %
Epoxidation 30 °C	-480 ²⁾	-400 ⁵⁾	20 %
Epoxidation 36 °C	-440 ²⁾	-410 ⁵⁾	7 %
Epoxidation	-450 ³⁾	-390 ⁶⁾	15 %

6.3 Combined evaluation of calorimetric and infrared data

In a second part of this work (see detailed description in Chapter 4) an evaluation algorithm was developed that allows the model-based evaluation of the calorimetric and infrared data measured during a chemical reaction. The task of the evaluation algorithm is to identify feasible reaction models with their parameters (such as **reaction rate constants, activation energies** or **reaction enthalpies**). To perform this task the **following input is required**:

- ❖ One or several reaction models that describe the **empirical kinetics**, the **stoichiometry**, the **feeds** or any other processes in terms of ordinary differential equations.
- ❖ **Initial conditions** of the specified reaction model, such as initial concentrations of the involved chemical components.
- ❖ **Calorimetric and infrared measurement data**. Several experiments at different temperatures and concentrations can be evaluated at the same time. If measurements at different temperatures are evaluated simultaneously the Arrhenius law will be used to model the rate constants of the reaction model.
- ❖ **Bounds for the unknown reaction parameters** such as rate constants, reaction enthalpies. No initial guesses for the unknown kinetic reaction parameters are required as ten different random start values are generated within the specified bounds. In order to evaluate the infrared data the unknown pure spectra of the involved chemical components are determined simultaneously. *If bounds for the pure spectra are known, they can be included but they are not required (see also discussion in Chapter 6.3.5).*

Based on this input data the developed algorithm performs the following three evaluations (for a detailed description see Chapter 4.4, Figure 4-5):

1. **Separate calorimetric evaluation:**

The thermodynamic (**reaction enthalpies ...**) as well as the reaction model parameters (**rate constants ...**) are identified **in one single step** based on the measured reaction power profiles. Similar methods are described in literature and were discussed in 2.3.2.3.

2. **Separate infrared evaluation:**

The spectroscopic (**pure component spectra**) as well as the reaction model parameters (**rate constants ...**) are identified **in one single step** based on the measured reaction spectra. Similar methods are described in literature and were discussed in 2.3.3.3. It is important to note that **several wave numbers are evaluated at the same time and overlapping absorption peaks of the pure components is allowed**.

3. **Combined evaluation of calorimetric and infrared data:**

Typically the separate evaluations of the **calorimetric and infrared data will not lead to the same reaction parameters** (see e.g. Chapters 5.4.4 and 6.3.3). Several reasons for this deviation are possible. But in the majority of the cases the reasons will be measurement errors and unmodeled processes. However **only one reaction parameter set can be used** for the purpose of reaction optimization as described in Chapter 1.1. In such cases a combined evaluation of the measured data is therefore essential. The aim is to **identify all reaction parameters** (reaction enthalpies, reaction rates and pure component spectra) **in one single step using both measured data sets** (reaction power profiles and infrared reaction spectra). Therefore an objective function has to be calculated that combines the calorimetric and infrared model-fit errors into one single value.

The combination of the calorimetric and infrared objective function, required for the third evaluation, represents the main challenge within all the three evaluations. As shown in Chapter 4.5 and Appendix E.3.8, a simple combination of the two different signals is not useful. It is necessary to scale the two error functions prior to the combined evaluation. This crucial task is generally left to the user of such optimization tools and therefore impedes their application. The **developed method however runs completely automatically and requires no time consuming user interaction**. For a detailed description see Chapter 4.5.

As all the three evaluations shown above are carried out using ten different start values it is then possible to characterize the robustness of the parameter identification. If all ten start values resulted in the same solution for the reaction parameters, the identification was robust whereas only a few identical best solutions indicates low robustness. If several reaction models are evaluated this robustness indicator is useful to distinguish between different models (see Chapter 4.3.2).

The developed evaluation algorithm was then applied to two example reactions, the hydrolysis of acetic anhydride (first-order one-step reaction, see Chapter 5.3) and the epoxidation of 2,4 di tert-butyl benzoquinone (two-step consecutive reaction, see Chapter 5.4). Based on these two case studies the following conclusions can be drawn.

6.3.1 Feasibility study with a simple reaction example

The evaluation performs accurate and robust for the simple reaction example of acetic anhydride (see Chapter 5.3). The combined as well as the separate evaluation of the calorimetric and infrared data gave the same results. The results were verified with classical evaluation principles that can be applied for such easy systems. The results (reaction enthalpy and rate constant) agree very well and are close to the reported literature references (see Table 5-3). It can therefore be concluded that the evaluation algorithm is correctly implemented.

6.3.2 Increased information content by measuring two different analytical signals

As an additional information the evaluation of calorimetric and infrared data of the hydrolysis reaction revealed that a heat of mixing occurs during the dosing phase of the acetic anhydride. As these effects are only visible in the calorimetric signal and do not affect the reaction spectrum, they could be identified (see Appendix E.2.4 and Chapter 5.3.1). This clearly demonstrates the benefit of measuring several different analytical signals in parallel. Especially the calorimetric and the infrared signal are well suited for combination as the reaction power is related to reaction rates whereas the reaction spectrum is related to the concentrations of the involved chemical components (see also Chapter 1.2 and Table 1-1).

Generally it should be considered that the calorimetric as well as the infrared signal have their own limits (see Chapter 6.1.1 for the calorimetric signal and Chapter 6.3.6 for the infrared signal). Therefore many cases might exist where only one of the signals will allow an identification of reaction parameters or only a combined evaluation will lead to reasonable results. *However no such reaction example was encountered during this work.*

6.3.3 A more complex reaction with different feasible reaction models

The evaluation of the consecutive epoxidation reaction (see 5.4) was much more complex, compared to the hydrolysis example, as different reaction kinetic models are feasible and the separate evaluations of the infrared and calorimetric data do not give the same results (see Pareto analysis in Chapter 5.4.4). The classical evaluation applied for the hydrolysis experiments (see Appendix E.2.4) is not possible any more.

By running the evaluation algorithm with several reaction models based on measurements at different initial concentrations of the educts it was further possible to show that the reaction kinetics is strongly depending on the concentration conditions (see Chapter 5.4.2). Only one of the eleven proposed reaction models was able to describe the reaction at different concentration conditions. The reaction orders of this model were also identified at the same time as the reaction rate constants (results see Chapter 5.4.2 and Table 5-10). This demonstrates that the evaluation algorithm is able to deal with complex reaction models. The robustness of the identification (“number of hits”, see above and Chapter 4.3.2) proved to be a useful indicator to select between different reaction models.

Several experiments were carried out at different temperatures but with constant initial concentrations of the educts. The evaluation however resulted in obviously unreasonable activation energies as well as temperature dependencies of the reaction enthalpies for any chosen reaction model (see Chapters 5.4.1 and 5.4.2). Consequently two additional physical constraints were introduced: 1) The reaction enthalpies are not allowed to change as a function of temperature and 2) The temperature dependency of the reaction rate constants is described by the Arrhenius law. Using these additional constraints the evaluation of all experiments at all temperatures was repeated and reliable results were obtained. The results are described in Chapter 5.4.3 and Table 5-5. They are similar to literature references. However care should be taken for this comparison as the literature data are problematic (see Appendix E.3.6).

This reaction example thus demonstrates that a critical analysis of the obtained reaction parameters based on chemical and physical knowledge will always be necessary. Otherwise mathematical artifacts might lead to misinterpretation of the final results.

6.3.4 Comparison of the three evaluation types: Separate Calorimetric, separate infrared and combined evaluation

Based on the different evaluations carried out for the epoxidation reaction (see comments in Chapters 5.4.1, 5.4.2 and 5.4.3 and the corresponding results in Table 5-5, Table 5-9 and Table 5-10) the following observations were made:

- ❖ The **separate calorimetric** evaluation was always the **most robust** estimation (“number of hits” maximal) but often resulted in **physically or chemically unreasonable reaction parameters**.
- ❖ The **separate infrared** evaluation was always the **less robust** estimation (“number of hits” minimal) but mostly resulted in **physically or chemically more reasonable reaction parameters** than the calorimetric evaluation.
- ❖ The **combined evaluation** was always able to find a **different solution** for the identification problem. The robustness of the identification was always between the two separate evaluations and the reaction parameters determined were physically reasonable. It is important to note that the combined evaluation did not result in a solution that is either similar to the infrared or calorimetric evaluation (see Appendix E.3.8). *The reaction parameters identified represent a real combined optimum that sometimes even lies outside of the range defined by the separate evaluation* (see e.g. Arrhenius plots Figure 5-13, Figure 5-16 and Figure 5-18). This fact and the further analysis of the automatic scaling method on the basis of a Pareto plot (see Chapter 5.4.4) allow the conclusion that the automatic calculation of the combined objective function performs well and that performing only a separate evaluation of the measured data might be misleading.

Basically two problems might be the reason for the difficulties encountered during the separate evaluation of the calorimetric data and the deviation of its results to the other evaluations:

1. The **calorimetric data contain physical effects (e.g. when the assumption $q_{tot} = q_{React}$ is not fulfilled) that were not modeled** by any of the reaction models and do not influence the reaction spectrum. This is supported by the fact that the integration of the total reaction power measured (q_{tot}) leads to significantly different total reaction enthalpies than the model-based evaluation (see Chapter 6.2). Further observations described in Appendix E.3.5 indicate that phase change effects and eventual side reactions occur.

2. The **evaluation task**, to identify two reaction rates and two reaction enthalpies in one step, is **mathematically robust** but leads to **physically unreasonable** results.

The reason for the low robustness of the infrared identification might be the larger degrees of freedom of the internal linear optimization problem (see Chapter 4.4.3, Equations (4-8) and (4-7)) compared to the internal linear optimization problem for the calorimetric evaluation (Equation (4-6)). In this reaction example eight different pure spectra but only two different reaction enthalpies have to be identified.

*Due to the developed algorithm the evaluation of the calorimetric data can be combined with evaluation of the infrared data. It was shown that both data sets support each other and lead to a medium robust identification with physically reasonable results. **The combined evaluation is thus clearly superior to the separate calorimetric and infrared evaluations, and essential for examples where the separate evaluations result in different reaction parameters.***

6.3.5 Determination of pure component spectra

For the simple reaction example, the **hydrolysis of acetic anhydride** (see Chapter 5.3), the identification of the pure component spectra was successful (see Figure 5-7), since only three components had to be identified (rank of the concentration matrix is also equal to three). *The estimated pure spectra differ significantly from the measured pure spectra and do not show a significant temperature dependency.*

However the identification of the pure spectra of the **epoxidation reaction** (see Chapter 5.4) is not possible because eight different spectra are identified and only five are mathematically possible (rank of the concentration profile matrix is equal to five, see discussion in Chapter B.2 and the identified pure spectra in Figure E-15). ***But it is important to note that the identification of the desired reaction parameters is still possible.***

In contrast to the hydrolysis reaction the identification of the reaction parameters failed when the pure component spectra were assumed to be constant in the investigated temperature range.

It can therefore be concluded that component spectra may vary in a reaction mixture with temperature (see also Chapter 2.2) and **may differ significantly from measured pure spectra**. *Care should thus be taken when measured pure component spectra are used in order to evaluate reaction spectra.*

6.3.6 Limits of the IR-ATR (infrared) signal

Based on the reactions investigated during this work the following limits were observed:

- ❖ In **suspensions** of solid and liquid components only the liquid phase can be observed. In the example studied (see Appendix B.2) the concentration of the solid component in the liquid phase was even too low to be visible in the infrared signal.
- ❖ During the epoxidation experiments (see Chapter 5.4) as well as during the industrial reaction example B (see Appendix E.4.2) **isomers** (stereo and regio isomers) are produced. However they could not be distinguished in the reaction spectrum as their pure component spectra are quite similar. Additionally an intermediate product would have been suggested for the industrial reaction example B, but could not be identified. The reason might be that the concentration is too low compared to the other concentrations and therefore the contribution to the overall reaction spectrum is not significant.
- ❖ As mentioned before, the reaction spectrum does mostly not contain enough information to identify all pure spectra of all involved chemical species as their **concentration profiles are linear dependent** (see discussion in Appendix B.2 and Chapter 5.4.1).
- ❖ Care must be taken when strong absorption bands are evaluated as the linear relation between absorption and component concentrations (**Lambert-Beer's Law**) might be violated (see Chapter 2.2 and Appendix B.1).
- ❖ The **maximal sampling frequency** (6 S/min) of the infrared signal is much lower compared to the calorimetric signal (600 S/min).
- ❖ Unfortunately the **spectral region** from 1800 to 2400 cm^{-1} is not available because diamond is used as ATR-crystal.

6.3.7 Limits of the model-based evaluation

As shown both data sets, the calorimetric as well as the infrared data, can be evaluated based on an empirical reaction model. The advantages and disadvantages of the model-based approach were already discussed earlier (see Chapters 2.3.4 and 6.2). Additionally it should be mentioned that most of the model-based approaches assume that the density of the reaction mixture is not changing during the reaction. As soon as such changes occur they should be considered in the reaction model.

However the often mentioned drawback of model-based approaches, it would be difficult to find appropriate reaction models, is not reasonable:

- ❖ Any person with adequate chemical background will always be able to suggest appropriate empirical reaction models. The reaction model does not have to represent the mechanistics of the reaction but the overall kinetics. As mentioned in Chapter 1.2 the proposed evaluation procedure is not designed to be used by people who have little or no chemical background about the reaction they would like to investigate. In practical situations there might be quite a lot of other analytical data available for the investigated reaction (chromatographic samples, isolated main products, identified side products ...). All this information can be used to suggest an appropriate empirical reaction model.
- ❖ Model selection based on the two indicators, quality and robustness of the model fit was shown to be easy and specific (see Chapters 4.3.2 and 5.4.2)

7 OUTLOOK

7.1 Reaction calorimeter

7.1.1 Reactor redesign

During the thesis a complete redesign of the presented reaction calorimeter (Chapter 3) was made. The main focus of the redesign was to improve the calorimetric properties of the intermediate thermostat but also to introduce a new type of ATR-Sensor. The Power-Compensation part is therefore not changed but the copper jacket is completely redesigned. The new device will be pressure resistant up to 20 bar. The calorimeter has already been built but no performance data are yet available. The new design is described in the following figures:

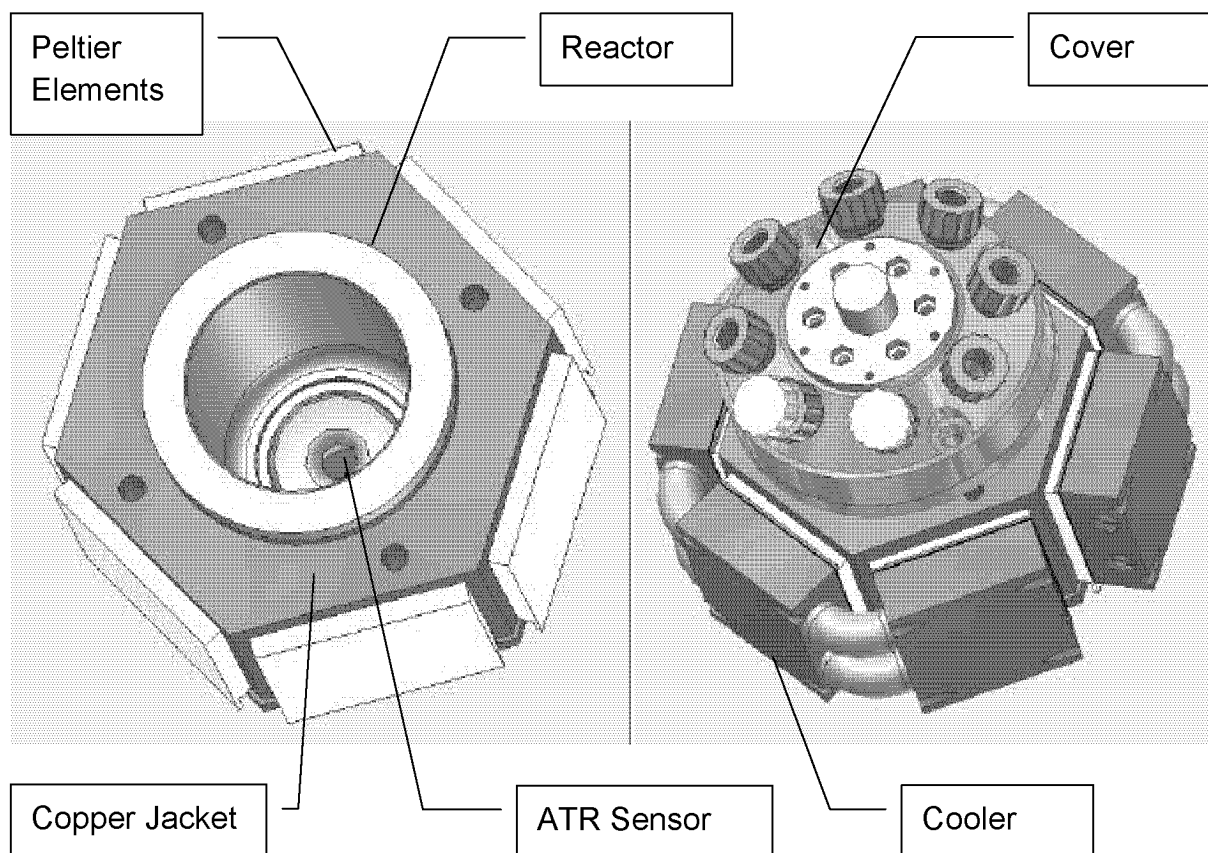


Figure 7-1: Left side: New design of the copper jacket using 6 Peltier elements from a side. The reactor can be replaced and is made of Hastelloy. The IR-ATR probe is directly mounted into the bottom of the reactor. Right side: The covered reactor as well as the six coolers of the Peltier elements are shown. (CAD – Drawings made by H. P. Schläpfer, Workshop ETH).

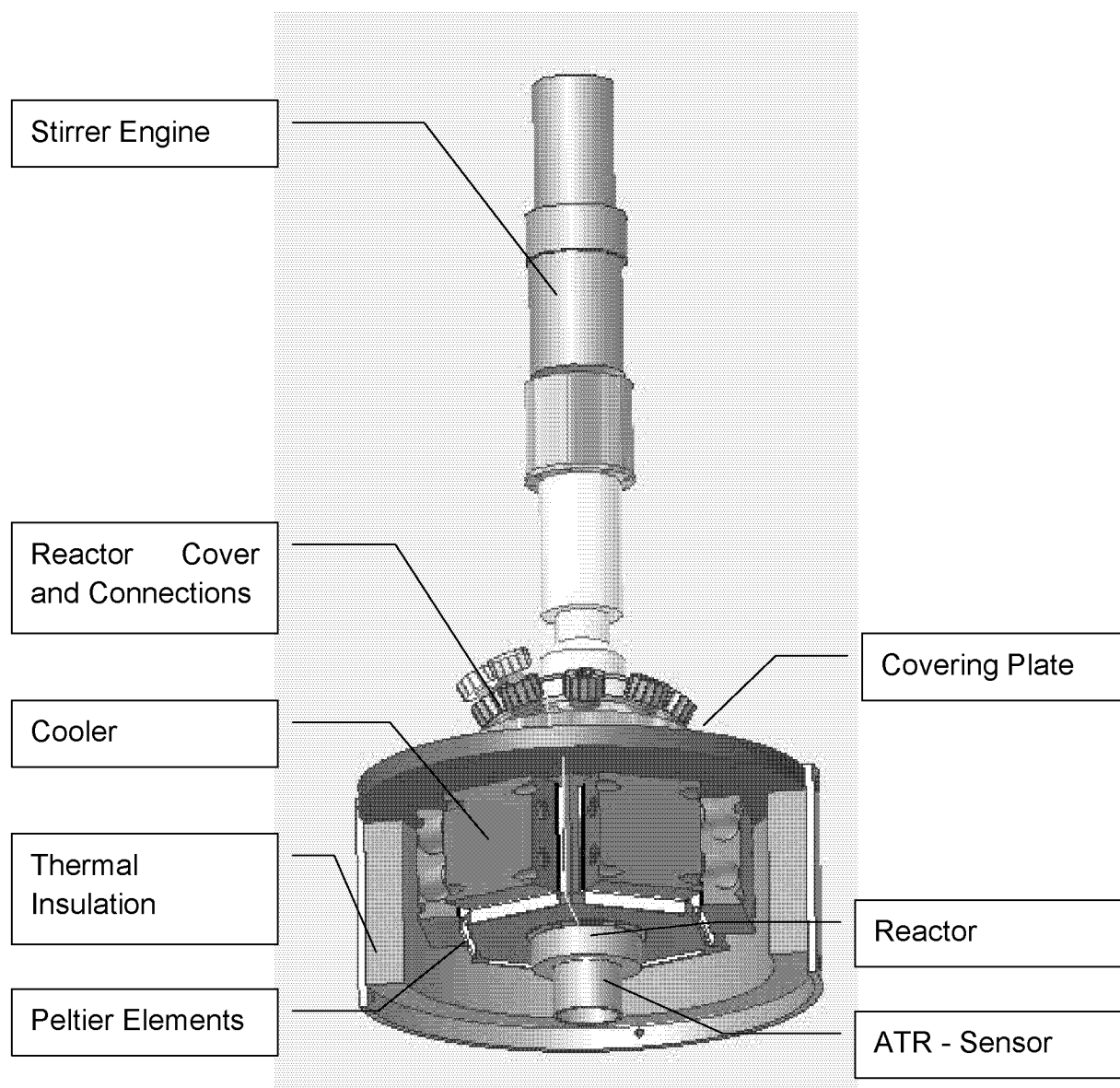


Figure 7-2: Final setup of the new reactor with the jacket insulation and the stirrer engine. (CAD – Drawings made by H. P. Schläpfer, Workshop ETH).

The main problems of the reaction calorimeter presented in Chapter 3 were mentioned in Chapter 6.1. Most of them but also more practical problems were addressed by this redesign:

- ❖ The problem of the **sealing of the infrared dipper** was completely solved by using a new type of ATR-Sensor kindly provided from the companies Mettler Toledo and ASI. The new ATR-Sensor should even show increased sensitivity.
- ❖ The reactor is not any more made of Teflon but of Hastelloy. It is now possible to **remove the reactor** from the copper jacket. Thus it should be possible to insert a dummy reactor that includes a separate heater. With such a dummy

reactor it will be possible to **calibrate the Peltier elements** systematically e.g. over night and not at the beginning and at the end of a reaction experiment. The same dummy reactor could also be used to calibrate the dynamics of the reactor jacket more systematically (see Chapters 3.7.2, 6.1.1 and 6.1.4). Another benefit will be the much **lower temperature gradients** caused by the reactor wall compared to the actual setup with Teflon as reactor wall. This will be useful if strongly exothermal reactions are studied at low temperatures.

- ❖ In order to further increase the calibration quality of the Peltier elements **twelve thermocouples** are introduced to measure T_{Pelt}^{up} and T_{Pelt}^{down} for each element (compare to the discussion in Appendix C.7.4 and D.1).
- ❖ The total **cooling performance** of the Peltier elements is three times larger. Therefore their operating conditions should be further away from the maximum cooling capacity. Consequently the calculation of the cooling power $q_{Cooling}$ should be more accurate (see Chapters 6.1.1 and 3.7.2).
- ❖ The **increased symmetry** of the reactor and reduced copper mass should improve the dynamic behavior of the reactor (see Chapters 6.1.1, 6.1.4 and 3.7.2). Additionally the temperature gradients inside the copper jacket will be further reduced. Six thermocouples will be used to calculate an average value for T_j (compare to Appendix C.6).
- ❖ The total **passive area** of the reactor jacket is heavily **reduced** compared to the actual setup. The **influence of the ambient temperature** should therefore be **decreased** significantly (see Chapters 6.1.5 and 3.7.3). Also the thermal insulation of the jacket is improved as it is now separated from the insulation of the reactor cover.
- ❖ The **mounting of the Peltier** elements can be carried out individually for each element and thus optimal thermal contact is guaranteed (compare to the discussion in Chapter 3.4.4). The mounting screws (see Chapter 3.4.4) are replaced by two springs around all cooler elements (not shown in the figures). Therefore the heat leakage due to the mounting screws is not present any more (see discussion in Chapter 3.4.4). The performance of the cooler is increased by circulation of the cooling liquid in two separate cooling turns in opposite direction. This is crucial as the six Peltier elements should all work at the same temperature. In order to further minimize the potential drift of the six elements they are electronically connected in the following way: Element 1, 3, and 5 in series. Element 2, 4, and 6 in series. The two blocks are then connected in parallel.
- ❖ The **separate thermal insulation of the reactor jacket** allows the purging of the whole box e.g. with N_2 in order to remove humidity of the air inside the thermal insulation. This is crucial for applications at low temperatures and should also increase the performance as well as the life time of the Peltier elements (see discussion in Appendix C.7.2).

7.1.2 Ideas for future developments

The following ideas could be investigated to further improve the reaction calorimeter:

- ❖ The problem of an accurate calibration of the Peltier elements could also be solved by introducing a **heat-flow sensor** analogous to the Chemisens reaction calorimeter. A heat-flow sensor measures the temperature difference over a specified distance. The heat flow between the two temperature measurements is proportional to the temperature difference as long as the heat conductivity of the material between the temperature sensors is constant. The temperature difference signal could be used as baseline function for the mathematical baseline correction (see Appendix D.3). A heat-flow sensor could be introduced between the Peltier elements and the copper jacket. However in the new reactor design it should also be possible to use the temperature difference between the Hastelloy reactor and the surface of the Peltier elements.
- ❖ Another solution to the Peltier calibration problem would be to **support the Peltier elements by an additional heater element**. Such a principle was already implemented by [Christensen et. al. 73]. However a big drawback of this method will be the increased cooling requirements for the cryostat.
- ❖ The **accuracy of the temperature measurement** is crucial for the detection limits of the whole device. Therefore Pt100 elements could be used to measure T_j and eventually T_r for slower applications. In parallel the sensor noise of the temperature measurement would be decreased.
- ❖ As mentioned the optimal **wall thickness of the copper jacket** was never calculated. A finite element calculation could be carried out in order to verify a possible improvement of the dynamic behavior.
- ❖ The switching of the controller settings at point ⑥ in Figure 3-15 could be automated. E.g. the switching could occur as soon as the changes of the $q_{Cooling}$ or q_{Comp} signals became small.

7.1.3 Ideas for the improvement of the heat-flow balance calculations

The following ideas are recommended to be investigated in order to further improve the quality of the heat-flow balance calculations:

- ❖ So far the **cooling power of the Peltier elements** $q_{Cooling}$ was directly used as in the heat-flow balance. However as discussed in Chapters 6.1 and 6.1.1 the accuracy of the $q_{Cooling}$ signal was not satisfying as an offset error occurred. This problem could be solved by not using $q_{Cooling}$ directly in the heat-flow balance but to use it as the baseline function $bl(t)$ in the mathematical baseline correction (see D.3).
- ❖ The **black-box time correction** of the $q_{Cooling}$ signal described in Chapter 3.7.2 could be replaced by a more physical based model of the dynamic heat flow through the reactor jacket (compare to Chapters 2.1.3.1 and 2.1.4). The steady-state equations that were used as the basis to calculate $q_{Cooling}$ could then be replaced. More possibilities to carry out a time correction are mentioned in [Velázquez-Campoy *et. al.* 99] and [Vincent *et. al.* 02].
- ❖ As mentioned no **changes of the Peltier parameters during a reaction** experiment were observed. However if such changes should be observed in future applications a temperature dependent correction of the Peltier parameters would be easy to implement in the heat-flow balance.
- ❖ The errors made by **neglecting the heat flow** q_{accu} in the isothermal heat-flow balance (see Chapter 6.1.1) could be eliminated by including this heat flow into the heat-flow balance. However the heat capacity of the reactor content (reaction mixture and reactor inserts) would have to be determined. **A fast and easy way to determine the heat capacity of the reactor content** would be to measure the initial slope of the reaction temperature T_r when a instant change of the compensation power q_{Comp} is applied. Feasibility tests for this quick determination of the heat capacity were already carried out and gave *promising results*. For the reaction examples shown in this work q_{accu} was calculated, assuming the heat capacity of water. Only during the initial reaction phase (start and end of the dosing) an improvement of the signal quality could be achieved. However the over all influence on the results was not significant.
- ❖ So far it was assumed that the heat flow caused by the **stirring** is constant during a reaction measurement (see Chapter 3.7.3). If this is no more the case, q_{Stirr} could be corrected according to the measured power consumption of the stirrer engine.

7.2 Evaluation algorithm

The following ideas could be investigated to further improve the combined evaluation algorithm:

- ❖ The **concept** of the calculation of the combined objective function must be tested on the basis of further reaction examples (e.g. parallel reactions).
- ❖ **Baseline drifts** of the infrared spectrometer were already taken into account during this work (see Chapter 4.4.1). However the baseline was assumed to be constant at all wave numbers. This assumption could fail for certain reaction examples. Therefore the evaluation methods based on target factor transformation described in Chapter 2.3.3.3 could be implemented and tested, instead of the direct least-squares approach used in the actual evaluation algorithm.
- ❖ Generally for the internal linear optimizations as well as the outside nonlinear optimization, the least-squares approach was used as objective **function type**. Of course many other objective function types exist such as absolute, relative, logarithmic, ... Approaches, different to the sum of squares, were also used in literature ([Taavitsainen et. al. 01], [Nomen et. al. 01], [Furusjö et. al. 00, b], [Tam et. al. 94], and [Bijlsma et. al. 98]).
- ❖ The model based evaluation of the infrared data used in this work (Equations (4-7) and (4-8)) could be replaced by one of the more sophisticated methods described in Chapter 2.3.3.3).
- ❖ The developed combined evaluation of calorimetric and infrared data (see Chapter 4.4.3) does not depend on any specific characteristics of the two signals. Also the calculation of the combined objective function (see Chapter 4.5) **does not need any specific input from outside**. It is therefore straightforward to **extend the proposed evaluation method to other analytical signals than calorimetry and infrared spectroscopy**. The only restriction is that a linear relationship between the measured signal (S) and the output of the reaction model exists. An extended version of the combined optimization (compare to 4.5, Equation (4-16)) could then be written as follows:

$$\min_{\theta_{1..N_p}} \left(S_Q \cdot [\Delta Q(\theta_{1..N_p}) - \Delta Q_{\min}] + S_{IR} \cdot [\Delta A(\theta_{1..N_p}) - \Delta A_{\min}] + S_S \cdot [\Delta S(\theta_{1..N_p}) - \Delta S_{\min}] \right) \quad (7-1)$$

8 REFERENCES

[ACSL]

ACSL Optimize, Aegis Technologies Group, Inc., www.acslsim.com

[am Ende et. al. 98]

D. J. am Ende, K. M. DeVries, P. J. Clifford, S. J. Brenek, *A Calorimetric Investigation To Safely Scale-Up a Curtius Rearrangement of Acryloyl Azide*, Organic Process Research & Development, Vol. 2, pp. 382-392, **1998**

[am Ende et. al. 99]

D. J. am Ende, P. J. Clifford, D. M. De Antonis, C. Santa Maria, S. J. Bernek, *Preparation of Grignard Reagents: FTIR and Calorimetric Investigation for Safe Scale-Up*, Organic Process Research & Development, Vol. 3, pp. 319-329, **1999**

[Amrhein et. al. 96]

M. Amrhein, B. Srinivasan, D. Bonvin, M. M. Schumacher, *On the rank deficiency and rank augmentation of the spectral measurement matrix*, Chemometrics and Intelligent Laboratory Systems, Vol. 33, pp. 17-33, **1996**

[Amrhein et. al. 99]

M. Amrhein, B. Srinivasan, D. Bonvin, *Target factor analysis of reaction data: use of data pre-treatment and reaction-invariant relationships*, Chemical Engineering Science, Vol. 54, pp. 579-591, **1999**

[Andersen 66]

H. M. Andersen, *Isothermal kinetic calorimeter applied to emulsion polymerization*, Journal of Polymer Science Part A-1, Vol. 4, pp. 783-791, **1966**

[Andersen 69]

H. M. Andersen, *Polymerization Rates by Calorimetry II*, Journal of Polymer Science Part A-1, Vol. 7, pp. 2889-2896, **1969**

[Anderson et. al. 96]

H.L. Anderson, A. Kemmler, R. Strey, *Erfahrungen mit vier Softwarepaketen für kinetische Auswertungen in der thermischen Analyse*, Journal of Thermal Analysis, Vol. 47, pp. 543-557, **1996**

[André et. al. 02]

R. André, L. Bou-Diab, P. Lerena, F. Stoessel, M. Giordano, C. Mathonat, *A New Reaction Calorimeter for Screening Purposes during Process Development*, Organic Process Research & Development, Vol. 6, pp. 915-921, **2002**

[Axiom]

Axiom Analytical Inc., <http://www.goaxiom.com>

[Balland et. al. 00]

L. Balland, L. Estel, J. M. Cosmao, N. Mouhab, *A genetic algorithm with decimal coding for the estimation of kinetic and energetic parameters*, Chemometrics and Intelligent Laboratory Systems, Vol. 50, No. 1, pp. 121-135, **2000**

References

- [Baranek et. al. 99]
B. Baranek, M. Gottfried, K. Korfhage, W. Pauer, K. Schulz, H. U. Moritz, *Closed Loop Control of Chemical Composition in Free Radical Copolymerization by Online Reaction Monitoring via Calorimetry and IR-Spectroscopy*, Mettler Toledo Publication, **1999**
- [BatchCAD]
BatchCAD, Hyprotech, www.hyprotech.com/batchcad
- [BatchReactor]
BatchReactor, ProSim, www.prosim.com
- [Bayada et. al. 95]
A. Bayada, G. A. Lawrance, M. Maeder, K. J. Molloy, *ATR-IR Spectroscopy for the Investigation of Solution Reaction Kinetics: Hydrolysis of Trimethyl Phosphate*, *Applied Spectroscopy*, Vol. 49, No. 12, pp. 1789-1792, **1995**
- [Becker 68]
F. Becker, *Thermokinetische Messmethoden*, *Chemie Ingenieur Technik*, Vol. 19, pp. 933-980, **1968**
- [Becker et. al. 65]
F. Becker, W. Walisch, *Isotherme Kalorimetrie mit automatisch gesteuerter Peltier-Kühlung und fortlaufender Integration der Kompensationsleistung. III. Die kalorimetrische Apparatur und ihre Anwendung*, *Zeitschrift für Physikalische Chemie Neue Folge*, Vol. 46, pp. 279-293, **1965**
- [Becker et. al. 67]
F. Becker, A. Maelicke, *Thermokinetische Messungen nach dem Prinzip der Wärmeflusskalorimetrie*, *Zeitschrift für Physikalische Chemie Neue Folge*, Vol. 55, pp. 280-295, **1967**
- [Bell et. al. 98]
W. C. Bell, K. S. Booksh, M. L. Myrick, *Monitoring Anhydride and Acid Conversion in Supercritical / Hydrothermal Water by in Situ Fiber-Optic Raman Spectroscopy*, *Analytical Chemistry*, Vol. 70, pp. 332-339, **1998**
- [BenAmor et. al. 02]
S. BenAmor, D. Colombié, T. McKenna, *Online Reaction Calorimetry. Applications to the Monitoring of Emulsion Polymerization without Samples or Models of the Heat-Transfer Coefficient*, *Industrial & Engineering Chemistry Research*, Vol. 41, pp. 4233-4241, **2002**
- [Bezemer et. al. 01]
E. Bezemer, S. C. Rutan, *Multivariate curve resolution with non-linear fitting of kinetic profiles*, *Chemometrics and Intelligent Laboratory Systems*, Vol. 59, pp. 19-31, **2001**
- [Bezemer et. al. 02]
E. Bezemer, S. C. Rutan, *Three-way alternating least squares using three dimensional tensors in MATLAB*, *Chemometrics and Intelligent Laboratory Systems*, Vol. 60, pp. 239-251, **2002**

- [Bijlsma et. al. 00]
S. Bijlsma, A.K. Smilde, *Estimating reaction rate constants from a two-step reaction: a comparison between two way and three-way methods*, Journal of Chemometrics, Vol. 14, pp. 541-560, **2000**
- [Bijlsma et. al. 01]
S. Bijlsma, H. F. M. Boelens, A. K. Smilde, *Determination of Rate Constants in Second-Order Kinetics Using UV-Visible Spectroscopy*, Applied Spectroscopy, Vol. 55, No. 1, pp. 77-83, **2001**
- [Bijlsma et. al. 02]
S. Bijlsma, H. F. M. Boelens, H. C. J. Hoefsloot, A. K. Smilde, *Constrained least squares methods for estimating reaction rate constants from spectroscopic data*, Journal of Chemometrics, Vol. 16, pp. 28-40, **2002**
- [Bijlsma et. al. 98]
S. Bijlsma, D. J. Louwse, A. K. Smilde, *Rapid Estimation of Rate Constants of Batch Processes Using On-Line SW-NIR*, AIChE Journal, Vol. 44, No. 12, pp. 2713-2723, **1998**
- [Bugnon et. al. 94]
P. Bugnon, J.C. Chottard, J.L. Jestin, B. Jung, G. Laurency, M. Maeder, A.E. Merbach, A.D. Zuberbühler, *Second-order globalization for the determination of activation parameters in kinetics*, Analytica Chimica Acta, Vol. 298, pp. 193-201, **1994**
- [Buist et. al. 94]
R. J. Buist, M. J. Nagy, *Thermoelectric heat sink modeling and optimization*, 13th International Conference on Thermoelectrics, TE Technology, Inc., Michigan, USA, www.tetech.com, **1994**
- [Casassas et. al. 93]
E. Casassas, N. Dominguez, G. Fonrodona, A. de Juan, *Factor analysis applied to the study of the effects of solvent composition and nature of the inert electrolyte on the protonation constants in dioxane-water mixtures*, Analytica Chimica Acta, Vol. 283, pp. 548-558, **1993**
- [Cesari et. al. 81]
E. Cesari, P. C. Gravelle, J. Gutenbaum, J. Hatt, J. Navarro, J. L. Petit, R. Point, V. Torra, E. Utzig, W. Zielenkiewicz, *Recent progress in numerical methods for the determination of thermokinetics*, Journal of Thermal Analysis, Vol. 20, pp. 47-59, **1981**
- [Chemisens]
Chemisens, www.chemisens.com
- [ChemCAD]
ConcIRT, Chemstations, Inc., <http://www.chemstations.net>
- [Christensen et. al. 73]
J. J. Christensen, J. W. Gardner, D. J. Eatough, R. M. Izatt, *An Isothermal Titration Microcalorimeter*, The Review of Scientific Instruments, Vol. 44, No. 4, pp. 481-484, **1973**
- [ConcIRT]
ConcIRT, ASI Applied Systems, <http://www.asirxn.com/>

References

[CRC]

CRC Handbook of Chemistry and Physics, CRC Press, 3rd electronic edition, **2000**

[Crevatin et. al. 99]

A. Crevatin, F. Mascarello, B. Leuthe, B. Minder, I. Kikic, *Kinetic Investigations of a Ketonization Reaction Using Reaction Calorimetry*, Industrial & Engineering Chemistry Research, Vol. 38, No. 12, pp. 4629-4633, **1999**

[de Juan et. al. 00]

A. de Juan, M. Maeder, M. Martínez, R. Tauler, *Combining hard- and soft-modeling to solve kinetic problems*, Chemometrics and Intelligent Laboratory Systems, Vol. 54, pp. 123-141, **2000**

[de Juan et. al. 01]

A. de Juan, M. Maeder, M. Martínez, R. Tauler, *Application of a novel resolution approach combining soft- and hard-modeling features to investigate temperature-dependent kinetic processes*, Analytica Chimica Acta, Vol. 442, pp. 337-350, **2001**

[Diewok et. al. 03]

J. Diewok, A. de Juan, M. Maeder, R. Tauler, B. Lendl, *Application of a Combination of Hard and Soft Modeling for Equilibrium Systems to the Quantitative Analysis of pH-Modulated Mixture Samples*, Analytical Chemistry, Vol. 75, pp. 641-647, **2003**

[Domenico et. al. 01]

G. D. Domenico, G. Maschio, D. G. Lister, A. Stassi, *Study of the hydrolysis of acetic anhydride by means of simple, low cost calorimeter*, Rivista dei Combustibili, Vol. 55, pp. 292-298, **2001**

[Dowd et. al. 91]

P. Dowd, S. W. Ham, S. J. Geib, *Mechanism of Action of Vitamin K*, Journal of the American Chemical Society, Vol. 113, pp. 7734-7743, **1991**

[Dyer et. al. 02]

U. C. Dyer, D. A. Henderson, M. B. Mitchel, P. D. Tiffin, *Scale-Up of a Vilsmeier Formylation Reaction: Use of HEL Auto-MATE and Simulation Techniques for Rapid and Safe Transfer to Pilot Plant from Laboratory*, Organic Process Research & Development, Vol. 6, pp. 311-316, **2002**

[Dyson et. al. 00]

R. M. Dyson, M. Hazenkamp, K. Kaufmann, M. Maeder, M. Studer, A. Zilian, *Modern tools for reaction monitoring: hard and soft modeling of 'non-ideal', on-line acquired spectra*, Journal of Chemometrics, Vol. 14, pp. 737-750, **2000**

[Erwin et. al. 01]

S. Erwin, K. Schulz, H. U. Moritz, C. Schwede, H. Kerber, *Increased reactor performance versus reactor safety aspects in acrylate copolymerization*, Chemical Engineering & Technology, Vol. 24, No. 3, pp. 305-311, **2001**

[Evans et. al. 80]

F. W. Evans, H. Frey, *Reaktionskinetik aus kalometrischen Untersuchungen, ein Beispiel der industriellen Verwendung*, Chimia, Vol. 34, No. 5, pp. 247-249, **1980**

- [Ferrotec]
Ferrotec, www.ferrotec.com
- [Fillion et. al. 02]
B. Fillion, B. I. Morsi, K. R. Heier, R. M. Machado, *Kinetics, Gas-Liquid Mass Transfer, and Modeling of the Soybean Oil Hydrogenation Process*, Industrial & Engineering Chemistry Research, Vol. 41, pp. 697-709, **2002**
- [Flowers et. al. 93]
R. A. Flowers, S. Naganathan, P. Dowd, E. M. Amett, S. W. Ham, *Thermochemical Investigation of the Oxygenation of Vitamin K*, Journal of the American Chemical Society, Vol. 115, pp. 9409-9416, **1993**
- [Franklin et. al. 02]
G.F. Franklin, J.D. Powell, A. Emami-Naeini, *Feedback Control of Dynamic Systems*, Prentice Hall, Reading, 4th edition, **2002**
- [Fringeli 03]
U.P. Fringeli, *Personal Communication*, **2003**
- [Fringeli et. al. 02]
U.P. Fringeli, D. Baurecht, M. Siam, G. Reiter, M. Schwarzott, T. Bürgi, P. Brüesch, *ATR Spectroscopy of Thin Films*, Handbook of Thin Film Materials, Volume 2: Characterization and Spectroscopy of Thin Films, H.S. Nalwa, pp. 191-229, Academic Press, San Diego, **2002**
- [Furusjö et. al. 00, a]
E. Furusjö, L.G. Danielsson, *Target testing procedure ofr determining chemical kinetics from spectroscopic data with absorption shifts and baseline drift*, Chemometrics and Intelligent Laboratory Systems, Vol. 50, No. 1, pp. 63-73, **2000**
- [Furusjö et. al. 00, b]
E. Furusjö, L. G. Danielsson, *Uncertainty in rate constants estimated from spectral data with baseline drift*, Journal of Chemometrics, Vol. 14, pp. 483-499, **2000**
- [Furusjö et. al. 03]
E. Furusjö, O. Svensson, L. G. ran Danielsson, *Estimation of kinetic parameters from non-isothermal batch experiments monitored by in situ vibrational spectroscopy*, Chemometrics and Intelligent Laboratory Systems, Vol. 66, pp. 1-14, **2003**
- [Furusjö et. al. 98, a]
E. Furusjö, L. G. Danielsson, E. Könberg, M. R. Jonas, B. Skagerberg, *Evaluation Techniques for Two-Way Data from in Situ Fourier Transform Mid-Infrared Reaction Monitoring in Aqueous Solution*, Analytical Chemistry, Vol. 70, pp. 1726-1734, **1998**
- [Furusjö et. al. 98, b]
E. Furusjö, L. G. Danielsson, *A method for the determination of reaction mechanisms and rate constants from two-way spectroscopic data*, Analytica Chimica Acta, Vol. 373, pp. 83-94, **1998**

References

- [Gampp et. al. 86]
H. Gampp, M. Maeder, C.J. Meyer, A. D. Zuberbühler, *Calculation of equilibrium constants from multiwavelength spectroscopic data - IV*, *Talanta*, Vol. 33, No. 12, pp. 943-951, **1986**
- [Gemperline 02]
P.J. Gemperline, *Characterizing Batch Reactions with in-situ Spectroscopic Measurements, Calorimetry, and Dynamic Modeling*, 3rd International Chemometrics Research Meeting, **2002**
- [Gemperline 84]
P.J. Gemperline, *A priori estimates of the elution profiles of the pure components in overlapped liquid chromatography peaks using target factor analysis*, *Chemical Information and Computer Science*, Vol. 24, No. 4, pp. 206-212, **1984**
- [Gemperline 86]
P. J. Gemperline, *Target transformation factor analysis with linear inequality constraints applied to spectroscopic-chromatographic data*, *Analytical Chemistry*, Vol. 58, No. 13, pp. 2656 - 2663, **1986**
- [Gemperline 98]
P.J. Gemperline, *A method for computing the range of feasible profiles estimated by constrained self-modeling curve resolution*, **1998**
- [Gemperline 99]
P.J. Gemperline, *Computation of the Range of Feasible Solutions in Self-Modeling Curve Resolution Algorithms*, *Analytical Chemistry*, Vol. 71, pp. 5398-5404, **1999**
- [Gemperline et. al. 99]
P.J. Gemperline, M. Zhu, E. Cash, D.S. Walker, *Chemometric characterization of batch reactions*, *ISA Transactions*, Vol. 38, pp. 211-216, **1999**
- [Goffe 94]
B. Goffe, *Simulated annealing (simann.f, Fortran routine)*, NetLib, <http://www.netlib.org/opt/simann.f>, **1994**
- [Göhring et. al. 96]
W. Göhring, J. Schildknecht, M. Federspiel, *Development of a Process to Prepare 2-cynopyrimidine on Commercial Scale*, *Chimia*, Vol. 50, pp. 538-543, **1996**
- [Guntern et. al. 98]
C. Guntern, A. H. Keller, K. Hungerbühler, *Economic Optimization of an Industrial Semibatch Reactor Applying Dynamic Programming*, *Industrial & Engineering Chemistry Research*, Vol. 37, No. 10, pp. 4017-4022, **1998**
- [Haario et. al. 98]
H. Haario, V. M. Taavitsainen, *Combining soft and hard modeling in chemical kinetic models*, *Chemometrics and Intelligent Laboratory Systems*, Vol. 44, pp. 77-98, **1998**
- [Hairfield et. al. 85]
E. M. Hairfield, E. W. Moonmaw, R. A. Tamburri, R. A. Vigil, *The Epoxidation of 2,5-Di-tert-butyl-1,4-benzoquinone*, *Journal of Chemical Education*, Vol. 62, No. 2, pp. 175-177, **1985**

- [Hamilton et. al. 90]
J. C. Hamilton, P. J. Gemperline, *Mixture Analysis using Factor Analysis. II: Self-Modeling Curve Resolution*, Journal of Chemometrics, Vol. 4, pp. 1-13, **1990**
- [Harre et. al. 01]
M. Harre, H. Neh, C. Schulz, U. Tilstam, T. Wessa, H. Weinmann, *Breaking the New Bottleneck: Our Way into Robotics*, Organic Process Research & Development, Vol. 5, pp. 335-339, **2001**
- [Harre et. al. 99]
M. Harre, U. Tilstam, H. Weinmann, *Breaking the New Bottleneck: automated Synthesis in Chemical Process Research and Development*, Organic Process Research & Development, Vol. 3, pp. 304-318, **1999**
- [Harrick 67]
N.J. Harrick, *Internal Reflection Spectroscopy*, Interscience Publishers, New York, **1967**
- [Heinzle et. al. 97]
E. Heinzle, K. Hungerbühler, *Integrated process development: The key to future production of chemicals*, Chimia, Vol. 51, pp. 176-183, **1997**
- [Heinzle et. al. 98]
E. Heinzle, D. Weirich, F. Brogli, V. H. Hoffmann, G. Koller, M. A. Verduyn, K. Hungerbühler, *Ecological and economic objective functions for screening in integrated development of fine chemical processes. 1. Flexible and expandable framework using indices*, Industrial & Engineering Chemistry Research, Vol. 37, pp. 3395-3407, **1998**
- [HEL]
HEL, www.helgroup.co.uk
- [Heldt et. al. 98]
K. Heldt, H. L. Anderson, B. Hinz, *Investigation of run-away reactions by precision calorimetry*, Thermochemica Acta, Vol. 310, pp. 179-184, **1998**
- [Hemminger et. al. 84]
W. Hemminger, G. Höhne, *Calorimetry: Fundamentals and Practice*, Verlag Chemie, Weinheim, **1984**
- [Hentschel 79]
B. Hentschel, *Ein automatisches, kontinuierlich registrierendes isothermes Kalorimeter - insbesondere zur Bestimmung der Polymerisationskinetik*, Chemie Ingenieur Technik, Vol. 51, No. 8, pp. 823, **1979**
- [Hinz et. al. 98]
B. Hinz, K. Heldt, H. L. Anderson, *Calorimetric analysis of the ethanolysis of 1,2-epoxybutane*, Thermochemica Acta, Vol. 310, No. 1-2, pp. 95-99, **1998**
- [House 72]
H.O. House, *Modern Synthetic Reactions*, W.A. Benjamin, Inc. Menlo Park, California, 2nd edition, pp. 306-310, **1972**
- [Huang et. al. 00, a]
B. J. Huang, C. J. Chin, C. L. Duang, *A design method of thermoelectric cooler*, International Journal of Refrigeration, Vol. 23, pp. 208-218, **2000**

References

- [Huang et. al. 00, b]
B. J. Huang, C. L. Duang, *System dynamic model and temperature control of a thermoelectric cooler*, International Journal of Refrigeration, Vol. 23, pp. 197-207, **2000**
- [Hugo 93]
P. Hugo, *Allgemeine Regel und Auswertverfahren für thermokinetische Messungen*, Chemie Ingenieur Technik, Vol. 65, No. 12, pp. 1497-1500, **1993**
- [Hungerbühler et. al. 98]
K. Hungerbühler, J. Ranke, T. Mettier, *Chemische Produkte und Prozesse: Grundkonzepte zum umweltorientierten Design*, Springer, Berlin, **1998**
- [Jansson et. al. 87]
L. Jansson, H. Nilsson, C. Silvegren, B. Törnell, *a study of rapid redox initiation by reaction calorimetry*, Thermochemica Acta, Vol. 118, pp. 97-105, **1987**
- [Jiang et. al. 02]
J.H. Jiang, Y. Ozaki, *Self-Modeling Curve Resolution (SMCR): Principles, Techniques, and applications*, Applied Spectroscopy Reviews, Vol. 37, No. 3, pp. 321-345, **2002**
- [Jödicke et. al. 99]
G. Jödicke, O. Zenklusen, A. Weidenhaupt, K. Hungerbühler, *Developing environmentally-sound processes in the chemical industry: a case study on pharmaceutical intermediates*, J. Cleaner Prod, Vol. 7, pp. 159-166, **1999**
- [Johnson et. al. 02]
G. L. Johnson, R. M. Machado, K. G. Freidl, M. L. Achenbach, P. J. Clark, S. K. Reidy, *Evaluation of Raman Spectroscopy for Determining cis and trans Isomers in Partially Hydrogenated Soybean Oil*, Organic Process Research & Development, Vol. 6, pp. 637-644, **2002**
- [Karlsen et. al. 84]
L. G. Karlsen, H. Soeberg, J. Villadsen, *Optimal data acquisition for heat flow calorimeter*, Thermochemica Acta, Vol. 72, pp. 83-94, **1984**
- [Karlsen et. al. 87, a]
L. G. Karlsen, J. Villadsen, *Isothermal Reaction Calorimeters - I a Literature Review*, Chemical Engineering Science, Vol. 42, No. 5, pp. 1153-1164, **1987**
- [Karlsen et. al. 87, b]
L. G. Karlsen, J. Villadsen, *Isothermal Reaction Calorimeters - II Data Treatment*, Chemical Engineering Science, Vol. 42, No. 5, pp. 1165-1173, **1987**
- [Keller 98]
A. H. Keller, *Stufengerechte Beurteilung und Optimierung der thermischen Prozesssicherheit mittels dynamischer Modellierung*, ETH Zürich, Diss. ETH Nr. 12607, **1998**
- [Kepco]
Kepco, www.kepco.com
- [Köhler et. al. 72]
W. Köhler, O. Riedel, H. Scherer, *Ein mit Heizpulsen gesteuertes isothermes Kalorimeter. Teil I: Aufbau und Messanordnung*, Chemie Ingenieur Technik, Vol. 44, No. 21, pp. 1216-1218, **1972**

- [Köhler et. al. 73]
W. Köhler, O. Riedel, H. Scherer, *Ein mit Heizpulsen gesteuertes isothermes Kalorimeter. Teil II: Anwendungsbeispiele für kalorische und kalorisch-kinetische Messungen*, Chemie Ingenieur Technik, Vol. 45, No. 22, pp. 1289-1294, **1973**
- [Koller et. al. 98]
G. Koller, D. Weirich, F. Brogli, E. Heinzle, V. H. Hoffmann, M. A. Verduyn, K. Hungerbühler, *Ecological and economic objective functions for screening in integrated development of fine chemical processes. 2. Stream allocation and case studies*, Industrial & Engineering Chemistry Research, Vol. 37, pp. 3408-3413, **1998**
- [LabVIEW]
LabVIEW, National Instruments, www.labview.com, Version 6.0.1
- [Laird 01]
T. Laird, *Special Feature Section Laboratory Automation in Process R&D*, Organic Process Research & Development, Vol. 5, pp. 272, **2001**
- [Landau 96]
R. N. Landau, *Expanding the role of reaction calorimetry*, Thermochemica Acta, Vol. 289, No. 2, pp. 101-126, **1996**
- [Landau et. al. 94]
R. N. Landau, D. G. Blackmond, H. H. Tung, *Calorimetric investigation of an exothermic reaction: Kinetic and heat flow modeling*, Industrial & Engineering Chemistry Research, Vol. 33, pp. 814-820, **1994**
- [Landau et. al. 95, a]
R. N. Landau, R. F. McKenzie, A. L. Forman, R. R. Dauer, M. Futran, A. D. Epstein, *In-situ Fourier transform infrared and calorimetric studies of the preparation of a pharmaceutical intermediate*, Process Control and Quality, Vol. 7, pp. 133-142, **1995**
- [Landau et. al. 95, b]
R. M. Landau, U. Singh, F. Gortsema, Y. Sun, S. C. Gomolka, T. Lam, M. Futran, D.G. Blackmond, *A reaction calorimetric investigation of the hydrogenation of a substituted pyrazine*, Journal of Catalysis, Vol. 157, pp. 201-208, **1995**
- [Landolt-Börnstein, a]
Landolt-Börnstein, *Numerical Data and Functional Relationships in Science and Technology*, Vol. 1, No. Part b, pp. 245, Springer, Berlin, New Series, Group IV
- [Landolt-Börnstein, b]
Landolt-Börnstein, *Numerical Data and Functional Relationships in Science and Technology*, Vol. 4, No. Part 4, pp. 850, Springer, Berlin, 6th edition
- [LeBlond et. al. 96]
C. LeBlond, J. Wang, R. D. Larsen, C. J. Orella, A. L. Forman, R.N. Landau, J. Laquidara, J.R. Sowa, D.G. Blackmond, Q.K. Sun, *Reaction calorimetry as an in-situ kinetic tool for characterizing complex reactions*, Thermochemica Acta, Vol. 289, No. 2, pp. 189-207, **1996**

References

- [LeBlond et. al. 98]
C. LeBlond, J. Wang, R. Larsen, C. Orella, Y.K. Sun, *A combined approach to characterization of catalytic reactions using in situ kinetic probes*, Topics in Catalysis, Vol. 5, pp. 149-158., **1998**
- [Lehtonen et. al. 97]
J. Lehtonen, T. Salmi, A. Vuori, H. Haario, *Optimization of the Reaction Conditions for Complex Kinetics in a Semibatch Reactor*, Industrial & Engineering Chemistry Research, Vol. 36, pp. 5196-5206, **1997**
- [Litz 83]
W. Litz, *The Thermokinetic Reactor TKR and its possible applications in chemical research and engineering*, Journal of Thermal Analysis, Vol. 27, pp. 215-228, **1983**
- [Litz 87]
W. Litz, *Development and Use of a constant flow stirred Thermokinetic Reactor*, Journal of Thermal Analysis, Vol. 32, pp. 1991-1999, **1987**
- [Lundstrom et. al. 98]
L. Lundstrom, T. Salmi, J. Lehtonen, L.P. Lindfors, S. Toppinen, J. Aittamaa, *Modeling of speciality chemicals production in liquid-liquid reactors--A case study: synthesis of diols*, Chemical Engineering Science, Vol. 54, No. 1, pp. 1-18, **1998**
- [Lunghi et. al. 02]
A. Lunghi, M. A. Alos, L. Gigante, J. Feixas, E. Sironi, J. A. Feliu, P. Cardillo, *Identification of the Decomposition Products in an Industrial Nitration Process under Thermal Runaway Conditions*, Organic Process Research & Development, Vol. 6, pp. 926-932, **2002**
- [Machado et. al. 96]
R. M. Machado, J. W. Mitchell, J. P. Bullock, B. E. Farrell, *Kinetics of the reaction of 4,4'-methylenedianiline with propylene oxide in ethylene glycol*, Thermochemica Acta, Vol. 289, No. 2, pp. 177-187, **1996**
- [Maeder 87]
M. Maeder, *Evolving Factor Analysis for the Resolution of Overlapping Chromatographic Peaks*, Analytical Chemistry, Vol. 59, pp. 527-530, **1987**
- [Maeder et. al. 86]
M. Maeder, A. Zuberbühler, *The resolution of overlapping chromatographic peaks by evolving factor analysis*, Analytica Chimica Acta, Vol. 181, pp. 287-291, **1986**
- [Maeder et. al. 90]
M. Maeder, A.D. Zuberbühler, *Nonlinear Least-Squares Fitting of Multivariate Absorption Data*, Analytical Chemistry, Vol. 62, pp. 2220-2224, **1990**
- [Maeder et. al. 97]
M. Maeder, K.J. Molloy, M.M. Schumacher, *Analysis of non-isothermal kinetic measurements*, Analytica Chimica Acta, Vol. 337, pp. 73-81, **1997**
- [Mak et. al. 97]
C. P. Mak, H. Mühle, R. Achini, *Integrated Solutions to Environmental Protection in Process R&D*, Chimia, Vol. 51, pp. 184-188, **1997**

- [Malinowski 02]
E.R. Malinowski, *Factor Analysis in Chemistry*, Wiley-Interscience, New York, 3rd edition, **2002**
- [Marison et. al. 98]
I. Marison, M. Linder, B. Schenker, *High-sensitive heat-flow calorimetry*, *Thermochimica Acta*, Vol. 310, No. 1-2, pp. 43-46, **1998**
- [Marlow]
Marlow Industries, www.marlow.com
- [Martin 75]
H. Martin, *Wärmeflusskalorimetrie unter präparativen Bedingungen und ihre Anwendung zur Verfolgung der Isomerisierungskinetik von Trimethylphosphit*, University of Basel, Basel, PhD Thesis, **1975**
- [Mason et. al. 01]
C. Mason, M. Maeder, A. Whitson, *Resolving Factor Analysis*, *Analytical Chemistry*, Vol. 73, pp. 1587-1594, **2001**
- [Matlab Ident]
Matlab System Identification Toolbox, Mathworks, www.mathworks.com/products/sysid, Version 5.0 (R12)
- [Matlab Optim]
Matlab Optimization Toolbox, Mathworks, www.mathworks.com/products/optimization, Version 2.1 (R12)
- [Matlab Signal]
Matlab Signal Processing Toolbox, Mathworks, www.mathworks.com/products/signal, Version 5.0 (R12)
- [Mayes et. al. 92]
D. M. Mayes, J. J. Kelly, J. B. Callis, *Non-invasive monitoring of a two step sequential chemical reaction with shortwave near-infrared spectroscopy*, *Near Infra-Red Spectroscopy, Bridging the Gap between Data Analysis and NIR Applications*, K.I. Hildrum, T. Isaksson, T. Naes, and A. Tandberg, pp. 377-387, **1992**
- [Meeks 68]
M.R. Meeks, *An Analog Computer Study of Polymerization Rates in Vinyl Chloride Suspensions*, *Polymer Engineering And Science*, Vol. 9, No. 2, pp. 141-151, **1968**
- [Melcor]
Melcor, www.melcor.com
- [Mettler Toledo]
Mettler Toledo, www.mt.com
- [Miller 00]
C.E. Miller, *Chemometrics for on-line spectroscopy applications - theory and practice*, *Journal of Chemometrics*, Vol. 14, pp. 513-528, **2000**
- [Mirabella 93]
F.M. Mirabella, *Internal Reflection Spectroscopy*, Marcel Dekker, Inc., New York, **1993**

References

[Moore 67]

H.W. Moore, *Mono- and Diepoxy-1,4-benzoquinones*, Journal of Organic Chemistry, Vol. 32, pp. 1996-1999, **1967**

[Nagy et. al. 96]

M. J. Nagy, R. J. Buist, *Transient Analysis of thermal junctions within a thermoelectric cooling assembly*, 15th International Conference on Thermoelectrics, TE Technology, Inc., Michigan, USA, www.tetech.com, **1996**

[National Instruments]

National-Instruments, www.ni.com

[Nilsson et. al. 82]

H. Nilsson, C. Solvegren, B. Törnell, *A Calorimetric Reactor System for Kinetic Studies of Heterogeneous Polymerizations*, Chemica Scripta, Vol. 19, pp. 164-171, **1982**

[Nilsson et. al. 83]

H. Nilsson, C. Silvegren, B. Törnell, *A Calorimetric Investigation of Suspension and Emulsion Polymerization of Vinyl Chloride*, Die Angewandte Makromolekulare Chemie, Vol. 112, pp. 125-142, **1983**

[NIST]

NIST Chemistry Webbook, *Standard Reference Database Number 69*, National Institute of Standards and Technology, online, **2003**

[Nomen et. al. 01]

R. Nomen, J. Sempere, K. Avilés, *Detection and characterization of water alcohol hydrates by on-line FTIR using multivariate data analysis*, Chemical Engineering Science, Vol. 56, pp. 6577-6588, **2001**

[Parker et. al. 90]

R. L. Parker, P. B. Stark, *Bounded Variable Least Squares (bvls.f, Fortran routine)*, StatLib, <http://lib.stat.cmu.edu/general/bvls>, Version 3/19/90, **1990**

[Pastré 00]

J. Pastré, *Beitrag zum erweiterten Einsatz der Kalorimetrie in frühen Phasen der chemischen Prozessentwicklung*, ETH Zürich, Diss. ETH Nr. 13840, **2000**

[Pastré et. al. 01]

J. Pastré, A. Zogg, U. Fischer, K. Hungerbühler, *Determination of Thermodynamical and Kinetic Parameters using a small Power Compensation Calorimeter with and integrated FTIR Probe*, Organic Process Research & Development, Vol. 5, No. 2, pp. 158-166, **2001**

[Pauer et. al. 99]

W. Pauer, J.P. Tchoukou, H.U. Moritz, D. Brown, *Ein neues isothermes Wärmebilanzkalorimeter*, Workshop Reaktionskalorimetrie, DECHEMA e. V., Frankfurt, **1999**

[Pinto Machado e Silva et. al. 02]

C.F. Pinto Machado e Silva, J.F. Cajaiba da Silva, *Evaluation of Kinetic Parameters from the Synthesis of Triaryl Phosphates Using Reaction Calorimetry*, Organic Process Research & Development, Vol. 6, pp. 829-832, **2002**

- [Pollard 01]
M. Pollard, *Process Development Automation: An Evolutionary Approach*, Organic Process Research & Development, Vol. 5, pp. 273-282, **2001**
- [RC1 Handbook]
RC1 Handbook, Mettler-Toledo GmbH, Switzerland, edition 01/08, **2001**
- [ReactIR]
ReactIR, ASI Applied Systems, <http://www.asirxn.com/>
- [Regenass 76]
W. Regenass, *Thermoanalytische Methoden in der Chemischen Verfahrensentwicklung*, 2. Symposium der Gesellschaft für Thermische Analyse, **1976**
- [Regenass 83]
W. Regenass, *Thermische Methoden zur Bestimmung der Makrokinetik*, Chimia, Vol. 37, No. 11, pp. 430-437, **1983**
- [Regenass 97]
W. Regenass, *The Development of Stirred-Tank Heat Flow Calorimetry as a Tool for Process Optimization and Process Safety*, Chimia, Vol. 51, No. 5, pp. 189-200, **1997**
- [Riesen et. al. 85]
R. Riesen, B. Grob, *Reaktionskalorimetrie in der chemischen Prozessentwicklung*, Swiss Chem, Vol. 7, No. 5a, pp. 39-43, **1985**
- [Rivera et. al. 01]
D. R. Rivera, J. M. Harris, *In Situ ATR-FT-IR Kinetic Studies of Molecular Transport and Surface Binding in Thin Sol-Gel Films: Reactions of Chlorosilane Reagents in Porous Silica Materials*, Analytical Chemistry, Vol. 73, pp. 411-423, **2001**
- [Römp]
Römp Lexikon, Georg Thieme, Stuttgart, online, **2003**
- [Sans et. al. 97]
D. Sans, R. Nomen, J. Sempere, *Interactive self-modeling of chemical reaction systems using multivariate data analysis*, Computers & Chemical Engineering, Vol. 21, pp. S631-S636, **1997**
- [Saurina et. al. 98]
J. Saurina, S. Hernandez-Cassou, R. Tauler, A. Izquierdo-Ridorsa, *Multivariate Resolution of Rank-Deficient Spectrophotometric Data from First-Order Kinetic Decomposition Reactions*, Journal of Chemometrics, Vol. 12, pp. 183-203, **1998**
- [Sbirrazzuoli et. al. 00]
N. Sbirrazzuoli, L. Vincent, S. Vyazovkin, *Comparison of several computational procedures for evaluating the kinetics of thermally simulated condensed phase reactions*, Chemometrics and Intelligent Laboratory Systems, Vol. 54, pp. 53-60, **2000**
- [Schildknecht 77]
J. Schildknecht, *Development and application of a mini-pilot reaction calorimeter*, 2nd Int. Symp. Loss Prevention and Safety Promotion in the Process Industries, Vol. III, pp. 139-143, **1977**

References

[Schildknecht 81]

J. Schildknecht, *Reaction calorimeter for applications in chemical process industries: Performance and calibration*, *Thermochimica Acta*, Vol. 49, pp. 87-100, **1981**

[Schlegel et. al. 97]

M. Schlegel, A. Löwe, *A reaction calorimeter with compensation heater and differential cooling*, *Chemical Engineering and Processing*, Vol. 37, pp. 61-67, **1997**

[Sempere et. al. 98]

J. Sempere, R. Nomen, J. L. Rodriguez, M. Papadaki, *Modeling of the reaction of N-oxidation of 2 methylpyridine using hydrogen peroxide and a complex metal catalyst*, *Chemical Engineering and Processing*, Vol. 37, pp. 33-46, **1998**

[Setaram]

Setaram, www.setaram.com

[Simms et. al. 00]

C. Simms, J. Singh, *Rapid Process Development and Scale-Up Using A Multiple Reactor System*, *Organic Process Research & Development*, Vol. 4, pp. 554-562, **2000**

[Singh 97]

J. Singh, *Reaction Calorimetry for Process Development: Recent Advances*, *Process Safety Progress*, Vol. 16, No. 1, pp. 43-49, **1997**

[Smilde et. al. 01]

A.K. Smilde, H. C. J. Hoefsloot, H. A. L. Kiers, S. Bijlsma, H. M. Boelens, *Sufficient conditions for unique solutions within a certain class of curve resolution models*, *Journal of Chemometrics*, Vol. 15, pp. 405-411, **2001**

[Snee et. al. 93]

T. J. Snee, C. Bassani, J. A. M. Ligthart, *Determination of the thermokinetic parameters of an exothermic reaction using isothermal, adiabatic and temperature-programmed calorimetry in conjunction with spectrophotometry*, *Journal of Loss Prevention in the Process Industries*, Vol. 5, No. 2, pp. 87-93, **1993**

[Stappers et. al. 02]

F. Stappers, R. Broeckx, S. Leurs, L. V. Den Bergh, J. Agten, A. Lambrechts, D. Van den Heuvel, D. De Smaele, *Development of a Safe and Scalable Amine-to-Nitrone Oxidation: A Key Step in the Synthesis of R107500*, *Organic Process Research & Development*, Vol. 6, pp. 911-914, **2002**

[Stockhausen et. al. 92]

T. Stockhausen, J. Prüss, H.-U. Moritz, *An Isoperibol Calorimeter - A Simple Apparatus for Monitoring Polymerization Reactions*, *Dechema-Monographien*, Vol. 127, pp. 341-349, **1992**

[Stoessel 97]

F. Stoessel, *Applications of reaction calorimetry in chemical engineering*, *Journal of Thermal Analysis*, Vol. 49, pp. 1677-1688, **1997**

[Svensson et. al. 99]

O. Svensson, M. Josefson, F. W. Langkilde, *Reaction monitoring using Raman*

- spectroscopy and chemometrics*, Chemometrics and Intelligent Laboratory Systems, Vol. 49, pp. 49-66, **1999**
- [Systag]
Systag, www.systag.ch
- [Taavitsainen et. al. 01]
V. M. Taavitsainen, H. Haario, *Rapid estimation of chemical kinetics by implicit calibration. I*, Journal of Chemometrics, Vol. 15, pp. 215-239, **2001**
- [Taavitsainen et. al. 03]
V. M. Taavitsainen, H. Haario, M. Laine, *Rapid estimation of chemical kinetics by implicit calibration. II*, Journal of Chemometrics, Vol. 17, pp. 140-150, **2003**
- [Tam 91]
H. W. Tam, *Livermore solver for ordinary differential equations (Isoda.c, C routine)*, CCL.NET, <http://ccl.net/cca/software/SOURCES/C/kinetics2/Isoda-dir/index.shtml>, Translation of Isoda.f, **1991**
- [Tam et. al. 94]
K. Y. Tam, F. T. Chau, *Multivariate study of kinetic data for a two-step consecutive reaction using target factor analysis*, Chemometrics and Intelligent Laboratory Systems, Vol. 25, pp. 25-42, **1994**
- [Tauler 01]
R. Tauler, *Calculation of maximum and minimum band boundaries of feasible solutions for species profiles obtained by multivariate curve resolution*, Journal of Chemometrics, Vol. 15, pp. 627-646, **2001**
- [Tauler et. al. 93, a]
R. Tauler, A. Izquierdo-Ridorsa, E. Casassas, *Simultaneous analysis of several spectroscopic titrations with self-modeling curve resolution*, Chemometrics and Intelligent Laboratory Systems, Vol. 18, pp. 293-300, **1993**
- [Tauler et. al. 93, b]
R. Tauler, B. Kowalski, S. Fleming, *Multivariate Curve Resolution Applied to Spectral Data from Multiple Runs of an industrial process*, Analytical Chemistry, Vol. 85, pp. 2040-2047, **1993**
- [Tauler et. al. 94]
R. Tauler, A. K. Smilde, J.M. Henshaw, L. W. Burgess, B. R. Kowalski, *Multicomponent Determination of Chlorinated Hydrocarbons Using a Reaction-Based Chemical Sensor. 2. Chemical Speciation Using Multivariate Curve Resolution*, Analytical Chemistry, Vol. 66, pp. 3337-3344, **1994**
- [Tauler et. al. 95]
R. Tauler, A. Smilde, B. Kowalski, *Selectivity, Local Rank, Three-Way Data analysis and Ambiguity in Multivariate Curve Resolution*, Journal of Chemometrics, Vol. 9, pp. 31-58, **1995**
- [Tauler et. al. 99]
R. Tauler, R. Gargallo, M. Vives, A. Izquierdo-Ridorsa, *Resolution of temperature dependent conformational multiequilibria processes*, Chemometrics and Intelligent Laboratory Systems, Vol. 46, pp. 275-295, **1999**
- [Technova]
Technova, www.technova.ch

References

[Thermocoax]

Thermocoax, www.thermocoax.com

[Tietze et. al. 96]

A. Tietze, A. Pross, K.H. Reichert, *Temperaturschwingungskalorimetrie in Rührkesselreaktoren*, Chemie Ingenieur Technik, Vol. 68, No. 1+2, pp. 97-100, **1996**

[Ubrich et. al. 99]

O. Ubrich, B. Srinivasan, P. Lerena, D. Bonvin, F. Stoessel, *Optimal feed profile for a second order reaction in a semi-batch reactor under safety constraints. Experimental Study*, Journal of Loss Prevention in the Process Industries, Vol. 12, No. 6, pp. 485-493, **1999**

[Valle et. al. 99]

S. Valle, W. Li, S.J. Qin, *Selection of the Number of Principal Components: The Variance of Reconstruction Error Criterion with a Comparison to Other Methods*, Industrial & Engineering Chemistry Research, Vol. 38, pp. 4389-4401, **1999**

[Van Loo et. al. 02]

M. E. Van Loo, P. E. Lengowski, *Automated Workstations for Parallel Synthesis*, Organic Process Research & Development, Vol. 6, pp. 833-840, **2002**

[Vandeginste et. al. 85]

B. G. M. Vandeginste, W. Derks, D. Kateman, *Multicomponent self-modeling curve resolution in high-performance liquid chromatography by iterative target transformation analysis*, Analytica Chimica Acta, Vol. 173, pp. 253-264, **1985**

[VDI Wärmeatlas]

VDI Wärmeatlas, Springer, Düsseldorf, 8th edition, **1997**

[Velázquez-Campoy et. al. 99]

A. Velázquez-Campoy, O. López-Mayorga, M.A. Cabrerizo-Vilchez, *Determination of the rigorous transfer function of an isothermal titration microcalorimeter with peltier compensation*, Journal of Thermal Analysis and Calorimetry, Vol. 57, pp. 343-359, **1999**

[Vincent et. al. 02]

L. Vincent, N. Sbirrazzuoli, S. Vyazovkin, *Evaluation of the Dynamic Response of a New Heat Flux*

Calorimeter for Kinetic Purposes, Industrial & Engineering Chemistry Research, Vol. 41, pp. 6650-6655, **2002**

[Walisch et. al. 65]

W. Walisch, F. Becker, *Isotherme Kalorimetrie mit automatisch gesteuerter Peltier-Kühlung und fortlaufender Integration der Kompensationsleistung. II Eine Messanordnung für thermokinetische Untersuchungen*, Zeitschrift für Physikalische Chemie Neue Folge, Vol. 46, pp. 268-278, **1965**

[Willms et. al. 98]

T. Willms, H.L. Anderson, K. Heldt, B. Hinz, *Calorimetric investigation of complex reaction courses in organic chemistry*, Thermochimica Acta, Vol. 310, pp. 141-145, **1998**

- [Zaldívar et. al. 96]
J. M. Zaldívar, H. Hernández, C. Barcons, *Development of a mathematical model and a simulator for the analysis and optimization of batch reactors: Experimental model characterization using a reaction calorimeter*, *Thermochimica Acta*, Vol. 289, No. 2, pp. 267-302, **1996**
- [Zeton Altamira]
Zeton-Altamira, www.zetonaltamira.com
- [Zhu et. al. 02]
Z.L. Zhu, W.-Z. Cheng, Y. Zhao, *Iterative target transformation factor analysis for the resolution of kinetic spectral data with an unknown kinetic model*, *Chemometrics and Intelligent Laboratory Systems*, Vol. 64, pp. 157-167, **2002**
- [Zilian 01]
A. Zilian, *In situ Analytics for Hydrogenation Reactions*, *Chimia*, Vol. 55, pp. 704-707, **2001**
- [Zogg 83]
M. Zogg, *Wärme- und Stofftransportprozesse*, Salle + Sauerländer, Frankfurt am Main, **1983**
- [Zogg 93]
M. Zogg, *Einführung in die Mechanische Verfahrenstechnik*, B.G. Teubner, Stuttgart, 3rd edition, **1993**
- [Zogg 99]
A. Zogg, *Bestimmung thermo-kinetischer Parameter mit Hilfe eines kleinvolumigen Reaktionskalorimeters: Modellentwicklung und Anwendung auf eine ausgewählte Reaktion*, ETH Zurich, Zürich, **1999**
- [Zogg et. al. 00]
A. Zogg, M. Wohlwend, U. Fischer, K. Hungerbühler, *Patent: "Kalorimeter"*, Application No. 00810797.1, No. EP1184649, WO0221089, **2000**
- [Zogg et. al. 02]
A. Zogg, U. Fischer, K. Hungerbühler, *A new Small Scale Reaction Calorimeter combined with a new Evaluation Principle for Kinetics Screening*, 2002 AIChE Annual Meeting, Indianapolis, Nr. 285e, **2002**
- [Zogg et. al. 03]
A. Zogg, U. Fischer, K. Hungerbühler, *A New Small-Scale Reaction Calorimeter That Combines the Principles of Power Compensation and Heat Balance*, *Industrial & Engineering Chemistry Research*, Vol. 42, pp. 767-776, **2003**
- [Zogg et. al. 03, submitted]
A. Zogg, U. Fischer, K. Hungerbühler, *Application of a Combined Evaluation Algorithm to identify Kinetic and Thermodynamic Parameters based on Calorimetric and Infrared Reaction Data*, *Analytical Chemistry*, submitted for publication, **2003**
- [Zürcher 01]
I. Zürcher, *Bestimmung Thermo-Kinetischer Parameter mit Hilfe eines neuen Kleinvolumigen Kalorimeters*, ETH Zurich, Zürich, **2001**

References

APPENDIX

A REACTION CALORIMETRY

A.1 Combinations and further developments of the three basic reaction calorimetric principles (isothermal)

As explained in Chapter 2.1 the three basic reaction calorimetric principles (Heat-Flow, Heat-Balance and Power-Compensation) all have their advantages and disadvantages. It is therefore clear, that many attempts were made in order to modify or combine the techniques to get improved calorimetric devices.

A.1.1 Combination of the Heat-Flow and Heat-Balance principle

Most of the commercial available Heat-Balance calorimeters can be used as Heat-Flow calorimeters as well [Systag], [Zeton Altamira], and [Baranek et. al. 99] because only little changes on the setup have to be made.

A.1.2 Peltier calorimeters

Becker ([Becker et. al. 65] and [Becker 68]) designed a first calorimeter using Peltier elements. A similar calorimeter was presented by [Nilsson et. al. 83], [Nilsson et. al. 82] and [Jansson et. al. 87]. Their setup can be compared to the one shown in Figure 2-1 but the whole reactor is immersed in a thermostat bath that replaces the reactor jacket. The reactor bottom consists of Peltier elements and the rest of the reactor wall is thermally insulated. The temperature of the reactor content (T_r) is controlled by varying the power the Peltier elements. In contrast to the Power-Compensation principle Peltier elements can be used for cooling and heating. The heat flow from the reactor content through the Peltier element into the cooling liquid (q_{Flow}) is calculated based on the required electrical power and the measured temperature gradient over the Peltier elements. The temperature of the cooling liquid (T_j) is controlled at a constant temperature by an external cryostat. Therefore the main heat flow out of the reactor flows through the Peltier elements. It is calculated by the steady-state heat-flow equations for the Peltier elements [Karlsen et. al. 87, a]. The device specific Peltier parameters in the heat-flow model had to be calibrated in advance. As the Peltier elements are the main dynamic element in the system, Nilsson introduced heat accumulation terms in the calculation of the calorimetric signal. The design of Nilsson was the basis for the commercial available CPA200 from [Chemisens]. In the CPA200 the heat flow through the reactor bottom is no more calculated by modeling the Peltier elements but a heat-flow sensor is introduced between the reactor bottom and the Peltier elements. The heat-flow sensor allows the measurement of a small temperature gradient over a well defined distance. Thus no more Peltier parameters have to be calibrated. The calorimetric signal measured by the CPA200 is independent of the heat-transfer changes on the reactor bottom as it works similar to a Heat-Balance calorimeter.

[Christensen et. al. 73] developed a Peltier calorimeter similar to the design of Becker or Nilsson. However the Peltier elements are operated at a constant cooling rate. The control of the reaction temperature is carried out with an additional heater element between the Peltier elements and the reactor bottom. Therefore the heat flow through the Peltier elements does not have to be described and thus no Peltier parameters have to be calibrated. The heat-flow change through the reactor bottom is directly measured by the power consumption of the heater element. The calorimetric signal measured by such a calorimeter is independent of the heat-transfer changes on the reactor bottom as it works similar to a Heat-Balance calorimeter.

A.1.3 Improvements of the Power-Compensation technique

Another group of calorimeters aims at combining the Power-Compensation technique with an additional outer heat-flow balance in order to correct the measured reaction power signal for changes of the heat transfer through the reactor wall. [Litz 83] reported a Power-Compensation calorimeter using an additional intermediate jacket that allows an online measurement of the heat flow through the reactor wall (detailed discussion in 3.3). [Schlegel et. al. 97] combined the Power-Compensation technique with a Heat-Balance calorimeter in order to improve the dynamics of the temperature control system and to measure the changing heat-transfer coefficient. In the Similar calorimeter from HEL [Singh 97] the Power-Compensation technique can be implemented optionally and is supported with a “pseudo” Heat-Balance measurement, the CMC approach: The changing baseline of the power-compensation signal is corrected proportional to the measured temperature difference between the inlet and the outlet temperature of the cooling liquid.

Schildknecht ([Schildknecht 81] and [Schildknecht 77]) designed a Power-Compensation calorimeter that uses the reactor wall as heater surface and therefore minimizes eventual hot spots on the heater surface.

A.1.4 Improvements of the Heat-Flow principle

[Tietze et. al. 96] addressed the problem of the changing heat-transfer coefficient in a Heat-Flow calorimeter and proposed an online measurement based on an oscillation of the temperature of the cooling liquid. [BenAmor et. al. 02] presented an algorithm for the online detection of the heat-transfer coefficient based on mathematical modeling.

A.1.5 Other Calorimeters

Moritz and coworkers ([Stockhausen et. al. 92] and [Erwin et. al. 01]) presented an isoperibol reaction calorimeter that is inserted into a compensation heater controlled Heat-Flow device. A changing heat-transfer coefficient during a reaction measurement does not influence the calculated reaction power.

A completely new design for an isoperibol reaction calorimeter was presented by [Setaram]. According to the differential measurement principle common for thermo

analytical calorimeters such as DSC or DTA, two reaction vessels are run in parallel. One is filled with the reaction components and the other one e.g. with the solvent. The basic signal used for the evaluation is the temperature difference of the two reactor contents [André et. al. 02].

It can be concluded that many successful efforts have already been taken to handle the problem of changing heat-transfer through the reactor wall during a reaction measurement. However the dynamics of the different calorimetric systems are hardly addressed.

B INFRARED SPECTROSCOPY

B.1 Applicability of Lambert Beer's Law in ATR spectroscopy

As ATR measurements are not transmission experiments the applicability of the Lambert Beer's law (Equation (2-20)) has to be verified. In this Chapter the theoretical basis required to test the applicability of the Lambert Beer's law will be given.

Figure B-1 shows the general behavior of an incident light beam that passes between two optically different media. In an ATR experiment, medium one would be e.g. diamond and medium two the reaction mixture to be investigated. According to Figure B-1 three different cases can occur: 1) Refraction ($\theta_2 > 90^\circ$) 2) Total reflection ($\theta_2 = 90^\circ$) 3) Internal reflection ($\theta_2 < 90^\circ$).

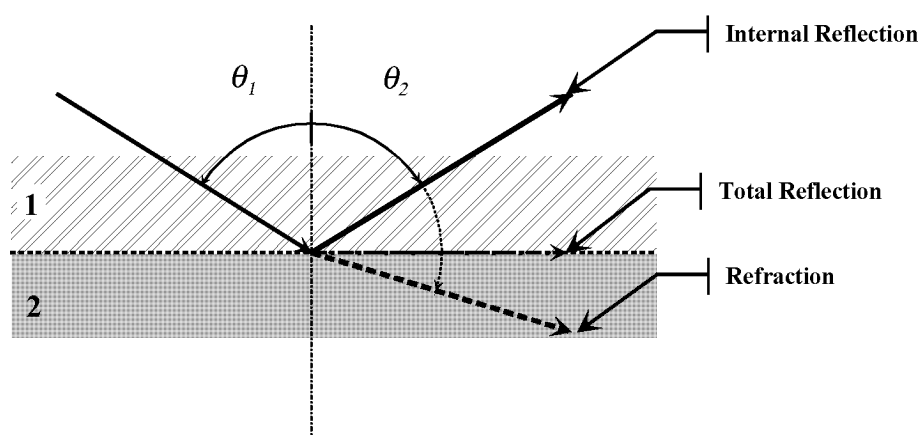


Figure B-1: Refraction and Reflection of the incident light beam between Medium 1 (e.g. Diamond) and 2 (e.g. reaction mixture)

According to the general law of refraction the situation for non-absorbing media one and two can be described as follows:

$$\frac{v_1}{v_2} = \frac{\sin \theta_1}{\sin \theta_2} = \frac{n_2}{n_1} = n_{21} \quad (\text{B-1})$$

Where v_1 and v_2 are the light velocities in media one and two and n_1 and n_2 the corresponding indices of refraction. If light absorption takes place, the refractive index of the absorbing media changes but Equation (B-1) is still valid. The refractive index of an absorbing medium is a complex number and can be expressed as follows [Fringeli et. al. 02]:

$$\hat{n} = n + i \cdot k \quad (\text{B-2})$$

Where n is the real part, normally referred to as refractive index and k the extinction coefficient. The extinction coefficient k is related to the absorption coefficient α according to the following equation

$$k = \frac{4\pi\alpha}{\lambda} \quad (\text{B-3})$$

n and k are related to each other by the Kramers – Kronig relation [Fringeli et. al. 02]. As a consequence of absorption one obtains anomalous dispersion of the refractive index at the positions of absorption bands (see Fig. 3 in [Fringeli et. al. 02], H₂O).

For a reaction spectrum it is important to note that α will vary as a function of time and consequently the complex refractive index will change as well.

In an ATR experiment the incident angle of the light beam (θ_1) will be chosen that total internal reflection (see Figure B-1) takes place. As the electromagnetic waves from the incident light beam are reflected at the interface of the two media they “travel” for a short distance through the optically rarer medium two. This is indicated in Figure B-2. During this short path length absorption could take place in medium two.

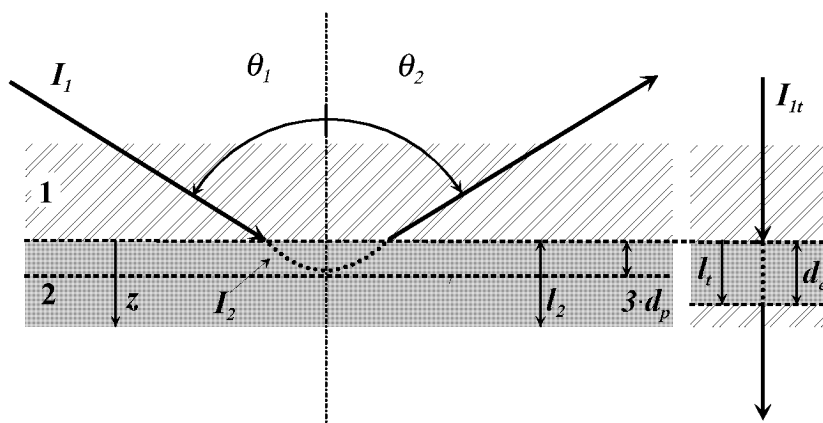


Figure B-2: Internal reflection in an ATR experiment. The penetration depth of the evanescent electric field in medium 2 is indicated ATR approximately to be $3 \cdot d_p$ (Equation (B-4)). The right side shows the hypothetical sample thickness d_e (Equation (B-6)) for a transmission experiment that results in the same absorption as the ATR experiment on the left side.

The most simple and straightforward treatment of total internal reflection is for an infinite plane wave at an interface between semi-infinite non-absorbing media [Mirabella 93]. The electric field in medium two caused by the incident light is described by an evanescent field. Its amplitude decays exponentially in the z – direction (see Figure B-2). The decrease of the electric field amplitude at the surface of the rarer medium two E_{20} to some value E_2 , at a distance z from the surface, can be expressed as follows:

$$E_2 = E_{20} \cdot e^{-\frac{2\pi}{\lambda_1} \sqrt{\sin^2 \theta_1 - n_{21}^2} \cdot z} = E_{20} \cdot e^{-\frac{z}{d_p}} \quad d_p = \frac{\lambda_1}{2\pi \sqrt{\sin^2 \theta_1 - n_{21}^2}} \quad (\text{B-4})$$

Where λ_1 is the wavelength of the electromagnetic field in medium one, n_{21} the relation of the refractive indices (B-1) and d_p the penetration depth of the evanescent field in medium two. As the decay is exponential the electrical field amplitude inside medium two is about zero at three times the distance of d_p (see Figure B-2).

Equation (B-3) is valid for non-absorbing species. However, the assumption that medium two is non-absorbing is unrealistic, since absorption of energy must occur if a measurement is to be made. Therefore the refractive index ratio n_{21} would have to be modified according to Equation (B-2).

It is important to keep in mind that for a reaction spectrum with time varying absorption coefficients α , also the refractive indices of medium two will vary and consequently the penetration depth d_p can change during an experiment.

Nevertheless Equation (B-3) allows an estimation of the penetration depth of the incident light beam into the reaction mixture during an ATR measurement. For the optical setup used in this work (see C.8.5) the parameters are as follows:

- The reaction mixture is assumed to be pure water.
- The calculation is carried out at 1640cm^{-1} ($\delta(\text{H}_2\text{O})$).
- The refractive index for the absorbing medium two is taken from Fig. 3a [Fringeli et. al. 02], $n_2 = 1.3$.
- $\theta_1 = 45^\circ$
- Refractive index of medium one (diamond): $n_1 = 2.4$
- The wavelength in medium one (diamond) at the chosen wave number is calculated by the following Equation: $\lambda_1 = 1/(\tilde{\nu}_{\text{vacuum}} \cdot n_1)$

Thus d_p can be calculated: $d_p \approx 0.9\mu\text{m}$.

It is therefore important to note that if a reaction is analyzed with an ATR experiment, absorption takes place only in a very thin layer on the surface of the ATR diamond crystal. The thickness of the layer is in the range of about $3\mu\text{m}$ and varies with the wave number, the refractive indexes n_2 and the absorbance coefficients α of the reaction mixture (n_2 and α can both change during a reaction experiment).

So far only the penetration depth of the evanescent electric field was calculated. As indicated in Figure B-2 this does not correspond to the sample thickness that is

necessary in order to apply Lambert Beer's law (Equation (2-20)). Therefore [Harrick 67] introduced the concept of effective thickness d_e . As shown in Figure B-2 a hypothetical sample with thickness d_e is introduced. In a transmission experiment the absorption of the hypothetical sample should be the same as obtained with the real ATR experiment. Therefore according to the descriptions in Figure B-2 and the fact that the intensity of light (I) is proportional to the square of the electric field amplitude (E), the following equation can be formulated:

$$\int_0^{d_e} I_{1t} \cdot \alpha \cdot dl_t = \int_0^{d_e} \cos \theta_1 \cdot I_1 \cdot \alpha \cdot dl_t = \int_0^{l_2} I_2 \cdot \alpha \cdot dz = \int_0^{l_2} I_{20} \cdot \left(e^{-\frac{z}{d_p}} \right)^2 \cdot \alpha \cdot dz \quad (\text{B-5})$$

Where I_1 and I_2 are the light intensities in the corresponding media, I_{1t} is the light intensity of the incident light in the hypothetical transmission experiment, I_{20} the light intensity of the incident light at the surface of medium two in the ATR experiment and l_2 the thickness of medium two. According to [Mirabella 93] the integration of Equation (B-6) gives the following result:

$$d_e = \frac{1}{\cos \theta_1} \frac{n_2}{n_1} (E_{02}^r)^2 \frac{d_p}{2} \quad (\text{B-6})$$

Equation (B-6) is only valid under the following constraints:

- ❖ Both media are electrical isolators (dielectrics)
- ❖ $l_2 \gg d_p$
- ❖ Both media are no or only weak absorbers

Again in the case of absorption the refractive indexes would have to be replaced by Equation (B-2). The relative electric field in the sample E_{02}^r can only be calculated for parallel or perpendicular polarized light [Fringeli et. al. 02]. But as the ATR setup used for this work does not use polarized light, the calculation will not be continued. However with Equation (B-6) the final link to the Lambert Beer's law can be made:

$$\ln \left(\frac{I}{I_0} \right) = \kappa \cdot c \cdot d_e \quad (\text{B-7})$$

Again it should be noted that the effective sample thickness d_e depends on the refractive indices. According to Equation (B-3) they change as the absorption coefficient changes during a reaction experiment.

B.2 Evaluation methods that do not require a reaction model

Any model-free evaluation of the spectroscopic data will not reveal the desired reaction parameters (reaction rates, activation energies) of the investigated reaction. Therefore they are not a direct contribution towards the goal of this thesis (see Chapter 1.2). Still they could be useful to design a proper reaction model.

The easiest and by far most applied approach to evaluate a measured reaction spectrum A is the univariate evaluation of single peaks. It is assumed that only one chemical component of the reaction system is responsible for the absorption peak. Generally the selected columns of A are used as qualitative information how the concentration of the corresponding component behaves as a function of time [Landau et. al. 95, a], [am Ende et. al. 98], and [am Ende et. al. 99]. The advantage of these methods is that no pure spectra (E) have to be identified.

For the general case of overlapping absorption bands multivariate methods have to be chosen. These methods, generally addressed as self-modeling curve-resolution (SMCR), decompose the measured reaction spectrum into the pure spectra and the concentration profiles of the involved components. Theoretically it would be possible to use these extracted concentration profiles in a subsequent step in order to identify the kinetic reaction parameters with classical kinetic fitting procedures. As will be shown this approach is rarely chosen in literature because the direct decomposition of the reaction spectra on the basis of a reaction model is much more robust.

However the SMCR methods will be useful for the step of reaction model design because they are able to identify possible intermediate or side products of the investigated reaction.

The first step in all SMCR techniques involves a principal component analysis (PCA). The procedure of PCA is well described in [Malinowski 02]. The result of the PCA is the decomposition of the measured reaction spectra A into three matrixes:

$$A = C_{abs} \times E_{abs} + R \quad A(N_t \times N_\lambda), C_{abs}(N_t \times N_{PC}), E_{abs}(N_{PC} \times N_\lambda), R(N_t \times N_\lambda) \quad (\text{B-8})$$

Where C_{abs} is the abstract concentration matrix, E_{abs} the abstract pure spectra matrix, R the residual matrix (containing measurement errors and noise) and N_{PC} the number of principal components. This decomposition is similar to Lambert-Beer's law (2-33) but the matrix elements of C_{abs} and E_{abs} do not have any physical meaning and are therefore called "abstract". Further the number of principal components N_{PC} is generally not equal to the number of chemical components in the reaction system (N_C). There are several reasons for this difference:

1. As mentioned not all chemical components must be absorbing species.
2. As explained in [Malinowski 02] and [Valle et. al. 99] the selection of N_{PC} is not a closed mathematical procedure. Several different statistical tests are proposed but often the selection is done on the basis of chemical knowledge. Generally it will be difficult to decide whether a component found by PCA represents measurement noise, a baseline drift or a real absorbing chemical species with low concentration.
3. Because A was measured during a chemical reaction, the concentration profiles of the absorbing chemical components might be linear dependent on each other. E.g. considering a reaction example of the following type:
 $A + B \rightarrow C + D$ It is obvious that the concentration profiles of components A and B as well as C and D are linear dependent. Therefore a PCA would only reveal two components. The subject of rank deficiency in measured reaction spectra was discussed by [Amrhein et. al. 96], [Nomen et. al. 01], and [Sans et. al. 97]. For an ideal reaction spectrum (no baseline drift, no measurement error), they concluded that the maximum number of linear independent components (equal to the rank of A) that can be identified from a reaction spectrum A is equal to $\min(N_{C,abs}, N_R + 1)$, where $N_{C,abs}$ is the number of absorbing species and N_R the number of chemical reactions (as long as no dosing occurs).

After the PCA the original reaction spectrum A will be replaced by the reduced reaction spectrum A^* :

$$A^* = C_{abs} \times E_{abs} = A - R \quad (\text{B-9})$$

After having chosen a feasible number of components (N_{PC}) in PCA, the next step in SMCR methods will be the transformation of the abstract concentration and pure spectra matrix (C_{abs} and E_{abs}) into physical meaningful matrixes (C_{real} and E_{real}):

$$A^* = [C_{abs} \times T] \times [T^{-1} \times E_{abs}] = C_{Real} \times E_{Real} \quad (\text{B-10})$$

Where T is any non-singular matrix of size $N_{PC} \times N_{PC}$. Many different approaches for this transformation are proposed in literature [Hamilton et. al. 90] and [Jiang et. al. 02]. As mentioned before the SMCR techniques are not the main focus of this work and therefore only some examples will be shortly explained.

Equation (B-10) clearly shows that during the reconstruction of physical meaningful E_{abs} and C_{abs} the problem of rotational ambiguities will come up because any new matrixes proposed for E_{abs} and C_{abs} can always be transformed into another pair of matrixes by any transformation matrix T . The task of SMCR is therefore to break these rotational ambiguities and to find a unique transformation of C_{abs} and E_{abs} into physical meaningful matrices C_{real} and E_{real} .

Iterative Target Testing Factor Analysis (ITTFA)

By target testing it is possible to test whether a test vector x corresponds to a principal component of A^* in Equation (B-9). Let's assume that a concentration profile c of one component could be guessed or determined by any method (one column in matrix C of Equation (2-33)). In order to test if this concentration vector c corresponds to one of the principal components in C_{abs} a transformation vector t has to be found that transforms C_{abs} as close as possible to the target vector c (least-squares solution):

$$\min_t [c - C_{abs} \times t]^2 \quad C_{abs} \times t = \hat{c} \approx c \quad \text{or} \quad t = (C_{abs}^T C_{abs})^{-1} C_{abs}^T \times c \quad (\text{B-11})$$

If \hat{c} is similar to c it can be concluded that the target concentration profile c corresponds to a real chemical component in the reaction system. This procedure can be repeated until N_{PC} successful target concentration profiles c_i and corresponding transformation vectors t_i are found. Finally the transformation matrix T in Equation (B-10) is constructed by adding the determined t_i to a matrix. The estimates of the desired C_{real} and E_{real} and the reproduced reaction spectra \hat{A}^* are given by the following equation:

$$\hat{A}^* = \hat{C}_{real} \times \hat{E}_{real} \approx A^* \quad \hat{C}_{real} = C_{abs} \times T \approx C_{real} \quad \hat{E}_{real} = T^{-1} \times E_{abs} \approx C_{real} \quad (\text{B-12})$$

The principle of target testing is used and implemented in the ITTFA method. ITTFA iteratively changes the estimated targets \hat{c}_i according to constraints, mostly non negativity and unimodality of the concentration profiles. These new targets are evaluated again by Equation (B-11). This step is repeated until convergence and the final estimates of the concentration profiles \hat{c}_i fulfill all the constraints. The start point is an initial guess for \hat{C}_{real} that contains the initial targets c .

ITTFA was developed by Gemperline ([Gemperline 84] and [Gemperline 86]) and [Vandeginste et. al. 85] for the analysis of HPLC elution profiles using non negativity and unimodality constraints for the concentration elution profiles. It was successfully applied for the decomposition of reaction spectra by [Bell et. al. 98], [Gemperline et. al. 99], [Dyson et. al. 00], [Johnson et. al. 02], and [Zhu et. al. 02]. In most of these works non-negativity and unimodality constraints were applied.

Alternating Least Squares (ALS)

The ALS method starts with an initial guess for the matrix C_{real} . The number of chemical components (columns) in C_{real} has to be chosen either on the basis of chemical knowledge or by PCA analysis. Then E_{real} can be calculated according to the following linear least squares:

$$E_{real} = (C_{real}^T C_{real})^{-1} C_{real}^T \times A \quad (\text{B-13})$$

The unconstrained E_{real} can now be constrained (e.g. to be non-negative) to get a new estimate \hat{E}_{real} :

$$E_{real} \xrightarrow{\text{constraints}} \hat{E}_{real} \quad (\text{B-14})$$

Then a new C_{real} can be calculated according to following linear least squares:

$$C_{real} = A \times \hat{E}_{real}^T (\hat{E}_{real} \hat{E}_{abs}^T)^{-1} \quad (\text{B-15})$$

The unconstrained C_{real} can now be constrained (e.g. to be non-negative and unimodal) to get a new estimate \hat{C}_{real} :

$$C_{real} \xrightarrow{\text{constraints}} \hat{C}_{real} \quad (\text{B-16})$$

The new \hat{C}_{real} can now be inserted in Equation (B-13). The iteration is continued until the difference the residuals R of the estimated and measured reaction spectrum do not change any more:

$$R = \left\| A - \hat{C}_{real} \times \hat{E}_{real} \right\|_2^2 \quad (\text{B-17})$$

It is also possible to replace the measured reaction spectrum A in Equations (B-13), (B-15) and (B-17) by the PCA reduced reaction spectrum A^* (Equation (B-9)).

The technique of ALS was discussed by [Casassas *et. al.* 93] and further developed by [Tauler *et. al.* 93, a]. The same method was applied in several reaction studies applying different constraints such as non-negativity, unimodality, closure, or more general shape constraints [Tauler *et. al.* 94], [Saurina *et. al.* 98], and [Tauler *et. al.* 99]. The technique was also applied by [Furusjö *et. al.* 98, a], [Bezemer *et. al.* 02], and [Miller 00].

Evolving Factor Analysis (EFA)

In the evolving factor analysis approach, sub matrices of A^* are decomposed by PCA. The procedure starts using only the first spectrum in the sub-matrix and proceeds, adding one spectrum at a time, until all spectra are decomposed, thus giving eigenvalues from a total of N_T sub-matrices. The same procedure is repeated in the backward direction, yielding N_T more sets of eigenvalues. If the eigenvalues from the forward and backward procedures are plotted, a picture showing at which times chemical components appear and disappear is obtained.

The sets of eigenvalues produced by EFA can be used to obtain initial estimates of the concentration profiles during the reaction. Assuming that the compound that enters the system first also leaves first, one can simply combine the eigenvalues from the forward and backward analysis to give concentration profiles. In a second step the matrix of combined eigenvalues is then fitted into A^* . For this second step an alternating least-squares procedure was proposed by [Maeder *et. al.* 86] and a non-iterative procedure similar to target transformation by [Maeder 87] and [Gampp *et. al.* 86]. As the technique was first applied for the decomposition of elution profiles from GC or HPLC measurements, both procedures used the existence of pure

concentration windows. The method was applied for the decomposition of a reaction spectrum by [Bell et. al. 98] who applied non-negativity constraints and ALS in the second step of EFA. EFA is mostly used to generate an initial guess of \hat{C}_{real} for an ALS method (see above).

Resolving factor analysis (RFA)

This technique is similar to the ALS method. In a first step the reaction spectrum A is decomposed into C_{abs} and E_{abs} by PCA. Then according to Equation (B-10) C_{abs} and E_{abs} are transformed by a transformation matrix T into C_{real} and E_{real} . The same physical constraints as applied in ALS, such as non-negativity of C_{real} and E_{real} or unimodality of C_{real} , are then applied to C_{real} and E_{real} in order to calculate \hat{C}_{real} and \hat{E}_{real} :

$$C_{real} = C_{abs} \times T \xrightarrow{\text{constraints}} \hat{C}_{real} \quad (\text{B-18})$$

$$E_{real} = T^{-1} \times E_{abs} \xrightarrow{\text{constraints}} \hat{E}_{real} \quad (\text{B-19})$$

As an initial guess of the unknown transformation matrix T random numbers can be chosen. The $N_{PC} \times N_{PC}$ unknown matrix elements of T are identified by a nonlinear least-squares optimization, given by the following equation:

$$\min_T \left\| A - \hat{C}_{real}(T) \times \hat{E}_{real}(T) \right\|_2^2 \quad (\text{B-20})$$

The number of unknown parameters in Equation (B-20) can be reduced to $N_{PC} \times N_{PC} - N_{PC}$ by normalizing T . This method was developed and applied to a simulated reaction example by [Mason et. al. 01]. No applications to a real example were found in literature.

ConcIRT

[ConcIRT] is one of the few commercial SMCR programs. An application example is reported by [Zilian 01]. Unfortunately the calculation principle is not public.

Conclusions:

Form the study of the literature about SMCR algorithms and own experience the following problems have to be considered when using these algorithms:

Rotational ambiguity of the solutions:

As discussed in [Gemperline 99], [Gemperline 98], [Tauler et. al. 95], [Tauler 01], [Smilde et. al. 01], [Miller 00], and [Diewok et. al. 03] the results of SMCR algorithms are generally not unique due to rotational ambiguities (Equation (B-10)). Even though constraints such as non-negativity, unimodality or closure are applied, the resolution will not be unique. In these cases, instead of unique profiles, a range or band of feasible profiles (\hat{C}_{real}) fitting equally well the experimental data and fulfilling the physical and chemical constraints of the system has to be considered. The more constraints applied the smaller will be the range of feasible solutions to the SMCR problem. Systems with good resolution in either the kinetic (time) or spectral direction will often yield a unique solution or a narrow band of possible solutions. However problems arise especially in kinetic evaluations, where lack of selectivity and similarly shaped profiles (either concentration profiles or spectra) are often encountered. Thus the ambiguities in the solution obtained by SMCR methods will often be severe [Furusjö et. al. 98, b], [de Juan et. al. 00], and [Diewok et. al. 03].

Rank deficiency of the reaction spectrum:

As mentioned before all SMCR will only reveal component information if their concentration profiles as well as pure spectra are linearly independent. Especially for the analysis of reaction spectra rank-deficiency has to be expected because the concentration-time profiles are linked by the chemical reactions taking place (see above).

Initial guess of a \hat{C}_{real} :

ALS, ITTFA are iterative and therefore depend on a good initial guess of \hat{C}_{real} [Zhu et. al. 02].

Intensity ambiguities:

Due to intensity ambiguities the resulting matrices \hat{C}_{real} and \hat{E}_{real} from any SMCR method will only contain relative values [Tauler et. al. 93, b] and [Smilde et. al. 01]:

$$A^* \approx \left(k \cdot \hat{C}_{real} \right) \times \left(\frac{1}{k} \cdot \hat{E}_{real} \right) \quad (\text{B-21})$$

Where k is an arbitrary scaling vector. In order to solve these intensity ambiguities more external knowledge, such as closure, has to be introduced into the constraints applied. However in many real applications these ambiguities will remain.

Baseline drifts:

If baseline drifts occur, all SMCR methods will treat them as additional components [Furusjö *et. al.* 98, b]. It is not possible to distinguish them from a chemical component.

Solutions to some problems:

A general and easy approach to address the problems of rank deficiency, rotational or intensity ambiguities is matrix augmentation, e.g. several reaction spectra measured at different concentration conditions but with the same components (and therefore same pure spectra) will be concatenated to a single reaction matrix A_{aug} :

$$A_{aug} = \begin{bmatrix} A_1 \\ \vdots \\ \vdots \\ A_{N_{exp}} \end{bmatrix} \quad (\text{B-22})$$

where N_{exp} is the number of experiments. Using A_{aug} instead of a single reaction spectra A all described SMCR techniques can still be carried out without any changes.

B.3 Comparison and combination of model-based and model-free evaluation methods

Generally the model-free (Appendix B.2) evaluation methods are applied as an initial step to the model-based evaluation (Chapter 2.3.3.3). The model-free analysis is essentially completely automatic and does not need any operator input (at least theoretically) and there is not much reason not to perform it. The results can serve as a basis for the elaboration of the correct reaction model. However in many cases the shape of the reaction spectra might already be sufficient in order to identify the underlying reaction model and an SMCR analysis will not reveal new information (see also Appendix E.2.2 and E.2.2.1). [Amrhein *et. al.* 99] reported a technique, based on target testing, to identify the stoichiometrics of the chemical reaction investigated.

However the most important role in the initial step of reaction model design will be the chemical intuition and knowledge about the reaction. For this step it might also be essential to use more specific offline analysis techniques such as NMR or chromatography [Dyson *et. al.* 00] in order to identify possible intermediate or side products.

The task that has to be solved by the model-free analysis is of course much heavier and much less constrained. In model-free analyses, the number of unknowns is usually orders of magnitude higher than in a model-based approach. The mathematical robustness of the evaluation is therefore much smaller. As discussed in Appendix B.2 the calculated concentration profiles are not unique and depend on the

initial guess. This was shown by [Furusjö *et. al.* 98, b] for a simple one-step reaction. The comparison showed a clear advantage of the model-based evaluation. There are, of course, many cases where a mechanism is too complex to be useful in modeling. In those cases the SMCR techniques will still be applicable as long as the component spectra are constant. An example reaction, where the reaction orders change as a function of reaction progress, was presented by [Zhu *et. al.* 02].

The advantages of the soft and hard modeling approaches were combined by [de Juan *et. al.* 00]. The evaluation is based on the ALS method explained in Appendix B.2. A new hard constraint is introduced to force some or all the concentration profiles to fulfill a reaction model, which is refined at each iterative cycle of the optimization process. This modification of the ALS method drastically decreases the rotational ambiguity associated with the kinetic profiles obtained using exclusively soft-modeling constraints (see Appendix B.2). The optional inclusion of some or all the absorbing species into the kinetic model allows the successful treatment of data matrices whose instrumental response is not exclusively due to the chemical components involved in the kinetic process, such as baseline drifts or absorption shifts. The method was applied to evaluate a two-step consecutive reaction example and compared to the classical model-free ALS and model-based approach reported by Maeder *et. al.* (see 2.3.3.3). The performance of the combined method was similar to the pure hard modeling approach. However they were both superior to the model-free ALS method. The same algorithm was used by [de Juan *et. al.* 01] in order to evaluate a three-step consecutive reaction example, where the classical ALS evaluation failed. A third application of the algorithm was presented by [Diewok *et. al.* 03]. A similar ALS algorithm with hard modeling constraints was used by [Bezemer *et. al.* 01] to evaluate a more complex chemical reaction system.

The same concept, of using a kinetic model as an additional constraint in a SMCR technique, was treated by [Smilde *et. al.* 01]. On a theoretical basis it was shown that rotational and intensity ambiguities (see Appendix B.2) of SMCR solutions can be eliminated for certain reaction systems.

[Dyson *et. al.* 00] compared the model-free ITTFA method with the model-based method developed by Maeder *et. al.* for the evaluation of a consecutive heterogeneous hydrogenation reaction. In a later publication by [Zilian 01] the same reaction system was additionally evaluated with ConciRT, another SMCR method. In both publications the SMCR as well as the hard modeling methods were both able to predict reasonable concentration time profiles. However the two different SMCR methods did not conclude in a unique result and showed worse performance compared to the model-based method.

Despite the combined application of Raman and IR techniques, it was not possible to explain the complete behavior of the reaction as measured by off line NMR analysis [Dyson *et. al.* 00].

C CONSTRUCTION DETAILS OF THE NEW REACTION CALORIMETER

C.1 IR-ATR Probe and Teflon inliner

As ATR probe a standard DMD-260 Probe from [Axiom] was used with Hastelloy C276 as tube material (see further specifications in C.8.5). The tube has a diameter of about 16 mm analogous to ATR Probes from other manufactures such as ASI [ReactIR].

The purpose of the Teflon inliner is to protect the copper block from chemical substances. For a good protection the thickness should be minimum 2 mm. Therefore Teflon coating techniques cannot be applied. The introduction of the Teflon inliner into the reactor is therefore shortly described in the following section.

As the IR-ATR probe from Axiom has a rather delicate sensor head the sealing caused some troubles. As shown in Figure C-1 is not possible to seal on top of the sensor head as there is no plane surface. The only solution was therefore to seal on the sides of the sensor head just before the tube begins (see right side in Figure C-1). Together with the company [Technova] the problem was solved as follows:

1. The copper block is heated to about 200 °C
2. The Teflon inliner, slightly too large in diameter, is then introduced into the reactor opening of the copper block. The hole for the ATR-Probe is prepared but too small, thus leaving enough Teflon material to be pushed back into the bore for the ATR-Probe (indicated in Figure 3-6).
3. Using a cone, the still hot and thus soft Teflon is pushed back into the bore for the ATR Probe. By doing this the thickness of the Teflon material decreases. The Teflon will cover the O ring that was previously inserted into the copper jacket (indicated in Figure 3-6). This O ring will press the Teflon that was pushed inside, onto the ATR probe.
4. The cone is then removed and with a special tool the ATR probe was inserted into the channel. The whole system was then cooled down. Thus the Teflon will have the exact form of the ATR-probe.

Using this technique the ATR-probe should be sealed pressure proof up to about 10 bar. It can be removed and reinserted for cleaning purposes using a special tool.

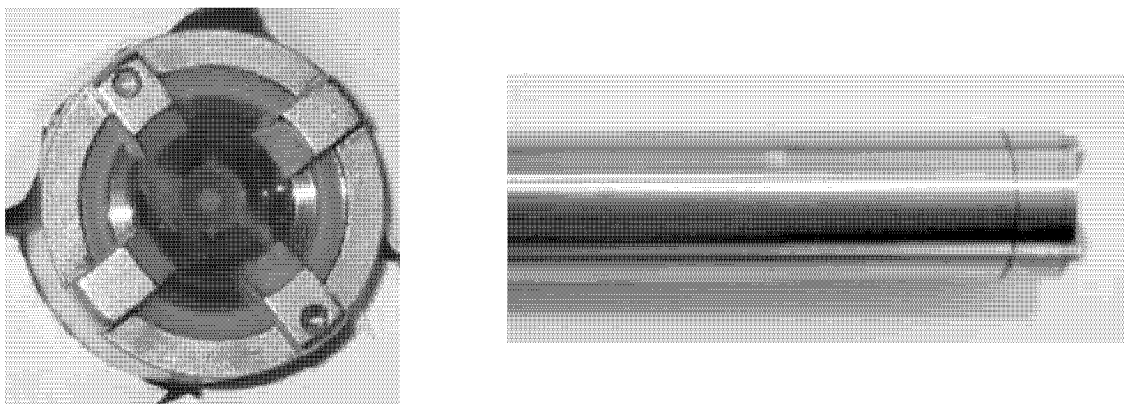


Figure C-1: Top view (left side) and side view (right side) of the IR-ATR Probe from Axiom.

C.2 Stirrer

The stirrer is made of two parts: A Hastelloy shaft and a Teflon part that forms the blades of the stirrer. The Teflon part is screwed onto the shaft and can therefore be replaced if another blade geometry is required. For all experiments done in this work only one stirrer was used (see Figure 3-5 and Table 3-2).

C.3 Thermal insulation

The insulation was made of Rohacell, resistant up to 180°C with a heat conductivity of about 0.03 W/mK. The different parts of the thermal insulation can easily be put together to get a reproducible insulation.

C.4 Stirrer Engine

The stirrer revolutions per minute rate can be adjusted between 0 and 600 rpm. The stirrer speed is controlled by an external controller and a speed meter mounted on the engine.

C.5 Baffles

The baffles were introduced in order to prevent a large vortex and to increase the intensity of mixing. They are made of Teflon and are strengthened by a syringe needle that is inserted into the Teflon. The baffles are screwed into the reactor cover and can be removed easily if desired.

C.6 Position of the temperature sensors inside the copper jacket

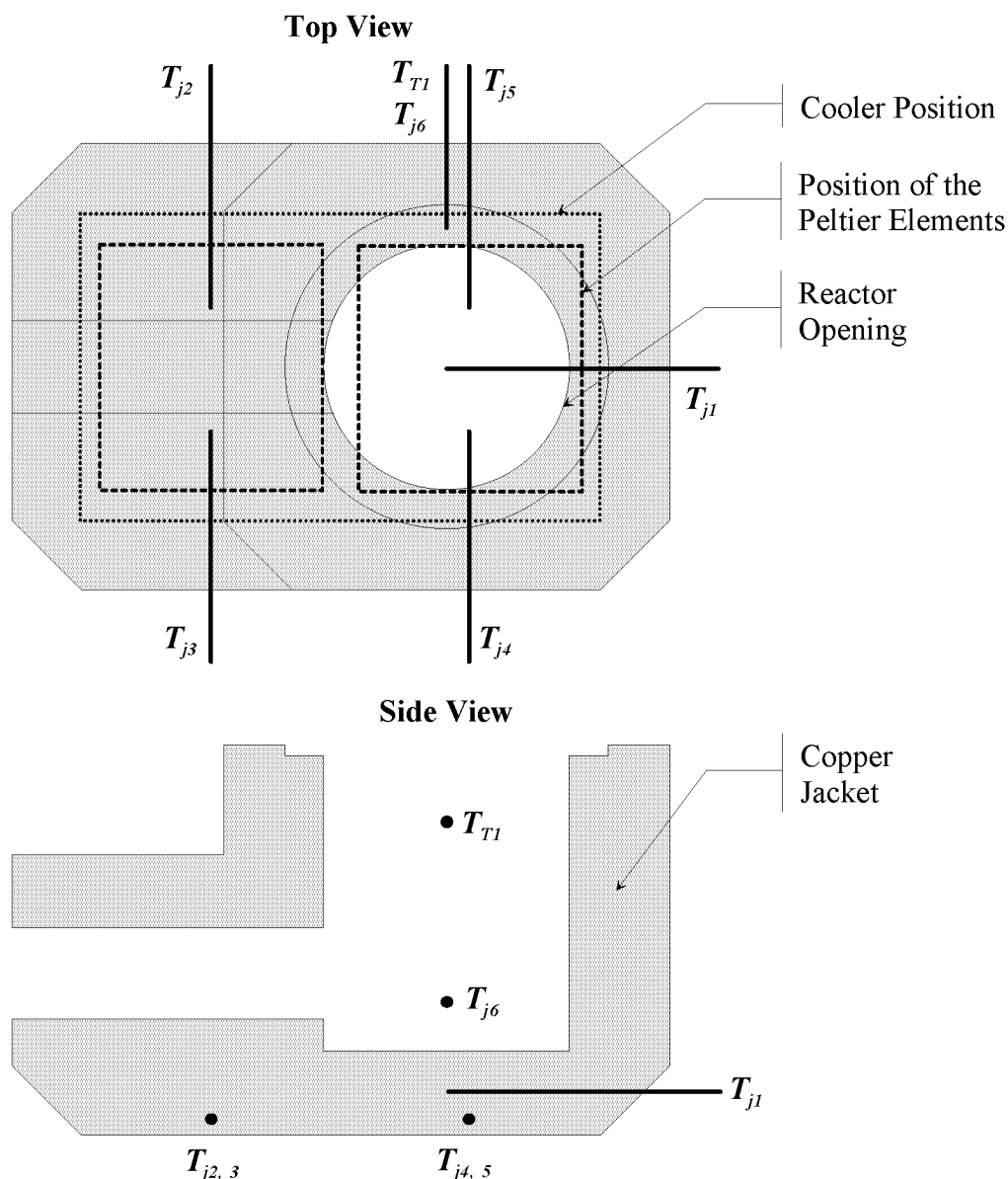


Figure C-2: Position of the temperature sensors inside the copper jacket of the intermediate thermostat.

Figure C-2 shows all the available temperature sensors inside the copper jacket. They were used to investigate the temperature gradients and to control the jacket temperature.

The same type of thermocouples was chosen as used for the measurement of T_r (see 3.4.3.2) and T_{Pelt}^{up} / T_{Pelt}^{down} (see C.7.4): Type K (1 mm diameter, time constant 0.6 s) Inconel® Alloy 600 as jacket material. In order to improve the measurement dynamics, thermal grease was put into the sensor bore prior to the introduction of the sensor.

However for the control of the jacket temperature only one temperature value can be used. Many different combinations of the sensors were tested but the following definition showed the best performance:

$$T_j = \frac{1}{4} \cdot \sum_{i=2}^5 T_{j,i} \quad (\text{C-1})$$

There are mainly three reasons for this selection:

1. By using the mean value of four sensors, the signal to noise ratio is reduced.
2. Possible inhomogeneities inside the reactor jacket are leveled out.
3. The two different heat-flow changes, shown in Figure 3-9, that have to be compensated by the intermediate thermostat are best acquired on the bottom plate of the copper jacket.

C.7 Cooler, peltier elements and cooling liquid

C.7.1 Different methods for thermal contact

A) Thermal grease

This is the standard technique. If care is taken during the mounting procedure and only as little thermal grease as possible is used, good performance can be expected. There are different classes of thermal greases, with different heat conductivities. Several of these were tested. However the standard thermal grease [*Melcor*] showed best applicability. Thermal greases cannot be used in vacuum [*Huang et. al. 00, a*] and [*Marlow*].

As thermal grease should not be applied in thick layers (only about 0.02 mm) care must be taken when several Peltier elements are mounted onto the same plate as they do not always show the same thicknesses. Therefore several Peltier elements were ordered and only pairs that showed the same thicknesses were fixed onto the cooler as described in 3.4.4.

B) Soldering and adhesive bonding

All metal parts used in this application could be soldered together. Special Peltier elements with metalized plates are available and could also be used for this technique. Of course the thermal performance of such a system is the best as compared to the other two techniques. However it should not be used for surfaces greater than 2 x 2 cm ([*Melcor*] and [*Ferrotec*]) due to the different thermal expansion coefficients of the connected materials. Temperature changes will thus lead to problems.

If parts cannot be soldered, adhesive bonding would be another possibility however shows the same drawback as the soldering technique.

C) Gels or films

Graphite films or silicon gels can also be used as thermal interface. Both materials were tested with the actual setup but the performance was bad. The reason might lie in the huge thickness of the films compared to thermal grease and the still relatively low thermal conductivities (as compared to copper). This mounting technique is useful if the contact surfaces show large inhomogeneities.

C.7.2 Peltier Elements

As shown in Figure 3-12 (Chapter 3.4.4) two Peltier elements were used in the cooler, electronically connected in series. Many different types of Peltier elements are available on the market. However if the application temperature is up to 200 °C only a few remain. For this calorimeter the HT series from Melcor (HT 6-12-40) was chosen. The cooling power $q_{Cooling}$ as a function of the temperature of the cooling liquid (T_{Cry}) is shown in Figure C-3. The calculations are carried out for a standard situation ($T_{PC} = 10$ °C (see Figure 3-4, Chapter 3.3.3), $I_{Pelt} = -4.5$ A, thermal resistance of the cooler 0.2 W/K). The cooling power of one Peltier element ($q_{Cooling}$) as well as the temperature of the hot side of the Peltier element (T_{PH} , see Figure 3-4) is calculated based on steady-state equations (see Chapter 3.7.2) as well as manufacturer values [Melcor] for the required Peltier parameters. The element shows a maximum cooling capacity of about 42 W if the temperature difference $T_{PH} - T_{PC}$ is zero ($T_{PH} = T_{PC} = 10$ °C). The cooling capacity drops down to 0 W if $T_{PH} - T_{PC}$ reaches a value of about 95 °K ($T_{PH} = 105$ °C, $T_{PC} = 10$ °C). It was therefore concluded that two Peltier elements in series should be powerful enough for this application.

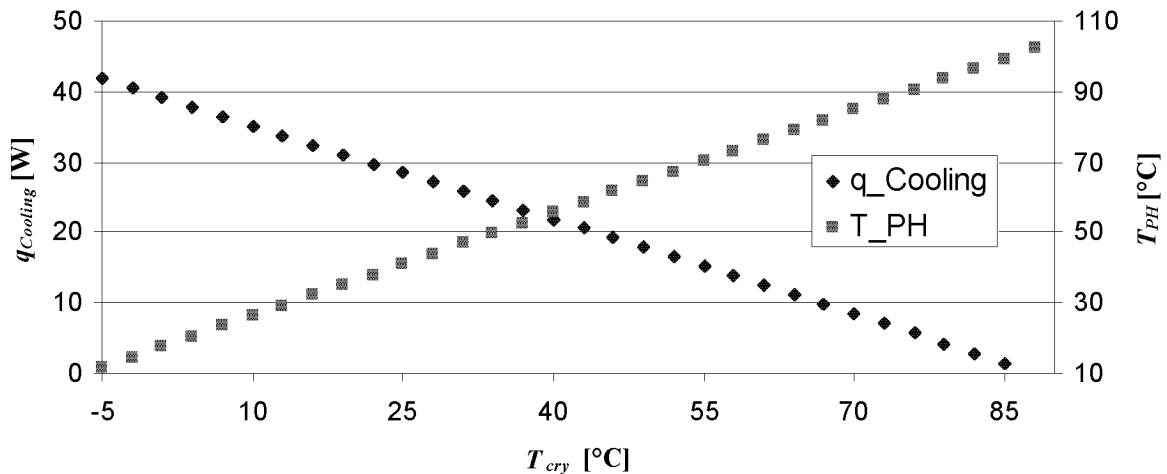


Figure C-3: Performance plot of one Peltier element (HT 6-12-40 series, manufacturer values for the Peltier parameters [Melcor]). T_{PC} is set to 10 °C, the temperature of the cooling liquid T_{Cry} is varied from -5 to 90 °C, the Peltier current is set to -4.5 A. The thermal resistance of the cooler is assumed to be 0.2 W/K.

Peltier elements should be protected against moisture. Therefore the Peltier elements are placed inside the bottom plate of the thermal insulation (see Figure 3-6). Best performance of the Peltier elements is achieved if they are operated in vacuum [Ferrotec], [Melcor] and [Huang et. al. 00, a]. However, as discussed above, there is no suitable mounting technique for the actual setup that can be used in vacuum.

Most of the manufactures guarantee a long life time of their elements. However the performance of the elements will not be constant over a long time period. Any calibrations carried out should therefore be repeated in the range of half a year [Melcor].

C.7.3 Cooler and cooling liquid

The task of the cooler is to remove the heat pumped by the Peltier elements. Therefore it should show smallest possible total heat resistance [Huang et. al. 00, a] and [Buist et. al. 94]. The total heat resistance is influenced by the following points:

Material of the cooler:

The material should show high heat conductivity, thus copper is the material of choice.

Cooling liquid:

Water is one of the best cooling liquids available. Unfortunately it cannot be used at temperatures lower than 0 °C. It is possible to use special oils as cooling liquids. The benefit is their high temperature range of application but they have bad heat-transfer performances.

As mentioned in 3.3.2 the new calorimeter reduces the temperature range required for the cooling liquid. Therefore for all applications discussed in this work a mixture of water and EtOH (2:1) or pure water was used.

Flow pattern and mass flow of the cooling liquid:

A cooler should maintain a homogeneous temperature distribution on the cooling surface and maximum heat transfer. If the cooler will have bad performance the two Peltier elements mounted on top can diverge and build up local temperature gradients inside the cooler. This can cause measurement drifts.

An optimal design for the actual setup might therefore be a quite complex and fine flow pattern that tries to get best thermal contact of the two different Peltier elements. However the more complex and fine a flow pattern is designed the bigger will be the pressure drop inside the channels. Consequently the flow rate of the cooling liquid will decrease as the cryostat will not be strong enough to maintain the flow rate. This will again lead to an increase of the temperature differences and consequently the goal of a homogeneous temperature distribution will not be achieved.

Therefore a compromise between pressure drop and complex flow patterns had to be found. The flow pattern chosen for this application is shown in Figure 3-12. Commercial coolers were also tested but showed worse performance.

C.7.4 Measuring of T_{Pelt}^{up} and T_{Pelt}^{down}

Figure 3-12 (Chapter 3.4.4) shows the position of the T_{Pelt}^{up} and T_{Pelt}^{down} sensors that will be used for the calculation of $q_{Cooling}$ (see later). The same thermocouples were chosen as used for the measurement of the jacket temperatures (see Appendix C.6): Type K, 1 mm diameter, time constant 0.6 s, Inconel® Alloy 600 as jacket material.

As T_{Pelt}^{up} and T_{Pelt}^{down} should be estimates of T_{PC} and T_{PH} (see Figure 3-6) they are placed as close as possible to the surfaces of the Peltier elements (0.3 mm shifted from the top of the cover plates). However it is clear that T_{Pelt}^{up} and T_{Pelt}^{down} will always differ from T_{PC} and T_{PH} as the alumina ceramics plates of the Peltier elements (heat conductivity 35 W/mK) cause significant temperature differences (see Figure 3-6).

C.8 Periphery devices according to Figure 3-14

C.8.1 Rotary valves and syringe pump

The two feeds that can be used with the current setup of the reactor cover (see Chapter 3.4.3.2) are each connected to a four position rotary valve (Omnifit, 11526), connection with Teflon tubes). The rotary valves are made of Teflon and are controlled by RS232 commands. The four inputs of the rotary valves are used as follows: 1) Closed (during the reaction) 2) Open (to connect to the syringe pump) 3) Nitrogen (to be able to remove oxygen from the reactor 4) Vacuum (in order to clean the reactor and to remove oxygen / moisture).

The syringe pump (kdS 200) can be connected to the open position of the rotary valves in order to dose reactants. The control of the syringe pump is done by RS232 commands. Gastight Hamilton syringes (series 1000) are used (volumes 25, 20, 5, 2.5, 1 ml).

C.8.2 Cryostat

The cooling liquid required to remove the heat pumped by the Peltier elements (see Figure 3-12 or Figure 3-3) is tempered by an outside cryostat (Haake F6 – C25) to reach the desired temperature T_{Cry} (see Figure 3-4). As cooling liquid pure water or water / ethanol mixtures were used (see description of the individual experiments).

C.8.3 Amplifiers for the Peltier elements and the compensation heater (U_{Pelt} , I_{Pelt} , U_{Comp} , I_{Comp})

As the control of the reactor temperature T_r as well as the jacket temperature T_j is done with the computer (Number I, in Figure 3-14, detailed description in Chapter 3.6), the output signal, in the range of -10 to 10 V, has to be amplified to the desired power range. The time constant of both amplifiers is smaller than the update rate of the computer signal (10 Hz).

The compensation heater is controlled by adjusting the voltage with an ATM-55-5M amplifier [Kepco]. The actual voltage on the compensation (U_{Comp}) heater is assumed to be equal to the output of the controller. This assumption is feasible because any voltage drops due to the cabling are constant during a reaction experiment and thus do not affect the calorimetric signal. The actual current required by the compensation heater (I_{Comp}), is monitored by the amplifier and acquired by the computer (indicated in Figure 3-14). As the monitored signal I_{Comp} is already scaled within the range of 0 to 10 V it can be directly feed to the AD converter without further signal conditioning (indicated in Figure 3-14).

The Peltier elements are controlled by adjusting the current with a BOP-36-6M amplifier [Kepco]. The actual voltage on the Peltier elements (U_{Pelt}) is assumed to be the same as the voltage monitored by the amplifier. This assumption is feasible as

U_{Pelt} is only used for evaluation purposes when I_{Pelt} is equal to zero. The actual current of the Peltier elements I_{Pelt} (\approx set point of the amplifier) and U_{Pelt} are both acquired by the computer (indicated in Figure 3-14). As the monitored signals U_{Pelt} and I_{Pelt} are already scaled within the range of -10 to 10 V they can be directly feed to the AD converter without further signal conditioning (indicated in Figure 3-14).

C.8.4 DA/AD converter, data acquisition, signal conditioning and signal generation

The computer (Number I in Figure 3-14) has mainly two different tasks within this application:

1. Data acquisition: Analog signals are converted to digital signals by an AD converter. These are the measured signals of the system.
2. Signal generation: In order to interact with the device, analog output signals have to be generated from digital values by a DA converter.

Both tasks are performed by the same PCI-MIO 16XE10 card from [National Instruments]. The frequency of signal acquisition and generation is 10 Hz and is triggered by a timer built in the PCI-MIO card.

The different signals acquired by the computer are listed in Table C-1. All signals that show low voltages are pre-amplified to the range of -10 to 10 V and filtered. The signal conditioning is carried out with SCXI 1125 (SCXI 1328 Terminal Block, input) and SCXI 1124 (SCXI 1325 Terminal Block, output) modules from [National Instruments]. The conditioned signals are then passed to the AD converter. The settings of the signal conditioning are shown in Table C-1.

Table C-1 Signal-conditioning specification of the measured input data in the new calorimeter.

Signal	Description	Amplified	Filter
T_r	Reaction Temperature (see Chapter 3.4.3.2)	yes	4 Hz
$T_j 1..6, T_{T1}$	Jacket Temperatures (see Appendix C.6)	yes	4 Hz
T_{Amb}	Ambient temperature, measured outside of the reactor (see Chapter 3.7.3)	yes	4 Hz
p_r	Reactor pressure (see Chapter 3.4.3.2)	yes	4 Hz
I_{stirr}	Current required by the stirrer engine to maintain the desired stirring speed (Figure 3-14).	yes	4 Hz
U_{Comp}, I_{Comp} U_{Pelts}, I_{Pelt}	See Appendix C.8.3 and (Figure 3-14). Directly fed to the PCI-MIO card without SCXI signal conditioning.	No	No

C.8.5 Infrared measurement

The infrared measurements were done with the same equipment that was already used in the previous work [Pastré 00]. It consists of the following elements:

- ❖ ATR-Probe: Axiom DMD 260 / 270, 3 reflections, angle of incidence 45°, Diamond as ATR crystal, 16 mm outside diameter, Hastelloy C-276, resistant up to 200°C and 30 bar, cutoff region 1800 to 2400 cm⁻¹.
- ❖ Detector: External MCT detector cooled with liquid nitrogen.
- ❖ Spectrometer: FT-IR spectrometer from Bruker (Equinox 55).
- ❖ Software: OpusNT from Bruker running on an second computer (number II in Figure 3-14)

In contrast to the previous work and most applications described in literature, the spectra during a reaction were not recorded at a fixed sampling rate. The sampling is triggered by the LabVIEW program running on the main computer (number I in Figure 3-14). In this way it is possible to adjust the sampling time according to the exact start of the reaction, the dosing actions and, if desired, to the rate of the reaction. The two computers are connected by Ethernet (indicated in Figure 3-14).

C.8.6 Endoscope

In order to be able to look inside the reactor an endoscope can be optionally inserted into the reactor. The endoscope was purchased from Storz.

D CALCULATION DETAILS REQUIRED FOR THE HEAT-FLOW BALANCE OF THE NEW REACTION CALORIMETER

D.1 Determination of S , R and κ

As described in Chapter 3.7.2 the calculation of $q_{Cooling}$ (corresponding to $q_{Cooling,corr}$) is based on the three steady-state Equations (3-14), (3-15) to (3-16). The calculation is only possible if the three parameters S (Seebeck coefficient [V/K]), R (electrical resistance [Ω]) and κ (heat conduction coefficient [W/K]) are known as a function of temperature. S , R and κ are device specific parameters and are independent from the reactor content. *It is therefore possible to calibrate these parameters once and then use them for any reaction measurement.*

The characterization of S , κ and R was not carried out in separate calibration experiments but always at the beginning and at the end of each reaction measurement described in Chapters 5.2 to 5.4. The individual values were then combined to a unique parameter set that can be applied for any reaction within the temperature range studied. As the Peltier elements had to be replaced during the work, two parameter sets were calculated.

All calculations and results shown in this work are carried out with one of these parameter sets and not with the individual calibration results. The two parameter sets are based on the following experiments:

Set A: Neutralization of NaOH (see Chapter 5.2) and Hydrolysis of Acetic anhydride (see 5.3).

Set B: Epoxidation reaction (see Chapter 5.4).

Parameter S

For the determination of S the Peltier elements were turned off for 25 s and the voltage of the elements as well as the temperature difference between the hot and the cold plate was measured (T_{Pelt}^{up} and T_{Pelt}^{down} see Figure 3-12). For the evaluation according to [Huang et. al. 00, a] the following equation was used (steady-state approximation; follows from Equations (3-14) to (3-16)):

$$S = \frac{U_{Pelt}(I_{Pelt} = 0)}{(T_{Pelt}^{up} - T_{Pelt}^{down})} \quad (D-1)$$

Where $U_{Pelt}(I_{Pelt} = 0)$ is the measured voltage over the Peltier elements after turning off the current supply. The value of S , determined according to (D-1), was plotted as a function of time. After about 5 seconds the value did not change any more, indicating that the steady-state approximation is sufficient. The mean value of the evaluation was therefore taken in the range of 5 to 25 s after the current was turned off. The whole procedure was repeated three times and averaged. This resulted in

one single value for S at the corresponding temperature. For the determination of S the accuracy of the temperature difference $\Delta T_{Pelt} = T_{Pelt}^{up} - T_{Pelt}^{down}$ is crucial. Therefore the offset of the two sensors was subtracted prior to the evaluation of Equation (D-1):

Set A: $\Delta\Delta T_{Pelt} = 0.05$ K, Set B: $\Delta\Delta T_{Pelt} = 0.085$ K

After having determined S at different temperatures a linear regression was applied to these values:

$$S = S_a \left(\frac{T_{Pelt}^{up} + T_{Pelt}^{down}}{2} \right) + S_b \quad (D-2)$$

The result for both sets A and B are shown in Figure D-1 and compared to the values provided by the manufacturer.

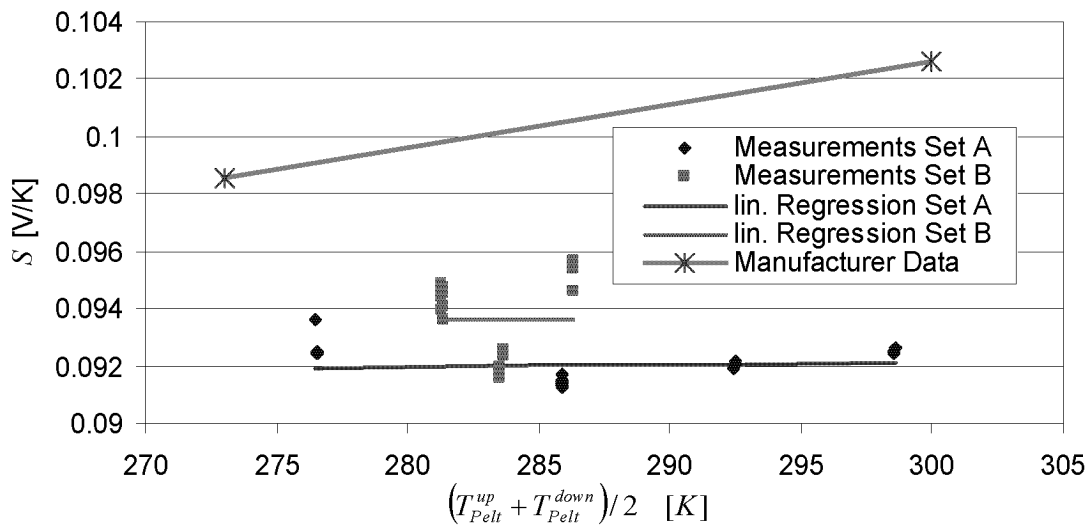


Figure D-1: Results of the calibration of the Seebeck coefficient S of both calibration sets A and B.

The deviation between the two sets A and B is only about 2 % whereas the deviation from the manufacturer values is in the range of 10% (see also sensitivity analysis in Chapter 6.1.3). The difference of the calibrations at the beginning and at the end of the reaction measurement was maximal 0.5 % in Set A and 0.8 % in Set B. These changes will be neglected in all evaluations done in this work and a single value of $S = S(T)$ determined by Equation (D-2) at $T = T_r$ will be used for the whole reaction period.

Parameter R

After having determined S by (D-2), the parameter R can be determined by the following equation (steady-state approximation; follows from Equations (3-14) to (3-16)):

$$R = \frac{U_{Pelt}}{I_{Pelt}} - \frac{S \cdot (T_{Pelt}^{up} - T_{Pelt}^{down})}{I_{Pelt}} \quad (D-3)$$

Several values were used to calculate a mean value for R . Again a linear regression was applied to the values determined in order to obtain R as a linear function of temperature:

$$R = R_a \cdot \left(\frac{T_{Pelt}^{up} + T_{Pelt}^{down}}{2} \right) + R_b \quad (D-4)$$

The result for both sets A and B are shown in Figure D-2 and compared to the values provided by the manufacturer.

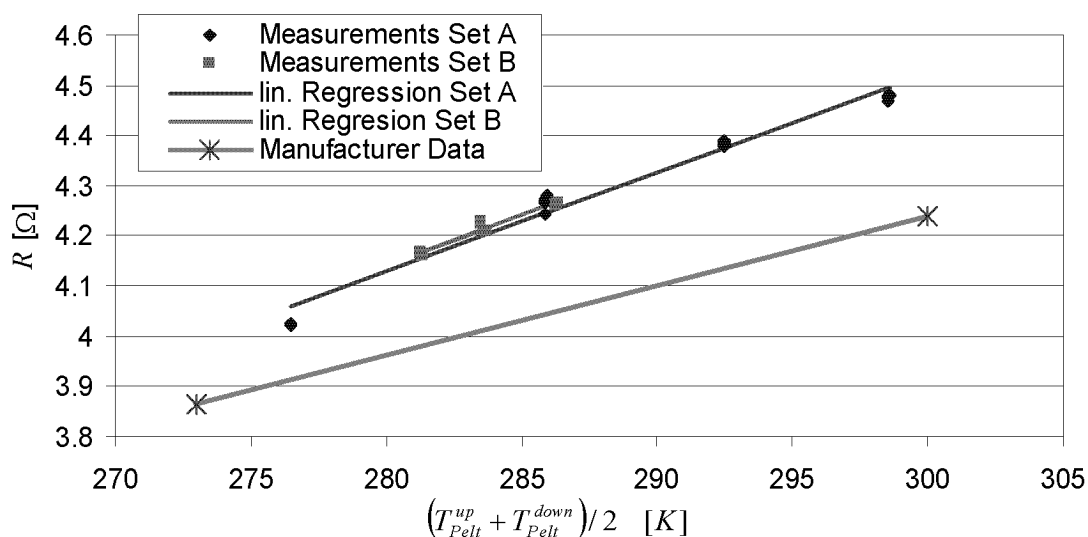


Figure D-2: Results of the calibration of the electric resistance R of both calibration sets A and B.

The deviation between the two sets A and B is smaller than 1 % whereas the deviation from the manufacturer values is in the range of 5% (see also sensitivity analysis in Chapter 6.1.3). The difference of the calibrations at the beginning and at the end of the reaction measurement was maximal 0.2 % in Set A and 0.1 % in Set B. These changes will be neglected in all evaluations done in this work and a single value of $R=R(T)$ determined by Equation (D-4) at $T = T_r$ will be used for the whole reaction period.

Parameter κ

The determination of κ is more difficult. It describes the passive thermal heat flow through the Peltier elements that is also present if no current flows through the Peltier elements ($I_{Pelt} = 0$). Since S and R are known from (D-2) and (D-4), κ can be determined by varying the temperature of the cooling liquid (T_{Cry} in Figure 3-4) and fixing all other parameters. The temperature of the cooling liquid was therefore changed by 0, +1, +2, -2, -1 and back to 0 K during a period of 20 to 30 minutes. The evaluation is done using the steady-state Equations (3-14) to (3-16) and the following linear least-squares optimization:

$$\min_{\kappa} \left(\sum_{i=1}^n \left(\text{mean}(q_{Cooling,SS_i}) - q_{Cooling,SS_i} \right)^2 \right) \quad (D-5)$$

$$q_{Cooling,SS_i} = -S \cdot I_{Pelt_i} \cdot T_{Pelt_i}^{up} - \frac{1}{2} \cdot R \cdot I_{Pelt_i}^2 + \kappa \cdot (T_{Pelt_i}^{up} - T_{Pelt_i}^{down}) \quad (D-6)$$

The indices i represent the i 'th measurement point during the variation of the temperature of the cooling liquid. The evaluation is based on the assumption that if T_r as well as T_j are controlled at a constant level and q_{tot} is zero (at the beginning and end of the reaction measurement) $q_{Cooling,SS}$ should remain constant though T_{Cry} and consequently T_{Pelt}^{down} will change (see Figure D-3). The linear least-squares optimization was carried out with different start values but always found the same optimum. For these rather slow changes of the heat flows the steady-state approximations were accurate enough. This can be seen in Figure D-3. The temperature changes of the cooling liquid can be seen in the varying T_{Pelt}^{down} . But the total measured heat production / consumption of the reaction mixture q_{tot} remains at zero.

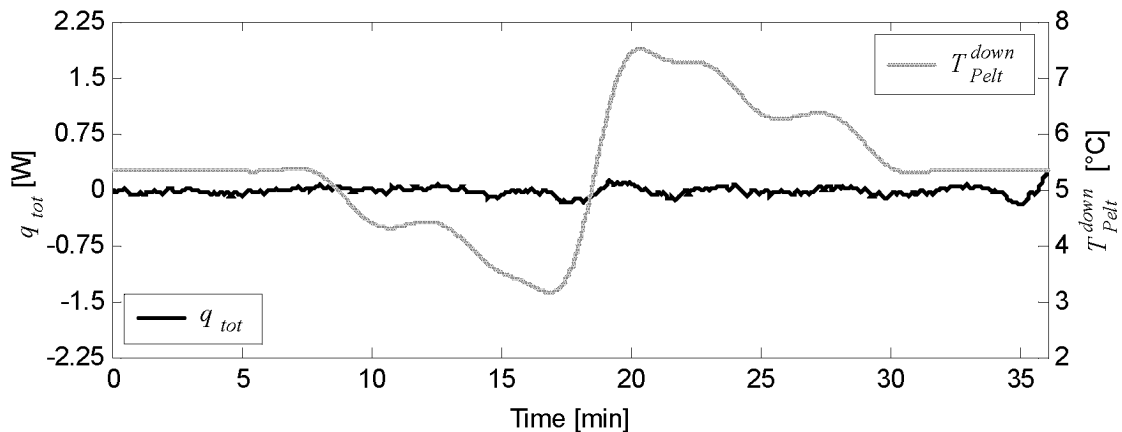


Figure D-3: Effect of temperature variations of the cooling liquid in the cooler on q_{tot} . The variation shown here was done by changing the cryostat temperature after a hydrolysis reaction of acetic anhydride at 25 °C.

Figure D-3 further demonstrates that the requirement set in Chapter 3.2 (q_{tot} should be independent to changes of the temperature of the cooling liquid) is met: The heat-flow balance to calculate q_{tot} (Equation (3-12)) is not influenced by changes of the temperature of the cooling liquid.

Again a linear regression was applied to the values determined by (D-5) in order to obtain κ as a linear function of temperature:

$$\kappa = \kappa_a \cdot \left(\frac{T_{Pelt}^{up} + T_{Pelt}^{down}}{2} \right) + \kappa_b \quad (D-7)$$

The result for both sets A and B are shown in Figure D-4 and compared to the values provided by the manufacturer.

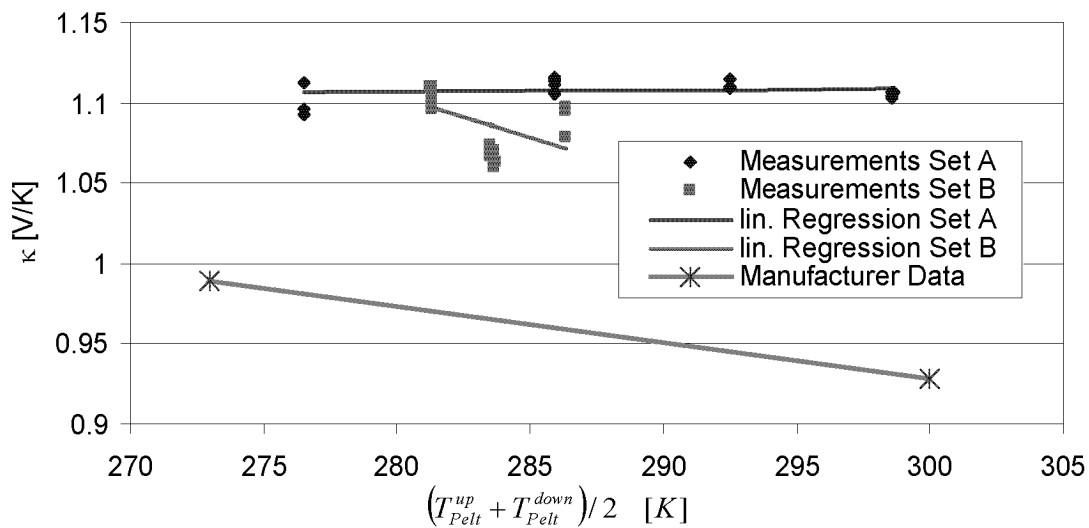


Figure D-4: Results of the calibration of the thermal conductivity κ of both calibration sets A and B.

The deviation between the two sets A and B is about 5 % whereas the deviation from the manufacturer values is in the range of 15% (see also sensitivity analysis in Chapter 6.1.3). The difference of the calibrations at the beginning and at the end of the reaction measurement was maximal 2 % in Set A and 2 % in Set B. These changes will be neglected in all evaluations done in this work and a single value of $\kappa = \kappa(T)$ determined by Equation (D-7) at $T = T_r$ will be used for the whole reaction period.

As mentioned by [Huang et. al. 00, a] it might be inaccurate to use values for the parameters S , κ and R that are provided by the manufacturer. In our case $R(T)$ was close to the reference values but $S(T)$ and $\kappa(T)$ deviated significantly from the values suggested by the manufacturer (see also sensitivity analysis in 6.1.3).

It was shown that parameter sets for $S(T)$, $R(T)$ and $\kappa(T)$ were found that can be applied for the measurement of any reaction example as they are device and not reaction specific parameters. The values of the two parameter sets used for the calculations in this work are given in Table D-1.

Table D-1: Values of the Peltier parameter sets A and B used for all calculations in this work.

	Set A	r^2	Set B	r^2
Experiments used for the determination	Hydrolysis of AcOAc (5.3) Neutralization of NaOH (5.2)		Epoxidation (5.4)	
S_a [V/K ²]	7.199E-06	0.008	7.299E-06	0.0001
S_b [V/K]	8.995E-02		9.155E-02	
R_a [Ω / K]	1.971E-02	0.97	2.044E-02	0.96
R_b [Ω]	-1.390E+00		-1.582E+00	
κ_a [W/K ²]	9.112E-05	0.016	-5.272E-03	0.27
κ_b [W/K]	1.081E+00		2.581E+00	

D.2 Determination of k_{Loss}

As described in Chapter 3.7.3 the calculation of q_{Loss} is based on Equation (3-21). The calculation is only possible if the parameter k_{Loss} [W/K] is known. Based on Figure 3-23 it was concluded that k_{Loss} must be a function of the temperature difference $T_{j,0} - T_{Amb,0}$. The coefficient k_{Loss} is a device specific parameter and is independent from the reactor content. It is therefore possible to calibrate it once and then use it for any reaction measurement.

The determination of k_{Loss} was not carried out in separate calibration experiments but always at the end of most reaction measurement used for this work. The individual values were then combined in order to get a unique $k_{Loss}(T_{j,0}, T_{Amb,0})$ that can be applied for any reaction within the temperature range studied. In contrast to the determination of the Peltier parameters (see Appendix D.1) only one $k_{Loss}(T_{j,0}, T_{Amb,0})$ will be determined and used as no changes in the thermal insulation of the reactor were done for all the experiments made during this work.

All calculations and results shown in this work are carried out using this unique k_{Loss} and not with the individual calibration results.

In a first step an individual and optimal $k_{Loss,opt}$ was determined for each experiment by the following linear least-squares optimization (derived from Equation (3-12) by setting q_{Dos} and q_{tot} 0 W):

$$\min_{k_{Loss,opt}} \left[\sum_{i=1}^n \left(q_{Cooling,i} - q_{Comp,i} + \Delta q_0 + k_{loss,opt} \cdot \left(|T_{J,i} - T_{Amb,i}| - |T_{j,0} - T_{Amb,0}| \right) \right)^2 \right] \quad (D-8)$$

Where the index i denotes the i 'th measurement point in time within the evaluated range. This time range is chosen after the reaction is finished (duration between 0.5 and 2 hours where it can be assumed that that $q_{tot} = 0$ W). Only experiments were used where the ambient temperature changed within this range. This identification was therefore not possible for all measurements done within this work. However most of the epoxidation and acetic anhydride hydrolysis experiments (see Chapters 5.3 and 5.4) were intentionally extended after the reaction was finished and could therefore be used for the identification of $k_{Loss,opt}$.

All reasonable $k_{Loss,opt}$ values identified by Equation (D-8) are plotted in Figure D-5. According to Equation (3-21) only positive values are reasonable for $k_{Loss,opt}$ otherwise q_{Loss} would be smaller than $q_{Loss,0}$ when the temperature difference $T_{j,0} - T_{Amb,0}$ increases. All $k_{Loss,opt}$ values shown in Figure D-5 are positive and thus reasonable. As mentioned before, Equation (3-21) presumes that q_{Loss} is proportional to the temperature difference $T_{j,0} - T_{Amb,0}$. The parameter k_{Loss} was therefore also calculated by taking the derivative of the curve shown in Figure 3-23 with respect to $T_{j,0} - T_{Amb,0}$. This derivative is shown as a thin straight line in Figure D-5. The fact that the values for k_{Loss} obtained by the derivation of the $q_{Loss,0}$ values are in the same range as the

$k_{Loss,opt}$ values determined by Equation (D-8) is a hint that the $k_{Loss,opt}$ values obtained are reasonable.

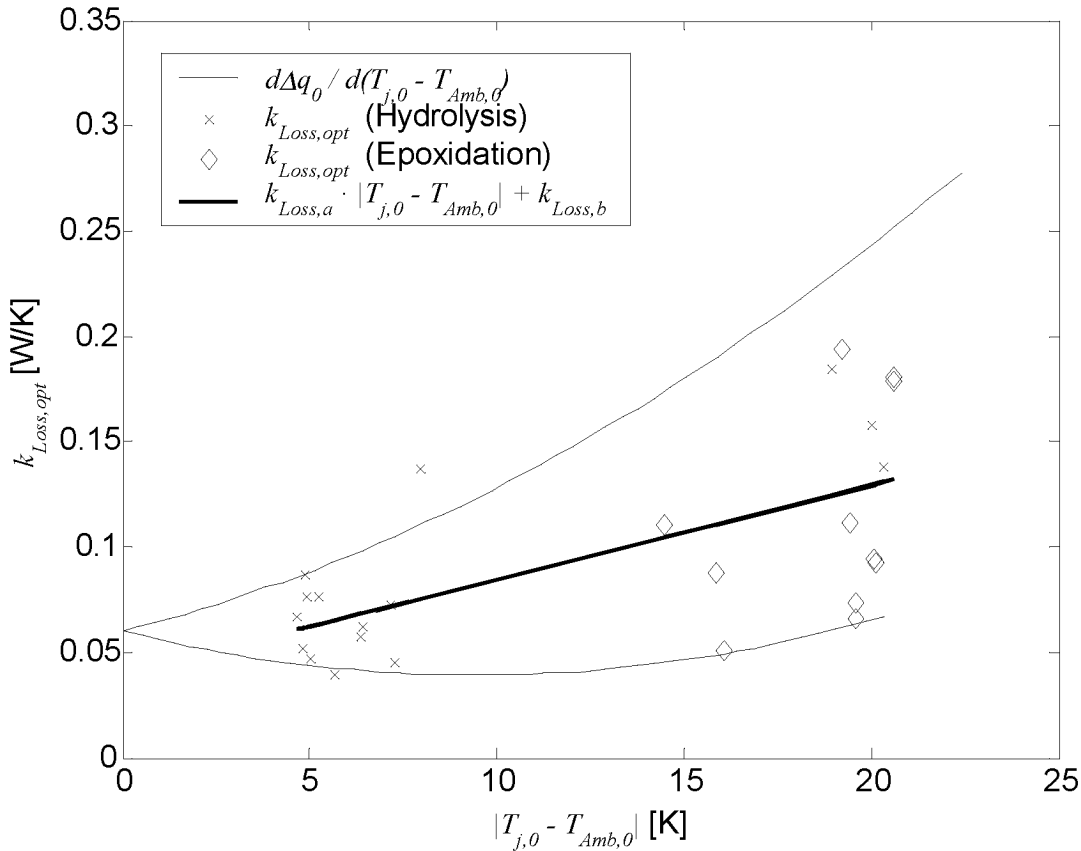


Figure D-5: $k_{Loss,opt}$ values determined at the end of some epoxidation and acetic anhydride hydrolysis experiments by Equation (D-8).

The temperature dependency of k_{Loss} was chosen as simple as possible:

$$k_{Loss} = k_{Loss,a} \cdot |T_{j,0} - T_{Amb,0}| + k_{Loss,b} \quad (D-9)$$

Where $k_{Loss,a}$ [W/K²] and $k_{Loss,b}$ [W/K] are determined by linear regression of the $k_{Loss,opt}$ values obtained by Equation (D-8). The absolute value of $T_{j,0} - T_{Amb,0}$ was taken in order to prevent negative values for k_{Loss} . Therefore the $k_{Loss,opt}$ values in Figure D-5 are plotted versus $|T_{j,0} - T_{Amb,0}|$.

The linear regression shown in Figure D-5 gave the following result:

- ❖ $k_{Loss,a} = 0.00448$ [W/K²]
- ❖ $k_{Loss,b} = 0.0398$ [W/K]

These values of $k_{Loss,a}$ and $k_{Loss,b}$ are used for all calculations in this work. It was shown a unique function $k_{Loss}(T_{j,0}, T_{Amb,0})$ was found that can be applied for the measurement of any reaction example as it is a device specific parameter. The importance of this correction of the ambient temperature was verified with a sensitivity analysis (see Chapter 6.1.5)

D.3 Mathematical baseline for the calculation of q_{tot}

Of course the calorimeter presented in this Chapter can also be used as a pure compensation calorimeter. For such an application only the heat-flow balance of the inner thermostat (Equation (2-14)) has to be considered:

$$q_{tot} = q_{Flow} + q_{Lid} - q_{Stirr} - q_{Dos} - q_{Comp} \quad (2-14)$$

Where q_{Comp} is the measured power consumption of the compensation heater (Equation (2-15)) and q_{Dos} the heat of dosing (Equation (2-4)). Generally the heat flows q_{Flow} and q_{Lid} cannot be calculated (see discussion in 2.1.3.1 and 2.1.3.3). Also q_{Stirr} is unknown but can be assumed to be constant during an experiment. However the sum of these three heat flows can be determined at the beginning ($q_{bl,0}$ [W]) and end of the reaction ($q_{bl,f}$ [W]) by Equation (2-14) ($q_{tot} = 0$ and $q_{Dos} = 0$):

$$q_{bl,0} = q_{Comp,0} = q_{Flow,0} + q_{Lid,0} - q_{Stirr,0} \quad (D-10)$$

$$q_{bl,f} = q_{Comp,f} = q_{Flow,f} + q_{Lid,f} - q_{Stirr,f} \quad (D-11)$$

As the change of the baseline between $q_{bl,0}$ and $q_{bl,f}$ cannot be measured, a mathematical function ($bl(t)$) has to be chosen (according to Equation (2-14)) that generates baseline values for the whole measurement period.

$$q_{tot} = q_{bl,0} + \frac{bl(t) - bl(0)}{\max(bl(t) - bl(0))} \cdot (q_{bl,f} - q_{bl,0}) - q_{Comp} - q_{Dos} \quad (D-12)$$

Generally the unknown function $bl(t)$ is approximated as follows:

- ❖ Equal to the volume of the reaction mixture calculated by the known quantities of reactants dosed during the reaction. This should compensate the change of the heat-transfer area A in q_{Flow} (see 2.1.3.1). Generally it has to be assumed that the volumes are additive.
- ❖ Equal to an online measured or estimated viscosity. This should compensate for changes of the overall heat transfer U in q_{Flow} (see 2.1.3.1).
- ❖ Any arbitrary mathematical function e.g. a straight line between $q_{bl,0}$ and $q_{bl,f}$.
- ❖ If the reaction kinetics is known, equal to the chemical conversion of the reaction.

As with the new calorimeter the baseline is directly measured by means of the Peltier elements and the additional measured heat flow $q_{Cooling}$, the task of generating a feasible baseline is not necessary.

E APPLICATIONS: EXPERIMENTAL PROCEDURES AND ADDITIONAL CALCULATIONS

E.1 Neutralization of NaOH with H₂SO₄

E.1.1 Experimental conditions

Initially 26 ml of NaOH (2.77N, 72mmol NaOH) were filled into the reactor. The jacket temperature was set to 0 °C and the reactor temperature was set to 25 °C. Afterwards H₂SO₄ was dosed into the closed reactor (see Table E-1). The stirrer speed was set to 400 rpm. The experiment was repeated three times (see Table E-2). The reaction conditions were chosen similar to the ones reported by [Schildknecht 81].

At the beginning and at the end of each reaction experiment the calibration experiments for the Peltier parameters were carried out (total duration about one hour) as described in Appendix D.1. The calibration experiments were only started when the reactor was in thermal equilibrium.

Table E-1: Different dosing settings for the neutralization experiments. ¹⁾ Settings at the syringe pump ²⁾ Calculated ³⁾ [Landolt-Börnstein, b]

Feed Type		Type I
Substance		H ₂ SO ₄ (4N)
Syringe Volume [ml]	¹⁾	25
Volume dosed [ml]	¹⁾	14.4
Dosing rate [ml/min]	¹⁾	3.5
Mass dosed [g]	²⁾	16.1
Moles H₂SO₄ dosed [mmol]		28.72
$c_{p,dos}$ [kJ/kgK]	³⁾	3.61
$c_{p,dos} \cdot f$ Eq. (2-4) [J/sK]		0.235

Table E-2: Experimental conditions for the neutralization experiments. ¹⁾ Set Point. ²⁾ Measured $(T_{Pelt}^{up} + T_{Pelt}^{down}) / 2$. ³⁾ See Table E-1. ⁴⁾ Used for the identification of reaction parameters. ⁵⁾ Used for the determination of the Peltier parameter set A (see D.1).

Experiment Name	T_r ¹⁾ °C	T_j ¹⁾ °C	T_{Cry} ¹⁾ °C	T_{Pelt} ²⁾ K	Feed Type ³⁾	Evaluation ⁴⁾	Peltier ⁵⁾
NaOHN1 25	25	0	5	276.5	I	✓	✓
NaOHN2 25	25	0	5	276.5	I	✓	✓
NaOHN3 25	25	0	5	276.5	I	✓	✓

Infrared Settings:

No infrared measurements were carried out.

Calorimeter Settings:

Cooling liquid: Water.

Peltier Parameter Set: Set A Appendix D.1

ΔT_{Pelt} (see Appendix D.1): 0.05 K

Filter settings: see Chapter 3.7.4

k_{Loss} settings: see Appendix D.2

Controller settings: see 3.6, Point ⑥ in Figure 3-15 was chosen 3 min after the end of the dosing.

E.2 Hydrolysis of Acetic Anhydride

E.2.1 Experimental conditions

First the reactor was brought to the desired jacket temperature T_j after being cleaned and purged with N_2 . After some minutes a reference background spectrum for the infrared measurement was taken. Then 35 ml of 0.1N HCl (Titrisol, Merck) were added to the reactor, the stirrer was turned on to 400 rpm and the desired reaction temperature T_r was set. Afterwards a mixture of acetic anhydride from Fluka (purum) and acetic acid from Scharlau were dosed into the closed reactor (see Table E-3). The acetic anhydride was fed together with acetic acid in order to increase the solubility of acetic anhydride in water. This experiment was carried out 8 times at $T_r = 25$ °C (including two experiments with different dosing settings), 4 times at $T_r = 40$ °C and 5 times at $T_r = 55$ °C (see Table E-4).

At the beginning and at the end of each reaction experiment the calibration experiments for the Peltier parameters were carried out (total duration about one hour) as described in D.1. The calibration experiments were only started when the reactor was in thermal equilibrium.

The reaction conditions were chosen similar to the ones reported by [Becker et. al. 65] to be able to compare the heat of mixing which depends on the chosen concentrations.

Table E-3: Different dosing settings for the acetic anhydride hydrolysis experiments. ¹⁾ Settings at the syringe pump. ²⁾ Experimentally determined. ³⁾ Calculated using the mass fractions and the heat capacities of the pure components

Feed Type		Type I	Type II	Type III
Substance		Mixture AcOAc / AcOH (334 : 277g)	Mixture AcOAc / AcOH (334 : 277g)	Mixture AcOAc / AcOH (334 : 277g)
Syringe Volume [ml]	¹⁾	2.5	2.5	5
Volume dosed [ml]	¹⁾	2	2	5
Dosing rate [ml/min]	¹⁾	5	3	3
Mass dosed [g]	²⁾	1.99 ± 0.01(0.5%)	1.99 ± 0.01(0.5%)	5.15 ± 0.02(0.3%)
Moles AcOAc dosed [mmol]		10.68	10.68	27.6
$c_{p,dos}$ [kJ/kgK]	³⁾	1.83	1.83	1.83
$c_{p,dos} \cdot f$ Eq. (2-4) [J/sK]		0.152	0.0912	0.0943

Table E-4: Experimental conditions for the acetic anhydride hydrolysis experiments. ¹⁾ Set Point ²⁾ Measured $(T_{Pelt}^{up} + T_{Pelt}^{down}) / 2$ ³⁾ See Table E-3 ⁴⁾ Used for the identification of reaction parameters, evaluation set I and II ⁵⁾ Used for the determination of the peltier parameter set A (see D.1). ⁶⁾ Only used for the classic determination of ΔH by integration (see E.2.4.1).

Experiment Name	T_r	T_j	T_{Cry}	T_{Pelt}	Feed Type	Eval. Set I	Eval. Set II	Peltier
	¹⁾ °C	¹⁾ °C	¹⁾ °C	²⁾ K	³⁾	⁴⁾	⁴⁾	⁵⁾
AcOAcN1 25	25	20	5	285.9	I	✓	✓	✓
AcOAcN4 25	25	20	5	285.9	I	✓	✓	✓
AcOAcN5 25	25	20	5	285.9	I	✓	✓	✓
AcOAcN8 25	25	20	5	285.9	I	✓	✓	✓
AcOAcN9 25	25	20	5	285.9	I	✓	✓	✓
AcOAcN10 25	25	20	5	285.9	I	✓	✓	✓
AcOAcN14 25	25	20	5	285.9	II	✓	✓	✓
AcOAcN15 25	25	20	5	285.9	III	✓ ⁶⁾		✓
AcOAcN11 40	40	33	5	292.5	I	✓	✓	✓
AcOAcN12 40	40	33	5	292.5	I	✓	✓	✓
AcOAcN13 40	40	33	5	292.5	I	✓	✓	✓
AcOAcN17 40	40	33	5	292.5	I	✓	✓	✓
AcOAcN2 55	55	45	5	298.6	I			✓
AcOAcN3 55	55	45	5	298.6	I	✓	✓	✓
AcOAcN6 55	55	45	5	298.6	I	✓	✓	✓
AcOAcN7 55	55	45	5	298.6	I	✓	✓	✓
AcOAcN16 55	55	45	5	298.6	I	✓	✓	✓

Infrared Settings:

Resolution: 4 cm⁻¹, *Zero filling:* 2, *Apodization:* Blackman-Harris 3-Term

Scan Mode: Double-Sided; Forward-Backward

Number of samples for the background measurement: 50

Temperature of the probe during the background measurement (25, 40, 55 °C):
20, 33, 45 °C (equal to T_j)

Number of samples for a reaction measurement: 15

Time required for a reaction measurement: 11.5 s

Sampling Time for the infrared measurement according to Figure 3-15:

Baseline: 4 min, 8 samples (2 samples / min)

Dosing period: 4 samples (4.4 samples / min)

Main Conversion (25, 40, 55 °C): 20, 20, 15 min, 40, 40, 45 samples (2, 2, 3 samples / min)

Reaction tail (25, 40, 55 °C): 0.5, 0.5, 1 samples / min

Calorimeter Settings:

Cooling liquid: Water.

Peltier Parameter Set: Set A Appendix D.1

$\Delta\Delta T_{Pelt}$ (see Appendix D.1): 0.05 K

Filter settings: see Chapter 3.7.4

k_{Loss} settings: see Appendix D.2

Controller settings: see Chapter 3.6, Point ⑥ in Figure 3-15 was chosen 20, 20, 25 (25, 40, 55 °C) min after the end of the dosing.

Additional dosing experiments:

As mentioned in Chapter 3.4.3.2, the temperature of the dosing liquid is measured inside the feed tube. If the heat capacity of the feed is known, the heat flow introduced by the dosing feed can be calculated according to Equation (2-4). In order to measure the accuracy of this approach three test experiments at $T_r = 25, 40$ and 55 °C were carried out analogous to the hydrolysis experiments explained above. However 35 ml of the acetic acid / acetic anhydride mixture were filled into the reactor as starting material and the same mixture was dosed (see Table E-3). The heat flow q_{Dos} was determined identically as for the hydrolysis experiments.

E.2.2 Pretreatment of the infrared data

E.2.2.1 Baseline correction and spectral region selection

Figure E-1 shows a raw measured reaction spectrum (reaction at 25°C). The initial absorbance is subtracted from the reaction spectrum in order to highlight the absorbance changes that occur during the reaction. Positive peaks indicate appearing products or mean products and negative peaks vanishing educts. As the educt (acetic anhydride) was dosed) no negative peaks are visible. Prior to all evaluations, the measured spectroscopic data was baseline-corrected as explained in Chapter 4.4.1.1. For the determination of the baseline, the absorbance profiles at four wave numbers were averaged (indicated in Figure E-1 and shown in Figure E-2). The resulting baseline-corrected spectrum is shown in Figure E-3 and Figure E-4. For all calculations described in Chapters 5.3.1 and 5.3.2 only the regions from 950 ... 1480 cm^{-1} and 1600 ... 1800 cm^{-1} were used.

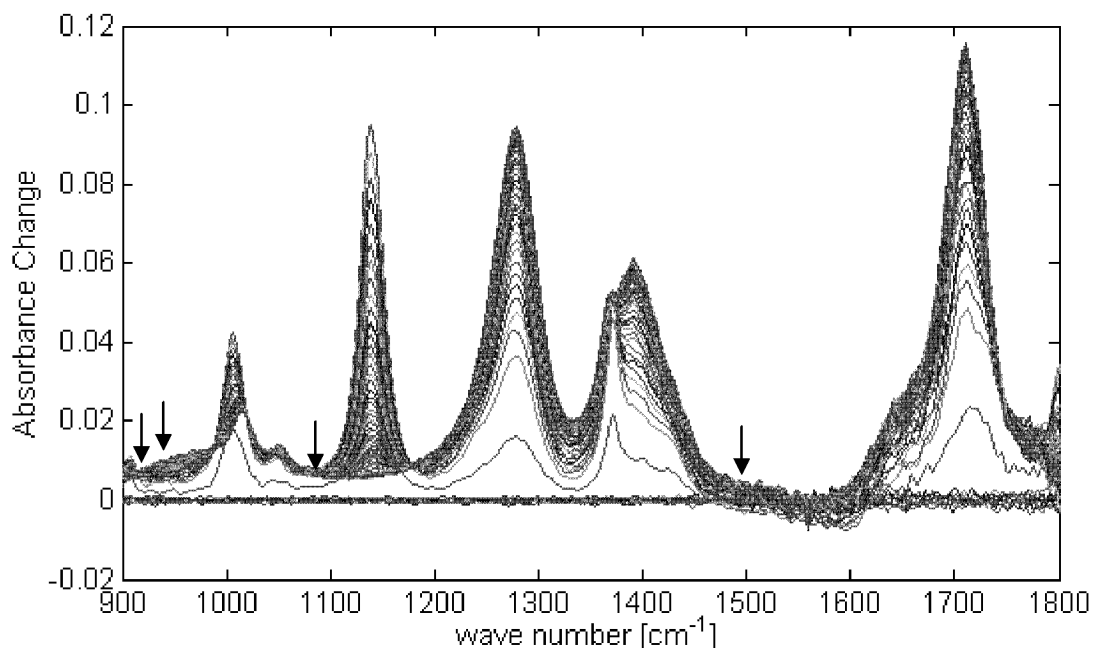


Figure E-1: Measured reaction spectrum of an acetic anhydride hydrolysis experiment at 25°C. The initial absorbance is subtracted from the spectrum. The wave numbers of the spectrum, used for the baseline calculation, are indicated with arrows (compare to Figure E-2).

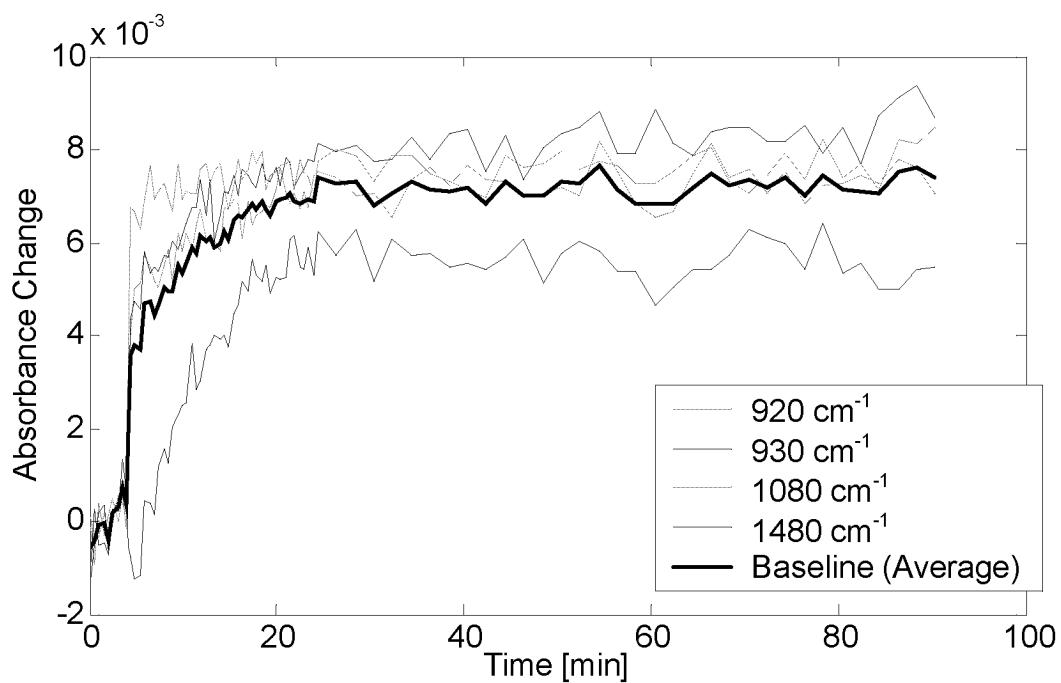


Figure E-2: Absorbance profiles of the wave numbers in A_{Data} selected to calculate the baseline (compare to Figure E-1).

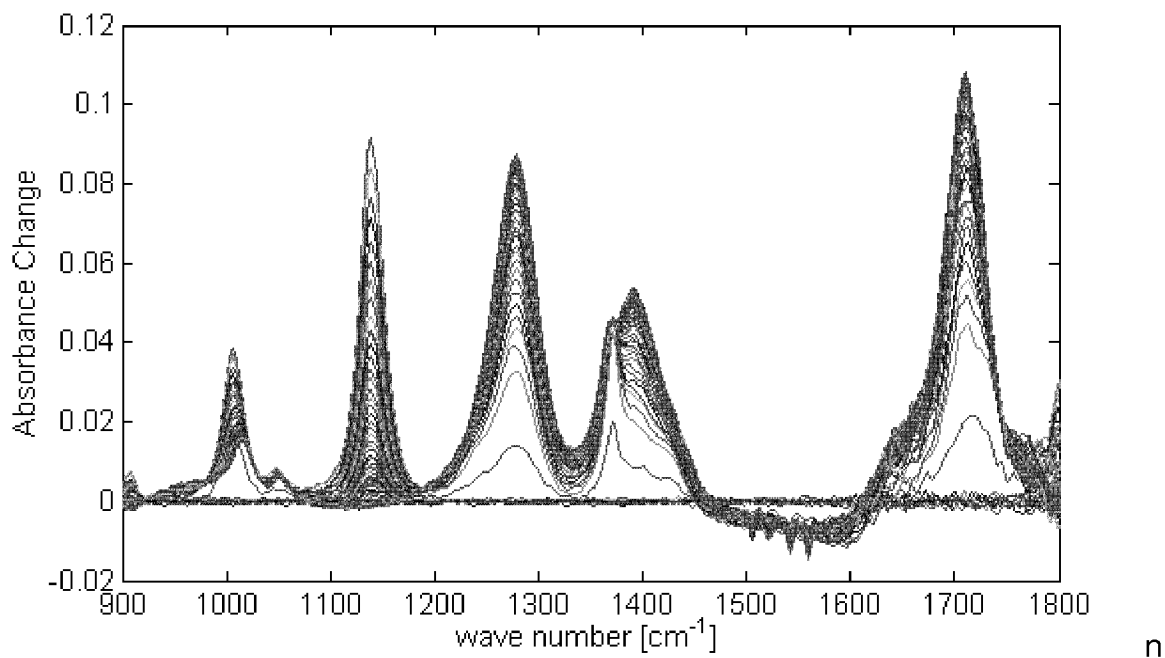


Figure E-3: Baseline-corrected reaction spectrum of an acetic anhydride hydrolysis experiment at 25 °C. The initial absorbance is subtracted from the spectrum.

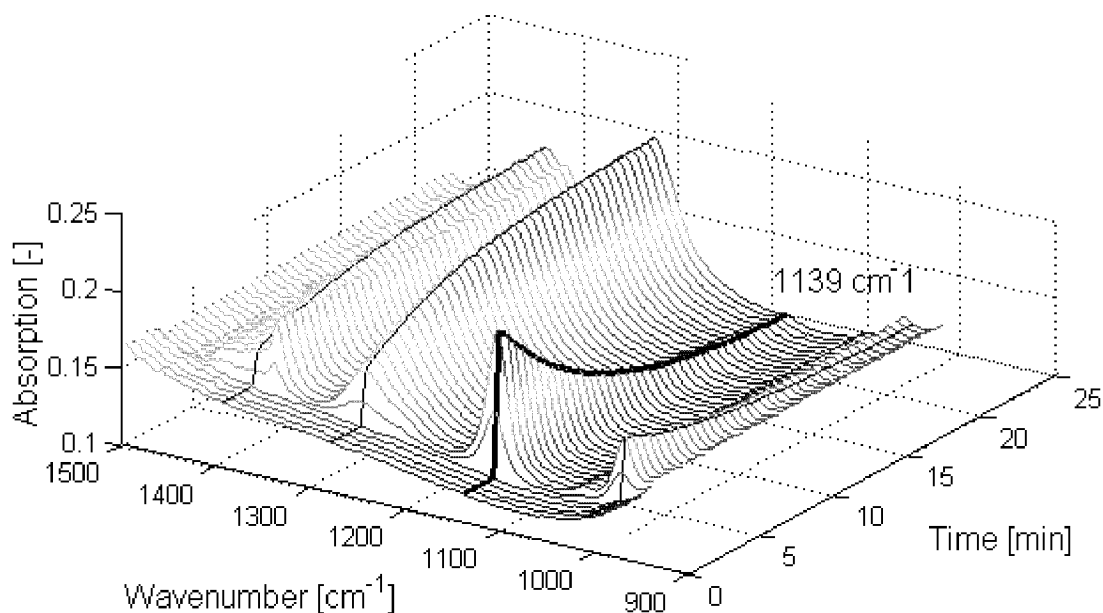


Figure E-4: Part of the reaction spectrum of an acetic anhydride hydrolysis experiment at 25 °C. The spectrum is baseline corrected. The peak at 1139 cm⁻¹ is indicated with a fat line and was used for the classical determination of the rate constant (see Appendix E.2.4.3). It was also used to judge the fit quality of the infrared evaluation (see Chapter 5.3.1).

E.2.2.2 Resampling and exclusion of data points

No resampling of the data is required. The sampling defined in Appendix E.2.3 was used. In none of the evaluation data sets I and II (see Table E-4) data points were excluded.

E.2.3 Pretreatment of the calorimetric data

As explained in Chapter 4.4.2 the only pretreatment applied to the calorimetric data is resampling and exclusion of data points. Two data sets I and II are required for the later evaluation. The experiments included in these data sets are indicated in Table E-4. The two data sets only differ in the number of points that are excluded. They are described in Table E-5 and Table E-6 according to Figure 3-15

Table E-5: Resampling and data exclusion settings for the evaluation data set I.

	25 °C	40 °C	55 °C
Number of baseline points	10	10	10
Duration of the baseline [min]	6	6	6
Number of points during the dosing	20	20	20
Number of points during the main conversion part	70	70	70
Duration of the main conversion part [min]	20	10	5
Number of points during the reaction tail	30	30	30
Duration of the reaction tail [min]	20	10	5
Exclusion before the dosing [min]	0.5	0.5	0.5
Exclusion during the dosing	all	all	all
Exclusion after the dosing [min]	1	1	0.5
Total number of points	130	130	130

Table E-6: Resampling and data exclusion settings for the evaluation data set II.

	25 °C	40 °C	55 °C
Number of baseline points	10	10	10
Duration of the baseline [min]	6	6	6
Number of points during the dosing	10	10	10
Number of points during the main conversion part	80	80	80
Duration of the main conversion part [min]	20	10	5
Number of points during the reaction tail	30	30	30
Duration of the reaction tail [min]	20	10	5
Exclusion before the dosing [min]	0	0	0
Exclusion during the dosing	none	none	none
Exclusion after the dosing [min]	0	0	0
Total number of measurement points	130	130	130

E.2.4 Classical, separate evaluation of the infrared and calorimetric data

E.2.4.1 Evaluation of the calorimetric data

In the following the total power release or uptake measured by the calorimeter (q_{tot}) will also be called q_{React}^{tot} as it contains mainly two different heat flows: 1) the reaction power (q_{React}) and the heat of mixing (q_{mix}) during the dosing period. q_{React}^{tot} is always calculated based on the measured data using Equation (3-23). For this classical evaluation no data pretreatment (see Appendix E.2.3) was applied. The two evaluation concepts applied are similar to principle B and C described in Chapter 2.3.2.2.

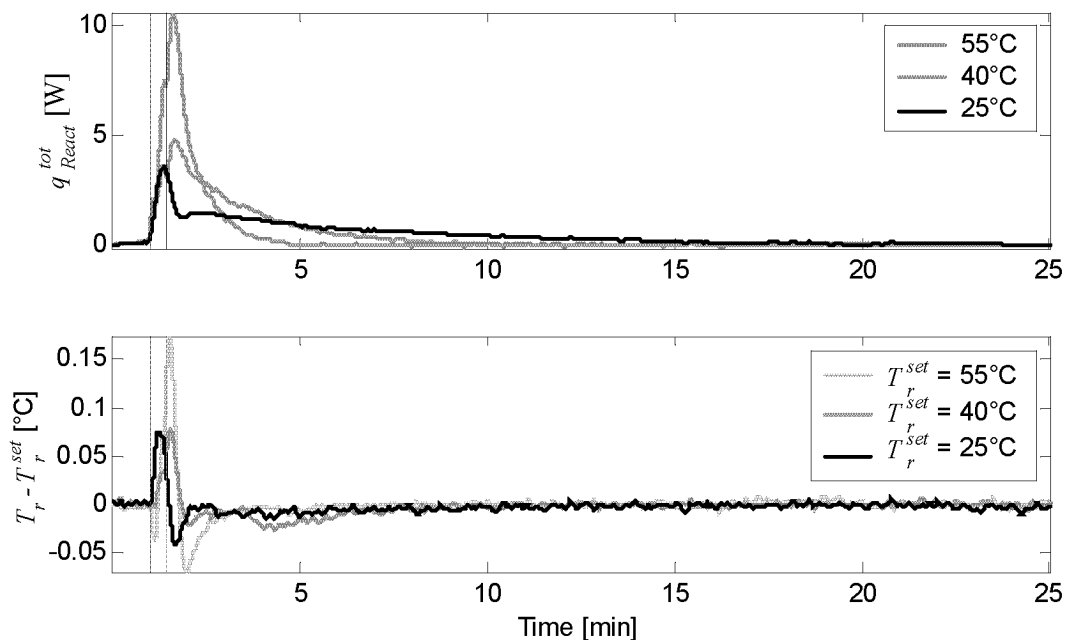


Figure E-5: Reaction power (q_{React}^{tot}) of the hydrolysis of acetic anhydride measured at 25, 40 and 55 °C. The dosing period of the mixture of acetic anhydride and acetic acid is indicated with dashed lines.

The hydrolysis of acetic anhydride (Figure 5-3) was chosen as a reference reaction because many literature data are available. The measured reaction power as a function of time (q_{React}^{tot}) at $T_r = 25, 40$ and 55 °C is shown in Figure E-5 together with the deviation of the reactor temperature from the set point. The q_{React}^{tot} curve of the measurement at 25 °C shows a significant peak at the beginning of the reaction. As reported by [Becker et. al. 65] and [Köhler et. al. 73] this initial exothermal heat flow corresponds to the heat of mixing released during the dosing phase. According to both authors the reaction kinetics of the hydrolysis in diluted aqueous solution is of the following type:

$$-\frac{dc_{AcOAc}}{dt} = (k' + k'' \cdot c_{H^+}) \cdot c_{AcOAc} \quad (E-1)$$

As the reaction is carried out in 0.1M HCl and acetic acid is also part of the feed the reaction kinetics is assumed to be of pseudo first order [Becker et. al. 65], [Köhler et. al. 73].

$$-\frac{dc_{AcOAc}}{dt} = k \cdot c_{AcOAc} \quad (E-2)$$

According to Equation (E-2) [Becker et. al. 65] and [Becker et. al. 67] could separate the observed heat of mixing at the beginning of the experiment from the reaction power. At 25 °C the heat of mixing is reported as -5 kJ/mol and the reaction enthalpy for the first order reaction as -57 kJ/mol [Becker et. al. 65] and [Becker et. al. 67]. Similar to this procedure the measurements done with the new calorimeter were evaluated in order to be able to split the total measured enthalpy (ΔH [J/mol]) into the enthalpy of reaction ($\Delta_r H$ [J/mol]) and the heat of mixing (Q_{mix} [J/mol]):

$$Q_{tot} = n \cdot \Delta H = n \cdot [\Delta_r H + Q_{mix}] \quad (E-3)$$

Where Q_{tot} is the total measured heat production / consumption by the calorimeter [J] (Equation (2-21)) and n the moles of acetic anhydride [mol]. Therefore in a first step the first order rate constant k of Equation (E-2) was calculated by linear regression of the natural logarithms of q_{React}^{tot} versus time. The time intervals used for regression were [4; 14], [2; 9], and [2.2; 3.8] min after the start of the reaction for the measurements at 25, 40 and 50°C, respectively.

The first order rate constant at 25 °C was determined to be $3.0 \pm 0.2 \cdot 10^{-3} \text{ s}^{-1}$ and is in good agreement with the value of $2.76 \pm 0.06 \cdot 10^{-3} \text{ s}^{-1}$ reported by [Martin 75] who carried out the experiments under the same conditions. The determination of the rate constant was repeated for the measurements at 40 °C and 55 °C. From the values determined at three different temperatures the activation energy E_A was determined with an Arrhenius plot (see Figure E-8 , thermal measurements) to be 57 kJ/mol and is again in good agreement with the literature value of 57 kJ/mol [Martin 75].

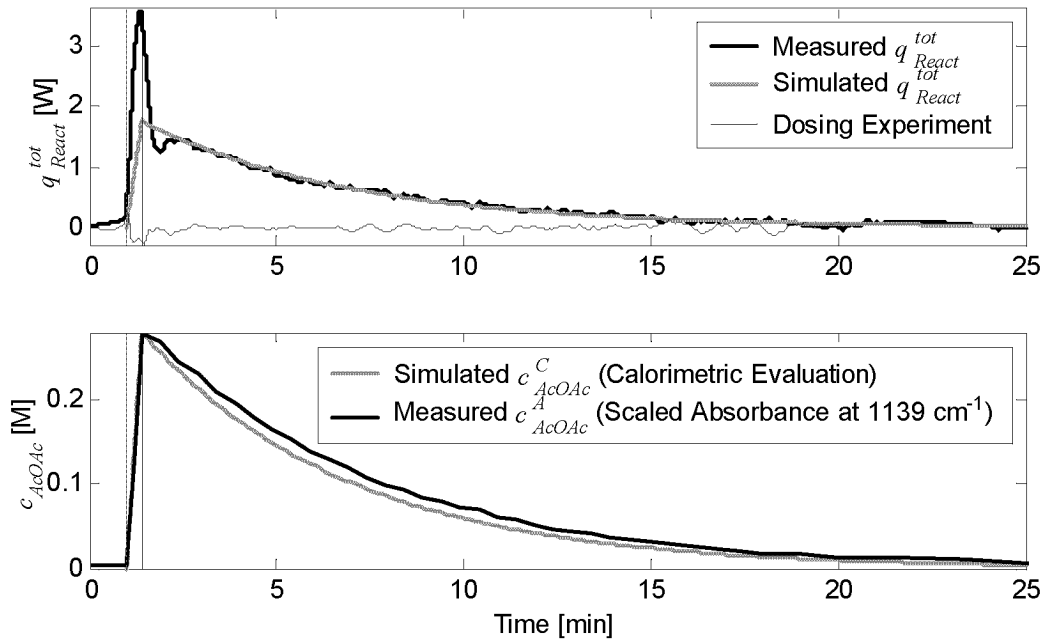


Figure E-6: Evaluation of the reaction power during the initial phase of the acetic anhydride hydrolysis reaction at $T_r = 25$ °C. The thin black line in the first plot shows the reaction power measured if a mixture of acetic anhydride and acetic acid is dosed into the same mixture without any reaction. The second plot shows the concentration time curve of acetic anhydride simulated with the parameters obtained from the calorimetric measurement compared to the one determined from the IR measurement at 1139 cm^{-1} . The dosing period of the mixture of acetic anhydride and acetic acid is indicated with dashed lines.

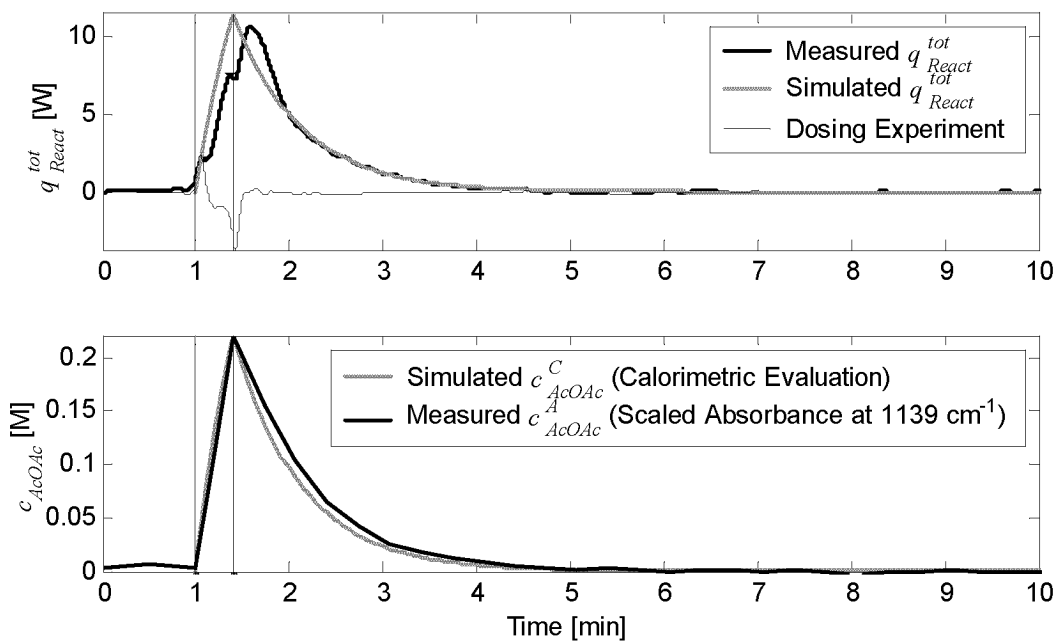


Figure E-7: Evaluation of the acetic anhydride hydrolysis experiments conducted at $T_r = 55$ °C. See Figure E-6 for further details.

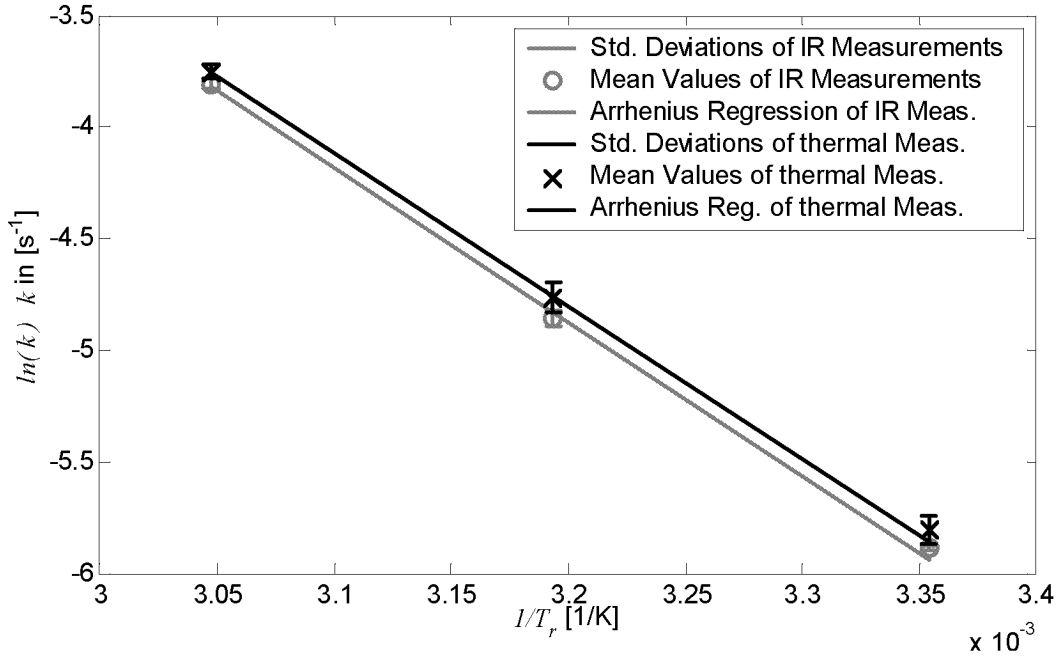


Figure E-8: Arrhenius plot of the rate constants determined at 25, 40 and 55 °C for the acetic anhydride hydrolysis reaction. The evaluation was done independently for the IR measurements and the calorimetric measurements.

As the rate constants are now known the following simple mass and energy balances can be made to describe the power of the hydrolysis reaction:

$$\frac{dn_{AcOAc}}{dt} = -k \cdot n_{AcOAc} + v_{dos} \cdot c_{dos} \quad \frac{dV_r}{dt} = v_{dos} \quad (E-4)$$

$$q_{react} = k \cdot n_{AcOAc} \cdot (-\Delta_r H) \quad (E-5)$$

Where n_{AcOAc} are the moles of acetic anhydride inside the reactor, v_{dos} the dosing rate [l/s], V_r the reactor volume [l] and c_{dos} the concentration of acetic anhydride in the feed [mol/l]. Using a linear least-squares approach the calculated n_{AcOAc} is then fitted according to Equation (E-5) into the measured q_{React}^{tot} curves and $\Delta_r H$ for the assumed first order reaction is identified (see Figure E-6 and Figure E-7 first plot, grey line):

$$\min_{\Delta_r H} \left(\sum_{i=1}^{N_t} \left(n_{AcOAc} \cdot k \cdot (-\Delta_r H) - q_{React}^{tot\ i} \right)^2 \right) \quad (E-6)$$

Where $q_{React}^{tot\ i}$ is the i 'th measurement point of the measured reaction power. Not all measurement points of q_{React}^{tot} were used to carry out this linear regression because in particular the initial phase is influenced by the heat of mixing. The time intervals used to identify $\Delta_r H$ were [4; 20], [3; 9], and [2.2; 3.8] min after the start of the reaction for the measurements at 25, 40 and 55°C, respectively. The estimated values for $\Delta_r H$ are shown in Table E-7. The direct integration of the q_{React}^{tot} curves shown in Figure E-5 gives the total enthalpy (ΔH), including the heat of mixing. These values are summarized in Table E-7 as well. According to [Becker et. al. 65] the difference

between ΔH and $\Delta_r H$ corresponds to the heat of mixing. These values are also shown in Table E-7 as Q_{mix} . All the literature values cited in Table E-7 were measured under the same conditions as applied for the experiments reported here. Many more literature references for the reaction enthalpy of this hydrolysis reaction example exist. However they were all measured at different concentration conditions and can thus not be compared to each other.

The total enthalpy ΔH measured at 25 °C is -60 ± 5 kJ/mol and is in good agreement with the mean value of -63 ± 2 kJ/mol reported in the literature (see Table E-7). The reaction enthalpy assuming first order kinetics ($\Delta_r H$) measured at 25 °C is -57 ± 1 kJ/mol and is also in good agreement with the literature reference of -57 kJ/mol. However, the estimated value of $\Delta_r H$ at 40 °C which is -62 ± 2 kJ/mol shows that the method to estimate $\Delta_r H$ based on Equation (E-6) is less accurate than the standard deviations of $\Delta_r H$ at 25, 40, and 50 °C suggest. The value estimated for Q_{mix} at 25 °C is -3 kJ/mol and is also on the order of the literature reference, which is -5 kJ/mol.

The measured values of ΔH (see Table E-7) seem to imply a temperature dependency. If the reaction enthalpy at 55 °C was calculated based on the value determined at 25 °C and the heat capacities of the pure components of the reaction (assumed to be constant between 25 to 55 °C), the value of ΔH would only change by 0.1 kJ/mol. The observed temperature dependency of ΔH is not visible for the values of $\Delta_r H$. Therefore it was concluded that the measured temperature dependency of ΔH might be caused by the heat of mixing included in ΔH . As shown in Table E-7 the estimated heat of mixing (Q_{mix}) shows a decreasing tendency from 25 to 55°C and could explain the observed temperature decrease of ΔH . However, a clear conclusion can not be drawn since the heat of mixing determined is of the same order of magnitude as the standard deviations of the measured reaction enthalpy. [Domenico et. al. 01] also reports that the heat of mixing is decreasing with increasing temperature in the range of 5 to 40 °C and change from exothermal to endothermal. As these experiments were carried out in another concentration region the absolute values cannot be compared. [Martin 75] reports only the total enthalpy (including the heat of mixing and the reaction enthalpy) in the range of 15 to 35°C (Table E-7) and does not observe such a change.

Table E-7: Summary of the results for the hydrolysis reaction of acetic anhydride using classical evaluation techniques. ^{a)} ΔH includes the heat of mixing. It is calculated by integration of q_{tot} (Equation (2-21), integration time = 60 min). The total integration time was 60 min for all experiments. ^{b)} $\Delta_r H$ is the reaction enthalpy assuming a first-order kinetic without heat of mixing. It is calculated similar to the principle C in Chapter 2.3.2.2, requiring the rate constant k . ^{c)} Determined by dosing a mixture of acetic anhydride and acetic acid into the same mixture (see Appendix E.2.4.2). ^{d)} Standard deviations were determined from 7 (25 °C), 4 (40 °C) and 4 (55 °C) measurements. ^{e)} Determined independently from ΔH and $\Delta_r H$, according to principle B in Chapter 2.3.2.2. ^{f)} Calculation corresponding to Chapter 2.3.3.2. ^{g)} [Köhler et. al. 73] ^{h)} [Martin 75] ⁱ⁾ [Becker et. al. 65] ^{j)} [Becker et. al. 67] ^{k)} Calculated based on tabulated standard enthalpies of formation [NIST]. ^{l)} Calculated based on tabulated standard enthalpies of formation [CRC]

T_r [°C]	This work			Literature			
	25	40	55	0	15	25	35
ΔH [kJ/mol] ^{a)}	-60 ± 5 ^{d)}	-59 ± 5	-57 ± 2	-57 ^{g)}	-59 ^{h)}	-65 ^{g)} -62 ^{i, j)} -61 ^{h)}	-59 ^{h)}
$\Delta_r H$ [kJ/mol] ^{b)}	-57 ± 1 ^{d)}	-62 ± 2	-60 ± 1	-	-	-57 ^{i, j)} -56 ^{k)} -58 ^{l)}	-
Q_{mix} [kJ/mol]	-3	+3	+3	-	-	-5 ^{i, j)}	-
error of q_{Dos} [kJ/mol] ^{c)}	± 0.5	± 1.7	± 2.1	-	-	-	-
k [10^{-3} s^{-1}] calorimetric data ^{e)}	3.0 ± 0.2 ^{d)}	8.5 ± 0.6	23.5 ± 0.8			2.76 ± 0.06 ^{h)}	
k [10^{-3} s^{-1}] infrared data ^{f)}	2.8 ± 0.2 ^{d)}	7.8 ± 0.3	22.2 ± 0.5				
E_A [kJ/mol] calorimetric data		57				57 ^{h)}	
E_A [kJ/mol] infrared data		57					

E.2.4.2 Evaluation of the dosing experiments

For semi-batch experiments it is important to consider the heat flow during the dosing phase caused by the feed (q_{Dos} , Equation (2-4)). Therefore the temperature of the feed (T_{Dos}) when it drops into the reaction liquid has to be measured as exactly as possible. As mentioned before (see Chapter 3.4.3.2) the measurement of T_{Dos} was done with a small thermocouple inserted into the dosing tube. In order to estimate the accuracy of this correction the same amount of mixture of acetic anhydride and acetic acid as used for the hydrolysis experiments was dosed into 35 ml of the same mixture. If the correction of q_{Dos} would be accurate, the calculated q_{tot} (by Equation (3-23)) should be zero during the whole experiment. The result of this experiment is shown in Figure E-6 and Figure E-7 (first plot, thin black line, q_{React}^{tot} equals q_{tot}). The integration of the q_{tot} curve of such dosing experiments gives 0.5, 1.7 and 2.1 kJ/mol at 25, 40 and 55 °C, respectively (see also Table E-7). When compared to the standard deviations of the determined heats of reaction ΔH (5, 5 and 2 kJ/mol) they become increasingly significant for an increasing temperature difference between T_{Dos} and T_r .

E.2.4.3 Evaluation of the infrared data

The hydrolysis reaction was further observed with the integrated IR-ATR-probe as for each measurement a simultaneous infrared spectrum was recorded. The reaction spectra, used for the evaluation shown in this Chapter, were first pretreated as described in Appendix E.2.2.1. A typical reaction spectrum is shown in Figure E-4.

The easiest and most efficient way to evaluate such a reaction spectrum is to find a wave number where only one component is absorbing (see Chapter 2.3.3.2). For simple reaction systems, such as the hydrolysis of acetic anhydride, there are generally several of these pure wave numbers. To determine the first-order rate constant on the basis of the infrared measurements the peak at 1139 cm^{-1} (see Figure E-5), which corresponds to the C-O-C stretch vibration of acetic anhydride, was chosen. The second plots of Figure E-6 and Figure E-7 show the absorbance profiles at 1139 cm^{-1} converted to concentration units (c^A_{AcOAc}). The conversion was done according to the following Equation:

$$c^A_{AcOAc} = (A_{AcOAc} - A_{AcOAc}^{final}) \cdot \frac{\max(c^C_{AcOAc})}{\max(A_{AcOAc} - A_{AcOAc}^{final})} \quad (\text{E-7})$$

Where c^C_{AcOAc} is the concentration profile of acetic anhydride (simulated using the rate constant determined on the basis of the thermal measurements), A_{AcOAc} the absorbance profile at 1139 cm^{-1} and A_{AcOAc}^{final} the absorbance at 1139 cm^{-1} at the end of the reaction. Figure E-6 and Figure E-7 show that c^A_{AcOAc} and c^C_{AcOAc} are in good agreement. Similar to the thermal evaluation (see Appendix E.2.4.1), the reaction rate constant k can be determined from c^A_{AcOAc} by a linear regression of $\ln(c^A_{AcOAc})$ vs. time. The regression was done for the same time period as was used for the regression of the thermal measurements. The first-order rate constant at $25\text{ }^\circ\text{C}$ was determined to be $2.8 \pm 0.2 \cdot 10^{-3}\text{ s}^{-1}$ and is in good agreement with the value determined from the calorimetric measurements ($3.0 \pm 0.2 \cdot 10^{-3}\text{ s}^{-1}$). The determination of the rate constant was repeated for the measurements at 40 and $55\text{ }^\circ\text{C}$ (see summary in Table E-7). From these values the activation energy E_A was calculated with an Arrhenius plot (see Figure E-8, IR measurements) to be 57 kJ/mol . It is in good agreement with the value determined from the thermal measurements (57 kJ/mol). Comparing the measured reaction power q_{React}^{tot} at $25\text{ }^\circ\text{C}$ with c^A_{AcOAc} (see Figure E-6) it is apparent that the initial peak of the q_{React}^{tot} curve is not visible in the infrared signal and is therefore not related to the chemical reaction but rather to the heat of mixing. Obviously even in this simple case the simultaneous measurement of a different signal than the thermal reaction power is able to reveal effects that are not related to the reaction power.

E.3 Epoxidation of 2,5-di-tert-butyl-1,4-benzoquinone

E.3.1 Experimental conditions

After the reactor was cleaned, evacuated and purged with N₂, 1.29g of 2,5-di-tert-butyl-1,4-benzoquinone (Aldrich, 5.85 mmol) were added. Care was taken that the benzoquinone did not touch the ATR Sensor (otherwise the background spectrum might be influenced by this substance). Then the reactor was brought to the desired jacket temperature T_j . During this period the air inside the reactor was removed by a constant flow of N₂. After some minutes a reference background spectrum for the infrared measurement was taken. Then 19.2 ml Dioxan (Baker), 8ml EtOH (Baker) and tert-butyl hydroperoxide (Aldrich, 70% solution in water, see Table E-8) were added sequently. The stirrer was turned on to 400 rpm and the desired reaction temperature T_r was set. Afterwards the solution was degassed for 3 min with N₂. After the power of the compensation heater did no more change (see Appendix E.3.5), Triton B (Fluka, 40% in methanol) was dosed into the closed reactor to start the reaction.

This experiment was carried at four different temperatures (17, 24, 30 and 36 °C) and at each temperature at least three times (see Table E-9). Three additional experiments at 30°C were carried out with different concentrations (see Table E-9). The reaction conditions were chosen similar to the ones reported by [Mayes *et. al.* 92] to be able to compare the kinetic rate constants.

At the beginning and at the end of each reaction experiment the calibration experiments for the Peltier parameters were carried out (total duration about one hour) as described in Appendix D.1. The calibration experiments were only started when the reactor was in thermal equilibrium.

Table E-8: Dosing settings for the epoxidation experiments. ¹⁾ Settings at the syringe pump. ²⁾ A dead volume of 0.11 ml was added to the syringe pump setting. ³⁾ Calculated. ⁴⁾ The heat capacity of Triton B solution was assumed to be equal to the heat capacity of methanol.

Substance		Triton B Solution (40% in MeOH)
Syringe Volume [ml]	¹⁾	1
Volume dosed [ml]	²⁾	0.8
Dosing rate [ml/min]	¹⁾	2
Mass dosed [g]	³⁾	0.74
Moles Triton B dosed [mmol]	³⁾	1.78
$c_{p,dos}$ [kJ/kgK]	⁴⁾	2.48
$c_{p,dos} \cdot f$ Eq. (2-4) [J/sK]		0.0769

Table E-9: Experimental conditions for the epoxidation experiments. ¹⁾ Set Point. ²⁾ Measured ($T_{Pelt}^{up} + T_{Pelt}^{down}$) / 2. ³⁾ Volume of the hydroperoxide used. ⁴⁾ Moles of the hydroperoxide used. ⁵⁾ Stirrer rate ⁶⁾ Used for the identification of reaction parameters, evaluation sets I and II. ⁷⁾ Used for the determination of the Peltier parameter set B (see Appendix D.1).

Experiment Name	T_r	T_j	T_{Cr}	T_{Pelt}	tert-Butyl Hydro Peroxide		Stirr. Rate	Eval. Set I	Eval. Set II	Pelt.
	¹⁾ °C	¹⁾ °C	¹⁾ °C	²⁾ K	³⁾ ml	⁴⁾ mmol				
EpoxidN4 17	17	5	15	283.5	8	58.5	400	✓		✓
EpoxidN5 17	17	5	15	283.5	8	58.5	400	✓		✓
EpoxidN8 17	17	5	15	283.5	8	58.5	400	✓		✓
EpoxidN13 17	17	5	15	283.5	8	58.5	400	✓		✓
EpoxidN7 24	24	5	15	283.7	8	58.5	400	✓		✓
EpoxidN11 24	24	5	15	283.7	8	58.5	400	✓		✓
EpoxidN15 24	24	5	15	283.7	8	58.5	400	✓		✓
EpoxidN6 30	30	5	10	281.3	8	58.5	400	✓	✓	✓
EpoxidN10 30	30	5	10	281.3	8	58.5	400	✓	✓	✓
EpoxidN14 30	30	5	10	281.3	8	58.5	400	✓	✓	✓
EpoxidN17 30	30	5	10	281.3	5	36.4	400		✓	✓
EpoxidN18 30	30	5	10	281.3	5	36.4	400		✓	✓
EpoxidN19 30	30	5	10	281.3	5	36.4	400		✓	✓
EpoxidN20 30	30	5	10	281.3	8	58.5	300			✓
EpoxidN21 30	30	5	10	281.3	8	58.5	300			✓
EpoxidN9 36	36	10	15	286.3	8	58.5	400	✓		✓
EpoxidN12 36	36	10	15	286.3	8	58.5	400	✓		✓
EpoxidN16 36	36	10	15	286.3	8	58.5	400	✓		✓

Infrared Settings:

Resolution: 4 cm⁻¹, Zerofilling: 2, Apodization: Blackman – Harris 3 Term

Scan Mode: Double-Sided, Forward -Backward

Number of samples for the background measurement: 50

Temperature of the probe during the background measurement (17, 24, 30, 36 °C):

5, 5, 5, 10 °C (equal to T_j)

Number of samples for a reaction measurement: 15

Time required for a reaction measurement: 11.5 s

Sampling Time for the infrared measurement according to Figure 3-15:

Baseline: 6 min, 12 samples (2 samples / min)

Dosing period: 4 samples (4.4 samples / min)

Main conversion: 20 min, 40 samples (2 samples / min)

Reaction tail: 1 samples / min

Calorimeter Settings:

Cooling liquid: Water, alcohol mixture (2:1).

Peltier Parameter Set: Set B Appendix D.1

$\Delta\Delta T_{Pelt}$ (see Appendix D.1): 0.087 K

Filter settings: see Chapter 3.7.4

k_{Loss} settings: see Appendix D.2

Controller settings: see Chapter 3.6, Point ⑥ in Figure 3-15 was chosen 20 min after the end of the dosing.

E.3.2 Pretreatment of the infrared data**E.3.2.1 Baseline correction and spectral region selection**

Figure E-9 shows an example of a raw measured reaction spectrum (reaction at 30°C). The initial absorbance is subtracted from the reaction spectrum in order to highlight the absorbance changes that occur during the reaction. Positive peaks indicate appearing products or mean products and negative peaks vanishing educts. Prior to all evaluations, the measured spectroscopic data was baseline-corrected as explained in Chapter 4.4.1.1. For the determination of the baseline, the absorbance profiles at several wave numbers were averaged (indicated in Figure E-9 and shown in Figure E-10).

The resulting baseline-corrected spectrum is shown in Figure E-11 and Figure E-12 (measurement at 17 °C). For all calculations described in Chapters 5.4.1 to 5.4.4 only the regions from 740 ... 860 cm^{-1} , 1150 ... 1450 and 1580 ... 1780 cm^{-1} were used.

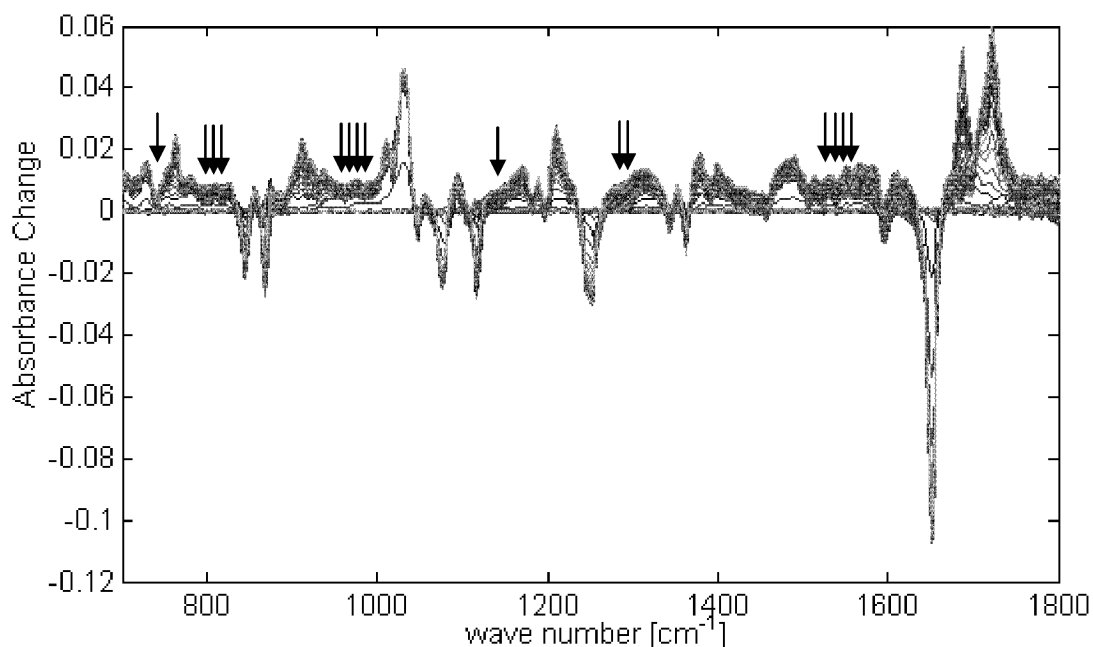


Figure E-9: Measured reaction spectrum of an epoxidation experiment at 30 °C. The initial absorbance is subtracted from the spectrum. The wave numbers of the spectrum, used for the baseline calculation, are indicated with arrows (compare to Figure E-10).

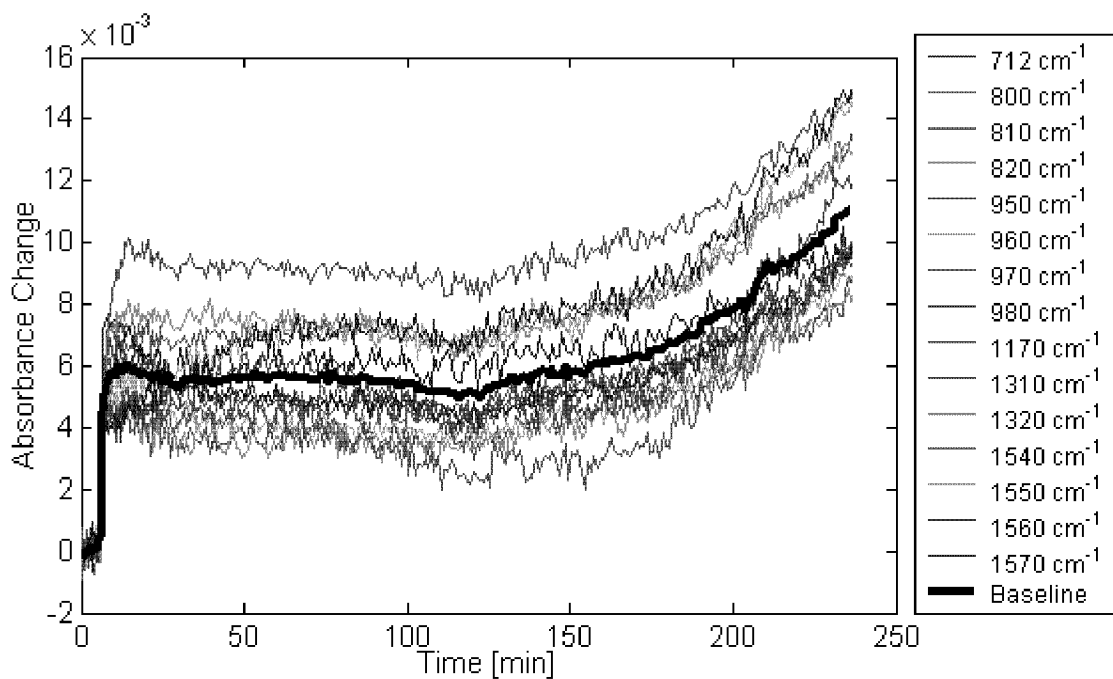


Figure E-10: Absorbance profiles of the wave numbers in A_{Data} selected to calculate the baseline (compare to Figure E-9).

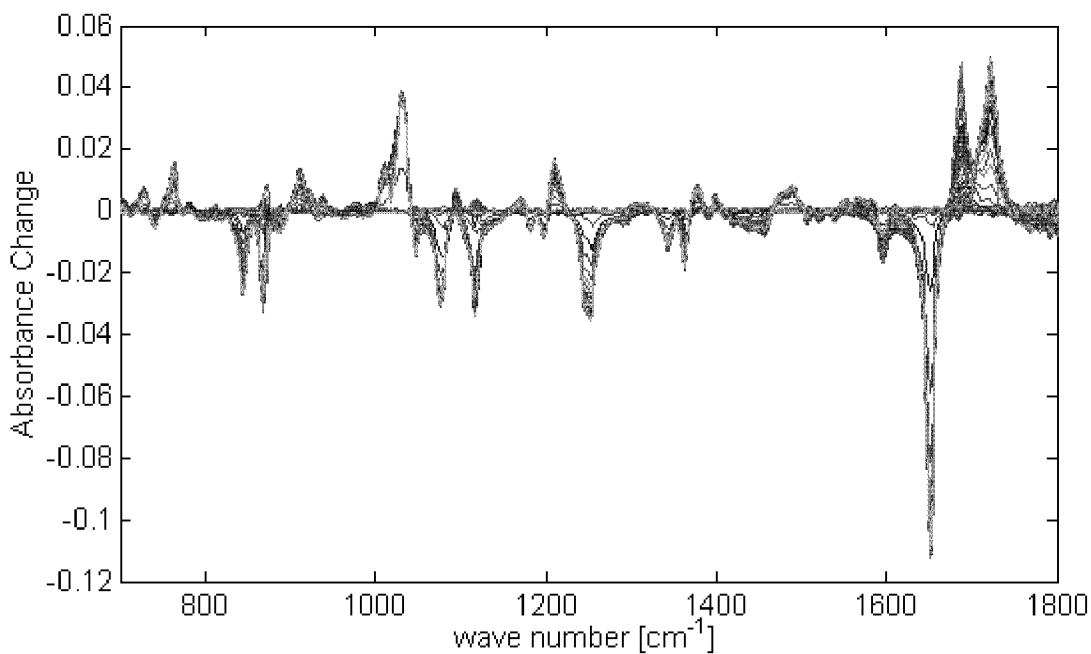


Figure E-11: Baseline-corrected reaction spectrum of an epoxidation experiment at 30 °C. The initial absorbance is subtracted from the spectrum.

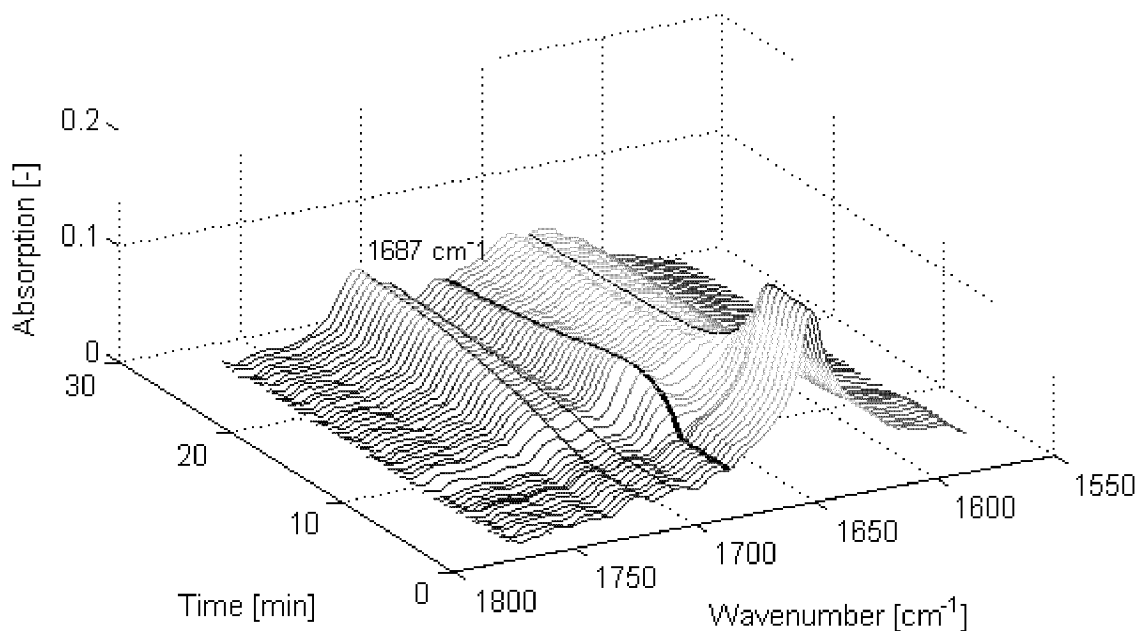


Figure E-12: Part of a reaction spectrum of an epoxidation experiment at 17 °C. The spectrum is baseline-corrected. The peak at 1687 cm^{-1} is indicated with a fat line and will be used to judge the fit quality during the combined evaluation procedure.

E.3.2.2 Resampling and exclusion of data points

No resampling of the data is required. The sampling defined in Appendix E.3.3 was used. In none of the evaluation data sets I and II (see Table E-9) data points were excluded.

E.3.3 Pretreatment of the calorimetric data

As explained in Chapter 4.4.2 the only pretreatment applied to the calorimetric data is resampling and exclusion of data points. Two data sets I and II are required for the later evaluations. The experiments included in these data sets are indicated in Table E-9. The data sets only differ in the included experiments. No measurement points are excluded. Therefore all data sets are described in a single Table E-10 according to Figure 3-15.

Table E-10: Resampling and data exclusion settings for the evaluation data sets I and II. Only data set I contains measurements at 17, 24 and 36 °C.

	17 °C	24 °C	30 °C	36 °C
Number of baseline points	10	10	10	10
Duration of the baseline [min]	6	6	6	6
Number of points during the dosing	20	20	20	20
Number of points during the main conversion part	60	60	60	60
Duration of the main conversion part [min]	25	15	10	10
Number of points during the reaction tale	40	40	40	40
Duration of the reaction tail [min]	95	70	60	60
Exclusion before the dosing [min]	0	0	0	0
Exclusion during the dosing	None	None	None	none
Exclusion after the dosing [min]	0	0	0	0
Total number of points	130	130	130	130

E.3.4 Classical, separate evaluation of the calorimetric data

In the following the total measured heat production / consumption by the calorimeter (q_{tot}) will also be called q_{React}^{tot} . It contains mainly one heat flow, the reaction power (q_{React}). q_{React}^{tot} is always calculated based on the measured data by Equation (3-23). The results shown in this Chapter are based on the evaluation data set I (see Table E-9).

The measured reaction power as a function of time at $T_r = 17, 24, 30$ and 36 °C is shown in Figure E-13 together with the deviation of the reactor temperature from the set point. The control of the reaction temperature was very precise in all cases. A maximum deviation of about 0.3 K was observed for the measurement at 36 °C with a maximum reaction power of about 700 W/l. It was not necessary to feed the catalyst at 0 °C in order to prevent large changes of the reaction temperature, as reported by [Bijlsma et. al. 98], [Hairfield et. al. 85] and [Mayes et. al. 92] who investigated the same reaction.

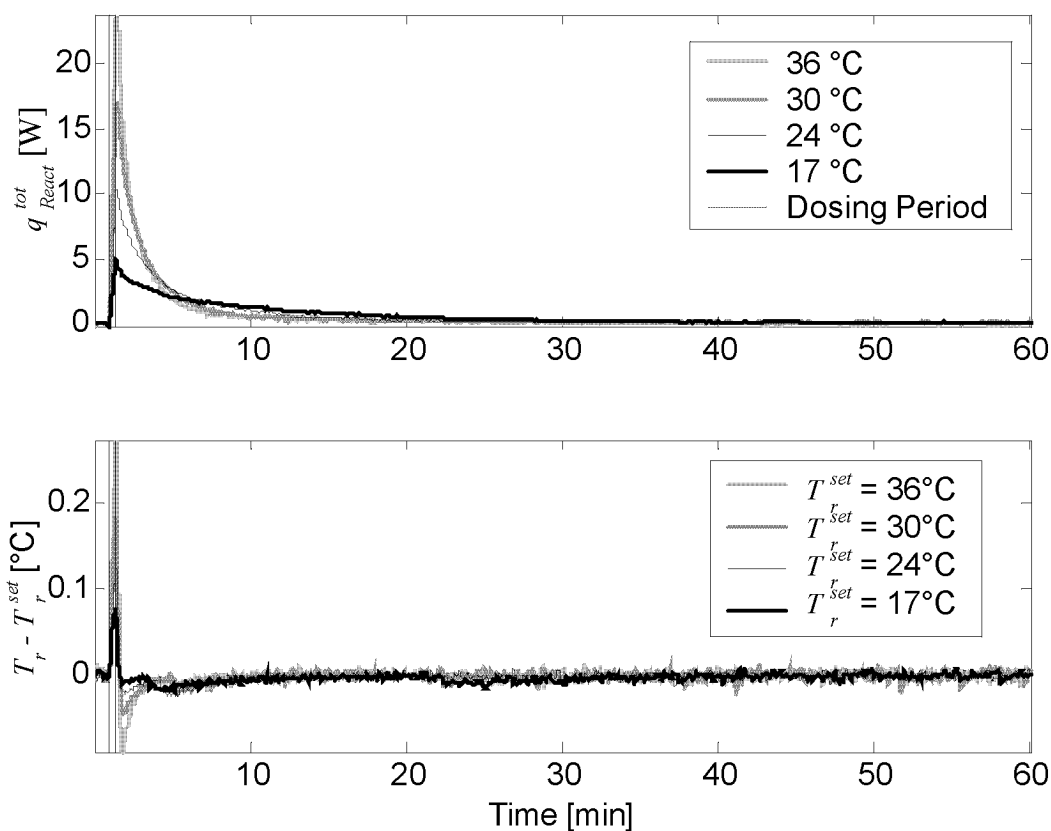


Figure E-13: Reaction power (q_{React}^{tot}) of the epoxidation reaction measured at 17, 24, 30 and 36°C. The dosing period of the catalyst is indicated with dashed lines.

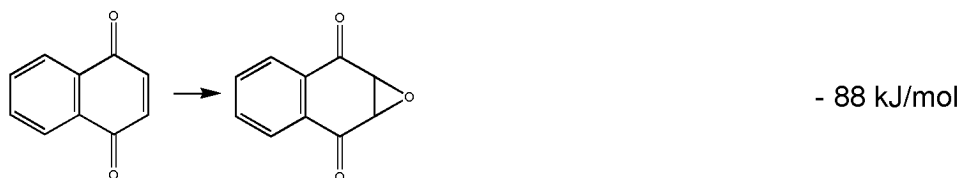
In contrast to the hydrolysis reaction of acetic anhydride, this epoxidation reaction is a consecutive reaction (see Figure 5-9). Therefore the total measured reaction power q_{React}^{tot} is mainly the sum of the reaction powers of the two reaction steps, taking place at the same time. Therefore the classical evaluation method applied in Appendix E.2.4.1 cannot be applied in this case. The only possibility to calculate the desired reaction parameters (enthalpies of reaction and rate constants) would be to apply method B reported in Chapter 2.3.2.3. This actually corresponds to the separate calorimetric evaluation carried out prior to the combined evaluation described in Chapter 4 (see Figure 4-5). The combined evaluation will be shown in the following Chapter.

The only reasonable classical evaluation that remains is the integration of the total measured reaction power q_{React}^{tot} to obtain a total reaction enthalpy ΔH [J/mol]

$$\Delta H = \frac{1}{n} \cdot \int_0^{120 \text{ min}} q_{React}^{tot} dt \quad (\text{E-8})$$

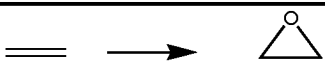
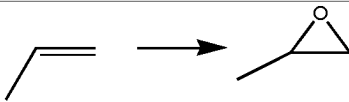
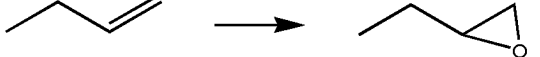
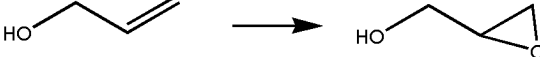
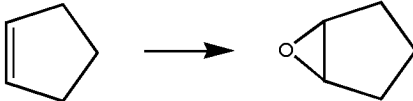
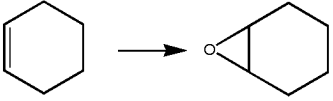
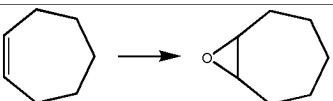
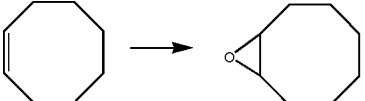
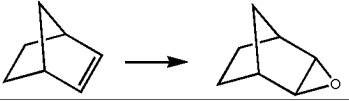
Where n is the number of moles of 2,5-di-tert-butyl-1,4-benzoquinone [mol]. The results are summarized in Table E-12. Despite a very intensive literature research {Chemical Abstracts, Beilstein, Ulman, Landolt-Börnstein, CRC Handbook of

chemistry and physics, Organic Chemistry Patai, Organic Chemistry Houben Weyl, NIST Chemistry Web book} only a single reference data for an epoxidation of a conjugated C=C double bond was found [Flowers *et. al.* 93] (the oxygen source is not included):



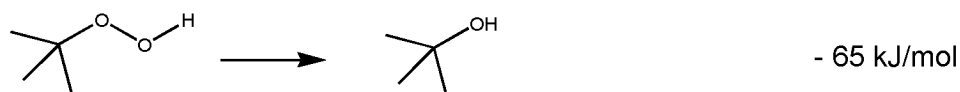
However this epoxidation enthalpy was not directly measured but is the result of a complex calculation scheme. Therefore it was compared to the epoxidation enthalpy of saturated C=C double bonds (calculated by the difference of the standard enthalpies of formation). The data is shown in Table E-11.

Table E-11: Enthalpies of epoxidation of saturated C=C double bonds calculated based on standard heats of formation. The oxygen source is not included. ^{a)} [Dowd *et. al.* 91] ^{b)} [NIST]

Epoxidation step	State	ΔH [kJ/mol]
	gas	-104 ^{a)} -105 ^{b)}
	gas	-115 ^{a)} - 115 ^{b)}
	liquid	-147 ^{a)}
	liquid	-127 ^{b)}
	gas	-131 ^{a)} , -133 ^{b)}
	Liquid	- 135 ^{b)}
	gas	-122 ^{a)} , -121 ^{b)}
	liquid	-128 ^{b)}
		-143 ^{a)}
		-138 ^{a)}
		-107 ^{a)}

All epoxidation enthalpies shown in Table E-11 are significantly higher than the -88 kJ/mol reported for the conjugated system. Considering Figure 5-9 it can be concluded that the reaction enthalpy of the first epoxidation step will probably be smaller than the reaction enthalpy of the second step as the C=C bond is less conjugated in the second step.

The second part of the investigated epoxidation reaction is the transformation of tert-butyl hydroperoxide (oxygen source for the epoxidation):



The total reaction enthalpy of the epoxidation of a C=C bond by tert-butyl hydroperoxide should therefore be in the range of -153 to -212 kJ/mol. For the investigated epoxidation the reaction enthalpy should be closer to -153 kJ/mol. In order to compare these literature values to the measured total reaction enthalpy ΔH it has to be multiplied by two, as two epoxidations are taking place. This value is also shown in Table E-12. It is apparent that the reaction enthalpies obtained by the integration of $q_{\text{React}}^{\text{tot}}$ curves are higher than the reference values. The high standard deviation of the reaction enthalpy at 17 °C (> 10%) will be discussed in E.3.5.

Table E-12: Total reaction enthalpy ΔH obtained by integration of the $q_{\text{React}}^{\text{tot}}$ curves shown in Figure E-13. ^{a)} Total integration time: 120 min

	17 °C	24 °C	30 °C	36 °C
ΔH [kJ/mol] ^{a)}	-440 ± 50	-440 ± 20	-480 ± 30	-440 ± 10
Literature	-307 ... -424			

E.3.5 Special observations

During these experiments several phenomena were observed. They are shortly described in this Chapter.

Heterogeneous reaction mixture at 17 °C

During the experiments at 17 °C it was observed that after the hydroperoxide was dosed the reaction mixture became a suspension. However, after about one hour of mixing the reaction mixture became a clear solution again. This process was observed optically by the endoscope and it was also registered in a drift of the measured q_{Comp} and q_{Cooling} signal. Obviously the heat-transfer coefficient was changing during this initial phase and thus caused a drifting q_{Comp} and q_{Cooling} signal. The calculated q_{tot} during this initial phase was close to zero, indicating that no reaction was taking place. Also in the infrared spectrum no changes were observed during this phase. Therefore the four reaction experiments at 17 °C, used for the evaluation, were only started when the measured q_{Comp} and q_{Cooling} signals were stable.

Changes of the heat-transfer coefficient during the reaction measurements

Figure 3-20 shows the measured total calorimetric signal q_{tot} in the first plot. The second plot shows the measured baseline signal (shifted q_{Cooling} signal) compared to the corresponding mathematical baseline (proportional to the volume change). The calculation was carried out analogous to the description in Chapter 5.2.1. This

second plot clearly shows that the behavior of the baseline changes with the temperature. The measurement at 17 °C shows the largest baseline change and deviates significantly from the supposed mathematical baseline. The measurement at 24 °C still shows a similar behavior but the changes are smaller. However the measured baselines at 30 and 36 °C show no more significant deviation to the supposed mathematical baseline. The reaction enthalpies can be obtained by the integration of the q_{tot} curves. The results deviate by 12 (17 °C), 6 (24 °C), 5 (30 °C) and 4 % (36 °C) if the measured baseline is replaced by the mathematical baseline. Figure 3-20 further shows the power consumption of the stirrer engine. No change was observed during all experiments.

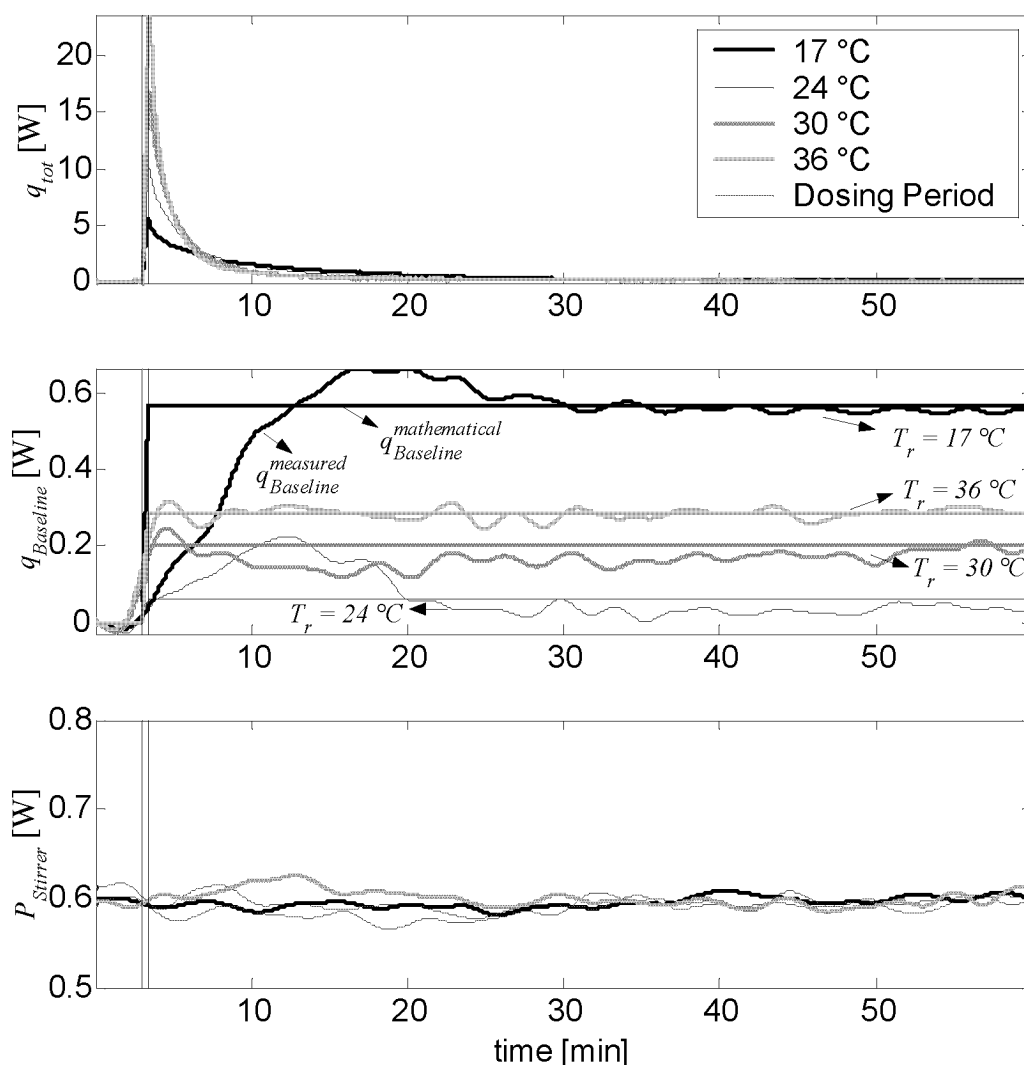


Figure E-14: Comparison of the mathematical and measured baseline for the epoxidation experiments. The dosing period of the catalyst is indicated with dashed lines. The changing baseline is mainly caused by the change of the heat-transfer coefficient and is changing with temperature.

Large standard deviation in the determined ΔH at 17 °C (see Table E-12)

The large standard deviation of the determined ΔH values of the four experiments carried out at 17°C (> 10%, see Table E-12) could be explained based on the observations discussed above as they are mainly related to the measurements at 17 °C.

Change of the color

Further it was observed that the color (slight orange) of the final reaction mixture showed increasing intensity with increasing temperature. The reaction mixtures were stored for some months at 4 °C and it was observed that during this time the color and thus the differences almost disappeared.

E.3.6 Comparison to literature values

Unfortunately the published kinetic data for this reaction example turned out to be rather unreliable. The three references found and the reported experimental conditions are summarized in Table E-13. The rate constants were all published as pseudo first-order rate constants in units of [1/min]. However the concentrations of tert-butyl hydroperoxide as well as the concentration of the catalyst were not chosen identically. It is therefore surprising that the reported pseudo first-order rate constants are similar. Based on the assumption that the reaction is first order in the concentration of tert-butyl hydroperoxide and first order in the concentration of the catalyst (Triton B), the reported pseudo first-order rate constants were transformed into third order rate constants. The calculation is summarized in Table E-13. During this calculation several problems were encountered (see comments below).

Table E-13: Epoxidation of 2,5-di-tert-butyl-1,4-benzoquinone. Comparison of the kinetic parameters reported in the literature. Comments marked with “?..” are listed below.

		T_r	<i>Bijlsma</i>	<i>Hairfield</i>	<i>Mayes</i>	<i>This Work</i>
Reported k_1	1/min	10		0.1		see Table 5-5
		17	0.3	0.24 ^{?1}	0.3	
		30		0.8	1.3	
Reported k_2	1/min	10		0.03 c		
		17	0.04	0.07 ^{?1}	0.05	
		30		0.26	0.17	
Reported $E_{A,1}$ [kJ/mol]				68.6	82	
Reported $E_{A,2}$ [kJ/mol]				73.4	69	
Reported $E_{A,2}$ [kJ/mol]					(74)^{?2}	
Tert-Butyl HP	mmol		12	50	36.5	58.3
Catalyst 40% in Methanol	ml		0.24	1	0.5 ^{?3}	0.8
V_r	ml		31.1	50	22.5	36
Tert-Butyl HP Concentration	mol/l		0.39	1	1.62^{?4}	1.62
Catalyst Concentration	mol/l		0.017	0.044	0.049	0.049
transformed k_1	[³ mol ² /min]	10		2.6		see following Table E-14
		17	45.3 ^{?5}	5.4	3.8	
		30		18.3	16.3	
transformed k_2	[³ mol ² /min]	10		0.7		
		17	6	1.6	0.6	
		30		5.8	2.1	

Comments to the experiment reported by [Hairfield et. al. 85]

²¹ The rate constants at 10, 17 and 30 °C were determined but only the activation energies and one pair of rate constants was reported. Unfortunately the corresponding temperature is not given. *Also after contacting the author the question was not answered.* Therefore the reference temperature was suggested to be 17°C.

Comments to the experiment reported by [Mayes et. al. 92]

²² In the article the activation energy of E_A^1 was reported to be 74 kJ/mol. However using the two reported rate constants k_1 at 17 and 30 °C E_A^1 was calculated to be 82 kJ/mol.

²³ Nowhere in the text it was clearly stated that the concentration of the catalyst solution is really 40 % in Triton B. For the calculations this was assumed.

²⁴ From the quantities reported in the experimental section a ten fold excess of the hydroperoxide to the benzoquinone was calculated. However in the text it is written that the excess is twenty fold. For the calculations the values given in the experimental section are used.

Unfortunately the author did not answer to any of these questions.

Comments to the experiment reported by [Bijlsma et. al. 98]

²⁵ According to the calculations shown in Table E-13 the concentrations applied deviated significantly from the concentrations applied by the other two authors. Therefore the scaled rate constants are completely out of the range compared to the values given by the other references. The author responded to this fact with the answer that the concentrations were indeed chosen smaller than in the publication of [Mayes et. al. 92] because otherwise the temperature could not be controlled isothermally. But the different concentrations were not considered in the reported rate constants. According to the author the difference caused by the different concentrations should not be significant.

Comparing the transformed rate constants in Table E-13 it becomes clear that the values reported by [Bijlsma et. al. 98] deviate significantly from the other references. The other two references however agree quite well. They are summarized in Table E-14 and compared to the values calculated in this work.

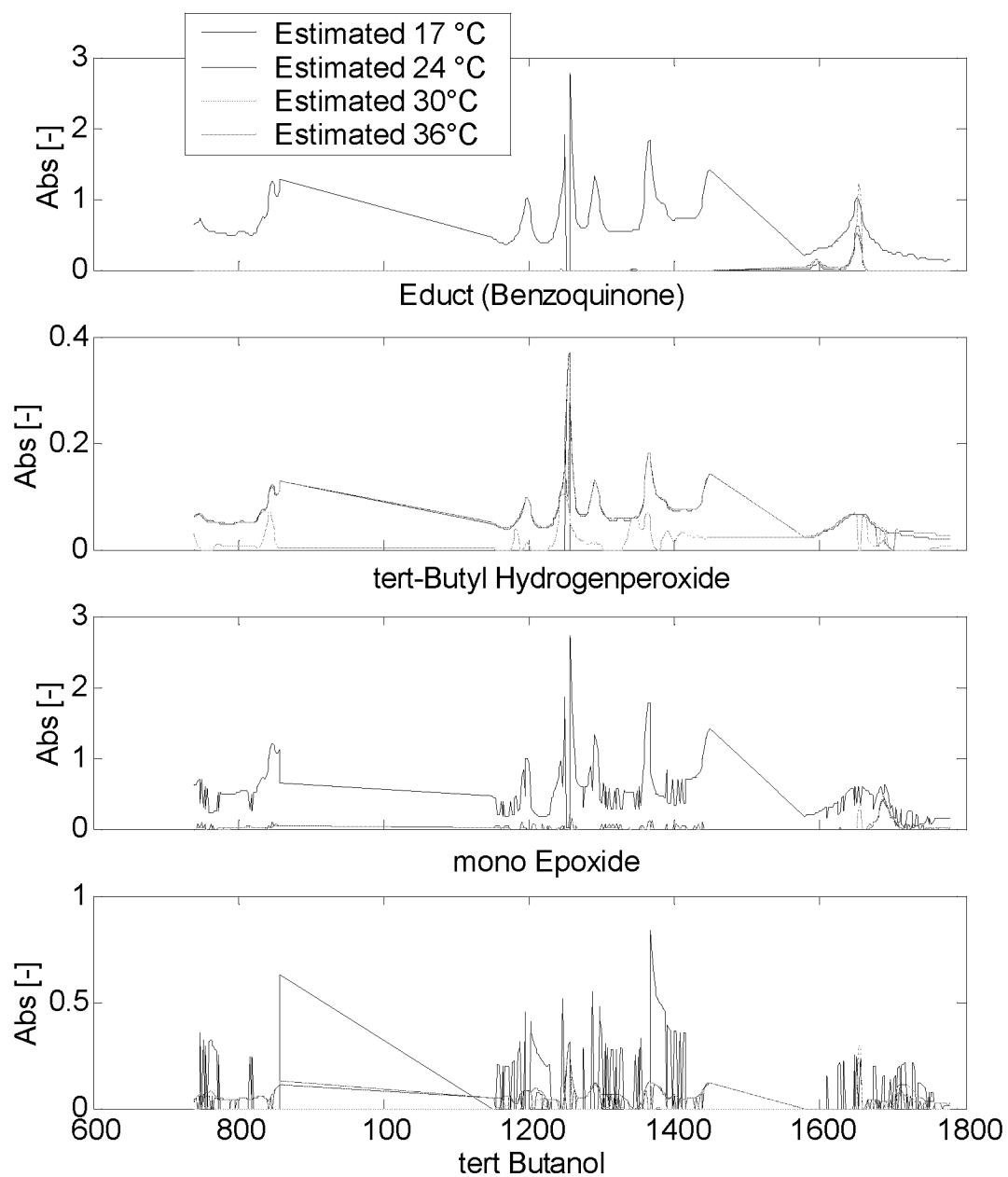
Table E-14: Epoxidation of 2,5-di-tert-butyl-1,4-benzoquinone. Summary of the kinetic reaction parameters reported in literature and comparison to the calculated values of this work. ^{a)} Mean value of the transformed rate constants shown in Table E-13 (only values of Mayes and Hairfield are used). ^{b)} Calculated based on the two average values of k_1 and k_2 at 17 and 30 °C. ^{c)} Separate evaluation of the measurements at each temperature (see Chapter 5.4.1). The values given in Table 5-5 are transformed according to Table E-13 ^{d)} Simultaneous evaluation of all measurements at all temperatures (see Chapter 5.4.3). The rate constants given in Table 5-5 are transformed according to Table E-13.

	k_1 17°C	k_1 30°C	k_2 17°C	k_2 30 °C	$E_{A,1}$	$E_{A,2}$
	[l ² /mol ² /min]				[kJ/mol]	
Literature	5 ± 1 ^{a)}	17 ± 1 ^{a)}	1 ± 1 ^{a)}	4 ± 3 ^{a)}	75 ^{b)}	72 ^{b)}
Combined Evaluation ^{c)}	8	14	1.1	4.5	34	72
Combined Evaluation ^{d)}	5	14	1.2	4.2	60	70

Although the values shown in the first row of Table E-14 are reasonable, care should be taken when using these values for comparison as their calculation was not straightforward (see problems discussed above). It should also be noted that the assumption, required to transform the reported rate constants, that the reaction is first order in tert-butyl hydroperoxide and the catalyst concentration might be incorrect (see Chapter 5.4.2).

However the combined evaluation of all measurements at all temperatures (see Chapter 5.4.3) agrees quite well with the literature values whereas the separate combined evaluation of each temperature results in a significantly different activation energy $E_{A,1}$.

E.3.7 Estimated pure spectra



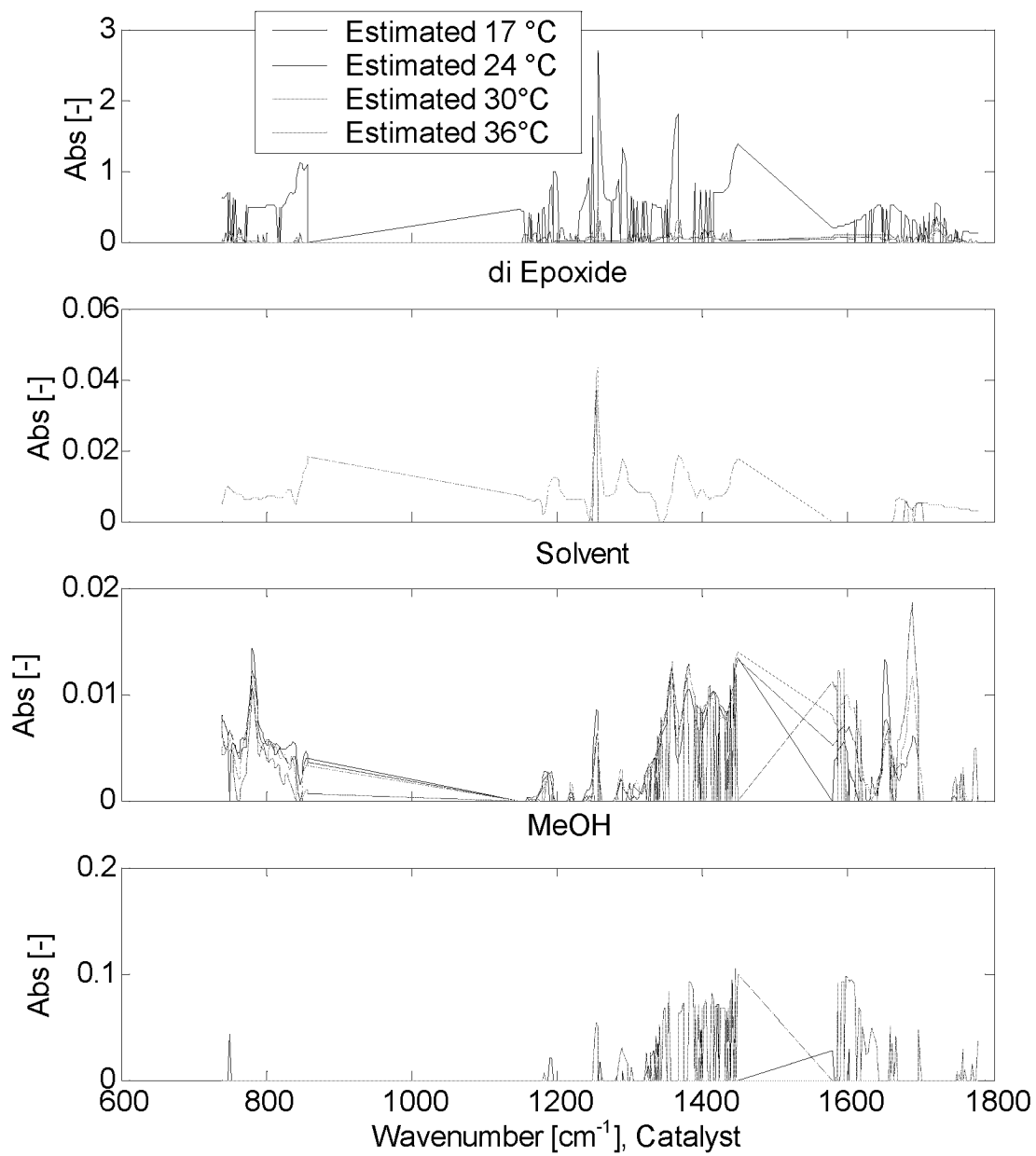


Figure E-15: *Epoxidation of 2,5-di-tert-butyl-1,4-benzoquinone*. Calculated pure spectra by the combined evaluation (data set I).

E.3.8 Importance of the automatic scaling method for the combined evaluation

On the bases of this reaction example the importance of the developed automatic scaling procedure for the combined evaluation of calorimetric and infrared data (see Chapter 4.5) can be demonstrated. Table E-15 shows the deviation of all reaction parameters determined by a combined identification to the reaction parameters determined by individual evaluations of the calorimetric and infrared data. The evaluation corresponds to the overall evaluation of all experiments at all temperatures (see Chapter 5.4.3 and results in Table 5-5). The combined evaluation is carried out two times:

Method 1: The error functions ΔQ and ΔA (sum of squares of the deviation of the simulated to the measured calorimetric and infrared data, Equations (4-6) to (4-8)) are simply added together. This corresponds to setting $S_Q = 1$, $S_{IR} = 1$ and $\Delta A_{min} = \Delta Q_{min} = 0$ in Equation (4-16).

Method 2: The automatic scaling method described in Chapter 4.5 is applied. The aim of this automatic scaling method is to achieve equal influence of the calorimetric and infrared data on the determined reaction parameters. This is achieved by a sensitivity analysis of the calorimetric and infrared error functions with respect to the reaction model parameters (equal to the evaluation shown in Chapter 5.4.3).

Table E-15: Comparison of two different combination methods: 1) Simply adding ΔQ and ΔA and 2) Developed automatic scaling method of ΔQ and ΔA (see Chapter 4.5). The evaluation corresponds to the evaluation over all temperatures described in Chapter 5.4.3 and Table 5-5.

Reaction Parameter	Deviation to separate the Calorimetric Evaluation [%]		Deviation to separate the Infrared Evaluation [%]	
	Method I	Method II	Method I	Method II
k_1 17°C	0	54	36	2
k_1 24°C	0	52	30	6
k_1 30 °C	0	51	25	13
k_1 36 °C	0	49	20	19
k_2 17°C	0	123	57	5
k_2 24°C	0	110	56	7
k_2 30 °C	0	99	54	10
k_2 36 °C	0	90	53	12
$E_{A,1}$	0	2	17	14
$E_{A,2}$	0	8	5	4
$\Delta_r H_1$	0	33	33	11
$\Delta_r H_2$	0	32	11	17

Table E-15 clearly shows that a combined evaluation by simply adding the two error functions does not lead to useful results: They are identical to the results obtained by a separate evaluation of the calorimetric data (deviations are all 0 %). The measurements of the infrared spectrum would therefore be without any use.

However it should be kept in mind that the dominance of the calorimetric data is no sign for a superior quality. It only tells that the error function ΔQ is more sensitive to changes of the reaction parameters compared to ΔA (compare to Chapters 5.4.4 and 6.3.4). But still the result might be influenced by measurement or model errors.

It is therefore essential to apply the developed automatic scaling method in order to get a real combined evaluation of the data sets. Table E-15 shows that the results obtained by this method are neither equal to the separate calorimetric evaluation nor to the separate infrared evaluation. They represent the best possible combined solution where the scaled ΔQ and ΔA have the same influence on the determined reaction parameters.

E.4 Industrial reaction examples

E.4.1 Experimental section, Reaction A: Acetylation

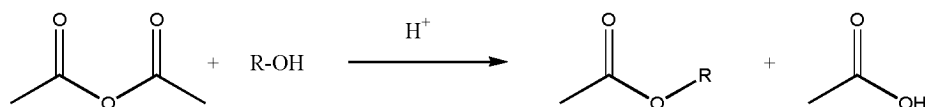


Figure E-16: Acetylation reaction. The catalyst was dosed into the reaction mixture in order to initiate the reaction.

First the reactor was brought to the jacket temperature $T_j = -5 \text{ }^\circ\text{C}$ after being cleaned and purged with N_2 . After some minutes a reference background spectrum for the infrared measurement was taken. Then 23.5 ml of the alcohol and 5.25 ml of acetic anhydride were added sequentially to the reactor. The stirrer was turned on to 550 rpm and the reaction temperature T_r was set to $60 \text{ }^\circ\text{C}$. To start the reaction 0.4 ml of acid were dosed within 48 seconds into the closed reactor. The temperature of the cooling liquid (water, alcohol mixture) connected to the cooler of the calorimeter was set to $-10 \text{ }^\circ\text{C}$ by the cryostat.

Calorimeter Settings:

Cooling liquid: Water, alcohol mixture (2:1).

Peltier Parameter Set: Set A D.1 and fitted values.

$\Delta\Delta T_{\text{Pelt}}$ (see D.1): 0.05 K

Filter settings: see 3.7.4

k_{Loss} settings: see D.2

Controller settings: see 3.6, Point ⑥ in Figure 3-15 was chosen 5 min after the end of the dosing.

E.4.2 Experimental section, Reaction B

A second reaction example was carried out using the pre-version of the presented calorimeter (described in the diploma work of I. Zürcher [Zürcher 01]).

25 ml of the educt solution was given into the reactor. The jacket temperature was set to $T_j = 60 \text{ }^\circ\text{C}$, the temperature of the cooling liquid to $T_{\text{Cry}} = 20 \text{ }^\circ\text{C}$ and the reaction temperature to $T_r = 100 \text{ }^\circ\text{C}$. The reaction was initiated by dosing 0.4 ml of the catalyst within 1.5 minutes. In a second experiment the catalyst was dosed within 25 seconds.

E.4.3 Measurement results

These reactions were only carried out in order to demonstrate that fast and strongly exothermic reactions can be handled with the presented calorimeter. Both reactions were investigated using a conventional reaction calorimeter (RC1 [Riesen et. al. 85] and [RC1 Handbook]). However the isothermal-temperature controlling caused serious problems. Deviations from the set point in the range of up to 30°C (example A) and 25 °C (example B) during a time period of several minutes occurred.

Infrared spectra were also recorded during these reactions and evaluated according to Chapter 2.3.2.2. The calorimetric and the infrared signals were then compared according to the predicted conversion profile of the reaction. The agreement was satisfying in all experiments.

No further evaluation of the measured data was carried out.

E.4.3.1 Reaction Example A: Acetylation

This reaction example shows the potential of the new calorimeter to control fast and highly exothermic reactions at strictly isothermal conditions. Although a maximum reaction power of about 1.3 kW/l is reached within a few seconds, the temperature of the reactor content is only changing by 0.6 K over a period of about 1 minute (see Figure E-17). However this reaction also showed the accuracy limits of the measured base line. Using the Peltier parameter set A the offset of the baseline at the end of the reaction is about 0.7 W. For all the standard experiments described in Chapter 5.2 to 5.4 this offset error was in the range of 0.1 to 0.2 W. The reason for this difference might be caused by the fact that the baseline change is larger (6 W) compared to all other experiments and that the cooling power of the Peltier elements was close to the maximum (see also Chapter 7.1).

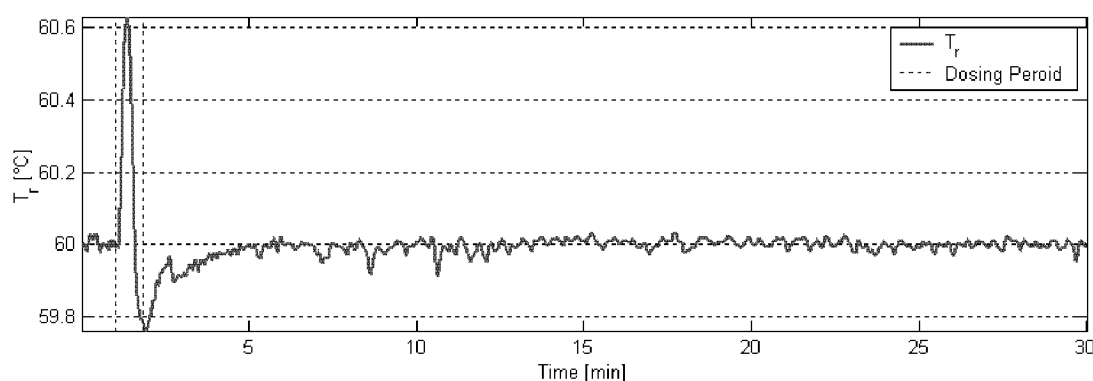


Figure E-17: Measured T_r of the reaction example A. A maximum reaction power of about 1.3 kW/l has to be removed. It only causes a temperature deviation of about 0.6 °C.

Analogous to Figure 5-2 (neutralization reaction of NaOH) and Figure E-14 (epoxidation reaction), Figure E-18 shows a comparison of the total measured reaction power q_{tot} (first plot, straight line) and the reaction power calculated using a mathematical baseline (first plot, dotted line). The mathematical baseline was calculated analogous to Equation (5-2) and is shown in the second plot of Figure

E-18 (dotted lines). The measured baseline was not calculated based on the Peltier parameter set A. The Peltier parameters were obtained by a linear least-squares minimization of the q_{tot} signal at the end of the reaction.

In contrast to the neutralization reaction of NaOH the measured baseline change is not caused by a changing heat-transfer area A as the reaction volume remains constant during the reaction (or slightly increases). The main reason for the baseline change might therefore be an increasing viscosity, resulting in a change of the heat-transfer coefficient h_r on the reactor wall during the reaction. The increase of the viscosity is indicated by an increasing power consumption of the stirrer engine (Figure E-18, third plot).

Such an effect cannot be correctly described by the mathematical baseline, that assumes a linear change of the baseline during the dosing of the catalyst. Therefore the mathematical and the measured baseline deviate significantly for this reaction example. The integration of the two q_{tot} curves (mathematical and measured baseline) deviates by 15%. This example clearly shows the benefit of an online measured baseline as more information about the process is available.

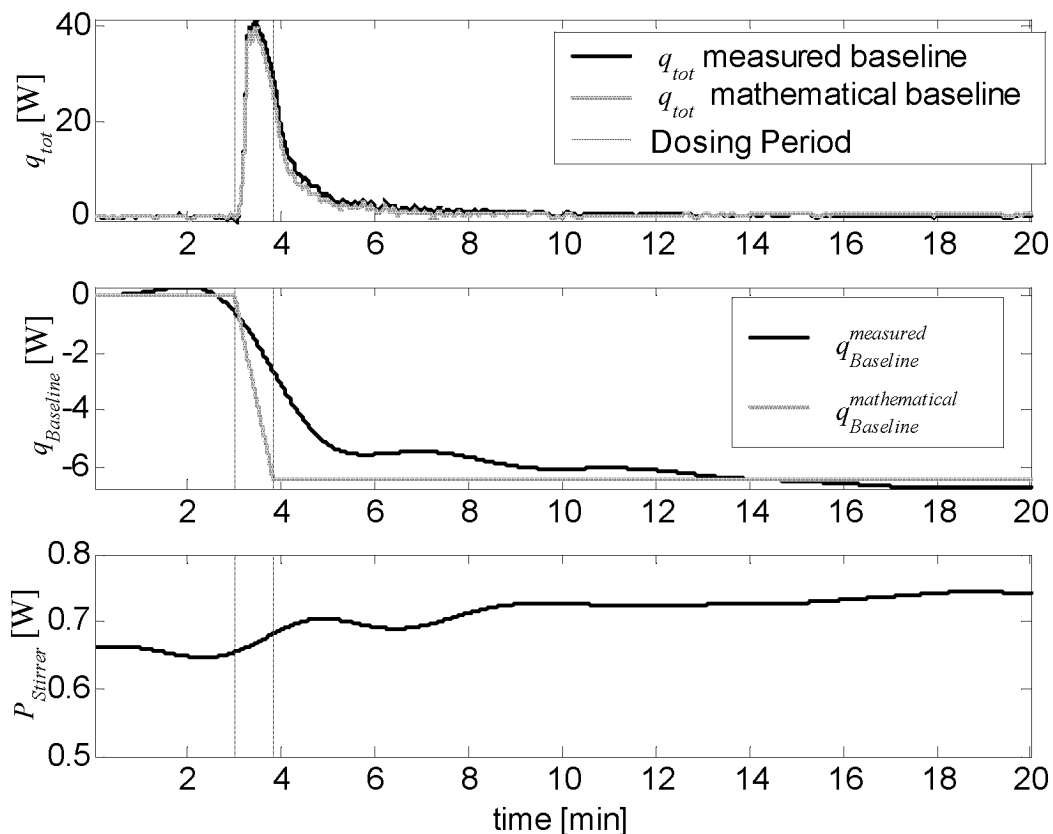


Figure E-18: Acetylation reaction at 60°C. The maximum reaction power equals 1.3 kW/l. The dosing period of the catalyst is indicated with dashed lines. The changing baseline is mainly caused by the change of the heat-transfer coefficient on the reactor wall due to the increasing viscosity.

E.4.3.2 Reaction Example B

As this reaction was measured with a pre-version of the presented reaction calorimeter only the measured data are shown in Figure E-19 and Figure E-20.

Both experiments show the potential and the limits of the new calorimeter to control fast and highly exothermic reactions at strictly isothermal conditions. In the first experiment, with slower catalyst addition and consequently slower reaction, a maximum reaction power of about 1.2 kW/l is reached within a few seconds. However the temperature of the reactor content is only changing by 0.4 K over a period of about 1 minute (see Figure E-19). In the second experiment, with faster catalyst addition, the reaction power reaches a maximum of about 2.8 kW/l resulting in a temperature deviation of about 4°C. This reaction example demonstrates the limits of the dynamics of the new reaction calorimeter.

Furthermore both measurements also show significant baseline changes of the q_{Comp} signal during the reaction. These baseline changes are compensated by the total cooling power ($q_{Cooling}$) of the Peltier elements. This example clearly shows the benefit of an online measured baseline as the observed baseline change is much slower than the initial burst during the reaction and would be difficult to predict.

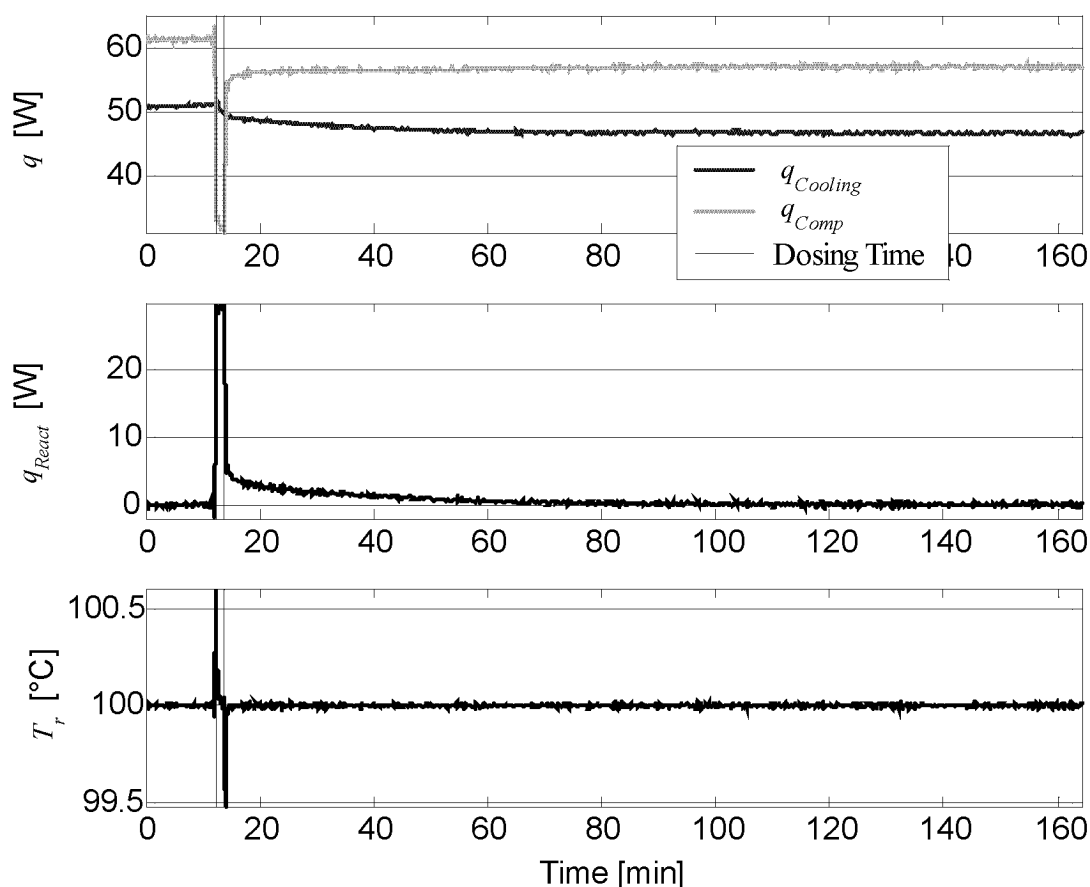


Figure E-19: Measured q_{Comp} and $q_{Cooling}$ (first plot), the calculated q_{React} (second plot) and the measured reaction temperature T_r (third plot) of reaction example B (1.5 minutes dosing time).

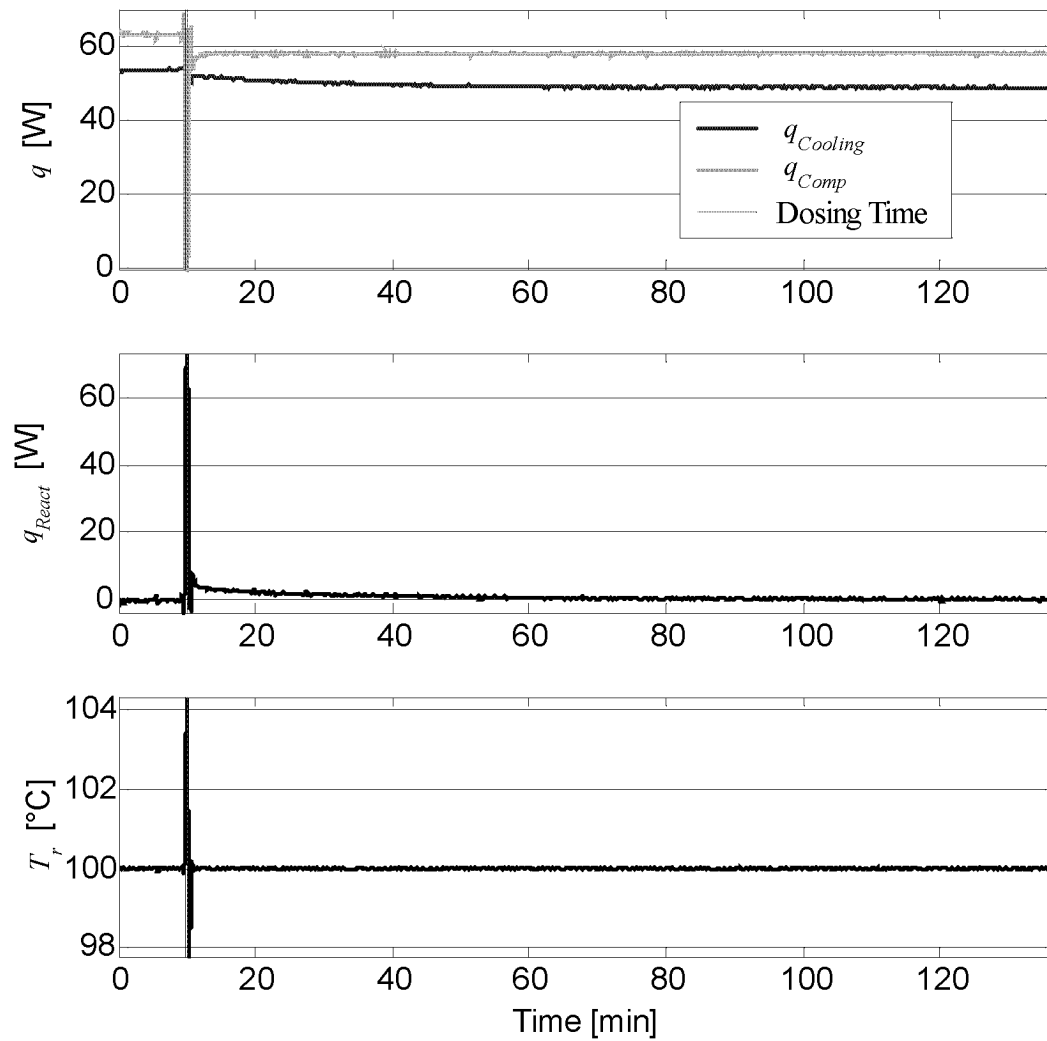


Figure E-20: Measured q_{Comp} and $q_{Cooling}$ (first plot), the calculated q_{React} (second plot) and the measured reaction temperature T_r (third plot) of reaction example B (25 seconds dosing time). A maximum reaction power of 2.8 kW/l has to be removed. It causes only a temperature deviation of about 4°C.

E.5 Heterogeneous Reaction Example

The following heterogeneous reaction example was investigated during the diploma thesis of I. Zürcher [Zürcher 01]:

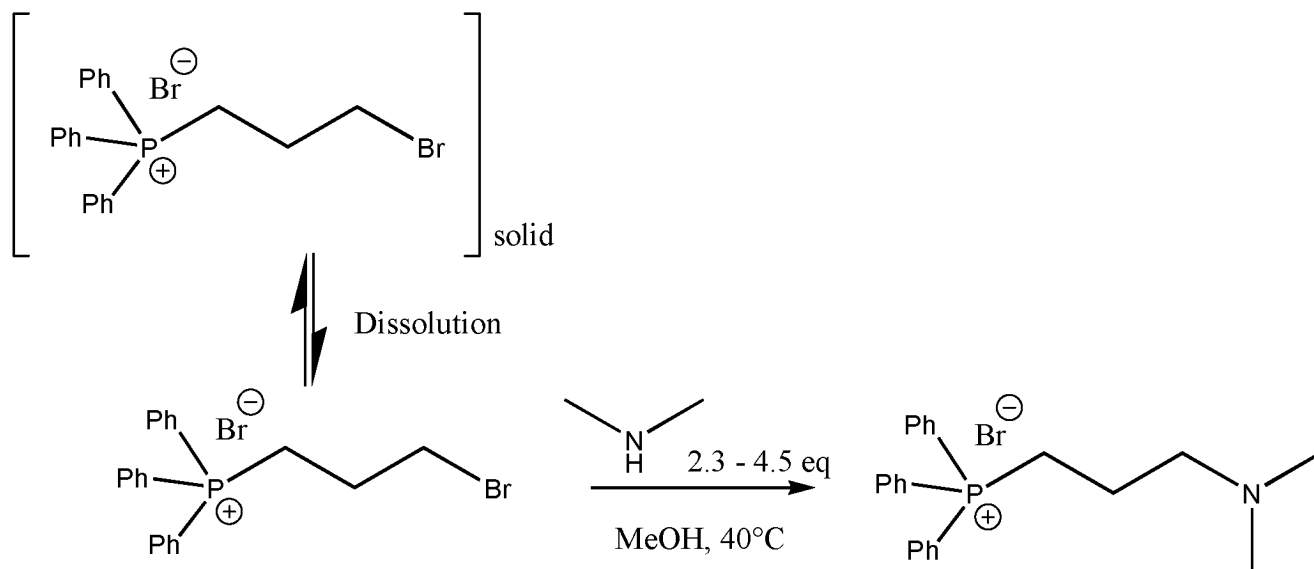


Figure E-21 Reaction scheme of the heterogeneous reaction investigated during the diploma work of I. Zürcher [Zürcher 01]

The applied reaction calorimeter as well as the evaluation algorithm were both pre versions of the presented final implementations. Though the results were promising they cannot be evaluated for this thesis.

Curriculum Vitae

Personal Data

Name: Andreas Zogg
Date of Birth: November 26, 1974
Birth place: Burgdorf, Switzerland

Education

1981-1987 Primary and secondary schools at Oberburg BE
1987-1994 Gymnasium at Burgdorf BE
1994 Matura certificate, type C
1994-1996 Basic studies in chemistry, Swiss Federal Institute of Technology (ETH Zürich)
1996-1998 Diploma studies of technical chemistry, Swiss Federal Institute of Technology (ETH Zürich)
1998-1999 Diploma thesis at the Institute for Chemical and Bioengineering, ETH Zürich, Safety and Environmental Technology Group (Prof. Dr. K. Hungerbühler). *“Bestimmung thermo-kinetischer Parameter mit Hilfe eines kleinvolumigen Reaktionskalorimeters: Modellentwicklung und Anwendung auf eine ausgewählte Reaktion.“*
1999 Diploma as Dipl. Chem. ETH
1999-2003 Doctoral student at the Institute for Chemical and Bioengineering, ETH Zürich, Safety and Environmental Technology Group (Prof. Dr. K. Hungerbühler). *“A Combined Approach using Calorimetry and IR-ATR Spectroscopy for the Determination of Kinetic and Thermodynamic Reaction Parameters “*